Copy No. 5

LOAD LOSSES IN SYNCHRONOUS MACHINES

- - - - -

A STUDY OF THE POLE FACE LOSS
CAUSED BY ARMATURE REACTION M.M.F. HARMONICS

A Thesis submitted for the degree of

MASTER OF SCIENCE

by

KENNETH JOHN ADDERLEY

The University of Aston in Birmingham

August 1968

Faculty of Engineering
Department of Electrical Engineering

Supervisor,
Professor E.J. Davies.

SUMMARY

The investigation divides into two main parts, the first relating to the power loss in the pole face of synchronous machines caused by the rotating space harmonics of armature reaction, the second to the surface e.m.f. distribution across the pole face.

The m.m.f. harmonic loss, important in modern machines with high specific current loadings, is calculated from established eddy-current coupling theory derived analytically from the diffusion equation. The theory accommodates the demagnetising effects of the surface currents and has been extended in generalised form by the author.

The theory, contains an analytical substitution for permeability and leads to simple formulae to predict the effect of changes in machine parameters. A comprehensive series of examples, using a digital computer, emphasises the importance of the slot openings, the gap to wavelength ratio, and the pole profile.

Tests on a range of production machines and an experimental model support the proposed formulae. The model machine, with a synchronously rotating laminated primary carrying a three-phase winding and a solid unwound secondary supported on a dynamometer frame, is designed to accentuate the harmonic loss.

Difficulties experienced in separating the losses therein include the accurate assessment of primary iron loss and secondary slot ripple loss. The primary iron loss is measured by considering the distribution of power supplied from mechanical and electrical sources. The slot ripple loss is calculated using equations derived from conformal-transformation theory together with established formulae.

The second part of this investigation, the distribution of surface e.m.f.s, is limited to the first pair of harmonic terms. It stresses the fundamental nature of the m.m.f. fluctuation at any point on the surface and the factors controlling its magnitude. Experimental evidence lends support to the author's mathematical treatment of this periodic non-sinusoidal fluctuation superposed on a polarising m.m.f. wave.

1. CONTENTS AND NOMENCLATURE

1.1 TABLE OF CONTENTS

1.1 TABLE OF CONTENTS cont.

1.1 TABLE OF CONTENTS cont.

1.1 TABLE OF CONTENTS cont.

1.1 TABLE OF CONTENTS cont.

1.1 TABLE OF CONTENTS cont.

1.2 LIST OF FIGURES AND PLATES

1.2 LIST OF FIGURES AND PLATES cont.

1.2 LIST OF FIGURES AND PLATES cont.

1.3 LIST OF TABLES

1.4. List of Principal Symbols

b	= slot width	m
B	= flux-density	
B_o	= peak value of B_x at the pole surface	Wb/m^2
C_1, C_2, C_3	= constants defined in sections 3.6.2, 3.6.3, 3.6.4, respectively	
d	= $1/\alpha$	m
D	= rotor diameter at airgap	m
e	= e.m.f. induced in a search coil on the secondary surface; subscripts detailed in section 7, identify either a particular coil or a particular component of the induced e.m.f.	V
e	= base of natural logarithms = 2.718	
E	= Electric Intensity	V/m
f_1	= synchronous frequency	c/s
F'	= primary (armature) ampere-turns, defined in section 3.2.	
F	= total ampere-turns for the hth harmonic in the primary (armature) m.m.f. wave $= F' \times k_{bh}$	
F_R (or F_2)	= eddy current reaction ampere-turns.	
F_ϕ	= flux component of F	
g	= airgap length	
G_0, G_1, G_2	= constants defined in section 3.6.5 & Appendix 12.1.2	
h	= order of space harmonic. As a subscript, the value of that harmonic quantity.	
H	= magnetic intensity	AT/m
H'	= magnetic intensity in c.g.s. units	

H_m	= peak value H at pole surface	AT/m
I	= armature phase current	A
I_A	= primary current in phase 'A' of the experimental load loss dynamometer	A
J	= current density in the pole face	A/m^2
J_m	= the peak value of J at the pole surface	A/m^2
K	= a positive integer	
k_1	= magnetisation parameter defined by equation 3.13	
k_b, k_d, k_p,	= slot width, winding pitch & winding distribution factors	
k_w	= $k_p \times k_d$	
k_2	= constant defined in section 3.6.1.	
K_L	= peripheral flux leakage factor defined in section 12.2.2	
L	= active pole length	
m	= magnetisation parameter defined by equation 3.13	
M	= auxiliary quantity defined in section 3.6.1	
n, N	= slip speed = speed of m.m.f. wave relative to the pole face	r.p.s., r.p.m.
n_m, N_m	= slip speed at maximum torque	r.p.s., r.p.m.
n_s, N_s	= synchronous speed	r.p.s., r.p.m.
p	= pole pairs	
P	= supply or loss power - for subscripts see Fig. 5.15 and section 5.8.1	
q	= slots per pole per phase	
Q	= auxiliary quantity defined in section 3.6.6	
R_1	= resistance factor defined by Kuyper.	

S	= reluctance	AT/Wb
T	= torque	Nm
T_m	= peak torque	Nm
w	= loss/unit surface area of pole face	W/m^2
w'	= loss/unit periphery of pole face	W/m
W_h	= predicted m.m.f. harmonic loss in a cylindrical rotor for the h-th term, neglecting peripheral flux leakage.	
W_{TOT}, kW_{TOT}	= the sum of a series of W_h values	W, kW
x	= peripheral direction in pole face	m
y	= radial direction into pole face ($y = o$ at pole/airgap surface)	m
z	= axial direction	m
$x, y, z,$	= as subscripts indicate the component of a quantity in that direction.	
α	$= \sqrt{\frac{\mu\omega}{2\rho}}$	m^{-1}
β and γ	= parameters used in the solution of Maxwell's equations	
β_1	= ratio: chamfered periphery/pole pitch	
β_2	= ratio: parallel-gap periphery/pole pitch	
δ	= angle between the inducing m.m.f. and the flux density wave.	
λ	= wavelength of electromagnetic quantities in drum surface	
λ_1	= fundamental wavelength	m
λ_s	= slot pitch	m
μ	= permeability = $\mu_o \mu_r$	H/m
μ_o	= permeability of free space $= 4\pi \times 10^{-7}$	H/m
ρ	= resistivity of the pole steel	Ω-m
ϕ, Φ	= flux linkages	
ϕ	= angle defined by equation 3.4, p 43.	

$(\phi_{ac})_h$	= total flux/pole for term of order h	Wb
θ_1	= angular displacement w.r.t. the primary (armature) surface	
θ_2	= angular displacement w.r.t. the secondary (pole) surface.	
ω	= angular frequency of electromagnetic quantities in drum surface	rad/s
ω	= angular velocity of the experimental machine	rad/s

Other symbols used mainly in one particular section are defined in that section.

2. INTRODUCTION

2. INTRODUCTION

2.1 The Problem

The calculation of eddy currents continues to be a subject of great interest to machine designers, on account of the undesirable losses caused by them and the difficulty of accurate predition. Eddy Current losses contribute to the total loss which, in a synchronous machine, may be classified as follows :

(i) Exciting circuit losses.

(ii) Fixed loss: no-load core loss, no-load surface losses, mechanical losses, including windage and brush friction.

(iii) Direct load loss: losses in armature circuits (I^2R) and brushes.

and (iv) Stray load loss.

With improved methods of cooling, modern machines have a much higher unit rating (Fig. 2.1) and specific current loading (Fig. 2.2.) Any increase in armature current means an increase in the losses associated with it, these have now become a significant proportion of the total loss in the machine.

The stray load loss, also referred to as the load loss[1], arises from changes in the flux distribution in various parts of the machine between the no-load and full load conditions due to the ampere-turns of the armature winding. Stray alternating fields induce eddy currents in the armature conductors, teeth, end clamps, pole pieces etc.

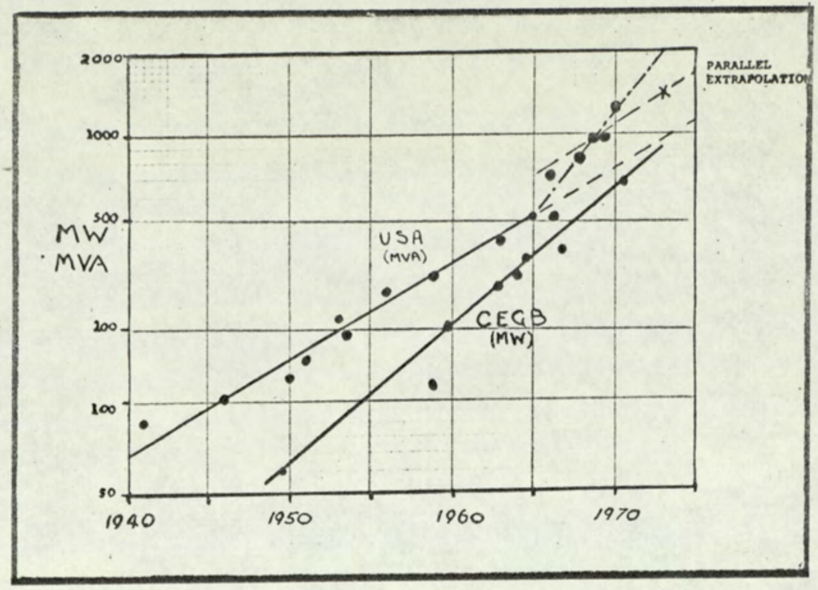

Fig.2.1. The Increase in Unit Rating of Turbo Alternators since 1940 (U.S.A.) and 1950 (U.K.)
Note the Logarithmic Scale.

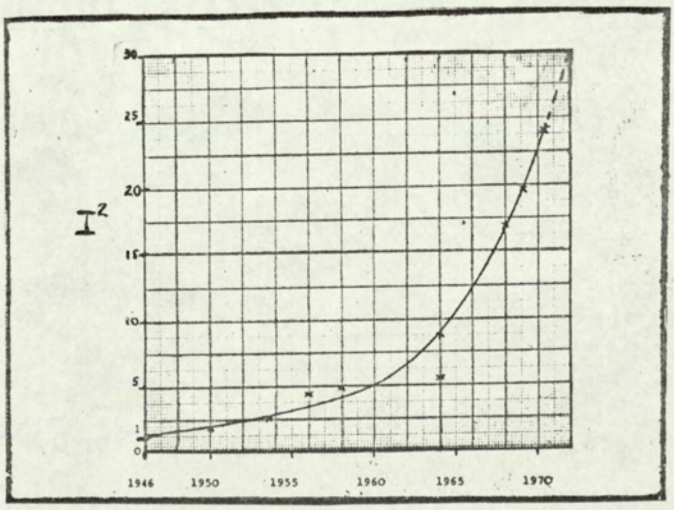

Fig. 2.2. The Way Problems Associated with the Current Loading of Large A.C. Generators is Illustrated by Plotting the Stator Current Squared Relative to 1946.

In the pole surface these eddy currents are caused by harmonics in the armature reaction m.m.f. wave. Barello[2] calls them stray rotating fields because they move at known speeds relative to the pole face.

The problem is to predict and measure this component of stray load loss. The proposed method of loss prediction, presented in chapter 3, is based on an established theory for eddy current couplings by Davies[3,4].

The loss measurements, which are difficult to obtain precisely on practical machines for the reasons given below, are taken on a specially designed experimental model (chapter 5), built following the encouraging results of applying the modified eddy current coupling theory to a range of large salient pole synchronous machines and turbo-alternators (Appendix 12.8 and chapter 6.) The work has highlighted a number of problems, many of which require further investigation (chapter 10). A summary of Davies' method and those of previous authors on pole face losses and related problems is given later in this chapter. Concluding remarks refer to the writer's own theoretical and experimental investigations into (a) the magnitude of the loss and (b) the variation in the surface e.m.f.s. over the pole surface (chapter 7.)

2.2. The Importance of the Investigation

The stray load loss is measured by the short circuit test and exists in many parts of the machine (Chalmers [6]). It can be subdivided into the following main components :

(i) Eddy current losses in the stator conductors due to the slot leakage flux,

(ii) End region losses in the stator, teeth, shields, clamps, end bracing rings (if metallic) and end windings due to end-leakage flux.

(iii) Increased iron losses in the stator teeth and core due to slot-leakage and harmonic fluxes.

(iv) Pole face losses due to armature reaction m.m.f. harmonics.

The test figure for the stray load loss is usually between 0.1 and 1% of the rated output power depending on a variety of design factors such as the type of mechanical construction, materials used, speed and MW and voltage ratings. Chalmers[6] takes a stray load loss of about 800 kW in a 75-MVA 6-pole synchronous machine which is about 13% of the total full load loss, or about 0.13% of the rated output power at 0.8 p.f. i.e. about the same order of magnitude as the slot ripple loss caused by the armature slot openings, calculated using Gibbs'[9] method. The pole face loss expressed as a percentage of the stray load loss also varies considerably with the machine construction. In the example quoted Chalmers takes this percentage as approximately 25% making the pole face loss about 3% of the total full load loss, or about 0.03% of the output. This small percentage is significant financially, because of its large capitalised value; and thermally, because of cooling requirements.

The capitalised value of all losses in large synchronous machines is currently rated at £120 per kW (£200 in parts of Switzerland). Therefore the capitalised value of the pole face loss in this example is £24,000.

Innovations designed to reduce losses and improve cooling, referred to in section 9. become economically viable as the unit rating and electric loading increases; a proportionate increase of stray load loss with electric loading, is thereby prevented.

For example in the 750 MVA 0.9 p.f. turbo-alternator design quoted by Anempodistov et al[17] the stray load loss is estimated at 0.17% of the full load output, i.e. 1168 kW,. Capitalised at £120 per kW over the life of the machine, this loss would cost the user £140,000 - a significant proportion of the machine cost of about £1 m.

The measured value of stray load loss is determined by subtracting from the shaft input power on short circuit the mechanical and resistance losses. The accuracy of measurement will therefore depend on the accurate estimation of these other losses involving the measurement of several quantities. Particular importance is attached to the mean winding temperature and the winding resistance because the copper losses are often of comparable magnitude to the stray load losses. Furthermore the unavoidable inclusion of the short circuit iron loss tends to make the measured value of stray load loss pessimistic.

The test value of stray load loss so obtained is difficult to subdivide without previous experience. Indeed, some firms simply estimate the design value of total stray load loss from test data on similar machines. This situation will continue until all the components can be predicted theoretically with greater accuracy than at present. A better understanding of the factors affecting each component therefore should enable these losses to be minimised at the design stage - just 10% reduction in the second example quoted would yield a substantial saving.

The object of the writer's investigation was to correlate the measured loss on (i) a special laboratory machine and (ii) a range of large synchronous machines, with the predicted pole face loss due to armature m.m.f. harmonics using a new method of calculation. This method accounts for variable permeability but avoids using numerical methods to solve the diffusion equation.

2.3 The Origin of Pole Face Loss

Eddy currents are induced in the solid pole faces of synchronous machines; at no-load by the modulation of the main flux density pattern by the stator slot openings, and on load by the combination of this and the armature reaction produced harmonic m.m.f.s. which move relative to the rotor surface.

The slot ripple surface losses have been widely discussed elsewhere. They are relevant to the present investigation in that they constitute a significant portion of the surface losses in the experimental load loss dynamometer machine. For this reason the relevant literature is reviewed later (section 2.4.5).

The m.m.f. harmonic losses have been discussed in references 1,2,14,18 and 24 and will be discussed qualitatively here and quantitatively in chapter 3. The m.m.f. waveforms produced by a balanced system of sinusoidal currents in a three phase integral slot armature winding are now considered. The selection of this particular m.m.f. pattern simplifies the initial discussion but does not restrict the application of the work to machines having other winding configurations and/or carrying unbalanced or non-sinusoidal armature currents.

It is well known that the armature reaction m.m.f. of a three phase winding infinitely distributed in discrete phase bands fluctuates between two extreme angular forms, Fig. 2.3.

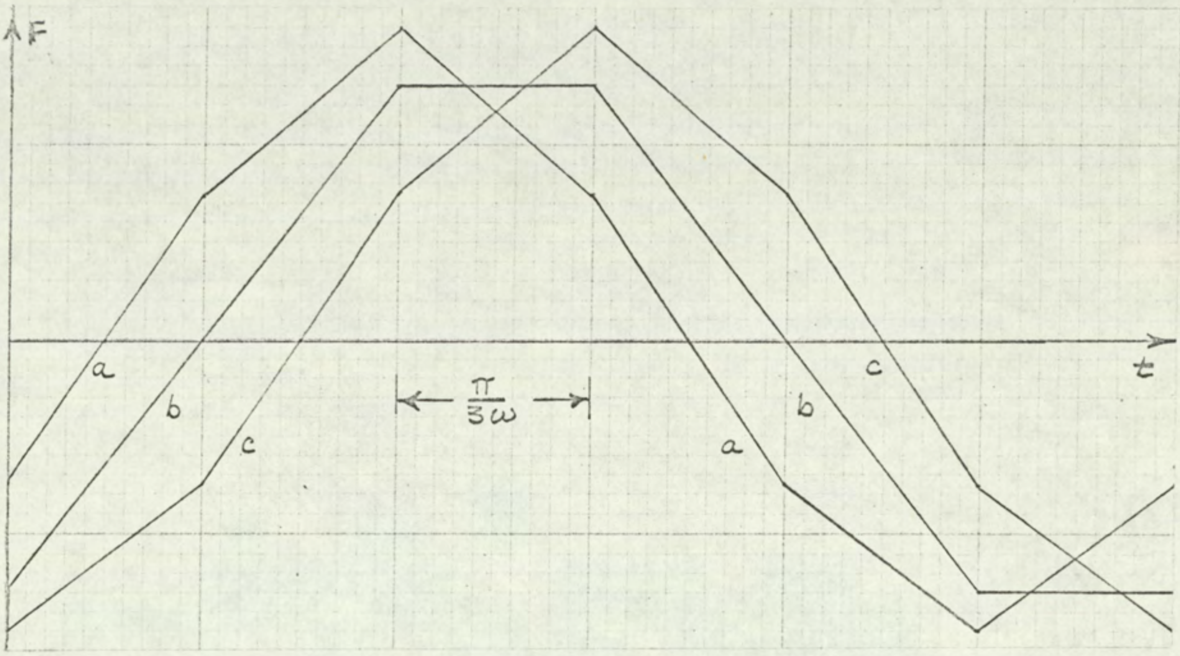

The m.m.f. waveform relative to the armature of an infinitely distributed three-phase 60° spread winding for the two limiting conditions :

(a) Maximum current in any one phase.
(b) $\pi/6\omega$ seconds later (current in the adjacent phase is zero).
(c) $\pi/3\omega$ seconds later than (a).

Fig. 2.3. The Travelling M.M.F. Waveform

The m.m.f. wave relative to the pole face is shown in Fig. 2.4 the difference in the two waveforms appears to be greatest at the direct axis of the m.m.f. wave and zero at the quadrature axis.

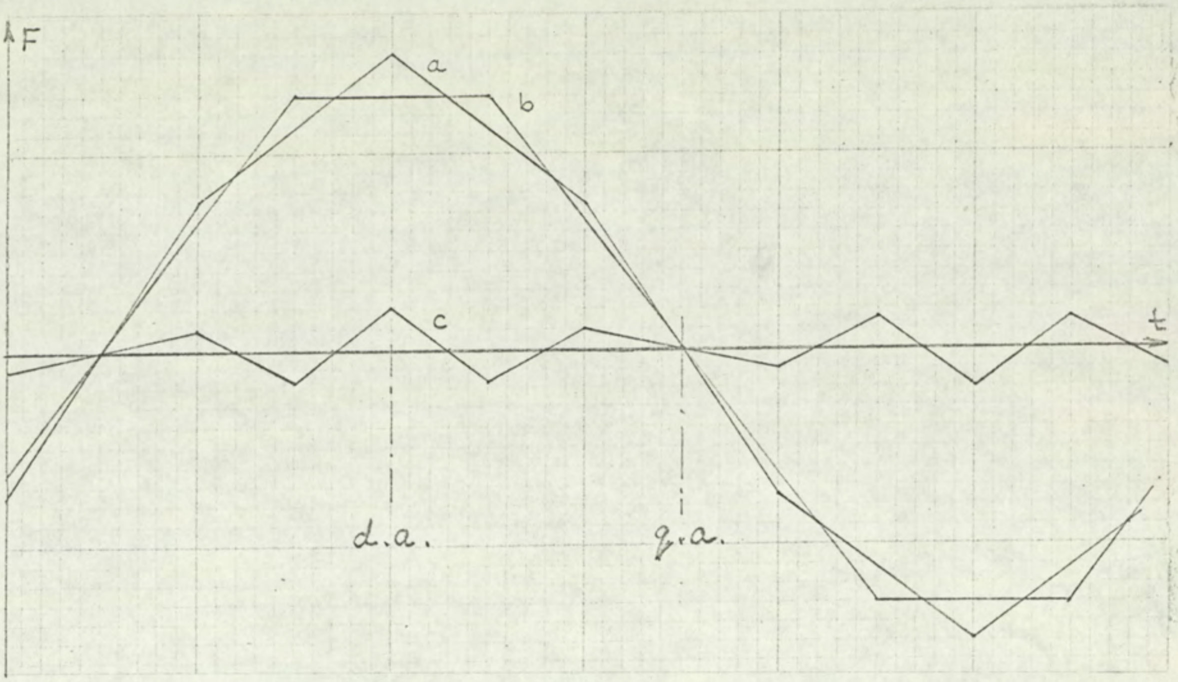

Fig. 2.4. Fluctuations in the armature m.m.f. Waveform relative to the pole shoe

Key : (a) and (b) as per Fig. 2.3.

(c) The difference between (a) and (b).

Further investigation using a larger scale and more m.m.f. waveforms drawn for equal increments in time, Fig. 2.5, shows that there is a fluctuation in m.m.f. on the quadrature axis. Waveforms (1) to (13) cover a complete sequence over a time interval of $60^oE/2\pi f_1$ ($= 1/6f_1$) seconds for which the fluctuation in impressed m.m.f. varies from that of curve (a) at the direct axis ($\theta_2 = 0$) to curve (h) at the quadrature axis. The inset shows the variation in the ripple amplitude over the pole surface.

It will be noted that Figs. 2.3 to 2.5 apply to an infinitely distributed full-pitched winding which does not apply in practice to large machines. The result of short pitching (which reduces the

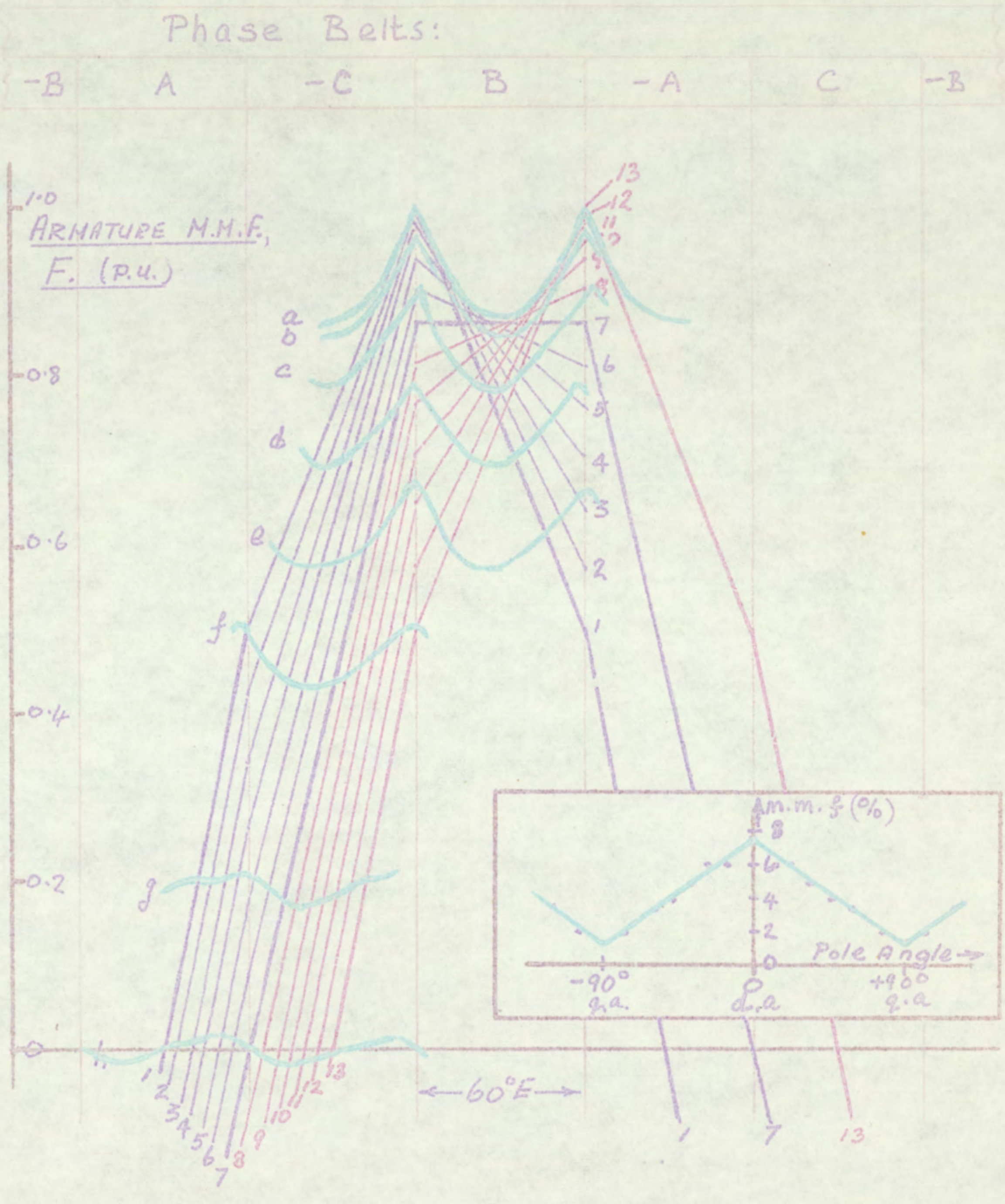

The time interval between each M.M.F Wave (1-13) = $\frac{\pi}{36\omega}$ sec.
Curves 'a' to 'h' show the time variation in M.M.F relative to the Pole Face: 'a' at the MMF Direct Axis and 'h' at the Quadrature Axis.
INSET: Peak to Peak value of M.M.F Fluctuation / Pole angle

FIG. 2.5 M.M.F WAVEFORMS FOR A 3-PHASE, INFINITELY DISTRIBUTED, FULL PITCHED, 60° SPREAD WINDING fluctuation is discussed in Chapter 7. It has been shown [36] that the magnitudes (but not the phase displacements) of the fundamental component m.m.f. and its harmonics are constant with time. The fundamental component travels at synchronous speed producing torque but no surface loss. The harmonic m.m.f.s. travel at known speeds relative to the pole face and induce eddy currents therein. The significant harmonics were divided by Rüdenberg [24] into two groups :

(i) the phase belt harmonics, arising from the grouping of the armature conductors into phase belts. These low order harmonics (of order h = 5, 7, 11, 13 ...) form the difference between the fundamental sine wave and the waveforms of Fig. 2.4 (a) and (b)

and (ii) the first order slot harmonics, arising from the practical windings being contained in discrete slots (Fig. 2.6.) and, not infinitely distributed. These two harmonics are of order $h = 6q \mp 1$, where q = the number of slots/pole/phase; they have wavelengths almost equal to the slot pitch and **are usually large** because together they most nearly fit the steps in the m.m.f. waveform.

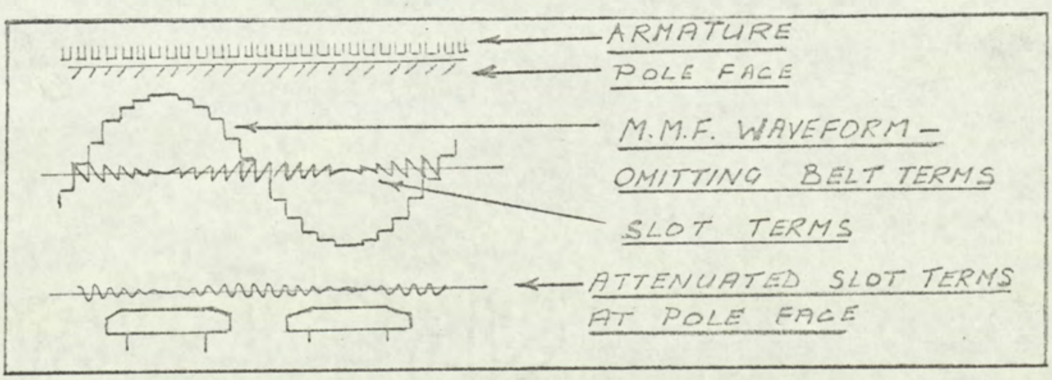

Fig. 2.6. The Effect of Slotting

Fig. 2.6 shows the result of placing a winding (which would otherwise give a sinusoidal m.m.f. wave) in discrete slots. For the moment the slots are assumed filamentary, the effects of the finite slot width being considered later (section 2.4.2 and Appendix 12.1.2.).
The superposed m.m.f. ripple is a distorted amplitude modulated sawtooth waveform. The unusual features of this waveform are that the positions of the saw teeth remain fixed relative to the stator but their amplitudes are fixed relative to the rotor. In contrast to the phase belt harmonics, the slot harmonics are seen to produce almost zero fluctuation at the centre line of the m.m.f. wave (direct axis) and maximum fluctuation at 90°E on either side (quadrature axis) when feeding a zero power factor load, or operating on short circuit the m.m.f. and rotor pole axes will be aligned (Fig. 2.6) giving maximum belt harmonic loss but minimum slot harmonic loss.

In the experimental model, designed to accentuate the m.m.f. harmonics, the induced e.m.f.s. due to the phase belt harmonics were, in contrast, a minimum on the m.m.f. direct axis and a maximum on the quadrature axis. The phenomenon is reconsidered in Chapter 7.

2.4 Previous Publications

2.4.1 Historical

Contributions to the understanding of the eddy current phenomenon date back to Oliver Heaviside[19] (1884) and J.J. Thompson[20] (1892). Heaviside considered the development of heat by eddy currents flowing in the core of a solenoid when excited with alternating current, Thompson the power loss in transformer cores.

It is well known that many other investigators have surveyed this field. Their works are collected in standard books some of which are listed in the bibliography.[21, 22].

The need to calculate the stray load losses in electrical machines was soon recognised, as references to early 20th century papers by more recent authors [1,2,3,18] will testify. Rudenberg [23], perhaps the most significant of these early writers, published in his paper on eddy current brakes and dynamos the basic principles for the analytical calculation of stray losses, including the armature current generated component of pole face loss (Germany 1906). In his later paper [24](1924), he divided the armature m.m.f. harmonics into the belt and slot terms described in section 2.3.

At the present time the methods of Kuyper[1](U.S.A., 1943), Barello[2] (France, 1955), Bratoljic[18](Switzerland 1966) and Postnikov[14](Russia 1958) are used to predict these losses. In their analytical solutions of the diffusion equation Rudenberg, Kuyper and Barello each make assumptions broadly similar to those made in this thesis (Section 3.3), but in their analyses the permeability is assumed constant throughout. Bratoljic has extended Barello's work to cover the problems of end effect and grooving.

The elimination of the constant-μ assumption is achieved by making an algebraic or empirical substitution for μ at the outset of the analysis. This introduces non-linear coefficients into the partial differential equations which cannot then be solved by normal analytical methods.

In recent papers (such as refs. 26, 27 and 28 : U.S.A. 1965, 1967 and 1966) on eddy currents in solid iron, the non-linear partial differential equations are replaced by finite difference equations and solved by numerical methods. This technique is now an extremely powerful one because of the current rapid increase in the size and speed of digital computers, indispensible with numerical solutions.

Davies'[3,4] method of tackling the problem of variable permeability (U.S.A. 1963, U.K., 1966) is to solve the partial differential equations for a linear system and then to make a logarthmic substitution for μ once the initial stages of integration are completed. This technique renders the treatment inexact but is probably superior to one which either ignores saturation altogether, or assumes a rectangular magnetisation curve having 100% saturation in both directions of magnetisation (Angst [29] U.S.A. 1962). The author's views on the problem of variable permeability are given in section 8.1.7. Davies' substitution can only be justified pragmatically by the results it gives in practice.

The papers directly concerning the calculation of the armature current generated component of pole face loss are introduced below, summarised in section 3.11, and used in section 6.4.

2.4.2. Pole Face Loss Theory

Both Kuyper[1] and Barello[2] analyse the electromagnetic field in the gap and the pole member of the idealised model produced by a single harmonic m.m.f., F_h, (Fig. 2.7). F_h is represented in the analysis by a current sheet, i_h, on the stator surface, the density of which

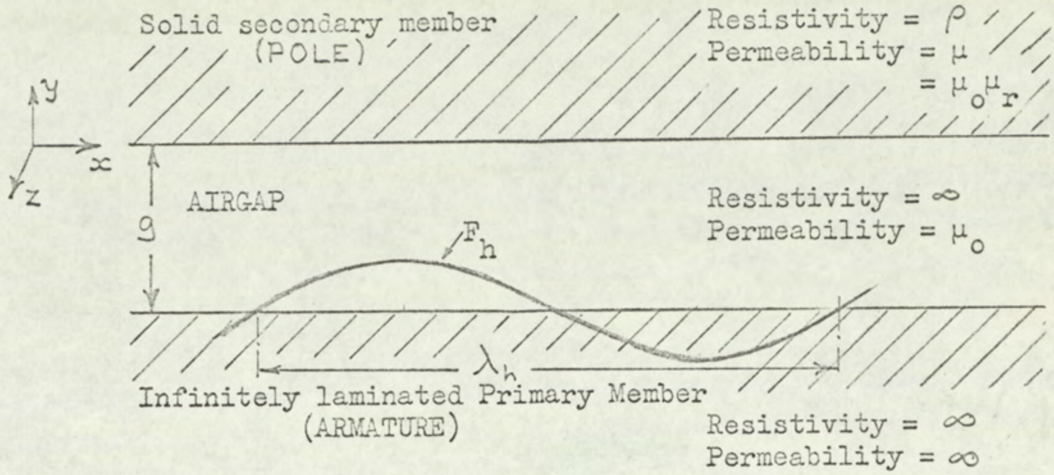

Fig. 2.7 The idealised model

$y_1 = y + g.$

F_h is the m.m.f. wave of harmonic order h.

varies sinusoidally in time and space.

The curvature of the rotor is disregarded, the solution being made in terms of rectangular rather than cylindrical coordinates. This is permissable where the ratios of gap/diameter and penetration depth/diameter are small. For large turbo generators where the air gap is 3-5% of the rotor diameter the use of Cartesian coordinates may lead to some error. Kuyper, Barello and the author consider this error small compared to that due to other assumptions. Anempdistov[17] (who only refers to the work of Postnikov, mentioned later) shows that the curvature severely modifies Postnikov's coefficient and therefore prefers to use cylindrical coordinates; resistivity and permeability are considered constant throughout.

End effects are neglected; the axial current paths in the secondary are considered long compared to the circumferential paths between harmonic poles. Limiting the direction of current density in this manner to J_z affords considerable mathematic simplification, reducing the investigation to a two dimensional problem in the plane xy.

The pole member is assumed to be homogenous, to extend from $y = o$ to $y = \infty$, and to have a smooth surface. Wedges made of metal different to that of the secondary member, and other discontinuities are neglected; so are the discontinuities in the primary surface due to the slot openings and cooling ducts. Damper windings, not normally provided on solid pole machines, are also neglected.

The choice of a suitable value for permeability is difficult, Chalmers[6] suggests a value of μ_r equal to several hundred, on the basis of surface saturation. The value seems to depend on experience in using the ultimate loss equations. Kuyper describes his choice as "relatively large" but less than 400. Some anomalies arise in his calculations which are discussed in section 6. His suggested value for surface flux density of 3.0 to 4.5 Wb/m^2 (200 to 300 Kilolines per square inch, about twice the saturation density for common steels) is unrealistic. The question of permeability and flux penetration is considered in sections 8.1.1 to 8.1.7.

Barello based his choice of μ_r on test results "carried out on similar machines and operating under similar load conditions" (his para.10). The permeability, resistivity and depth of penetration are so inter-related that Barello decided to specify the product $\mu_r \rho$ rather than μ_r itself. The surface heating causes the resistivity to decrease with depth causing some changes in the values of J, B, and μ_r at the surface. Barello found that an overall figure for the product $\mu_r \rho = 3 \times 10^{-4}$ ohm-metres gave satisfactory results with his loss formula for most of the machines he investigated. Taking the rotor resistivity = 25×10^{-8} ohm-metres Barello's value of μ_r becomes 1200. This differs considerably from Kuyper's value but not appreciably from the author's recommendation in Section 8.1.7. Since the loss is proportional to $\sqrt{\mu_r}$ any error in estimating the value of μ_r will produce a smaller (per unit) error in the predicted loss.

The methods ofboth Kuyper and Barello include the effects of circumferential flux leakage in the air gap. These effects are quite large in alternators especially for the higher order armature reaction m.m.f. harmonics because the air gap is quite large compared to the harmonic pole pitch. For the slot harmonic terms in particular it is essential to replace the idealised model of Kuyper and Barello with one resembling more closely the practical machine (chapter 10).

These two authors place no limitation on the gap length although Kuyper has found that the R_1 factor departs fromFig. 3.8 at very low harmonics (the upper part of the curve) and at very high harmonics (below the range of the plot). He therefore chooses to limit the ratio to the range 0.06 to 0.35. For the larger g/λ_h ratios (i.e. for the slot harmonic terms) the circumferential flux leakage is so high that harmonic losses may become small enough to be neglected. Furthermore the influence of the armature slot openings becomes considerable. These considerations throw doubt on the validity of Chalmer's extension of Kuyper's graph to $g/\lambda_h = 0.9$.

The method of solution is outlined in section 3.11.

The calculations are done in chapter 6 - Kuyper claims that the predominant losses are due to phase-belt harmonics (K = 1,2) and concentrates on these to the exclusion of the higher orders. Barello shows correctly that the slot harmonic terms (K = q(slots/pole/phase)) will often be important because their winding factors are the same as the fundamental winding factors. The harmonic m.m.f. F'_h however is modified further by the armature slot openings. The expressions for F_h' assume an abrupt change in gap m.m.f. at the centre of the slot i.e. the conductors are considered filamentary. The finite width of the conductor (and slot) results in a gradual change in m.m.f. across the slot opening. Kuyper introduces a factor to account for this gradual change in F_h' (k_{bh} in appendix 12.1.2, of this thesis), but omits it from his loss equation. Although this omission by both Kuyper and Barello introduces only a slight error for the belt harmonic terms, for the slot harmonic terms the harmonic m.m.f. is drastically reduced.

This reduction in F_h' must not be confused with the reduction in normal d.c. flux density or "ripple" caused by the change in gap permeance at the slot openings. The slot ripple is treated separately in sections 2.4.5 and Appendix 12.6

2.4.3. Eddy Current Coupling Theory

In 1946 Gibbs [5] published a paper entitled "The Theory and Design of Eddy Current Slip Couplings" which analyses the behaviour of eddy-current couplings on load, dealing mainly with the inductor coupling although (Davies[3] claims) his approach is equally valid for all couplings since he ignores the saturating effects of the direct flux. He assumes constant coefficients and sinusoidal space and time variations of magnetic quantities in the solid iron. He eventually obtains expressions for :

(i) the total loss, w in terms of $H^2\sqrt{\rho\mu\omega}$

and (ii) the flux per pole interms of w, H, and ω (p.175 Reference 5).

The performance characteristics are determined by first assuming the main mechanical parameters for a given load condition, and then calculating the quantity $H^2\sqrt{\mu}$ (and hence $\mu^{\frac{1}{4}}H$) from the formulae derived in his paper. The maximum surface value of magnetic intensity H is then determined from the empirical relationship between $\mu^{\frac{1}{4}}H$ and H, plotted for the particular drum material used. The flux per pole and the total excitation are then calculable.

Davies[3] observed that for many ferromagnetic materials the graph of $\mu^{\frac{1}{4}}H$ against H when plotted on log-log paper is linear above the knee for a considerable range of H. This led to the relationship $\mu^{\frac{1}{4}}H = 0.99H^{0.77}$ in the saturated region of the iron used. This was presumed to apply to the surface layer. He therefore used this algebraic substitution for μ at the point where Gibbs resorted to empiricism, thereby producing relationships between the electromagnetic quantities in the drum which are completely analytical, and yielding the normalised equations of section 3.6. Davies' method of solution follows Gibbs' closely in some of the early stages but he extends the theory to include the space distribution of electromagnetic quantities in the drum (with the support of experimental results on a model coupling) and some comments on conditions pertaining at low frequency. Davies' solution is now summarised.

An m.m.f. wave produced by a primary member and sinusoidally distributed in space at the smooth air gap surface is considered to move relative to a ferromagnetic secondary member (the drum) which has constant permeability and resistivity. An expression for the consequent current density wave, J_z, in terms of an assumed peak surface current density J_m, is obtained by solving the diffusion equation for J_z. Maxwell's equations are then used to find the inducing flux density wave, the total loss and the magnetic field components everywhere in the drum; all these in terms of the assumed J_z wave. The elimination of J_z together with the substitution for μ then gives expressions for the fundamental flux per pole and armature reaction m.m.f. per pole in terms of torque, slip speed, the physical parameters of the coupling (poles, diameter, length, and drum resistivity) and the coefficient and index of H. The combination of gap m.m.f. (F_ϕ) and the armature reaction m.m.f. (F_R) lead to useful expressions for the peak torque and the slip at which it occurs. These are combined with the torque at a given slip to give a normalised torque/speed curve describing the behaviour of any eddy current coupling using the same steel, Fig.3.4 The use of the normalised torque/speed curve is explained in the next chapter. The working equations are derived in Section 3.6. They use the normalised curve to account for F_R.

The methods used by Gibbs and Davies to sum F_{ϕ} and F_R differ fundamentally. Gibbs' addition is purely arithmetic, ignoring any space angle between F_{ϕ} and F_R. To $(F_{\phi} + F_R)$ Gibbs adds the much smaller ampere-turns needed to sustain the total (d.c.) flux in the primary member. For an inductor coupling, the ampere turns in the unslotted portion of the secondary are also added. Davies' addition is vectorial, F_{ϕ} and F_R being added at an angle of 135^o $(=\frac{\pi}{2}-\phi)$ to give the total excitation. Experimental evidence by Davies [3] and James [38] confirms that vectorial addition is essential and that the primary ampere turns are small enough to be neglected. Neither Davies nor Gibbs include the ampere turns for the harmonic fields, considering them of second order importance.

In reference 3 these ideas were developed in detail and verified experimentally by tests performed on a specially built Lundell coupling (suitable up to 100 h.p.) A critique of Davies's substitution for permeability is given in section 8.1.3.

2.4.4 The loss distribution over the pole face

In a paper presenting methods of calculating the important elements of load loss in synchronous machines, Pollard [33] states correctly that both the fifth and seventh space harmonics in the armature reaction m.m.f. wave produce an m.m.f. at the pole surface which fluctuates at 6 times mains frequency. Unlike Rüdenberg[24] and Richardson[8], Pollard does not distinguish between the pole centre of the physical pole and the m.m.f. direct axis i.e. the position of peak fundamental armature m.m.f. F_h. In fact he refers to the latter as the pole centre implying alignment of the two centre lines. This is only correct when the pole or torque angle is 90°, i.e. for zero p.f. loads and for the short circuit test, assuming the synchronous reactance >> armature resistance. When the load angle has a different value to this, the loss distribution will change because the m.m.f. centre and the physical pole centre are misaligned.

Pollard then points out (again correctly) that the 5th and 7th harmonic m.m.fs. F_5 and F_7 are 'in time phase' at the m.m.f. direct axis and in antiphase at the m.m.f. quadrature axis'. The resultant m.m.f. at any point is therefore the vector sum of F_5 and F_7. This resultant is derived for the general case of the 6K - 1 and 6K + 1 pair of terms, in terms of the fundamental m.m.f. and the harmonic winding factors in section 7 and Appendix 12.5. The change in phase angle between F_5 and F_7 along the pole surface is a result of the different wavelengths and speeds of the two m.m.f. waves. Consequently the surface loss will be a maximum where $(\bar{F}_5 + \bar{F}_7)$ has its greatest value, i.e. at the m.m.f. direct axis and a minimum, but not necessarily zero, at the m.m.f. quadrature axis (assuming that the winding factors are both positive, Section 7.2.)

Under short circuit test conditions, when the torque angle tends to zero the m.m.f. fluctuation would decrease from pole centre to pole tip and the reduction in s/c loss arising from the shaping of the pole tips would be minimal. The comments by Spooner and Kinnard, which were quoted by Gibbs[5]; "that shaping the pole tips does not affect the surface loss" apply to the slot ripple loss and not, in general, to the m.m.f. loss.

The summation of the 5th and 7th harmonic m.m.f.s. at the pole face is also mentioned by Richardson[8] in his paper on stray losses. He points to the complexity of the problem but does not suggest any alternative method of loss calculation. On the other hand Barello[2] proved, on the assumption of constant permeability, that the loss over 180°E of the pole face calculated from the resultant m.m.f. $(\bar{F}_5 + \bar{F}_7)$ equals the sum of the losses by the two individual m.m.f.s.

The theory and results of this investigation are presented in Chapter 7.

2.4.5. Other Relevant Publications

(i) Slot Ripple Loss

It is well known that the pole face losses resulting from the armature current generated m.m.f.s. are not the only losses in the pole faces of synchronous machines. Under all load conditions the non-uniform air gap permeance resulting from the armature slots superimposes a ripple on the gap flux density. The resulting tooth ripple, or slot ripple losses in the pole face are significant in the no load test. They are considered insignificant in the short circuit test because the gap flux density is quite small. They are significant however in the tests on the experimental load loss dynamometer when they are estimated from published data. The small gap of 0.012", designed to yield a high m.m.f. loss, results in an unusually large slot/gap ratio and consequently a high slot ripple loss.

The publications on this subject, from that of Carter in 1901 to Aston and Rao[15] in 1953, have been collated by Mukherji[30] in an E.R.A. report published in 1955. Since then Laurenson[7] has published a comprehensive set of computed results of surface flux density for a wide range of design parameters. He shows both experimentally and theoretically that the reaction of eddy currents on the inducing field, previously considered to be negligible (Gibbs[9]), can be very large. His results, quote : "are not presented as a basis of a quantitative test of theory ... nevertheless the measured results can be correlated with the theoretical ones by means of a simple artifice". Because the magnitude of this "artifice" for the experimental machine was unknown the slot ripple loss therein was calculated using Gibbs's[9] method. Further comments on Laurenson's paper are incbded in Sections 8.1 and 10.15.

Aston and Rao[15] used an experimental homopolar machine to verify Gibbs'[9] method of predicting the slot ripple loss due to eddy currents. The slot pitch λs, slot width s, and air gap g, were varied by having different sleeves shrunk on to the rotor, the loss in each being measured by the retardation test, since exploited at Kings College, London. The correlation between Gibbs's predictions and Aston's test results is between - 4% and + 14% for most sleeves. This fact together with the satisfactory prediction of the open circuit losses on practical machines both inspire confidence in Gibbs's method and explain its widespread use. It is therefore used in this thesis to calculate the slot ripple loss in the experimental machine. The extremely low slot/wavelength ratio of the experimental machine lies outside the range of Gibbs' β_1 and β_2 curves. It has therefore been necessary to calculate the values of β_1 and β_2 applicable to the experimental machine. This calculation necessitates calculating the field distribution at the pole surface using the Schwartz-Christoffel Transformation and then determining the harmonic components by Fourrier Analysis. The requisite loss curves are derived in Appendix 12.6 where the loss is calculated for a range of frequency, flux density and temperature.

(ii) <u>Hysteresis</u>

The prediction of losses in a ferromagnetic material is incomplete without an estimation of the hysteresis loss. In laminated materials, it has been found that the hysteresis loss and the eddy current loss are of equal importance. In solid materials the eddy current loss predominates. Pohl[16] (1944) argues theoretically that the hysteresis and eddy losses cannot be added arithmetically. The presence of hysteresis reduces the eddy current loss such that :

$$\text{The combined loss} = W\ \text{eddy}\ (1 + W\ \text{hysteresis}/\ W\ \text{eddy})^{\frac{1}{2}}.$$

His theoretical deduction that the hysteresis loss may be 16% of the combined loss is refuted by Gibbs [9](1947) who states unequivocally that in all practical applications the hysteresis loss is negligible - Gibbs's computation that the hysteresis loss is of the order of 1% of the total (iron) loss would seem a little optimistic in view of the experimental results by Aston and Rao[15] where the hysteresis loss for most sleeves was found to be higher than Gibbs's but much less than Pohl's. Pohl obtained good agreement between the predicted combined loss and measurements on an iron toroid, a device not as closely related to the real machine as that used by Aston and Rao. The author therefore considers the latter more applicable to the pole face loss problem. It could be argued that the test value of hysteresis loss (= 2 - 4% of the total iron loss) is not negligible, but it must be remembered that the error (in watts) in neglecting hysteresis loss is much less than that incurred in predicting the slot ripple loss itself (- 4 to + 14%). For the purpose of this thesis it would seem reasonable to consider secondary hysteresis loss due to surface flux density changes of second order importance.

The question of rotational hysteresis in the pole face loss problem is complicated by the presence of the d.c. polarising field.

The investigations by Boon and Thompson[31,32] on single crystal specimens in sheet form revealed that the rotational power loss exceeded the alternating power loss by up to 100%. Their paper shows reasonable agreement between their experimental work and their theory which was based on simple domain considerations. The presence of rotational hysteresis would explain why the hysteresis loss measured by Aston and Rao [15] exceed the alternating hysteresis loss calculated by Gibbs[9]. Gibbs used the formula presented by Ball[34] in 1915 based on a comprehensive series of experiments on laminated ring specimens. Ball's test results also show that d.c. polarisation increases the loss attributable to hysteresis.

(iii) Solid Secondary Induction Devices

The pole face loss due to the armature reaction m.m.f. harmonics is analogous to the loss in the secondary member of electromagnetic clutches, eddy current brakes, solid rotor induction motors, linear induction motors and self starting synchronous motors. It follows that a proven theory for any of these devices could be applied to the pole face loss problem (providing direct field effects are not ignored). Some of these induction theories use the rectangular magnetisation curve[29] (Fig. 8.11), some the empirical curve[27] and some an analytical approximation[3] to it. The relative merits of each method of dealing with the variable μ are discussed in section 8.1.7. This thesis uses the last method which is introduced in the next section, 2.5.

(iv) Secondary Remanence Torque

The secondary remanence torque of the experimental load loss dynamometer was particularly troublesome making the measurement of pole face loss by torque measurement impossible (section 5.7). The work by Rawcliffe and Menon[12] on induction motor losses was particularly helpful in overcoming this major difficulty. The technique is detailed in section 5.13 and the experimental measurements of remanence power (= Torque x angular velocity) in section 5.10.5.

2.5. The Approach Used in this Thesis

It is convenient to confine this section to the problem of loss measurement and prediction and defer the introductory remarks concerning the distribution of harmonic m.m.f.s. to section 7.1.

There is a close analogy between the induction of eddy currents in the loss drum of an eddy current coupling and in the solid pole face of a synchronous machine (Fig. 3.2), as the papers by Gibbs on eddy-current couplings[5] (U.K. (1946) and tooth-ripple losses[9] U.K.(1947) serve to illustrate. It seems likely therefore that an existing coupling theory could be applied to the present problem.

The eddy current coupling design equations relate torque, speed and excitation. The power loss due to currents flowing in the drum of the coupling can therefore be expressed in terms of the torque T, and the relative speed n. In the pole face loss problem the magnitude and relative speed of the harmonic m.m.f. wave is known leaving the harmonic torque to be found. It is proposed to calculate this torque by modifying the eddy current coupling equations presented by Davies[3]. The modifications will allow for a different gap permeance and magnetisation characteristic. Davies'[3] method is preferred to that of Gibbs[5] because it includes a substitution for permeability and a more realistic calculation of eddy-current reaction effects (section 2.4.3).

The theory avoids the actual calculation of the armature reaction of drum currents (but accounts for their presence) by using the normalised curve and the existing expressions for the peak torque and the speed at which the peak torque would occur.

The total loss for a cylindrical rotor machine is the arithmetic summation of the losses for all harmonics -a clear case for the application of a digital computer. The calculation assumes superposition and, for salient poles, the resultant loss must be reduced to allow for the pole profile (ref. Section 12.2.1).

The theory is applicable to machines with other winding configurations with "short" airgaps, i.e. where the airgap is much less than the wavelength of the highest significant harmonic. In applying this theory to harmonic terms for which s/λ_h is not 'small' a reduction factor must be introduced to account for the attenuation of the field across the gap. (Appendix 12.2.2). In section 3.6 and in reference 4 the theory of reference 3 is extended to consider the substitution for permeability in more detail. The coefficient and index of H in sec. 2.4.3 are manipulated as true parameters represented by algebraic symbols and not numerical constants. Numerical substitution in the final equations depends on the magnetisation characteristic of the particular steel used. This generalised theory has already been published by Davies [4]. It is included in section 3.6 of this thesis because it was carried out independently by the author before the publication of reference 4 providing, incidentally, a useful check on secton 2 of that paper. The comparison between the predicted loss using these equations and the loss measurements on the experimental machine (section 5.11) is most promising. The major source of error is the calculation of the slot ripple loss (section 2.4.5. above).

By deriving the equations in general terms they present a clear picture of the relevantmachine parameters and their various indices, and are put fotward as a reliable method of predictingthe effect of parameter changes (sections 3.8.3 and 3.8.4). The changes in the stray load loss figure, measured by the short circuit test on practical machines, when one parameter is changed are recorded in section 6.3 and compared with the change in predicted loss.

2.6 The Experimental Load Loss Dynamometer

The experimental load loss dynamometer machine was designed to accentuate the pole face loss due to the rotating m.m.fs. of armature reaction. Its primary function was to verify the theory derived for a machine with a uniform gap, leaving the effects of surface discontinuities for a second investigation.

It was decided to assess the loss in the pole face from the product (ωT) of the measured torque on the pole face and the shaft speed. To measure the torque and surface e.m.f.s easily an inverted construction was adopted, Fig. 4.1. The armature was driven at synchronous speed and a torque arm attached to the solid secondary member.

The fundamental component of the armature m.m.f. wave was held stationary in space thereby producing, in effect, a d.c. field. The secondary hysteresis (or remanence) torque (section 5.10) associated with this d.c. field so affected the measured torque (section 5.7) that a method of loss separation had to be used. The primary iron loss was determined experimentally over a range of armature current, frequency, and secondary surface temperature (sections 5.10 and 5.11). The slot ripple loss (due to dips in the flux density pattern at the secondary surface opposite the slot openings) was calculated using Gibbs'[9] method, for reasons given in Section 2.4.5. Unfortunately the requisite curves of β_1 and β_2 published by Gibbs do not accommodate the high slot opening to gap ratio of the experimental machine ($s/g = 13.3$). Consequently the calculation of the slot ripple loss in section 12.6 forms a disproportionately large portion of this thesis because β_1 and β_2 had to be calculated using the Schwartz-Christoffel transformation - Appendix 12.6. Suggestions for overcoming the slot ripple loss are put forward in chapter 10. The variation in induced e.m.f. between the m.m.f. direct and quadrature axes of the d.c. field, discussed in section 2.4.4, was investigated using search coils set into the secondary surface of the experimental machine.

3. THEORY

3. THEORY

3.1 Introduction

In this chapter the equations for calculating the eddy current loss caused by the armature reaction m.m.f's. are derived. The calculation of the slot ripple loss in the experimental machine, which is needed in chapter 5, has been deferred to Appendix 12.6. The magnitude of the m.m.f. harmonic loss is assumed to be independent of the distribution of the induced harmonic e.m.f's. across the pole face. It is therefore more convenient to consider the implications of the e.m.f. distribution in a separate chapter and concentrate on the modifications to the eddy current coupling theory.

This theory[3] includes an analytical substitution for permeability and a method of combining vectorially the inducing and reaction m.m.f's. It uses expressions for the maximum torque, T_m, and the speed n_m at which T_m would occur. The loss in an ingot iron pole face is calculated by extending the theory of reference 3 and compiling a digital computer programme. The theory is derived in generalised form in section 3.6 and the effect of changes in the predominant parameters considered in sections 3.8 and 3.9. Section 3.7 describes the method of calculation and the development of the computer programmes designed to accommodate materials with different magnetisation characteristics. A means of accounting for the pole profile is suggested. This is applied to a 60MVA machine in chapter 6. Finally, the theoretical work of other authors is summarised.

3.2 The Properties of the M.M.F. Wave

The armature-reaction m.m.f. wave in an ideal machine would be sinusoidally distributed in space, and of fundamental wave-length (λ_1), producing no losses in the rotor. Because the normal machine is wound with concentrated phase-bands and relatively few slots/pole/phase, harmonics are found in the m.m.f. pattern. When fundamental frequency (f_1) balanced currents flow in the practical 3-phase integral slot winding with 60° phase-bands carrying sinusoidal currents, it is well-known[6] that:

i) the harmonics are of ($6K \mp 1$) order ($K = 1, 2, 3,$ etc.)

ii) their wavelength is $\lambda_1/(6K \mp 1)$

iii) the ($6K - 1$) harmonics move backwards relative to the stator at a speed $n_h = n_s/(6K - 1)$

iv) the ($6K + 1$) harmonics move forwards relative to the stator at a speed of $n_h = n_s/(6K + 1)$

v) their peak magnitudes are usually taken as

$$F'_h = \frac{(k_p k_d)(6K \pm 1)}{(k_p k_d)_h} \cdot \frac{F_1}{6K \mp 1}$$

where the peak fundamental armature reaction m.m.f.,

$$F_1 = \frac{6\sqrt{2}}{\pi} (NI)q\ (k_p k_d)_1$$

and (NI) is the r.m.s. ampere-turns of a single coil.

vi) their speeds, relative to the rotor, are

$$\frac{6K}{6K \mp 1}\ n_s \text{ r.p.s.}$$

vii) the frequency induced in the rotor by the $(6K \mp 1)$ harmonics is $6Kf_1$ for both harmonics.

That is to say, the forward and backward rotating harmonic waves associated with a given value of K induce currents of the same frequency in the pole face, which incidentally yields a degree of simplification to the analysis. Barello indicates in para. II A.3 of ref. (2) that the winding factor has considerable influence on the pole face loss.

The harmonic m.m.f. is modified further by the effect of slot width and will therefore be expressed in this thesis as $F_h = F'_h \times k_{bh}$. The derivation of k_{bh} and its variation with harmonic order and with some machine parameters is discussed in detail in Appendix 12.1.2.

The rotating m.m.f. wave is expressed as:

$$F = \frac{2\sqrt{2}}{\pi} NIqr \left[K_{w1}\cos(\theta_1 - \omega t) + \frac{1}{5} K_{w5}\cos(5\theta_1 + \omega t) \right.$$

$$\left. + \frac{1}{7} K_{w7}\cos(7\theta_1 - \omega t) + \ldots + \frac{1}{h} K_{wh}\cos(h\theta_1 \mp \omega t)\right] \ldots \quad (3.1$$

where $h = 6K \mp 1$

$\theta_1 = 2\pi x/\lambda_1$ the peripheral angular displacement (^{o}E).

$k_{wh} = k_{ph} \times k_{dh} \times k_{bh}$

$\sqrt{2}$ NI = the peak ampere-turns of a single coil

q = the number of slots/pole/phase

r = the number of phases

3.3 Assumptions

The mathematical analysis is simplified by the assumptions described in section 2.4.2 and 2.5. These are summarised below:

(1) The pole member is composed of a semi-infinite, homogeneous block of magnetic material, having a smooth surface.

(2) Rotor curvature is ignored, the solution being derived in terms of rectangular rather than cylindrical coordinates.

(3) The values of electromagnetic field quantities in the pole face vary sinusoidally in time and space, and satisfy the diffusion equation.

(4) The field is constant in the axial ("z") direction, and the current density, J, is everywhere axial.

(5) The permeability of the pole face material is considered constant in the initial stages of the theory only, after which a substitution for μ is made.

(6) The resistivity of the pole shoe is constant throughout its depth. There is no damper winding.

(7) The airgap is constant (i.e. has a smooth boundary) and in the initial stages of the calculation is small compared to the wave length of the harmonic term under consideration. A correction factor is then applied to account for gap flux-leakage.

(8) The loss due to each harmonic term can be calculated independently of that due to other terms, all the harmonic losses being added arithmetically to yield the total loss figure. This premiss is discussed in section 7.

(9) The effect on the gap flux of any harmonic currents induced in the stator laminations is negligible, i.e.

$$\mu_{stator} = \infty = \rho_{stator}$$

(10) The d.c. field is ignored but is discussed in sections 8.1 and 12.6.

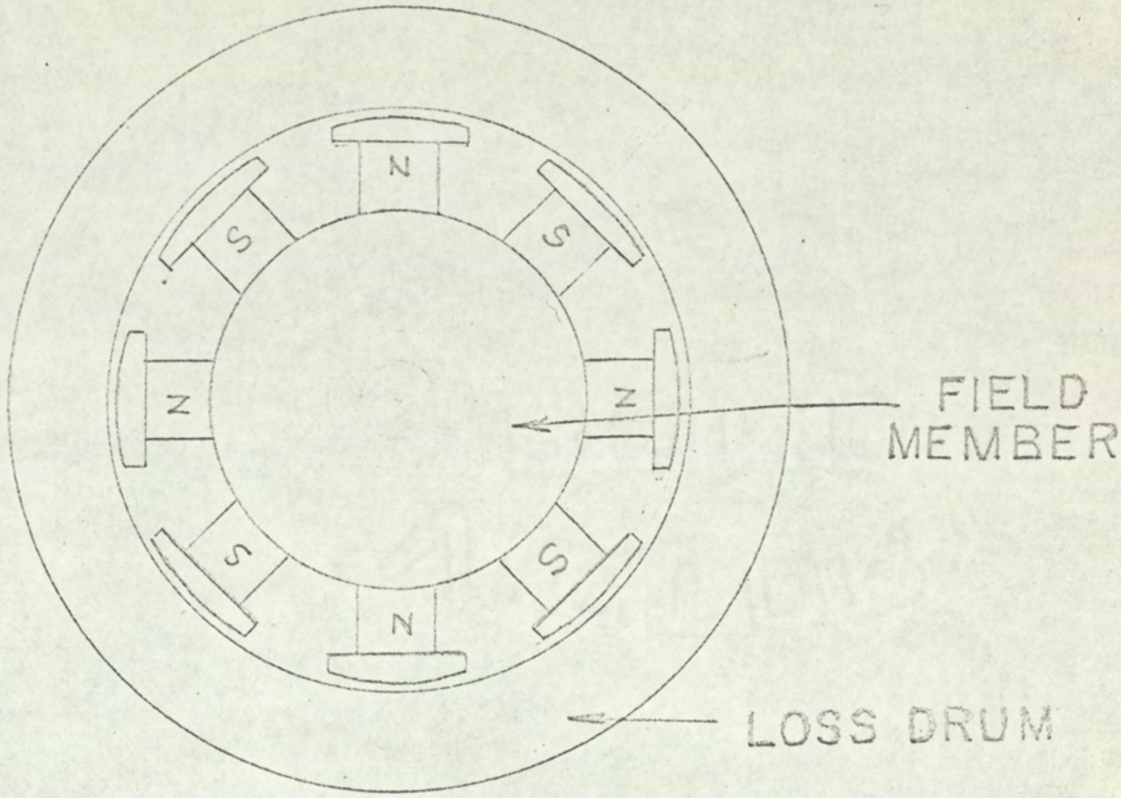

FIG. 3.1. Schematic diagram of an eddy current coupling.

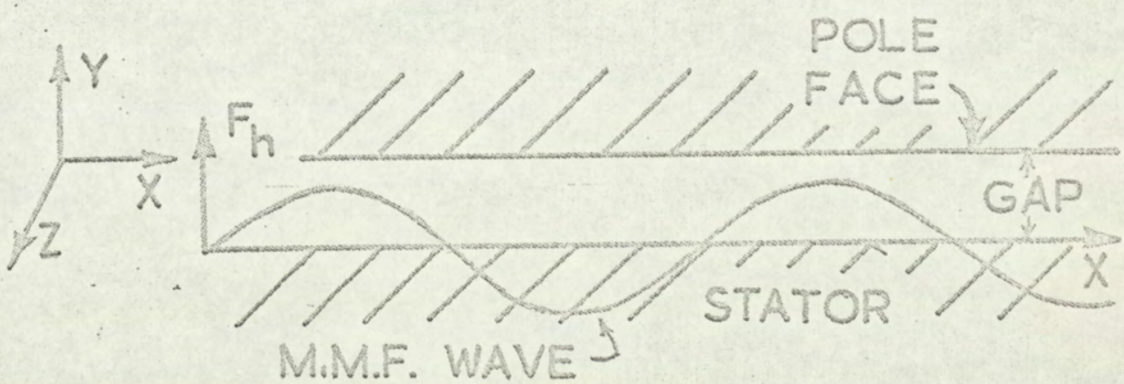

FIG. 3.2. The Travelling M.M.F. Wave.

3.4 Modifications to the Eddy Current Coupling Theory

One shaft of the eddy current coupling of Fig. 3.1 carries the field member which rotates inside an unwound iron loss drum connected to the second shaft. The field member is excited with direct current and the flux pattern moves past the loss drum at the airgap surface causing losses. The magnitude of these losses depends on the relative speed n (also termed the slip speed), the excitation, and the physical constants of the machine. The eddy current coupling theory[3] is used to calculate the loss caused by each harmonic of the armature m.m.f. wave in turn — Fig. 3.2.

Since the harmonic pole pitch is $1/(6K \mp 1)$ times the fundamental pole pitch, many harmonic poles exist in one (fundamental) pole pitch of the machine. The harmonic poles face a parallel gap, and the equations for peak torque and speed at peak torque must therefore be modified to accommodate a constant gap permeance instead of the square wave permeance of the salient pole coupling. The axial current paths in the pole face are much larger than the circumferential paths between harmonic poles so that the end effect factor derived by Gibbs[5] tends to unity.

The use of a different ferromagnetic material affects the numerical substitution of the permeability $\mu(=\mu_o \mu_r)$. The substitution, which assumes operation above the knee

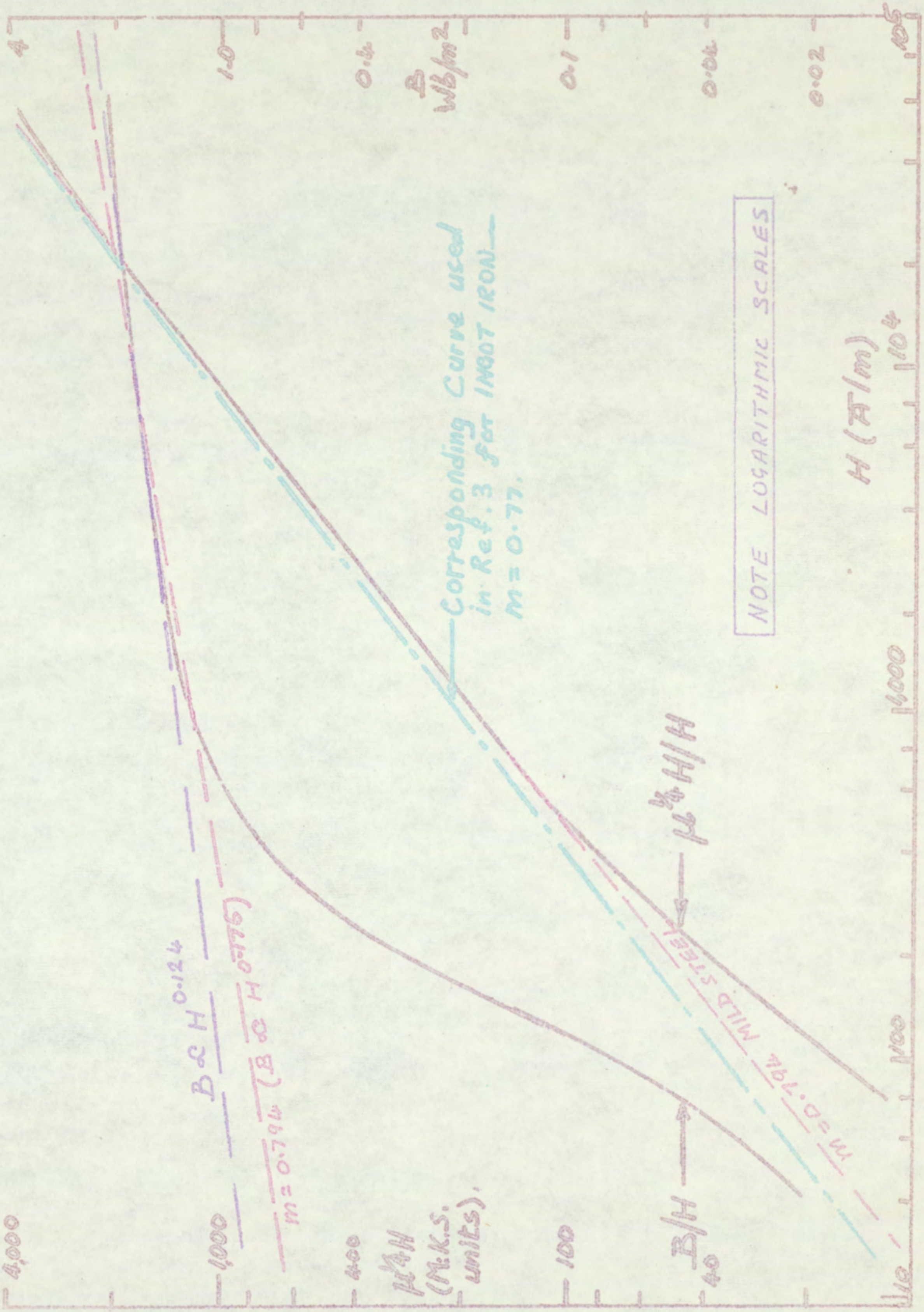

FIG.33. MAGNETISATION CURVES FOR THE SECONDARY STEEL OF THE EXPERIMENTAL MACHINE.

of the magnetisation curve, is derived by plotting $\mu^{\frac{1}{4}}H$ against H on log-log paper and measuring the slope of the linear portion above the knee. For the mild steel used for the secondary member of the experimental machine, the slope is 0.794 (Fig. 3.3) and the substitution for μ is:

$$\mu^{\frac{1}{4}}H = 0.769H^{0.794} \quad .. \quad .. \quad .. \quad (3.2)$$

Both the coefficient and the index of H vary with the material used and must therefore be determined in each case. e.g. for the ingot iron of ref. 3, the substitution is:

$$\mu^{\frac{1}{4}}H = 0.99H^{0.77} \quad .. \quad .. \quad .. \quad (3.2A)$$

The theory is developed in a similar manner to reference 3 for a sinusoidal impressed m.m.f. wave, F_h. However, since the number of poles for the hth harmonic term are h times that for the fundamental, 'p' in the eddy current coupling theory is replaced by p_h(=hp) in the pole face loss theory. To simplify the initial equations, the subscript will be omitted.

A suitable expression for the gap reluctance will be developed shortly but first the salient points of the eddy current coupling theory, already introduced in section 2.4.3 will be presented. Initially this theory follows a similar pattern to that of Kuyper and Barello (summarised in section 3.11). Then, after the analytical substitution for μ, expressions in terms of the machine parameters are obtained for the inducing m.m.f., and the eddy current reaction m.m.f.

which act at a space angle to each other. The vector combination of the inducing m.m.f. and the eddy current reaction m.m.f., acting on the airgap surface, produces the resultant flux-density wave that causes the loss.

A solution of the diffusion equation for the axial current denstiy J_z in the eddy current coupling drum (Fig. 3.2), presented in references 1, 2 and 3, indicate that J_z decreases exponentially with drum depth, y, and varies sinusoidally with time, t, and distance, x, around the circumference:

$$J_z = J_m e^{-\beta y} \cos(\omega t - 2\pi x/\lambda - \gamma y) \quad .. \quad .. \quad .. \quad (3.3)$$

The substitution of J_z in the equations:

$$\nabla \times (\rho J_z) = -\frac{\partial \overline{B}}{\partial t}$$

and

$$w = \frac{\omega}{2\pi} \int_{t=0}^{\frac{2\pi}{\omega}} \int_{y=0}^{\infty} \rho J_z^2 \ dt \ dy \quad \text{watts/sq. metre}$$

yields the surface magnetic intensity and loss both in terms of J_m :

$$H_x = \frac{R J_m e^{-\beta y}}{2\alpha^2} \sin(\omega t - 2\pi x/\lambda - \gamma y + \phi) \quad \overline{A}/m$$

and $w = \rho J_m^2 / 4\beta$

where $R^2 e^{2j\phi} = k^2$

$$= 4\pi^2/\lambda^2 - 2j\alpha^2,$$

$$\left.\begin{aligned} \beta &= R\cos\phi, \\ \text{and} \quad \gamma &= R\sin\phi \\ \text{i.e } Re^{j\phi} &= \beta + j\gamma \end{aligned}\right\} \quad (3.4)$$

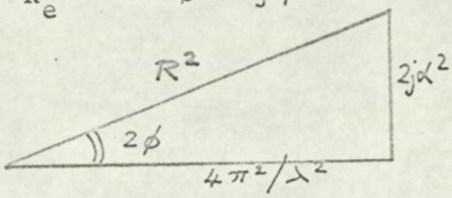

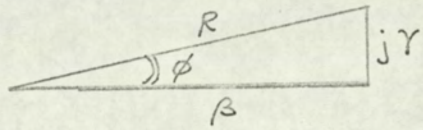

If the depth of penetration $(1/\alpha)$ is small (equation 3.32), then

$$\sqrt{2}\alpha \gg 2\pi/\lambda$$

$$, \quad R \longrightarrow 2\alpha, \ \gamma \longrightarrow \alpha, \ \beta \longrightarrow \alpha, \ \phi \longrightarrow \pi/4$$

H_x becomes much greater than H_y (quoted in section 12.5.1). Consequently, the resultant magnetic intensity $H \longrightarrow H_x$. The equations become much simpler and (Davies claims) very little accuracy is lost in eddy current coupling design since the assumption is true over most of the working range. The surface value H_m of the magnetic intensity H will therefore be :

$$H_m = \frac{J_m}{\sqrt{2}\alpha} \qquad (3.5)$$

and the loss per unit surface area:

$$w = \frac{\rho J_m^2}{4\alpha} \qquad \text{(Ref. 3 eq. 9A)} \qquad (3.7)$$

Elimination of J_m from these equations leaves α (and hence μ) in the final expression for loss:

$$\mu^{\frac{1}{4}}H = \left(\frac{8w^2}{\rho\omega}\right)^{\frac{1}{4}} \qquad \text{M.K.S Units} \qquad (3.8)$$

The flux per pole needed to produce the J_z wave corresponds to the usual definition of flux per pole used on a.c. generators:

$$\phi_{ac} = (\text{mean } B_y) \times (\text{pole area})$$

which is shown to be,

$$\phi_{ac} = \frac{2\rho L}{\omega} J_m \qquad (3.6)$$

The equations 3.5. to 3.8 can be combined to give an expression for ϕ_{ac} in terms of H_m:

$$\phi_{ac} = 4\sqrt{2}\ \frac{L\,w}{\omega H_m} \qquad (3.9)$$

Up to this point Davies' analysis has run parallel to Gibbs'. Since all the quantities on the R.H.S. of equation 3.8. are known, $\mu^{\frac{1}{4}}H$ can be calculated. Gibbs then uses a curve of $\mu^{\frac{1}{4}}H$ plotted against H to determine H_m which is substituted in equation 3.9. The a.c. flux required to produce a given loss can now be calculated.

The substitution by Davies of equation 3.2A into equation 3.8 eliminated the permeability and, eventually, led to expressions for torque and speed (section 2.5). Such expressions are therefore applicable only to a magnetic material satisfying equation 3.2A.

3.5 Working Equations for the Experimental Machine

The next step in the author's work therefore was to derive the expressions for the maximum torque (and for the corresponding speed) for the experimental machine using the magnetic constants applicable to its mild steel secondary.

It became obvious at any early stage that some indices in the final equations for T_m and n_m were independent of the material used. Following this observation, generalised expressions were derived and recorded in the next section. It is therefore unnecessary to record the derivation of the expressions for mild steel in particular and these will just be quoted against those for ingot iron:-

(i) Mild Steel

$$\mu^{\frac{1}{2}}H = 0.769H^{0.794}$$

$$\phi_{ac} = \frac{0.805L^{0.630}\,\rho^{0.315}\,T^{0.370}}{D^{0.370}\,p^{0.685}\,n^{0.315}}$$

$$T_m = \frac{\mu_o}{0.9(2 + C_3)} \times \frac{F^2DLp}{g}$$

$$n_m = \frac{0.5(2 + C_3)^{0.412}}{\mu_o^2} \times \frac{pg^2\,p^{2.18}}{D^{3.18}\,F^{0.82}}$$

(ii) Ingot Iron

$$\mu^{\frac{1}{2}}H = 0.99H^{0.77}$$

$$\phi_{ac} = \frac{1.05L^{0.65}\,\rho^{0.325}\,T^{0.35}}{D^{0.35}\,p^{0.675}\,n^{0.325}} \qquad (3.10)$$

$$T_m = \frac{\mu_o}{0.9(2 + C_3)} \times \frac{F^2DLp}{g} \qquad (3.11)$$

$$n_m = \frac{1.3(2 + C_3)^{0.56}}{\mu_o^2} \times \frac{\rho g^2\,p^{2.08}}{D^{3.08}\,F^{0.93}} \qquad (3.12)$$

Although the coefficient and indices in the two equations for ϕ_{ac} are very different, those for T_m are both identical and whole numbers. In the equations for n_m, the integral indices are also identical, the remainder depending on the magnetisation curve of the material.

3.6 The Generalised Theory

3.6.1 The Flux per Pole

The indices and coefficients in equations 3.10 to 3.12 depend on the index and coefficient of H in equations 3.2 and 3.2A which may be written in a generalised form:

$$\mu^{\frac{1}{4}}H = k_1 H^m \tag{3.13}$$

The theory was developed from this equation on the lines of Davies'[3] earlier paper but in terms of k_1 and m. Because the work has since been published in section 2 of reference 4, only the main steps will be given here. The nomenclature of reference 4 is used.

The subscript "h" is now introduced to indicate the number of harmonic pole pairs:

$$p_h = hp$$

The angular frequency of the hth harmonic is:

$$\omega_h = 2\pi n_h p_h$$

and the loss per unit surface area is:

$$w_h = \frac{2\pi n_h T_h}{\pi DL}$$

These expressions are substituted into equation 3.9 to give the harmonic flux per pole required to produce a torque T_h at the pole surface:

$$(\phi_{ac})_h = \frac{4\sqrt{2}}{\pi} \cdot \frac{T_h}{Dp_h H_{mh}}$$

The substitution for μ is made by combining equations 3.8 and 3.13 to give:

$$H_m = k_1^{-1/m} \left(\frac{8w_h^2}{\rho\omega}\right)^{1/4m}$$

H_m can now be eliminated from the expression for the flux per pole to give:

$$(\phi_{ac})_h = \frac{4\sqrt{2}\; k_1^{1/m}\; \pi^{1/4m}}{\pi 2^{1/m}} \times \frac{\rho^{1/4m}\; L^{1/2m}}{p_h^{1-1/4m}\; D^{1-1/2m}} \times \frac{T_h^{1-1/2m}}{n_h^{1-1/4m}},$$

or

$$(\phi_{ac})_h = k_2 M \left(T_h\right)^{\frac{2m-1}{2m}} \left(n_h\right)^{\frac{-1}{4m}} \qquad (3.14)$$

$$\text{where } k_2 = 1.8\pi^{1/4m}\left(\frac{k_1}{2}\right)^{1/m} \qquad (3.15)$$

$$\text{and } M = \frac{L^{1/m}\, p^{1/4m}}{D^{1-1/2m}\; p_h^{1-1/4m}} \qquad (3.16)$$

The flux $(\phi_{ac})_h$ is established by an impressed m.m.f., F_h, containing two components - an armature reaction component, F_{Rh} and a flux component $F_{\phi h}$. $F_{\phi h}$ is obtained by multiplying $(\phi_{ac})_h$ by a reluctance S_h defined below.

3.6.2 The Gap Reluctance S_h

The torque, T_h, has been expressed in terms of F_h, the peak m.m.f. of the hth harmonic. The flux $(\phi_{ac})_h$ associated with a component of F_h is equal to the harmonic pole area times the average flux density. It is therefore convenient to define the reluctance as the ratio

$$S_h = \frac{\text{the ampere turns across the gap for the hth harmonic, } F_h}{\text{the total harmonic flux per pole, } (\phi_{ac})_h}$$

S_h will now be derived for a cylindrical rotor machine with a uniform air gap. The average flux density in the air gap $= \dfrac{(\phi_{ac})_h}{DL/2p_h}$

$\therefore$ The peak value of gap m.m.f. $= F_{\phi h} = H_{peak} \times$ gap length

$$= \frac{\pi}{2} \times \frac{B_{ave}}{\mu_o} \times g$$

$$\frac{(\phi_{ac})_h \times p_h \times g}{\mu_o DL}$$

$$\therefore \text{ For a uniform gap, } S_h = \frac{F_{\phi h}}{(\phi_{ac})_h} = \frac{phg}{\mu_o DL} \qquad (3.17)$$

The "Flux Component" of the total excitation for the same machine is therefore

$$F_{\phi h} = (\phi_{ac})_h \times S_h$$

i.e.

$$\left.\begin{aligned} F_{\phi h} &= C_1 T_h^{\,1-1/2m}\, n_h^{-1/4m} && \text{Ampere turns} \\ \text{where} \quad C_1 &= k_2 M S_h && \text{M.K.S. units} \end{aligned}\right\} \qquad (3.18)$$

3.6.3 Armature Reaction

The combined effect of single frequency sinusoidal currents flowing throughout the depth of the pole face is to produce a sinusoidally distributed armature reaction m.m.f. which Davies[3] calculated by integrating J_z throughout the depth of the pole-face and integrating the result with respect to x:

$$F_R = \frac{\lambda}{2\pi} \frac{J_m}{R} \text{ Cos } (\omega t - 2\pi x/\lambda - \phi + \pi/2)$$

On substituting for J_z, Davies obtained an expression for the peak armature reaction ampere-turns:

$$F_{Rh} = \frac{\lambda_h}{2\pi} \times 4\sqrt{2} \times \frac{Lw_h}{\omega_h (\phi_{ac})_h}$$

This expression can be checked by applying the circuital law to a section of the secondary bounded by $y = 0$, $y = \infty$, $x = x_1$ and $x = x_1 + \delta x$.

On substitution for w_h, ω_h, and λ_h; F_{Rh} becomes:

$$F_{Rh} = \frac{2\sqrt{2}}{\pi} \times \frac{T_h}{p_h^2 \ (\phi_{ac})_h}$$

Using equations 3.14 to substitute for $(\phi_{ac})_h$, we get

$$F_{Rh} = \frac{2\sqrt{2}}{\pi k_2} \times \frac{T_h^{1/2m} \ n_m^{1/4m}}{p_h^2 \quad M}$$

which can be written:

$$\left.\begin{aligned} F_{\phi Rh} &= C_2 T_h^{1/2m}\, n_h^{1/4m} && \text{Ampere-turns} \\ \text{where} \quad C_2 &= \frac{0.901}{k_2 p_h^2 M} && \text{M.K.S units} \end{aligned}\right\} \quad (3.19)$$

In the eddy current coupling theory, an armature reaction modifying factor f is used. When a uniform gap is considered, f equals 1 and is therefore omitted from the above equations.

3.6.4 The Total Excitation

The peak m.m.f. provided by the stator winding for the hth harmonic F_h is the vector sum of $F_{\phi h}$ and F_{Rh} whose mutual phase displacement, $\pi/2 - \phi$, tends to 135° when the depth of penetration is small ($\sqrt{2}\alpha >> 2\pi/\lambda$), Fig. 12.5.1. Using the cosine rule the total excitation is given by:

$$F_h^{\,2} = F_{\phi h}^{\,2} + F_{Rh}^{\,2} - 2F_{\phi h} F_{Rh} \cos(\pi/2 - \phi)$$

$$\text{or} \quad F_h^{\,2} = C_1^2 \frac{T_h^{\frac{2m-1}{m}}}{n_h^{1/2m}} + C_2^2\, T_h^{1/m}\, n_h^{1/2m} + C_1 C_2 C_3 T_h \quad (3.20)$$

$$\text{where } C_3 = -2\cos(\pi/2 - \phi)$$

3.6.5 Equations for Calculation

The maximum torque, T_{mh}, and speed at maximum torque, n_{mh}, may be obtained[3] by differentiating 3.20 with respect to speed, keeping F_h constant and equating to zero to give, at the peak torque point:

$$\frac{C_1}{C_2} = T_{mh}^{\;1/m-1}\; n_{mh}^{\;1/2m} \tag{3.21}$$

Substituting equation 3.21 into 3.20 gives an expression for the peak torque:

$$F_h^2 = C_1 C_2 (2 + C_3) T_{mh} \tag{3.22}$$

It might be mentioned in passing that

$$F_{\phi h}^{\,2} = C_1 C_2 T_{mh} = F_{Rh}^{\,2}$$

i.e. at the peak torque point the two components of F_h are numerically equal.

The equations which follow involve both the product and quotient of C_1 and C_2, defined in equations 3.18 and 3.19. It is interesting to note that the product is independent of the magnetisation characteristic:

$$C_1 C_2 = \frac{0.9 S_h}{p_h^2}$$

Their quotient may be written as:

$$C_1/C_2 = 1.11\; k_2^2\; M^2\; p_h^2\; S_h$$

By rewriting equation 3.22, the peak torque is expressed as a function of k_1, m and the machine parameters:

$$T_{mh} = \frac{F_h^{\,2}}{C_1 C_2 (2 + C_3)}$$

Substituting for $C_1 C_2$ (above) and for S_h (equation 3.17), we get:

$$T_{mh} = \frac{\mu_o}{0.9(2 + C_3)} \times \frac{F_h^2 P_h DL}{g} \quad \text{Nm} \qquad (3.23)$$

where

$F_h = G\, k_{bh} k_{dh} k_{ph}/h$ (see appendix 12.1.2 equation 12.1.1)

Eliminating T_{mh} from equations 3.21 and 3.23 yields an expression for n_{mh} in terms of the machine parameters:

$$n_{mh} = \frac{C_1}{C_2}^{2m} \times T_{mh}^{\ 2m-2}$$

$$= \frac{k_2^{4m} M^{4m} p_h^{4m} S_h^{2m}}{0.9^{2m}} \times \frac{\mu_o^{2m-2} F_h^{4m-4} p_h^{2m-2} D^{2m-2} L^{2m-2}}{0.9^{2m-2} (2 + C_3)^{2m-2} g^{2m-2}}$$

$$\therefore \; n_{mh} = \frac{k_2^{4m} (2 + C_3)^{2-2m}}{(0.9)^{4m-2} \mu_o^2} \times \frac{\rho g^2 (ph)^{4m-1}}{D^{4m} F_h^{4-4m}} \quad \text{r.p.s.} \qquad (3.24)$$

where

$k_2^{4m} = 0.196(1.8)^{4m} k_1$

and $p_h = p \times h$

For mild steel having $m = 0.794$ and $k_1 = 0.769$, the above equations become 3.11(i) and 3.12(i) of section 3.5.

When calculating a number of harmonic terms for one particular machine, it is convenient to rewrite equation 3.23 and 3.24 in the form:

$$T_{mh} = G_1 F_h^2\, h \quad \text{Nm} \qquad (3.23A)$$

$$\text{and } N_{mh} = G_2 h^{4m-1} F_h^{4m-4} \quad \text{r.p.m.} \tag{3.24A}$$

$$\text{where } G_1 = \frac{\mu_o}{3.074} \times \frac{pDL}{g} \quad \text{M.K.S. units}$$

$$\phi = 45^o$$

and

$$G_2 = 6 \times 10^4 \times 2^{4m} k_1^{4m} (3.414)^{2-2m} \times \frac{p^{4m-1} \rho g^2}{D^{4m}}$$

ρ is in $\mu\Omega$-cm, g and D in metres

The coefficients G_0, G_1 and G_2, being the same for each harmonic term, are determined in the initial stages of calculation.

By using these expressions for the peak torque, T_{mh}, and the speed at which the peak torque would occur, n_{mh}, the theory accounts for the armature reaction of surface currents but avoids the actual calculation of them. It is evident that the peak torque and the speed at peak torque depend only on the machine parameters and the inducing m.m.f. (At the peak torque point, the inducing m.m.f. is equally divided between the gap and the armature reaction ampere turns).

T_{mh} is independent of the index m and coefficient k_1, i.e. it can be calculated with confidence irrespective of any inaccuracy in the magnetisation curve. In contrast, N_{mh} is rather sensitive to changes in m. Furthermore

T_{mh} is independent of ρ, whilst N_{mh} is directly proportional to ρ, as in the induction motor where the magnitude of the peak torque is independent of rotor resistance whilst the slip at which it occurs is directly proportional to rotor resistance.

3.6.6 The Normalised Curve

The normalised curve relates the normalised torque, T_h/T_{mh}, to the normalised speed, n_h/n_{mh}. With n_h known, n_h/n_{mh} and T_{mh} are calculated from the equations 3.23A and 3.23B. T_h is then read off the normalised curve derived as follows. Subscripts are omitted but it is to be understood that all the equations refer to the term of harmonic order 'h'. The peak torque is expressed in terms of F_h in equation 3.22. This is now substituted into the equation for the total m.m.f., 3.20:

$$(2 + C_3)T_m = \frac{C_1}{C_2}(T)^{2-1/m}(n)^{-1/2m} + \frac{C_2}{C_1}(T)^{1/m}(n)^{1/2m} + C_3 T$$

C_1 and C_2 are now eliminated using equation 3.21:

$$2 + C_3 = \frac{T^{2-1/m}}{T_m^{2-1/m}} \cdot \frac{n^{-1/2m}}{n_m^{1/2m}} + \frac{T^{1/m}}{T_m^{1/m}} \cdot \frac{n^{1/2m}}{n_m^{1/2m}} + C_3\frac{T}{T_m}$$

This implicit equation can be rearranged in terms of Q, where

$$Q = \left[\frac{T}{T_m}\right]^{\frac{1-m}{m}} \left[\frac{n}{n_m}\right]^{\frac{1}{2m}} \qquad (3.25)$$

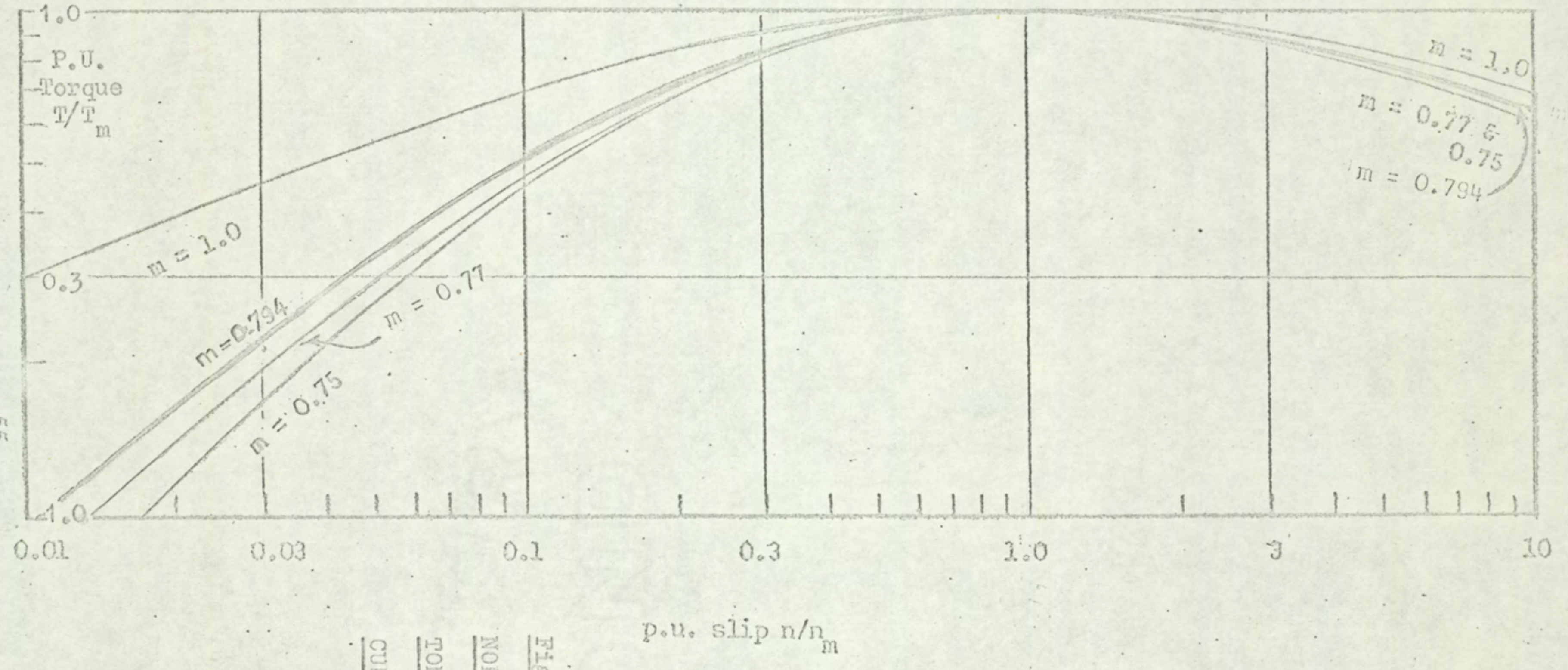

Fig.3.4.

NORMALISED

TORQUE/SLIP

CURVES

to give the normalised torque:

$$\frac{T}{Tm} = \frac{Q(2 + C_3)}{1 + C_3 Q + Q^2} \tag{3.26}$$

In Table 3.1, a few typical values of T/T_m and n/n_m are calculated for assumed values of Q, for the experimental machine. A few normalised curves are plotted in Fig. 3.4 for selected values of m . Note that they are all independent of k_1 and applicable to any other solid secondary device having the same value of m. For all these curves the angle ϕ is taken as 45^o, in accordance with the theory that the depth of penetration is small. Until further experimental evidence is available, it is difficult to select a suitable alternative value of ϕ.

<u>The Slope of the Normalised Curve</u>

The equation of a tangent at any point P on the normalised curve of Fig. 3.4, plotted on Log-log paper could be written:

$$\text{Log}\,\frac{T}{T_m} = \text{Log (const)} + \text{(slope) Log}\,\frac{n}{n_m}$$

$$= \text{Log}\left\{ (\text{const})\left(\frac{n}{n_m}\right)^{\text{slope}} \right\}$$

$$\therefore \qquad \frac{T}{T_m} \propto \left(\frac{n}{n_m}\right)^{\text{slope}}$$

Table 3.1 The Normalised Curve for Mild Steel

The three sample calculations are based on equation 3.26. The complete curve is tabulated in appendix 12.3 programme MS-16 and FS-4.

$m = 0.794$ $\qquad \phi = 45^{o}$ $\qquad \therefore C = \sqrt{2}$

$$\therefore \quad Q = (T/T_m)^{0.260} \, (n/n_m)^{0.630}$$

$$\frac{n}{n_m} = \left\{\frac{Q}{(T/T_m)^{0.260}}\right\}^{1/0.630} = \left\{\frac{Q}{F}\right\}^{1.587}$$

where $F = (T/T_m)^{0.26}$

Q	Denominator, $D = 1 + \sqrt{2}Q + Q^2$	$\frac{Q}{D}$	$T/T_m = 3.414\ Q/D$	F	$\frac{Q}{F}$	$\frac{n}{n_m}$
0.01	1.014	0.00987	0.0337	0.414	0.02315	0.0026
0.1	1.151	0.087	0.297	0.729	0.1372	0.0425
1.0	3.414	-	1	1	1	1
10	115	0.087	0.297	0.729	13.72	104

The slope is determined in the simplest way by drawing tangents. The value of the slope for a particular normalised speed, Fig. 3.5, will determine the way the predicted loss varies with the machine parameters, section 3.8.

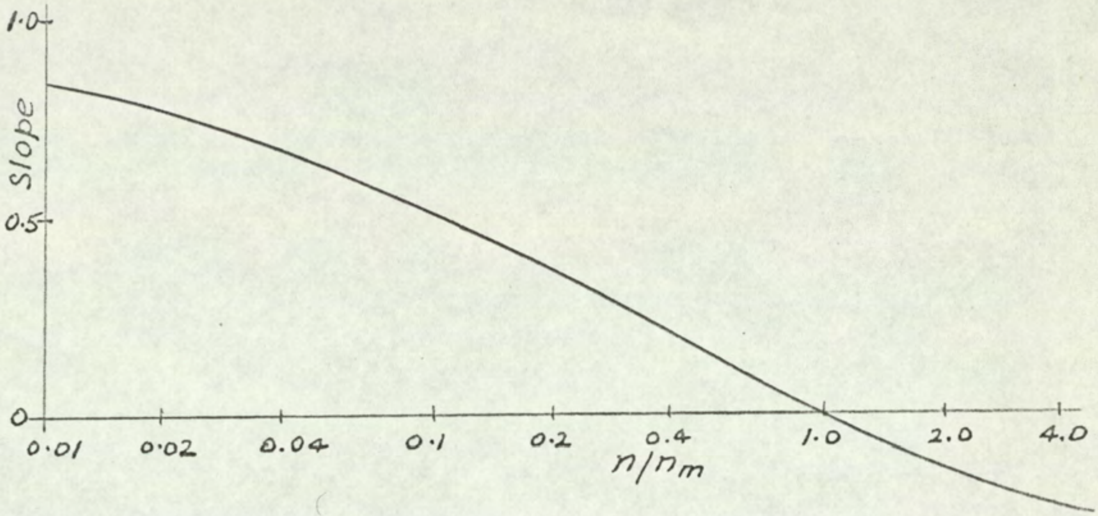

Fig. 3.5 The Slope of the Normalised Curve for Experimental Machine having m = 0.794

3.7 Method of Calculation

3.7.1 Cylindrical Rotors

Having determined k_1 and m for the material being used, the normalised curve is calculated in the manner described above.

The order and magnitude of the harmonic m.m.f's. are then determined from the winding geometry, and the coefficients, G_0, G_1, and G_2, calculated. The loss for each harmonic present is then determined by carrying out the following computations paying particular attention to the gap/wavelength ratio of the slot harmonic terms, see section 12.2:

N_{mh} using equation 3.24A R.P.M.

T_{mh} using equation 3.23A Newton-metres

N_h/N_{mh}

T_h/T_{mh} by reading off the normalised curve at the above value of N_h/N_{mh}

$T_h = (T_h/T_{mh}) \times T_{mh}$ Newton-metres

The pole face loss for the hth harmonic is:

$$W_h = \frac{2\pi}{60} N_h T_h \times 10^{-3} \quad \text{kW} \qquad (3.27)$$

In order to allow for peripheral flux leakage (appendix 12.2) W_h must be multiplied by a reduction factor such as K_{Lh} (Fig. 12.2) to obtain the harmonic loss figure. The total loss for a cylindrical rotor is $\Sigma W_h K_{Lh}$.

The calculation of the normalised curve and $\Sigma W_h k_{Lh}$ can be done using a digital computer. The data sheet and print-up of a typical computation, Tables 3.2 and 3.3, illustrate the above procedure using computer programme

Table 3.2 Data Sheet used for Computer Programme No. 4

Pole Face Loss Due to M.M.F. Harmonics

LABEL: = cr. lf. cr.	sp ^{55} ...... cr. lf. cr.		REF.	CEGB/K	
	sp ^{55} ...... bl.		DATE	28.1.64	/ /
A 0 †	P †	Pole pairs		1	
A 1	NS	Synchronous speed	r.p.m.	3000	
A 2	Z	Conductors/slot		2	
A 3	Y	Parallel paths/coil side		1	
A 4	C	Parallel paths/phase		2	
A 5	I	Total phase current	amp	3670	
A 6	S/P/P	Slots/pole/phase		10	
A 7	PITCH	Per unit pitch	p.u.	0.833333	0.
A 8	SPREAD	Spread	deg.	60	60
A 9	D	Rotor diameter	m.	0.94	
A10	G	Effective air gap	m.	0.0381	
A11	L	Rotor length	m.	4.44	
A12	RHO	Rotor iron resistivity	μΩ - cm	27.5	
A13	A13	Parameter *		-1	1
A14	K	Highest term required	$(h \pm 1)6$	11	

FOOTNOTES * Put A13 = positive integer to print k, h, k_{ph}, k_{dh}, T/T_m, T, KW, KW TOT, only

Put A13 = negative integer to print complete data

† 1st and 2nd columns = symbols used in programme and print-out respectively

TABLE 3.3 TYPICAL COMPUTER PRINT-UP USING PROGRAMME NO.4.

Note: (i) The parameters k_1 and m refer to the Ingot Iron of Ref.3.

(ii) The KW coloumn gives the loss for a cylindrical rotor neglecting peripheral flux leakage.

(iii) The magnitude of the slot harmonic terms is large.

(iv) Column $FH9 = F_h^{\ 0.925}$, ref. equation 3.12 (ii).

TABLE 3.3

PROBLEM NO CEGB/K
DATE 28/1/64

LOSS DUE TO HARMONICS IN MMF WAVEFORM

PPRS	NS	Z	Y	C	I	PROG
1.0000	3000.0	2.0000	1.0000	2.0000	3670.0	4

S/P/P	PITCH	SPREAD	D	G	L	RHO
10.000	.83333	60.000	.94000	.03810	4.4400	27.500

CF	CT	CN
.49545/ 05	.44694/-04	.42311/ 05

K	H	KPH	KDH	T/TM	T	KW	KW TOT
1.0	5.00	.25882	.19319	.996	.547/ 02	20.60	20.60
1.0	7.00	.25882	-.13952	.654	.134/ 02	3.598	24.20
2.0	11.0	.96593	-.09180	.557	.437/ 02	14.96	39.16
2.0	13.0	-.96592	.07945	.331	.165/ 02	4.776	43.93
3.0	17.0	-.25881	.06434	.059	.106/ 00	.0352	43.97
3.0	19.0	-.25883	-.05962	.037	.509/-01	.0151	43.98
4.0	23.0	-.96593	-.05356	.066	.848/ 00	.2778	44.26
4.0	25.0	.96592	.05176	.047	.520/ 00	.1567	44.[illegible]2
5.0	29.0	.25880	.05007	.010	.660/-02	.0021	44.42
5.0	31.0	.25883	-.05007	.008	.473/-02	.0014	44.42
6.0	35.0	.96593	-.05176	.020	.157/ 00	.0508	44.47
6.0	37.0	-.96592	.05356	.017	.134/ 00	.0409	44.51
7.0	41.0	-.25880	.05962	.004	.272/-02	.0009	44.51
7.0	43.0	-.25884	-.06434	.004	.268/-02	.0008	44.52
8.0	47.0	-.96593	-.07945	.012	.171/ 00	.0548	44.57
8.0	49.0	.96592	.09180	.012	.212/ 00	.0651	44.64
9.0	53.0	.25879	.13952	.004	.116/-01	.0037	44.64
9.0	55.0	.25885	-.19319	.005	.250/-01	.0077	44.65
10	59.0	.96593	-.95537	.055	.877/ 02	28.01	72.66
10	61.0	-.96592	-.95537	.049	.750/ 02	23.18	95.83
11	65.0	-.25879	-.19319	.003	.133/-01	.0042	95.84
11	67.0	-.25885	.13952	.002	.440/-02	.0014	95.84

H	FH	FH9	TM	N	NM	N/NM
5.00	.495/ 03	.307/ 03	.549/ 02	.360/ 04	.392/ 04	.919
7.00	.256/ 03	.167/ 03	.204/ 02	.257/ 04	.145/ 05	.177
11.0	.399/ 03	.252/ 03	.784/ 02	.327/ 04	.246/ 05	.[illegible]33
13.0	.292/ 03	.189/ 03	.497/ 02	.277/ 04	.465/ 05	.060
17.0	.485/ 02	.360/ 02	.179/ 01	.318/ 04	.426/ 06	.007
19.0	.402/ 02	.303/ 02	.137/ 01	.284/ 04	.639/ 06	.004
23.0	.111/ 03	.775/ 02	.128/ 02	.313/ 04	.371/ 06	.008
25.0	.991/ 02	.696/ 02	.110/ 02	.288/ 04	.492/ 06	.006
29.0	.221/ 02	.174/ 02	.635/ 00	.310/ 04	.267/ 07	.001
31.0	.207/ 02	.164/ 02	.594/ 00	.290/ 04	.326/ 07	.001
35.0	.708/ 02	.510/ 02	.784/ 01	.309/ 04	.135/ 07	.002
37.0	.693/ 02	.500/ 02	.794/ 01	.292/ 04	.155/ 07	.002
41.0	.186/ 02	.149/ 02	.637/ 00	.307/ 04	.643/ 07	.000
43.0	.192/ 02	.153/ 02	.708/ 00	.293/ 04	.692/ 07	.000
47.0	.809/ 02	.577/ 02	.137/ 02	.306/ 04	.220/ 07	.001
49.0	.897/ 02	.634/ 02	.176/ 02	.294/ 04	.219/ 07	.001
53.0	.338/ 02	.257/ 02	.270/ 01	.306/ 04	.634/ 07	.000
55.0	.450/ 02	.336/ 02	.499/ 01	.295/ 04	.525/ 07	.001
59.0	.775/ 03	.464/ 03	.158/ 04	.305/ 04	.440/ 06	.007
61.0	.750/ 03	.450/ 03	.153/ 04	.295/ 04	.486/ 06	.006
65.0	.381/ 02	.288/ 02	.422/ 01	.305/ 04	.867/ 07	.000
67.0	.267/ 02	.207/ 02	.214/ 01	.296/ 04	.128/ 08	.000

No. 4 for ingot iron.

Note that despite the ratio N/N_m being as low as 0.007 for the slot harmonic term, T_m is very high, thereby yielding a high loss figure. This is modified by K_L in section 6.2.1.

TABLE 3.4 THE M.M.F. HARMONIC LOSSES FOR A 1.5 MVA. MACHINE - AS PRINTED UP BY THE COMPUTER.

Note: (i) The parameters k_1 and m refer to the experimental load loss dynamometer.

(ii) N/N_m is now printed by punch 1.

(iii) Version 1M prints the significant terms only.

Version 1ML prints all terms.

(iv) Column FH9 = $F_h^{0.824}$ for the mild steel used, ref. equation No. 3.12(i).

TABLE 3.4 LOSS DUE TO HARMONICS IN MMF WAVEFORM PROG MS-1ML

PROGRAMME ACCOUNTS FOR SLOT WIDTH AND PRINTS ALL TERMS

PPRS	NS	Z	Y	C	I	A13	KMAX	REF
2.000	1800	2.000	1.000	4.000	2460	1.0	9.0	1.40250

S/P/P	PITCH	SPREAD	D	G	L	RHO	SLOT
9.0000	.81481	60.000	686.00	7.9500	490.00	21.000	10.50

G0	G1	G2
.14945@+05	.34502@-04	.63133@+04

Total loss for a Cylindrical Rotor

K	H	KPH	KDH	KBH	T/TM	N/NM	KW	KW TOT
1.0	5.00	.11609	.19371	.99628	.855	.329	.1495	.1495
1.0	7.00	.44881	.14026	.99271	.713	.200	.4949	.6444
2.0	11.0	.99831	.09303	.98205	.480	.089	.5753	1.220
2.0	13.0	.80211	.08096	.97498	.248	.034	.1024	1.322
3.0	17.0	.23064	.06649	.95744	.054	.005	.0011	1.323
3.0	19.0	.72739	.06217	.94701	.077	.008	.0102	1.333
4.0	23.0	.91820	.05709	.92293	.057	.006	.0088	1.342
4.0	25.0	.54948	.05593	.90933	.033	.003	.0014	1.344
5.0	29.0	.54954	.05593	.87917	.022	.002	.0008	1.344
5.0	31.0	.91823	.05709	.86267	.026	.002	.0024	1.347
6.0	35.0	.72734	.06217	.82701	.016	.001	.0010	1.348
6.0	37.0	.23057	.06649	.80792	.005	.000	.0000	1.348
7.0	41.0	.80215	.08096	.76742	.013	.001	.0012	1.349
7.0	43.0	.99831	.09303	.74610	.014	.001	.0022	1.351
8.0	47.0	.44875	.14026	.70153	.008	.001	.0005	1.352
8.0	49.0	.11616	.19371	.67838	.003	.000	.0000	1.352
9.0	53.0	.95801	.95547	.63057	.040	.003	.3732	1.725
9.0	55.0	.95797	.95547	.60601	.036	.003	.2845	2.009

TABLE 3.5. COMPUTED HARMONIC LOSSES FOR THE EXPERIMENTAL LOAD LOSS DYNAMOMETER.

Note: (i) Programme Version 1L uses inch units.

(ii) Parameter A 13 is made negative to call punch 2.

TABLE 3.5

A 38 14.10.65

LOSS DUE TO HARMONICS IN MMF WAVEFORM PROG MS-1L

PROGRAMME ACCOUNTS FOR SLOT WIDTH AND PRINTS ALL TERMS

PPRS	NS	Z	Y	C	I	A13	KMAX	REF
2.000	1500	8.000	1.000	1.000	29.80	-1.0	8.0	102.000

S/P/P	PITCH	SPREAD	D	G	L	RHO	SLOT
1.0000	1.0000	60.000	11.420	.01200	9.8500	20.000	.1570

CF	CT	CN
.32184@+03	.19429@-03	.13603@+03

K	H	KPH	KDH	KBH	T/TM	N/NM	KW	KW TOT
1.0	5.00	1.0000	1.0000	.99687	.587	12.3	.4427	.4427
1.0	7.00	1.0000	1.0000	.99386	.875	3.19	.3346	.7774
2.0	11.0	1.0000	1.0000	.98489	.999	1.04	.3037	1.081
2.0	13.0	1.0000	1.0000	.97893	.950	.530	.2043	1.285
3.0	17.0	1.0000	1.0000	.96413	.800	.269	.1465	1.432
3.0	19.0	1.0000	1.0000	.95532	.671	.171	.0965	1.528
4.0	23.0	1.0000	1.0000	.93493	.520	.104	.0652	1.594
4.0	25.0	1.0000	1.0000	.92340	.437	.074	.0452	1.639
5.0	29.0	1.0000	1.0000	.89777	.333	.050	.0303	1.669
5.0	31.0	1.0000	1.0000	.88371	.269	.038	.0208	1.690
6.0	35.0	1.0000	1.0000	.85323	.208	.027	.0141	1.704
6.0	37.0	1.0000	1.0000	.83686	.175	.021	.0102	1.714
7.0	41.0	1.0000	1.0000	.80203	.139	.016	.0070	1.721
7.0	43.0	1.0000	1.0000	.78362	.115	.013	.0051	1.726
8.0	47.0	1.0000	1.0000	.74498	.091	.010	.0035	1.730
8.0	49.0	1.0000	1.0000	.72482	.078	.008	.0026	1.732

102.000

H	FH	FH9	TM	N	NM	T
5.00	.642@+02	.308@+02	.400@+01	1800	.146@+03	.235@+01
7.00	.457@+02	.233@+02	.284@+01	1286	.403@+03	.249@+01
11.0	.288@+02	.159@+02	.177@+01	1636	.157@+04	.177@+01
13.0	.242@+02	.138@+02	.148@+01	1385	.261@+04	.141@+01
17.0	.183@+02	.109@+02	.110@+01	1588	.591@+04	.881@+00
19.0	.162@+02	.991@+01	.967@+00	1421	.832@+04	.649@+00
23.0	.131@+02	.832@+01	.765@+00	1565	.150@+05	.398@+00
25.0	.119@+02	.769@+01	.686@+00	1440	.195@+05	.300@+00
29.0	.996@+01	.665@+01	.559@+00	1552	.311@+05	.186@+00
31.0	.917@+01	.621@+01	.507@+00	1452	.385@+05	.137@+00
35.0	.785@+01	.546@+01	.419@+00	1543	.571@+05	.871@-01
37.0	.728@+01	.513@+01	.381@+00	1459	.685@+05	.667@-01
41.0	.630@+01	.455@+01	.316@+00	1537	.965@+05	.438@-01
43.0	.587@+01	.430@+01	.287@+00	1465	.113@+06	.330@-01
47.0	.510@+01	.383@+01	.238@+00	1532	.155@+06	.217@-01
49.0	.476@+01	.362@+01	.216@+00	1469	.179@+06	.168@-01

In Table 3.4, G_2 is calculated using the values of k_1 and m obtained from the linear portion above the knee of the $\mu^{1/4}H/H$ curve for mild steel in Fig. 3.3 These are $m = 0.794$ and $k_1 = 0.769$. It was decided at this initial stage to use the same values of k_1 and m for all calculations on steel rotors. The last column gives a progressive summation based on a cylindrical rotor design. This figure must therefore be modified to account for the peripheral flux leakage and the pole profile in practical machines. Modification is not needed in the experimental machine.

3.7.2 Salient Pole Rotors

Tapered or chamfered pole faces may be accounted for by repeating the above calculation for different air gaps and obtaining a loss figure by a graphical method. This procedure was adapted for machines E, F, and G Table 6.13.

Alternatively a simple approximate formula, derived in Appendix 12.2.1, can be used for machines having a parallel air gap and chamfered pole tips. The loss for chamfered poles

$$= \quad kW_{TOT}\ (2\beta_1\frac{g_1}{g_2} + \beta_2) \qquad kW$$

Applying this formula to Table 3.4 gives the results in Table 6.11, Column B.

The graphical and algebraic methods compare favourably in section 6.3.1.

3.8 Predominant Parameters

It is useful for the design engineer to know how the loss depends on various parameters. The loss has already been shown to be the product of T_h/T_{mh}, T_{mh} and n_h. These quantities have been defined, but the way in which T_h changes with the machine parameters is very dependent on the operating point on the generalised torque-slip curve. Since this point varies with the harmonic order over a wide range, it is impossible to be precise. However, two broadly defined regions are considered. The subscript "h" is again omitted for clarity with the exception of p_h which is written as p x h to avoid masking the influence of the harmonic order on the operating point.

3.8.1 At Low Values of Normalised Slip

(this applies mainly to the slot harmonic terms)

For any harmonic, when n/n_m is small,

T/T_m is also small, so that $Q << 1$

from equation 3.26 $\left(\frac{T}{T_m}\right) \propto Q$

$$\text{i.e.} \quad T/T_m \propto (n/n_m)^{1/2m} \times (T/T_m)^{\frac{1-m}{m}}$$

$$\propto (n/n_m)^{\frac{1}{4m-2}}$$

Therefore for mild steel having m = 0.794,

$$T/T_m \propto (n/n_m)^{0.85}$$

$$\therefore \text{ Loss } W_h \propto (n/n_m)^{0.85} \times T_m \times n$$

Using equations 3.11(i) and 3.12(i) for mild steel, we get:

$$W_h \propto \frac{D^{3.18} F^{0.824} n^{0.85}}{\rho g^2 (ph)^{2.18}} \times \frac{F^2 (ph) DL}{g} \times n$$

i.e. $$W_h \propto \frac{D^{3.7} F^{2.7} L n^{1.85}}{\rho^{0.85} g^{2.7} p^{1.85} h^{1.85}} \qquad (3.28)$$

for all values of $n/n_m < 0.1$

3.8.2 At Higher Values of Normalised Slip

(This applies mainly to the phase belt harmonics.)

When n/n_m exceeds 0.1, the slope of the generalised (log-log) curve varies from 0.85 at stall to zero at the peak torque point, Fig. 3.5. An upper limit of $n/n_m = 0.4$ covers most practical machines so far examined. The slope is then about 0.25 so that the harmonic loss,

$$W_h \propto \left(\frac{n}{n_m}\right)^{0.25} \times T_m \times n$$

(3.8.2)

$$\propto \left\{ \frac{D^{3.18} \; F^{0.824} \; n}{\rho g^2 \; (ph)^{2.18}} \right\}^{1/4} \times \; \frac{F^2 (ph) \; DL}{g} \; \times n$$

$$\propto \frac{D^{1.8} \; F^{2.2} \; Lp^{0.45} \; h^{0.45} \; n^{1.3}}{\rho^{0.25} \; g^{1.5}} \qquad (3.29)$$

3.9 Effect of Parameter Changes

The designer is interested in reducing the losses by altering the machine parameters. This section gives examples of the change in measured and computed loss obtained by altering one or more of these parameters in a practical machine. Equations 3.28 and 3.29 which form a useful guide in making design decisions are first summarised with the indices rounded off. In the initial computations on practical machines, the normalised slip was found to exceed 0.1 for the first two harmonic terms but to be very much lower for the slot harmonic terms. Since any given machine produces the whole range of harmonic m.m.f's. both equations 3.28 and 3.29 must be considered. The effects of parameter changes on the belt harmonic loss is governed mainly by equation 3.29 and on the slot harmonic loss by equation 3.28.

3.9.1 Changes in Main Dimensions

As the slot harmonic order increases the loss in the pole face due to armature reaction m.m.f. harmonics increases as:

D^2 to D^4

$F_h^2 \sqrt{h}$ to F_h^3/h^2

L

n to n^2

and decreases as:

$\rho^{0.3}$ to $\rho^{0.9}$

$g^{1.5}$ to g^3

$\frac{1}{\sqrt{p}}$ to p^2

These relationships form the basis of a design study of the experimental machine in section 4.1. Their relevance to practical machines is discussed below and in section 6.3. The change in F_h with the width of the armature slot opening is discussed in appendix 12.1.2.

3.9.2 Changes in Winding Geometry

Since the harmonic m.m.f. F_h decreases linearly with harmonic order, we must consider both F_h and h simultaneously. Substituting for F_h in equation 3.29 by using equation 12.1.1, Appendix 12.1.2, the loss due to the lowest harmonic orders (high normalised slip) is proportional to

$$(k_{wh}\ k_{bh}\ F\ )^{2.2}/h^{1.7}$$

As the harmonic order increases (and normalised slip lessens), the loss becomes proportional to

$$(k_{wh}\ k_{bh}\ F_1)^{2.7}/h^{4.5}$$

The loss is greatest when large harmonic winding factors occur with comparatively low harmonic orders, hence the established practice of short pitching to reduce the belt harmonic winding factors. When the number of slots/pole/phase, q, is reduced there is a notable increase in the contribution of the slot harmonic terms which have the fundamental winding factor but lower slot width and flux leakage factors.

For example, take the 3.4MVA machine, reference C in Table 6.11, section 6.3.2, and vary q by ± 50%. The relevant data is summarised in Table 3.6, columns C4 to C8, and Fig. 3.6 curves (a) and (c). The calculations are not corrected to account for flux leakage. This is small for the belt harmonics for which the pole face loss increases by 40% over the range of q from 8 to 4. The flux leakage increases with q (Fig. 12.2.4), so that the corrected loss curve will be below curve (a) and have a greater slope. The corrected loss for the slot harmonic terms which is the difference between (a) and (c) will therefore increase by more than 13 times over the same range of q.

Variation of loss with pole resistivity, ρ, is not

Table 3.6 - Computed Loss for machine C

Variation of q and ρ

Machine Reference / Cross Reference			C1 330/0	C2 330/5	C3 330/6	C4 330/7	C5 330/2	C6 330/1	C7 330/3	C8 330/4
Slots/pole/phase		q	6	6	4	4	5	6	7	8
Resistivity		$\mu\Omega$ - cm	19.7	30	← 25.4 →					
Surface Temperature		°C	20.0	-	← 75.0 →					
Specific Electric Loading		ac/mm	← 46.5 →							
Per Unit Pitch			0.778	0.778	1.0	0.833	0.800	0.778	0.809	0.792
Effective Conductors/slot			10	10	14	14	12	10	10	8
Total Phase Current		amp.	179	179	193	193	179	179	154	168
Slot width		mm	18	18	27	27	21.5	18	15.5	13.5
Computed loss times pole arc/pole pitch ratio	belt	kW	3.9	3.4	26	3.6	2.7	3.6	2.1	2.45
	slot	kW	5.6	3.8	21	19.5	8.8	4.4	4.6	1.65
	total	kW	9.5	7.2	47	23	11.5	8	4.7	4.1

All other details listed in Table 6.11, Column C.

so large - columns C1 and C2, and Fig. 3.6 (b) and (d). The full pitched winding of column C3, for which the belt harmonic loss has increased about 7 times, illustrates the influence of short pitching.

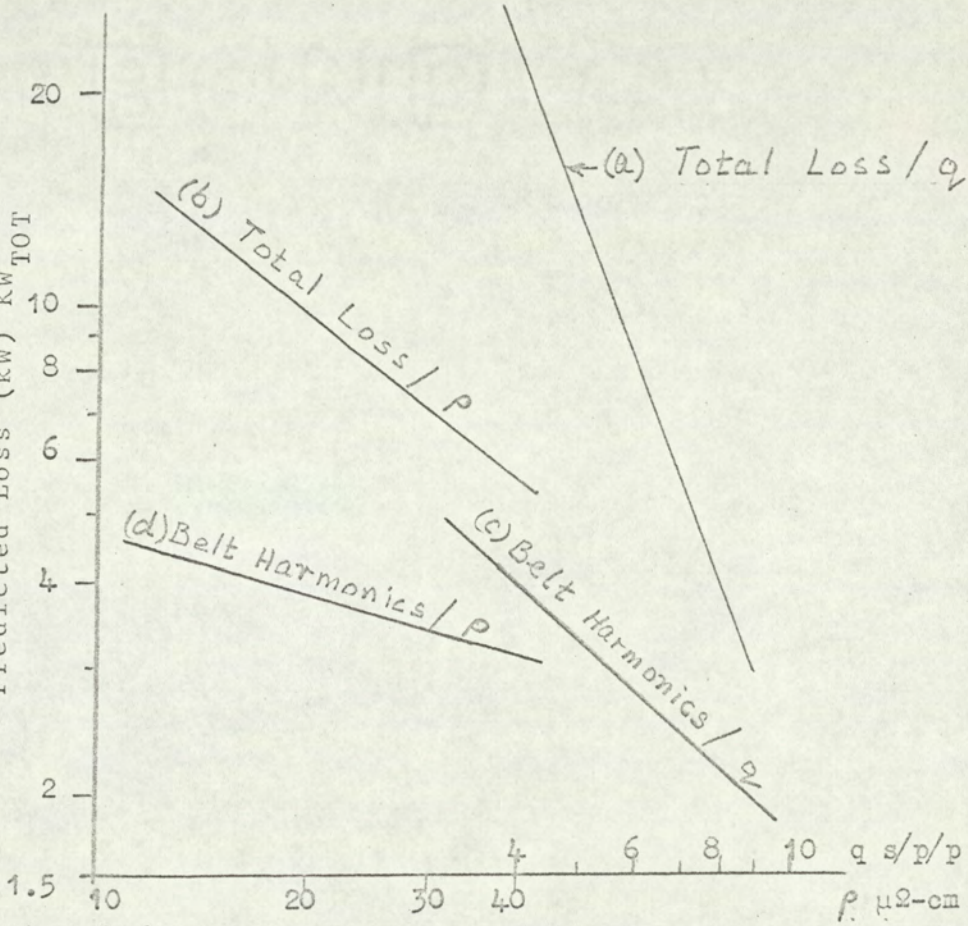

Fig. 3.6

Variation of predicted loss with q and ρ for machine C in Table 3.6

The peripheral flux leakage factor is not included

In order to highlight the effect of one parameter, only the slot width to slot pitch ratio (b/λ_s) and the specific electric loading have been retained throughout sometimes at the expense of generated e.m.f. and slot utilisation.

Designs C3, C4 and C5 (4, 4, and 5 s/p/p), which have the highest pole face loss, will also have excessive o.c. core loss because of the high b/g ratio. The 100% pitch of C3, needed to maintain the rated value of e.m.f. demonstrates the utility of Table 3.6 in revealing a bad machine in the early design stages. Designs C7 and C8 (7 and 8 s/p/p) look promising if the higher generated e.m.f. can be tolerated and if the ratio of copper to slot area can be improved.

The influence of the slot width on the loss is evident from Tables 6.3 and 6.7 which give the results of two computer runs on the same machine. Table 6.7 includes the slot width factor, k_{bh}; Table 6.3 does not. The omission of k_{bh} from the expression:

$$F_h = \frac{k_{bh} k_{dh} k_{ph} F_1}{k_{b1} k_{d1} k_{p1} h}$$

can lead to error of 2-10% in the calculated value of F_h for the belt harmonics and of 20-40% for the slot harmonic terms of machines with open slots (Figs. 12.1.3 and 12.1.4). Since the loss has been shown to be proportional to k_{bh}^2 for belt harmonics and k_{bh}^3 for slots harmonics, the loss will be considerably overestimated if k_{bh} is not included.

In appendix 12.1.2 k_{bh} is discussed at length, and although the method of determination is an approximate one, the author believes its importance justifies its inclusion in all calculations. Incidentally, the unfavourable influence of an increase in slot width on the tooth pulsation is partly compensated by the decrease in magnitude of the armature reaction m.m.f. harmonics.

3.10 Peripheral Flux Leakage

The problem of flux leakage between poles of the eddy current coupling with its very small gap is very different from that between the harmonic poles of a synchronous machine where the larger gap/wavelength ratio results in flux leakage between harmonic poles. This peripheral flux leakage is small for the phase-belt harmonics but considerable for the slot harmonics in most practical machines. The loss predicted by the 'modified' eddy current coupling theory assumes all the flux crosses the gap. This loss is reduced by a flux leakage factor K_L derived in Appendix 12.2 from the work of Alger[36] on the leakage reactance of induction motors. The derivation assumes infinite permeability of both rotor and stator iron and neglects the reaction of the pole face currents on the inducing field. It should therefore give a pessimistic estimate of the loss.

The omission of eddy current reaction effects renders the treatment inexact, but it should not seriously affect the loss reduction for the predominant harmonics: for the belt harmonics the flux leakage itself is comparatively small, while for the slot harmonics the flux linkage is small and consequently the eddy current reaction will also be small.

3.11 Previous Publications

This section summarises the work of Kuyper and Barello who solved Maxwell's equations by assuming μ and ρ constant. At the frequencies considered, the electric intensity in the solid secondary member, Fig. 2.7, satisfies the diffusion equation:

$$\nabla^2 E = \frac{\mu}{\rho} \frac{\partial E}{\partial t}$$

Assuming that the direction of E is purely axial and its time rate of change is sinusoidal,

$$E = E_z = f(y). (\cos \omega t - 2\pi x/\lambda) \qquad (3.30)$$

the diffusion equations becomes:

$$-(\frac{2\pi}{\lambda})^2 E_z + \frac{\partial^2 E_z}{\partial y^2} = j \frac{\omega\mu}{\rho} E_z \qquad (3.31)$$

which can be rewritten:

$$\frac{\partial^2 E_z}{\partial y^2} - k^2 E_z = 0$$

where $k^2 = 4\pi^2/\lambda^2 - j2\alpha^2$

and $\alpha = \sqrt{\mu\omega/2\rho} = 1/(\text{depth of penetration})$ (3.32)

The known solution of this equation is:

$$E_z = C\, e^{+ky} + D\, e^{-ky} \quad (3.33)$$

<u>In the solid secondary member</u> the indices are complex; the boundary conditions are $E_z = 0$ when $y = \infty$

and $E_z = E_m = \rho J_m$ when $y = 0$

Hences equation 3.32 becomes:

$$E_z = E_m e^{-ky} \cos(\omega t - 2\pi x/\lambda) \quad (3.34)$$

Remembering that $E_z = \rho J_z$, the loss/unit surface area is obtained by integrating ρJ_z^2 over the drum depth (see section 3.4).

The treatment so far is the same as Davies'[3]. It now differs in the way E_z is related to F_h via the gap flux.

<u>In the airgap</u> E_z satisfies the Laplacian equation, y_1 replaces y, the indices in (3.33) are real and α disappears from the auxiliary equation:

$$m^2 - 4\pi^2/\lambda^2 = 0$$

which leads to the solution

$$f(y) = E_1\, e^{2\pi y_1/\lambda} + E_2 e^{-2\pi y_1/\lambda} \quad (3.35)$$

The constants E_1 and E_2 are fixed by the boundary conditions. They are expressed in terms of μ, α, g and λ. They are complex, and indicate the manner in which the electric field intensity, E_z, is attenuated by the length of the airgap and the demagnetising effects of the eddy currents.

From now on, the two treatments by Kuyper and Barello differ. Barello derives expressions for E_1 and E_2 by applying the boundary conditions at the two iron/gap interfaces, remembering that B_y is solenoidal and that H_x is continuous. The quantities E_z and B_y can then be expressed in terms of the machine parameters, giving the loss per unit surface area as the arithmetic sum of all the harmonic losses present. The loss associated with each harmonic,

$$P_B = \Sigma \rho J_m^2 / 4\alpha \qquad \text{(see equation 3.7)}$$

is shown to be

$$P_B = \sum \frac{5.65\, N^2 I^2 k_{wh}^2 h^{-2} (bKf_1)^{1.5} \times 10^{-8}}{\sqrt{\mu_r \rho}\left[\sinh \frac{2\pi g h}{\lambda_1} + \frac{1}{\mu_r} \cdot \frac{\lambda_1}{2\pi h} \cdot \alpha \cosh \frac{2\pi g h}{\lambda_1}\right]^2 + \left[\frac{1}{\mu_r} \cdot \frac{\lambda_1}{2\pi h} \cdot \alpha \cosh \frac{2\pi g h}{\lambda_1}\right]^2} \qquad (3.36)$$

watts/unit area - M.K.S. units throughout

where N = number of conductors in series per pole per phase

I = the current per phase in amps.

k_{wh} = the winding factor for the harmonic of order h

f_1 = the frequency of the armature current

λ_1 = the fundamental wavelength = $h\lambda_h$

and $\alpha = \sqrt{\pi\mu\ (h \pm 1)\ f_1/\rho} = \sqrt{6Kf_1\mu\ \pi/\rho}$ (3.37)

— derived from 3.32 when

$$\omega = 2\pi(6Kf_1) = 12\pi f_1(h \pm 1)$$

Kuyper's approach is to derive an equivalent impedance, Z, offered to the assumed armature current sheet. The resistive component, R_1, of this impedance is determined for each harmonic in terms of the machine parameters. The subscript h is omitted for clarity:

$$R_1 = \frac{q_i(1 - \tanh^2(2\pi g/\lambda))}{(\tanh^2(2\pi g/\lambda) + q_r)^2 + q_i^2} \qquad (3.38)$$

where

$$q_r + jq_i = \frac{\lambda}{2\pi\mu_r}\ \sqrt{(2\pi/\lambda)^2 + j2\alpha^2} \qquad (3.39)$$

i.e. $q_r + jq_i = \frac{\lambda}{2\pi\mu_r}\ (\beta + j\gamma)$, in terms of eddy current coupling quantities (section 3.4). (3.40)

Note that the gap/wavelength ratio is a dominant feature in both Barello's and Kuyper's loss equations; it will be discussed later. By using the identity:

$$\text{loss} = (\text{current})^2 \times R_1$$

Kuyper shows that the pole face loss may be expressed:

$$P_K = \sum\left(\frac{A_1 k_{wh}}{k_{w1}}\right)^2 \times \frac{pLf_r}{h} \times R_1 \times 10^{-9} \qquad (3.41)$$

where $A_1 = \pi/_4$ (peak value of the fundamental armature m.m.f.)

$= \frac{\pi}{4} F_1$ (ampere-turns)

f_r = the frequency of currents generated in the rotor for the harmonic of order h (c/s)

p = pole pairs

and L = rotor length (inches)

Note the introduction of f.p.s. units

For an integral slot winding $f_r = 6Kf_1$ (section 3.1) Kuyper claims that "under most conditions encountered in the determination of pole face losses ...... $q_r = q_i$" in equation 3.39. This implies that the depth of penetration is small, i.e. that $\sqrt{2}\alpha >> 2\pi/\lambda$ (section 3.4.) giving

$|\beta| = |\gamma| = |\alpha|$ in equation 3.40.

For these conditions a family of R_1-curves for discrete $g/_\lambda$ ratios can be plotted against a factor proportional to $\frac{\alpha\lambda h}{\mu}$, namely $\sqrt{f_h \lambda^2{}_h/10^9\mu_r\rho}$ (C.g.s. units).

Kuyper shows this family in his Fig. 2 for which he assumes an unspecified but "relatively large value of μ". The curves have maxima within the region plotted and are reproduced in Fig. 3.7.

The resistance factor R_1 is a function of g/λ ($=hg/\lambda_1$), f_r, μ and ρ. Because of inadequate knowledge of suitable values of μ and ρ, a pessimistic value of the loss can be

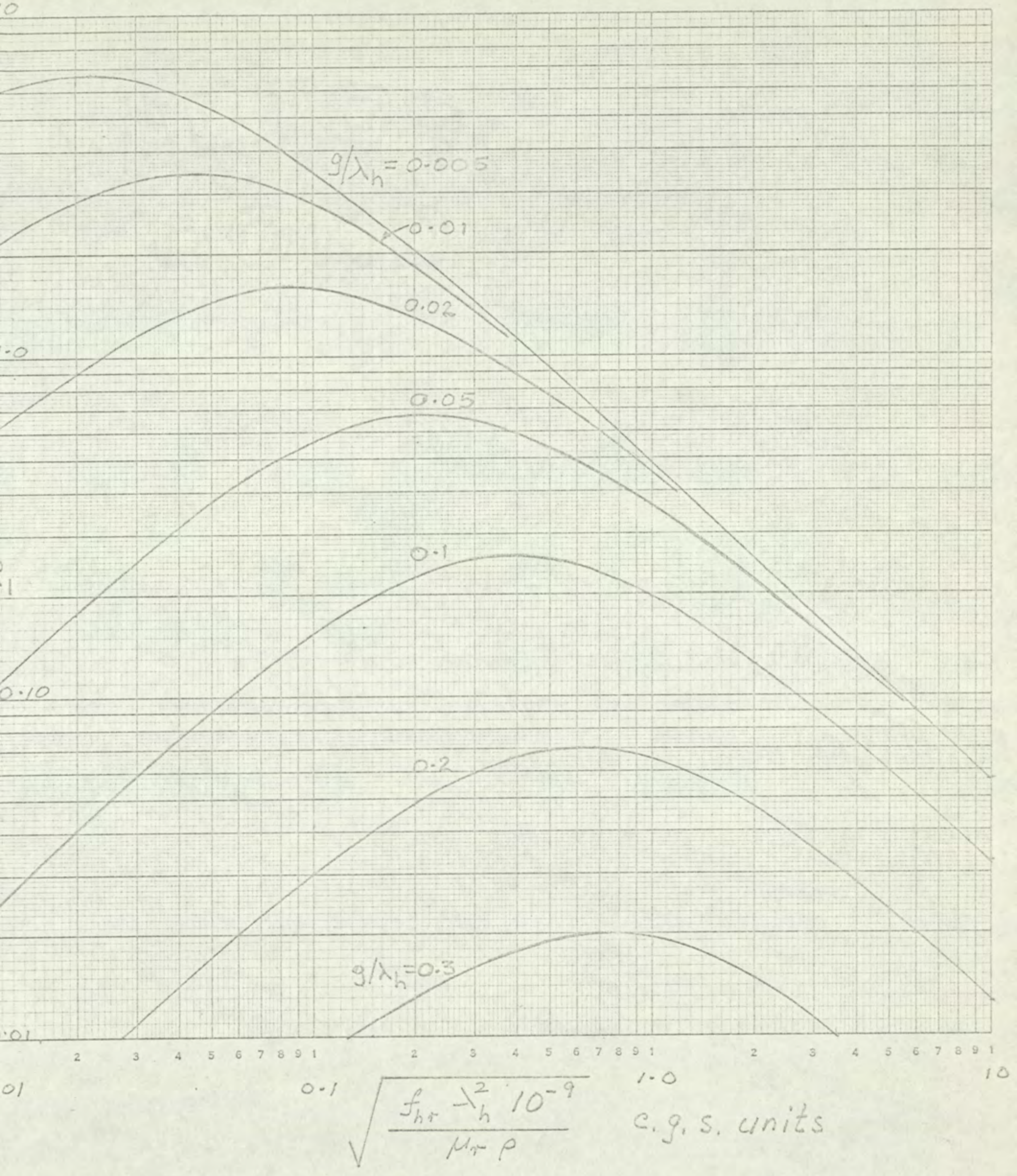

FIG. 3.7. KUYPER'S RESISTANCE FACTOR R_1

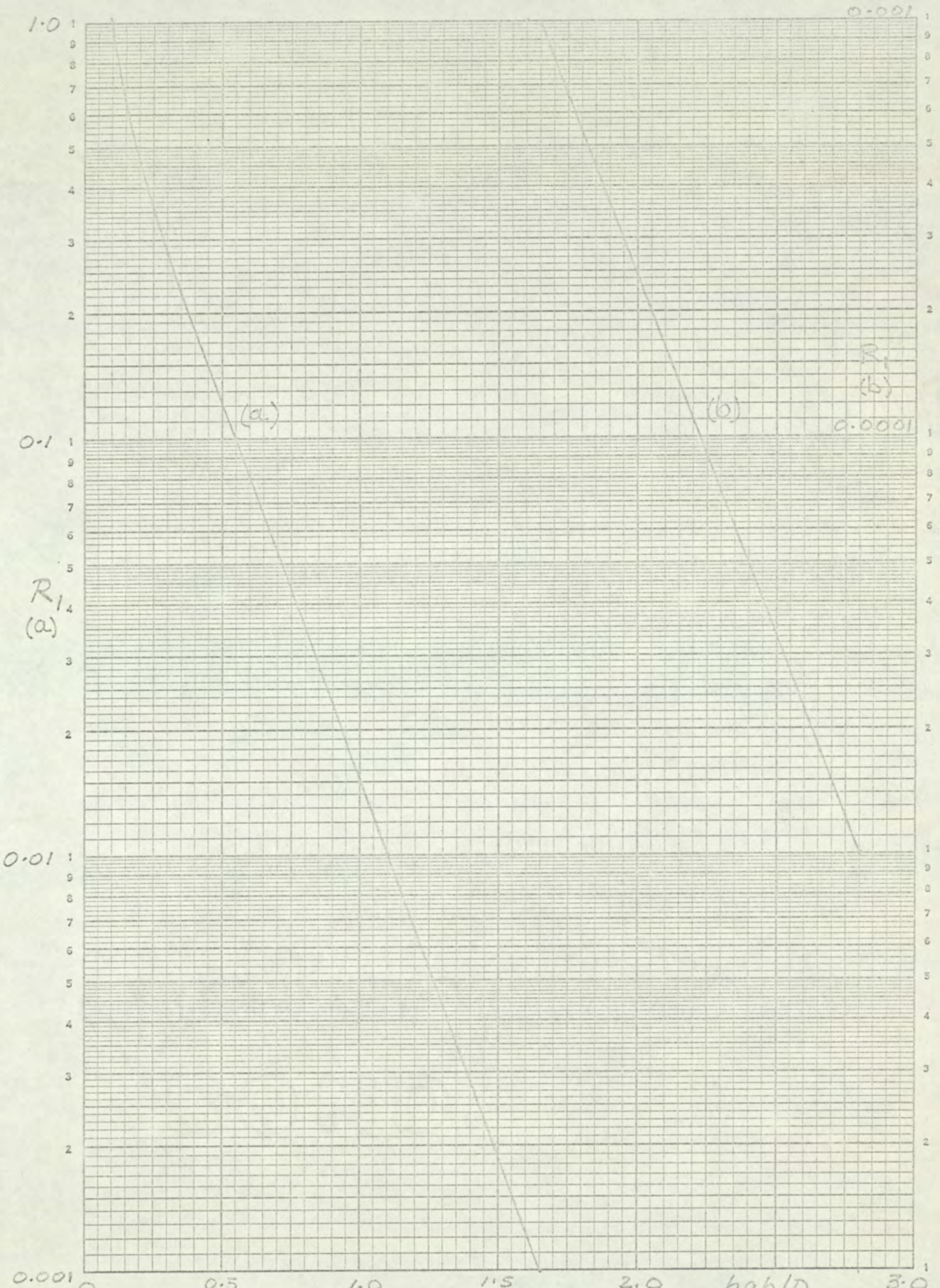

FIG 3.8. KUYPER'S RESISTANCE FACTOR R_1

obtained by reading the maximum value of R_1 from Kuyper's Fig. 2. In fact, Kuyper found that in many of his calculations the parameters were so related that the factor R_1 was a maximum or nearly so. Kuyper's Fig. 3, in which the values of these maxima are plotted against g/λ_h, is reproduced in Fig. 3.8 and discussed in section 6.4.2.

Postknikov[14] solves Maxwell's equations for a uniform gap and expresses the surface flux density as:

$$B_{h0} = \frac{\Lambda_o (ac) \sqrt{2}\, k_{wh}\, k_{h1-2}\, k_{rh}}{2hgk_c/D_m} \tag{3.42}$$

where Λ_o = gap permeance

(ac) = specific electric loading

k_{h1-2} = reduction factor to represent the attenuation of the hth harmonic across the gap

k_{rh} = eddy current reaction coefficient for the hth m.m.f. harmonic

k_c = airgap coefficient

D_m = mean gap diameter

The other symbols are the same as for this thesis, listed in section 1.

The harmonic loss is obtained by first calculating B_{h0} (using published curves[14] to obtain the various coefficients) and then substituting this value of B_{h0} in his expression 38:

$$w_h = \frac{B_{ho}^{\;2}\ (\lambda/2)^2 f_1^{1.5}\ (6K)^{1.5}}{h^2\ \sqrt{\pi\mu\rho}} \qquad \text{watts/cm}^2$$

These formulae have not been used in this thesis since Postnikov writes, "the method gives too small a value for the losses."

The hyperbolic functions contained in the above equations are the inevitable result of solving the Laplacian equation in the airgap. An analytical substitution for permeability is not made here as readily as in the eddy current coupling theory[3] because the latter assumes a "short" airgap thereby excluding awkward trigonometric functions.

4. THE EXPERIMENTAL MACHINE

4. THE EXPERIMENTAL MACHINE

4.1 Factors Influencing the Design

The problem of separating the pole face loss from the other components of the measured stray load loss in a practical machine has been mentioned in Section 2.2. To overcome this problem an experimental load loss dynamometer machine was designed to produce a pole face loss which greatly exceeded the other components of stray load loss. The functions of the experimental machine were (i) to verify the modified eddy current coupling method of loss prediction for a machine with a uniform air gap, (ii) to examine the e.m.f. distribution across the pole surface and (iii) to investigat the effects of surface discontinuities such as slotting and grooving. Item (iii) has been deferred for the moment.

In order to measure the torque and the e.m.f.s easily the inverted construction of Fig. 4.1 was adopted. The wound primary member was driven at synchronous speed inside the secondary so that the fundamental component of the primary m.m.f. wave remained stationary in space (ref. section 2.6). The secondary member was unwound and made in the form of a thick mild steel cylinder mounted in trunnion bearings. The torque arm attached to the secondary Fig. 4.6 section 4.3.1, was arranged to exert a downward pull on the scale pan of the Avery balance seen in Fig. 4.1. The design details are summarised in section 4.2. Three secondary members were made. Copper end rings, to minimise end - effects, were brazed onto two of them.

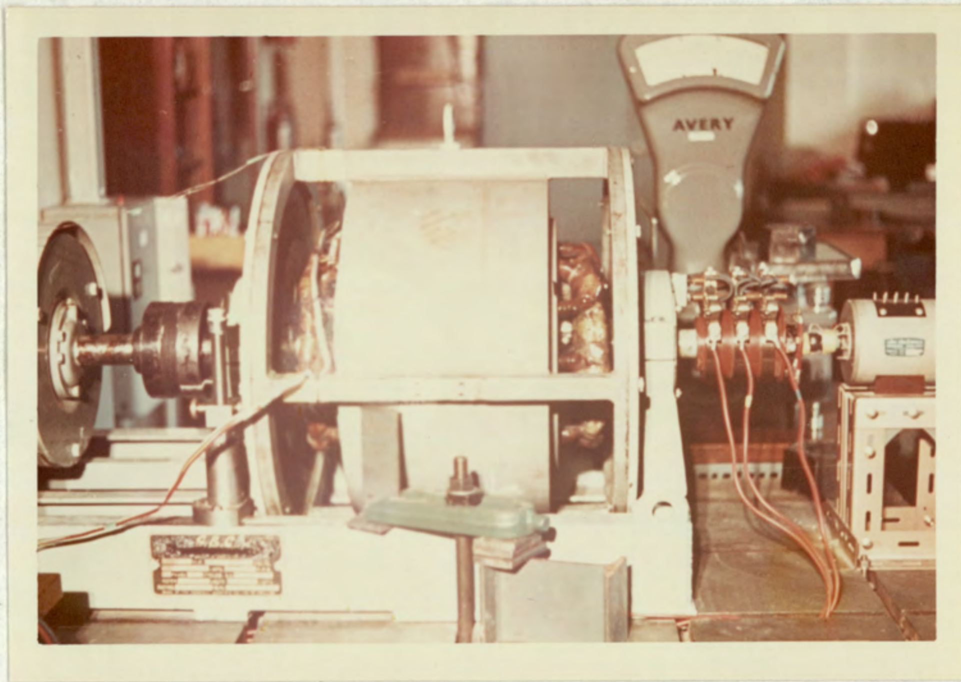

Fig. 4.1(a) The Experimental Synchronous Load Loss Dynamometer.

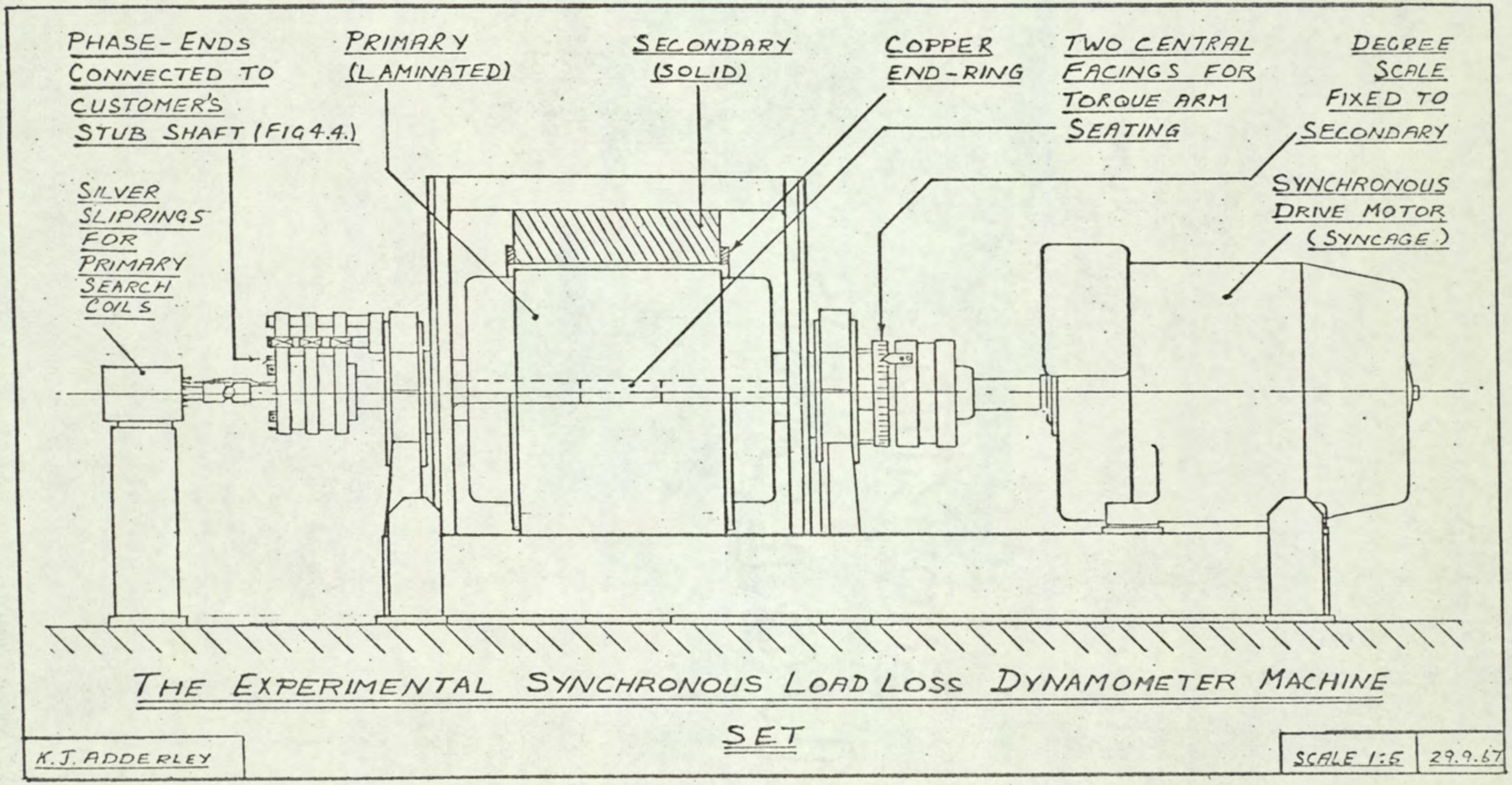
PHASE-ENDS CONNECTED TO CUSTOMER'S STUB SHAFT (FIG 4.4.)
PRIMARY (LAMINATED)
SECONDARY (SOLID)
COPPER END-RING
TWO CENTRAL FACINGS FOR TORQUE ARM SEATING
DEGREE SCALE FIXED TO SECONDARY
SILVER SLIPRINGS FOR PRIMARY SEARCH COILS
SYNCHRONOUS DRIVE MOTOR (SYNCAGE)
THE EXPERIMENTAL SYNCHRONOUS LOAD LOSS DYNAMOMETER MACHINE SET
K.J. ADDERLEY
SCALE 1:5
29.9.67

FIG. 4.1.(b)

The design of the primary member was influenced by sections 3.7 and 3.8, D and L were made as large as could be accommodated in the University Electrical Machines Research Laboratory and Workshop. The effect of changing the main parameters was predicted using the computer programme. From these computed results, Fig. 4.2, a design specification was made

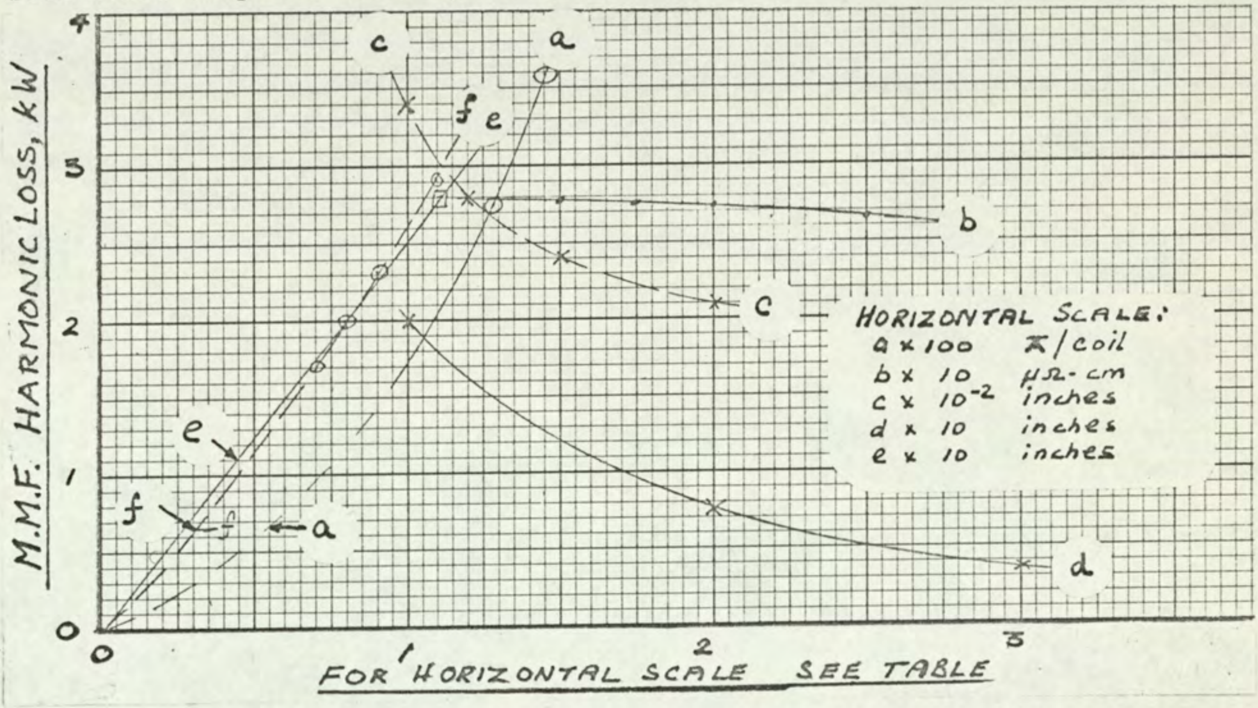

Key: (a) Loss/Ampere turns per coil; for D = 11" and L = 14"
(b) Loss/Resistivity, ρ ; for D = 11" and L = 14"
(c) Loss/gap length, g; for D = 11" and L = 14"
(d) Loss/slots per pole per phase, q ; for D = 8", g = 0.010"
(e) Loss/core length, L; for D = 11", g = 0.012 "
(f) Loss/core diameter, D; for L = 14", g = 0.012 "

Fig. 4.2 Variation in Predicted Loss with Main Parameters

out. Curves (c) and (d) illustrate the importance of choosing a small gap and a small number of slots/pole/phase. The gap was limited by mechanical considerations to 0.012", q was made equal to one. The core dimensions L and D, curves (e) and (f), were approximately 10" and 11" respectively. The armature current was determined by limiting the flux density in the teeth at the 1/3 point to about 100 Kl/in^2(1.55 Wb/m^2).

The copper section was unusually small since it only carried sufficient current to provide the magnetising ampere-turns and primary iron loss (ref. Appendix 12.7). The winding was underrated by 50% to allow for any unforseen increase in primary current and for a progressive increase in gap length at a later stage. With L = 10", D = 11" and g = 0.012" the predicted pole face loss $\triangleq 2\frac{1}{4}$ kW and the calculated primary iron loss = 0.8kW (Appendix 12.4). A 6-kW drive motor was therefore specified to ensure ample reserve power. Semi-closed slots were used to reduce the slot ripple loss, Fig. 4.3.

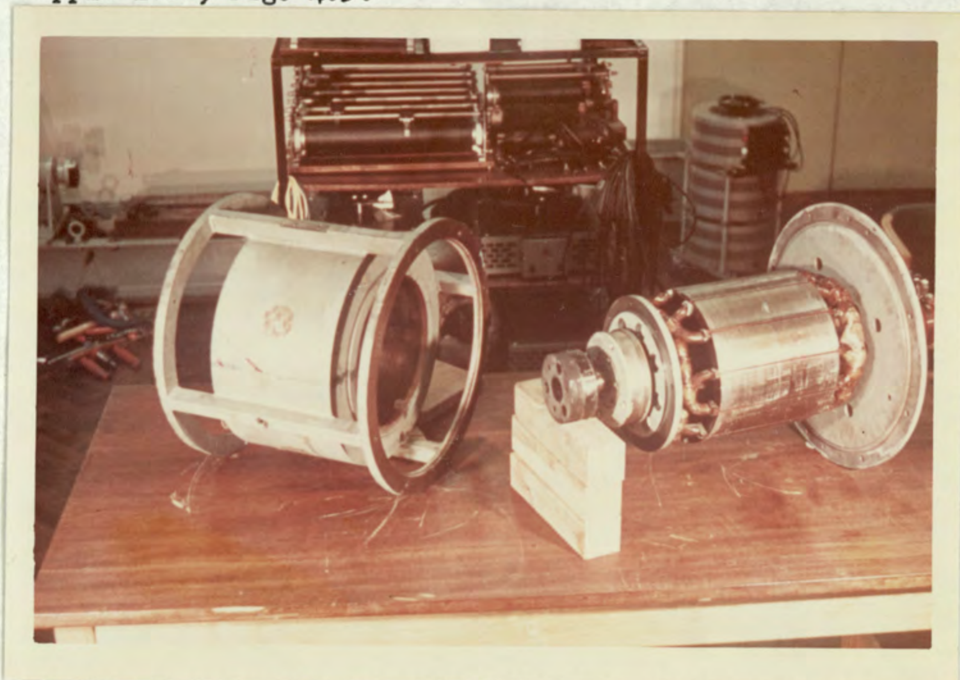

Fig. 4.3 The Primary and Secondary Members of the Experimental Machine

4.2 The Design Details

The final electrical and mechanical design details were carried out by the manufacturers in co-operation with the author. The design specification describes the main features of the machine and is included verbatim. At a later stage an array of search coils was set in fine axial grooves in the pole face. These are detailed in section 7. The rotor terminal block is shown in Fig. 4.4 and the trunnion bearing arrangement in Fig. 4.5.

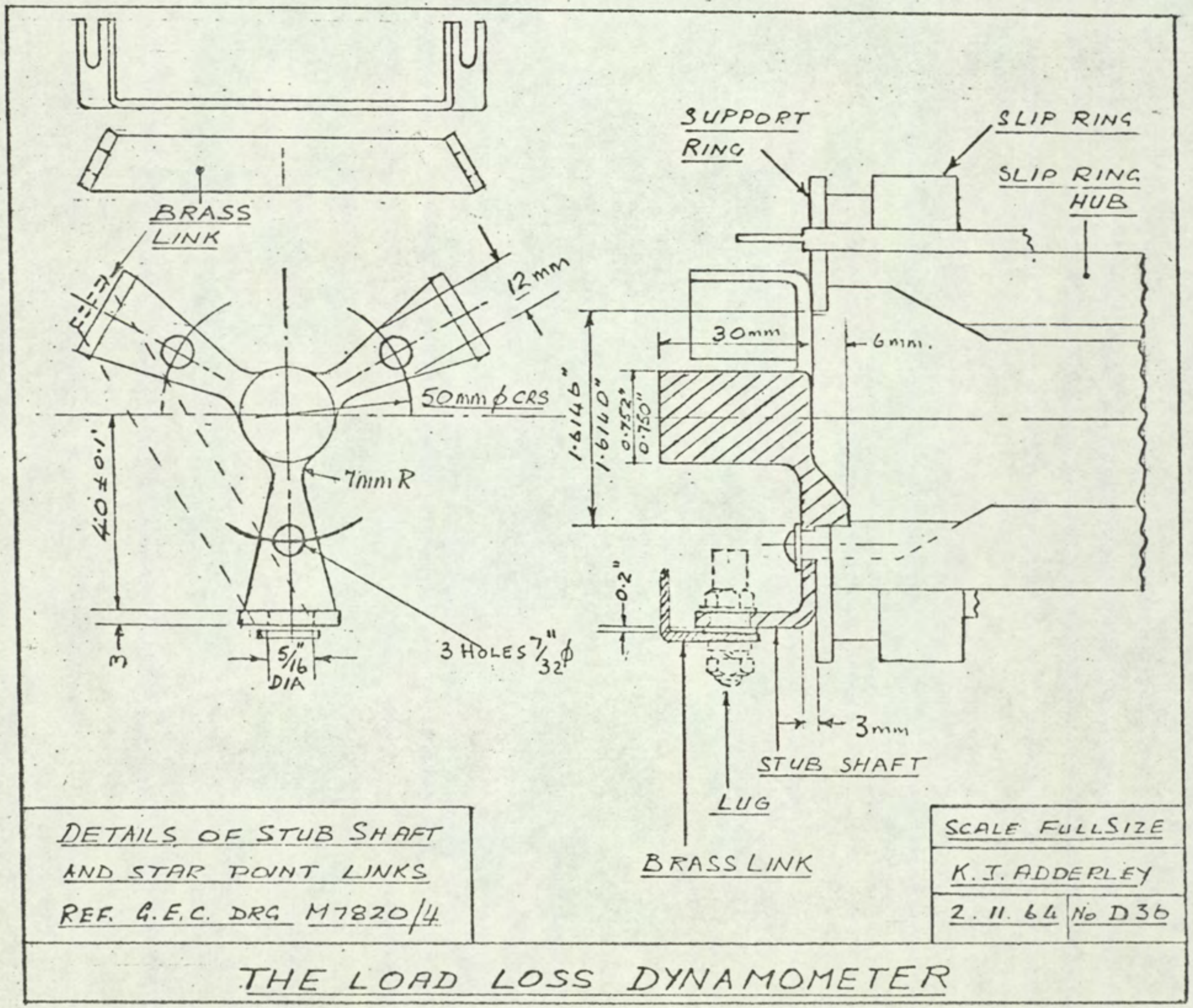
BRASS LINK
12 mm
50mm ϕ CRS
7mm R
4.0 ± 0.1"
3
5/16" DIA
3 HOLES 7/32" ϕ
SUPPORT RING
SLIP RING
SLIP RING HUB
30mm
6mm.
1.6146"
1.6140"
0.752"
0.750"
0.2"
3mm
STUB SHAFT
LUG
BRASS LINK
DETAILS OF STUB SHAFT
AND STAR POINT LINKS
REF. G.E.C. DRG M7820/4
SCALE FULLSIZE
K.J. ADDERLEY
2. 11. 64
No D36
THE LOAD LOSS DYNAMOMETER

FIG 4.4

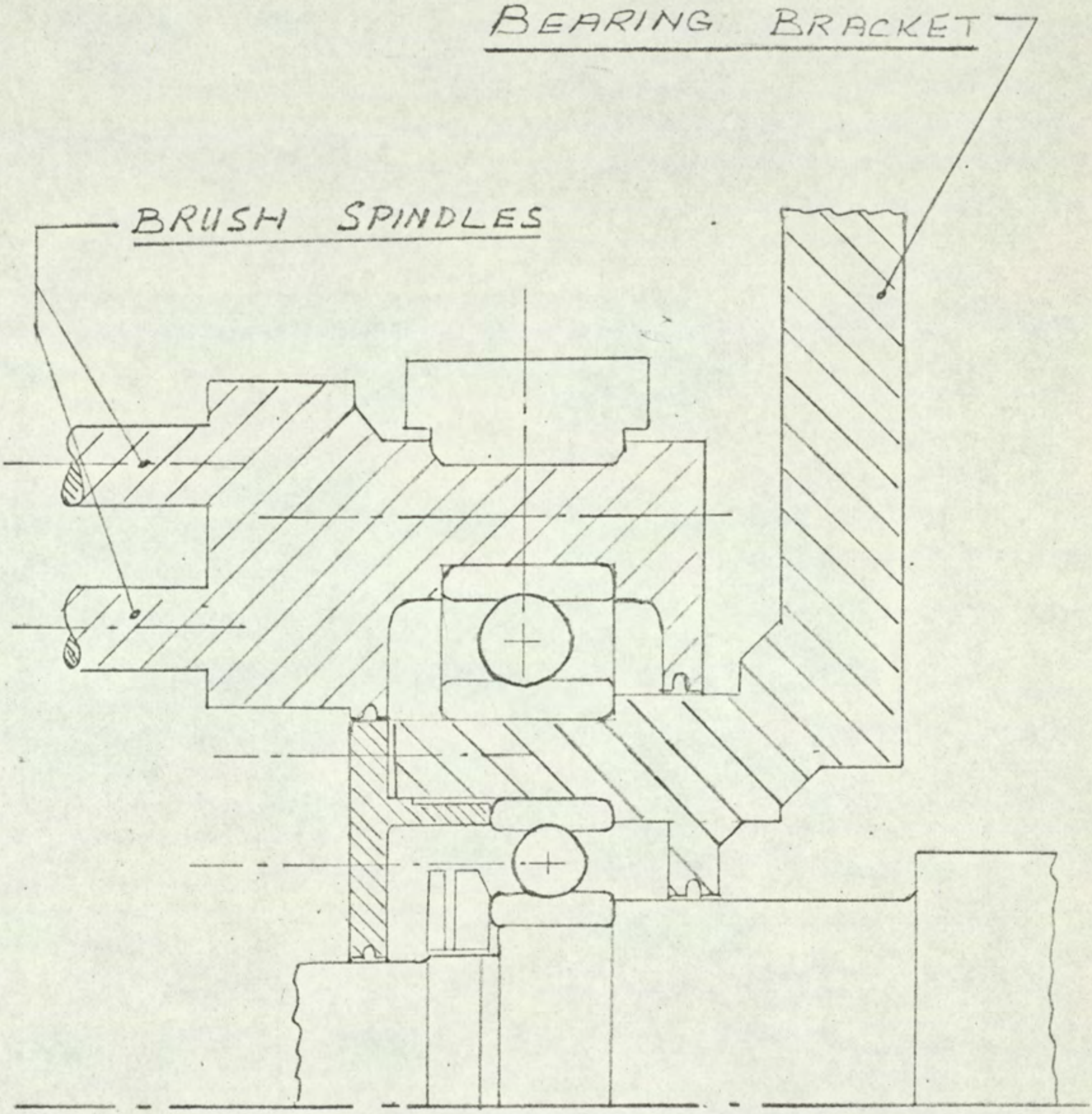

ARRANGEMENT OF BEARING AT O.D.E

SCALE FULL SIZE	FIG. 4.5	W.O: SS 25526
REF. GEC/M54970		29. 9. 67

4.2.1 The Specification

(i) Stator

(1) A solid mild steel core, flame cut from the solid. Maximum carbon content 0.25%.

(2) The resistivity of the core material over the range 20-100°C to be quoted by the manufacturers.

(3) One ring sample of the core material to be supplied for magnetic measurements, cut from one end of the secondary core and subjected to the same heat treatment as the core.

(4) The stators to be complete with copper end rings, each copper and ring to be 10mm. axial length by 20mm. radial thickness, flush with the bore, with a low resistance brazed joint between it and the core.

(5) A machined facing on each side of the side of the stator frame, to which the customer's torque arm will be attached. The facings to be centrally disposed with respect to the core. Expected maximum torque = 40 Newton metres (6 kW at 1500 r.p.m.)

(6) The stator frame to be free to rotate on pedestal bearings. The free movements between removable stops to be ± 1".

(7) The core to be annealed (1½ hours at 900°C) before final machining of the internal diameter. Very gradual cooling is most important.

(8) Air gap to be 0.012", by machining the stator core.

Great care is requested to ensure concentricity.

(9) The bearing brackets to be spigotted for easy exchange of stator shells.

(ii) Rotor

(1) Laminated core of 0.016" electrical sheet steel grade Losil 25, to be 29 cm. diameter, 25 cm. axle length.

Rotor winding to be single layer lap winding having 100% pitch, 4 poles, 1 slot per pole per phase (i.e. 12 slots), 8 conductors per slot each made of six strands of 14½ swg copper wire (cross section 17.52 mm^2). The calculated magnetising current=29.8 amps (giving a current density = 1.6A/mm^2 the slot). The six outgoing leads to be brought out to the slip ring sub-assembly. 100 amp polychloroprene cables to be used giving a oontinuous embedded rating of 70A. The banding to be non-magnetic.

(2) Slip rings to be rated at 70A and situated at the O.D.E.

(3) Slots to be semi closed, slot opening to have minimum width 1mm. depth.

(4) The peak value of flux density in the teeth (1/3 point) to be 1.55 Wb/m^2 (100 Kl/in^2). This should produce approximately 210V, (star connected) 34.2 mWb per pole and B_{mean} of 0.6 Wb/m^2.

(5) One single turn 14/.0076 P.V.C. (250V) full pitched search coil situated in slots 1 and 4 to be taped to the appropriate armature coil with the ends brought out through the shaft and slip ring sub-assembly. The free ends to be 12" long, for connected to the silver slip rings. Agreed with manufacturers that the shaft bore will be 15/16" diameter.

(6) 3 pairs of search coil outgoing leads from a terminal block at O.D.E. end of the rotor winding to be brought alongside 5 above. These leads, supplied by the customer, to be given a 500V

insultation test but not a 2000V flash test.

(7) The detailed drawing of slip ring assembly to be supplied to the customer so that the rotor sub-shaft and terminal block can be designed and made by the customer. Assembly and testing of same to be undertaken by the manufacturer.

(iii) The Assembly

The fabricated steel bedplate is to be designed and built by G.E.C. The 7.5 h.p. drive, a synchronous induction motor (Syncage) and metalastic flexible coupling to be supplied by and sent direct from Messrs. Mawdsleys Ltd. to G.E.C. Ltd. Witton Works. Coupling and lining up to be undertaken by the latter.

(iv) Ancilliary Equipment

The torque arm, stator locking gear, degree scale, and silver slip rings to be the entire responsibility of the customer.

4.2.2 The Actual Dimensions of the Manufactured Machine

Rotor curvature makes the measurement of gap length with feeler gauges imprecise. It was therefore decided to determine the gap length by carefully measuring the stator bore and rotor diameter in several places. The rotor diameter was measured in three places along its length: at the DE, ODE, and centre using a Vernier height gauge. Each reading was taken between the centres of two diametrically opposite teeth and recorded in Table 4.1. Reading N^{o} 3. refers to the tooth in axial alignment with the rotor terminal D1. The table shows that the rotor has negligible ovality but a taper of 0.0008 inches, the diameter being smaller at the O.D.E.

Table 4.1 Rotor Diameter

Tooth No.	O.D.E. inches	Centre inches	D.E. inches
1	11.3390	11.3395	11.3400
2	11.3395	11.3395	11.3400
3	11.3395	11.3395	11.3400
4	11.3390	11.3400	11.3400
5	11.3395	11.3395	11.3400
6	11.3395	11.3395	11.3400
Ave.	11.3393	11.3396	11.3400
Overall ave.		11.3397	
Tolerance on the measurement = $\pm$		0.00025"	
Reading accuracy = $\pm$		0.00025"	
Overall accuracy = +		0.0005"	

The stator bore, measured at each end of the core, ¼" inside the active length at two radial positions using an internal micrometer, is recorded in Table 4.2.

The tolerance on the measurement = $\pm$ 0.005 mm.

Reading accuracy = $\pm$ 0.005 mm.

$\therefore$ Overall accuracy = $\pm$ 0.01 mm.

= $\pm$ 0.0004 inches.

Table 4.2. Stator Bore Dimensions

	Stator I mm	Stator II mm	Stator III mm
ODE Vert	293.60	293.62	293.57
Horz	293.60	293.62	293.58
Ave.	293.60	293.62	293.58
DE Vert	293.63	293.67	293.62
Horz	293.64	293.66	293.62
Ave.	293.64	293.67	293.62
Overall Ave.	293.62	293.64	293.60
Ovality	nil	nil	nil
Taper	0.04mm.0.0016"	0.05mm,0.002"	0.04mm,0.0016"
Increase in bore w.r.t. Stator I:		+0.02(+0.0008")	-0.02(-0.0008")
Airgap = Bore - 11.3397"		0.012"	

It is observed that each stator has taper of 0.001 to 0.002 inches the diameter being smaller at the ODE in each case. i.e. both rotor and stator taper towards the same end.

Stators I and II have brazed copper and rings but stator III has not. Stator II is chosen for the uniform gap tests because (of the two stators having end rings) this one had the better concentricity.

4.3 Ancillary Equipment

4.3.1 The Torque Arm

The mild steel torque arm, shown in Fig. 4.6, was arranged to be sufficiently flexible to facilitate the use of a 4-arm strain gauge bridge, should this be required. The loss power indicated by the torque arm is ωT watts.

Where ω = the shaft speed in rad/s

and T = the indicated torque in Nm.

If F = the pull in Kg at 0.500m. radius

then $\omega T = \frac{2\pi N_s}{60} \times \frac{9.81F}{2}$

$$\therefore \omega T = 514 \times 10^{-6} \times N_s F \quad \text{Nm.} \qquad (4.1)$$

$$\text{i.e. } \omega T = 0.771F \quad \text{Nm. at 1500 r.p.m.} \qquad (4.2)$$

4.3.2 The Stator locking gear

A simple $\frac{5}{8}$"W boltbearing on the ODE end bracket and screwed into the bedplate is used to lock the secondary member. A rack and pinion arrangement is fitted at the driving end. This facilitates a controlled angular movement of the secondary over a range of about 30°M, Fig. 4.7. By fitting the peg into a succession of evenly spaced holes in the DE end bracket (visible in Fig.4.7) a controlled 360° angular displacement of

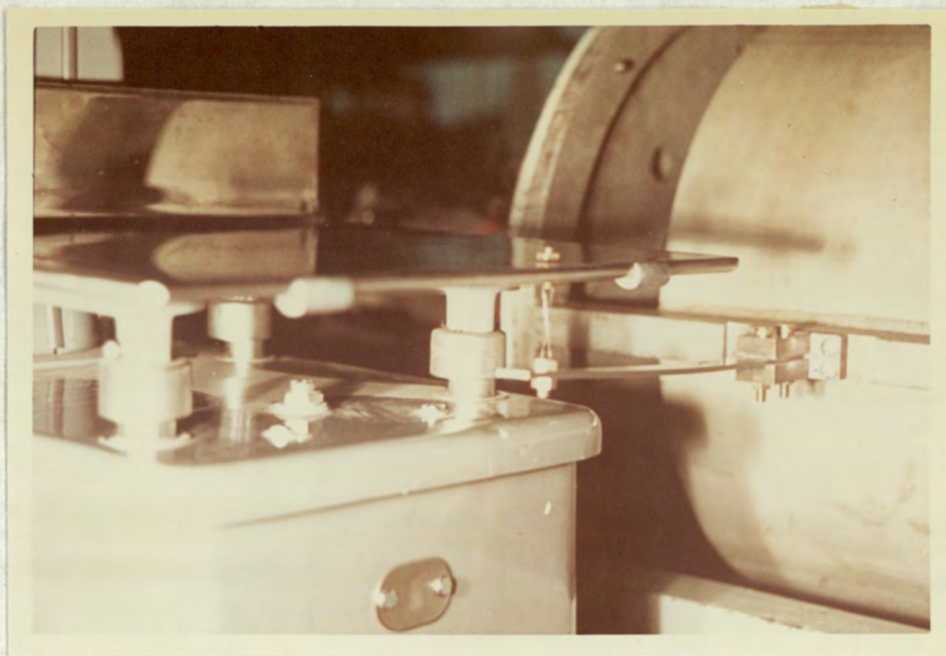

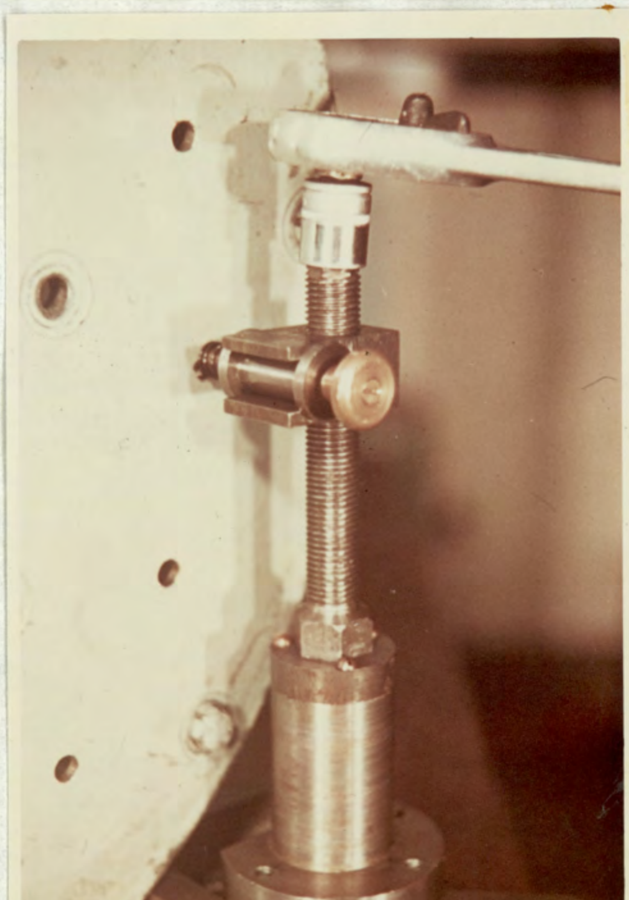

Fig.4.6 THE SECONDARY TORQUE ARM

Close-up showing the flexible coupling and the scale pan.

Fig.4.7 STATOR LOCKING GEAR
Rotation of the screw using the 'Woolf' ratchet spanner will turn the secondary through 30° Mech.

the secondary is achieved

4.3.3 The Ring Sample

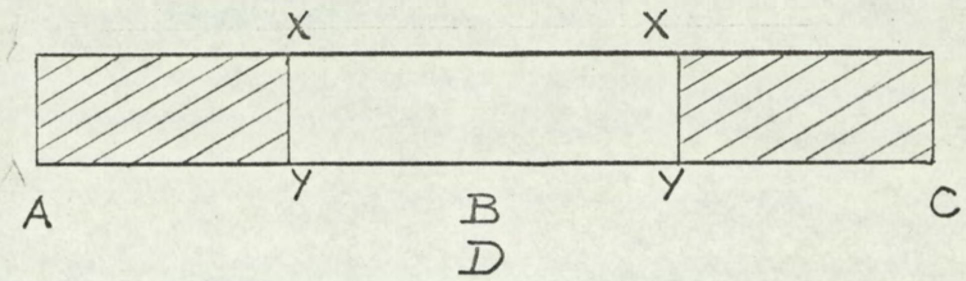

The dimensions were taken by micrometer at 4 equally spaced points are given in Table 4.3.

The axial length being taken at both inner and outer diameters.

Table 4.3 Dimensions of the Ring Sample

Circumferential Position :	A	B	C	D	mean
(i) Axial length(mm)					
at outer dia	23.80	28.84	28.89	28.82	28.79 mm.
at inner dia	28.70	28.73	28.77	28.71	
(ii) Radial Thickness (inches)					
	3.230	3.230	3.231	3.229	3.230" = 82.0 mm.
(iii) Internal Diameter (inches)					
at XX	11.067	11.065			11.066"
at YY	11.065	11.065			= 282 mm.

$\therefore$ Cross sectional area = 28.79 x 82.0 = 2360 mm^2

Mean diameter = 282 + 82 = 364 mm

$\therefore$ Length of the magnetic path at the mean diameter
= 364π mm = 1.14 m.

Because the B/H curve was not available for this particular steel the magnetising force necessary to saturate this sample to the extent of 2.2 Wb/m^2 had to be estimated. Published data on ordinary mild steel suggested about 100,000 A. 595 turns of 162/0.007 gauge T.R.S. flexible cable were wound by hand. At its continuously rated current of 31 Amp. this coil would only give 18,500 $\bar{A}$. As the 595 turns filled a large proportion of the winding space it was decided to obtain a B/H curve and then decide whether to wind on more turns.

By considerably overloading the magnetising winding for short periods (section 5.1) a flux density of 2.03 Wb/m^2 was achieved (40,000A) and oonsidered sufficiently high for the initial stages of the investigation.

4.3.4 The Degree Scale

The position of the standing flux pattern relative to the secondary changes with the load angle of the drive motor and with the movement of the scale pan. For some tests it is essential to know the position of the standing flux relative to the secondary. The degree scale, is therefore attached to the secondary and not to the bedplate. A pointer on the coupling, illuminated by a stroboflash at synchronous frequency, indicates any change in alignment of the standing flux with a secondary datum. The scale is calibrated so that the angle increases positively when the secondary is moved in the direction of shaft rotation.

5. EXPERIMENTAL RESULTS

5.0 EXPERIMENTAL RESULTS

5.1 Introduction

The overall purpose of the tests on the experimental load loss dynamometer was to verify the theory given in section 3. The original intention was to measure the pole face loss by measuring the mechanical power associated with the loss, i.e. the product of the synchronous angular speed and the measured secondary torque, ωT. It is shown in Appendix 12.7 that the loss is effectively supplied by a mechanical power source.

Preliminary tests showed that the measured value of torque varied when the loss was maintained constant. Whilst the torque arm provided a very convenient and useful means of calibrating the 'Syncage' driving motor it was unsuitable for measuring the pole face loss. The method of loss summation was therefore used. This entailed calibrating the driving motor and assessing all the mechanical and electrical losses. The method used to measure the iron losses in the rotating primary was quite simple. It is carefully considered in 5.9.3 5.10.5 and 5.13.

The results are presented in chronological order with two principal exceptions: the Syncage calibration which is grouped with other preliminary test data towards the beginning of the chapter, and the induction motor loss/slip test programme which is deferred until the end, in order to preserve the continuity of the major part of the work.

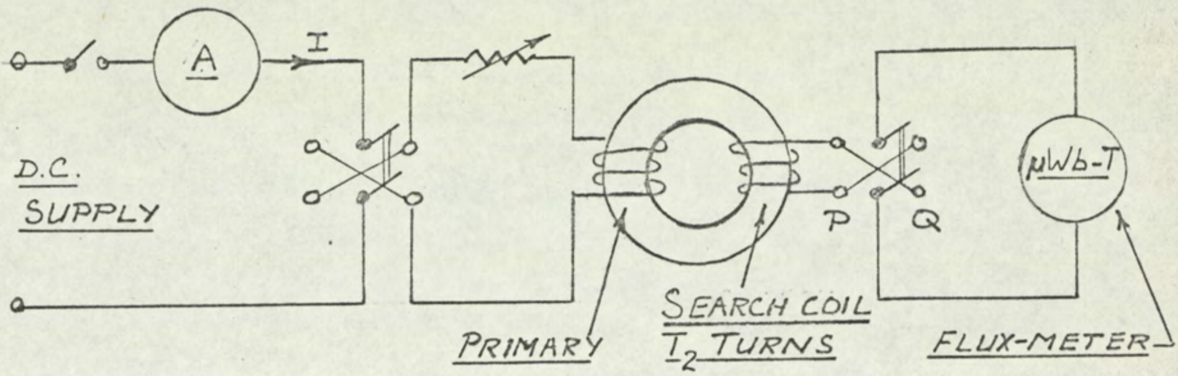

Toroid Details :

Primary Winding = 595 Turns (2 x 100 yds.) of 162/.0076 Rubber covered copper cable.

Secondary Search Coils: T_2 = 1, 1, 4, 10 Turns of 20 SWG enamelled copper wire.

Mean diameter, D_m = 0.364 m

Mean Cross sectional area = $2.36 \times 10^{-3} m^2$

Mean length = 0.082 m

Mean Flux Density B = $10^3 \times \frac{1}{2}$(Fluxmeter deflection)/$2.36 T_2$ Wb/m^2

= $\Delta\Phi / 4.72\ T \times 10^{-3}$

Magnetic Intensity at the mean diameter, D_m,

$$H = \frac{595\ I_1}{0.364\pi} = 521\ I_1\ \bar{A}/m$$

Fig 5.1 Test Circuit for Magnetic Measurements

Before taking loss measurements, samples of the secondary iron were tested to determine its magnetisation characteristics and its temperature coefficient of resistivity.

The measured and derived values of the various losses are presented only in graphical form, but a typical set of calculations is included to illustrate the method of loss separation detailed in section 5.8.4. The magnitudes of the torque produced by remanence in the secondary member and the power associated with this torque were found to be considerable. (section 5.10). The power is akin to the stand still secondary hysteresis loss in induction machines but will be referred to as "the remanence power" to avoid any confusion with hysteresis loss. It is shown in section 5.13 that although there is no fundamental hysteresis loss in the secondary at synchronism there is a transference of power due to the hysteresis property of the secondary iron.

The slot ripple loss, discussed in sections 2.4.5 and 2.6 is calculated in appendix 12.6 and used in section 5.11.

5.2 The Magnetic Characteristics of the Pole Steel

5.2.1 Test Procedure

The ring sample detailed in section 4.4, closely wound with a large number of turns, was used to determine the B/H curve and one B/H loop of the pole steel. Details of the test equipment are given in Fig 5.1. The Fluxmeter was calibrated against a Hibbert Standard.

The sample was demagnetised when necessary, by the usual procedure of reversing a progressively smaller current. Demagnetisation was considered complete when flux changes indicated by Fig. 5.2. were equal :

$AB = DC$

and $CA = BD$

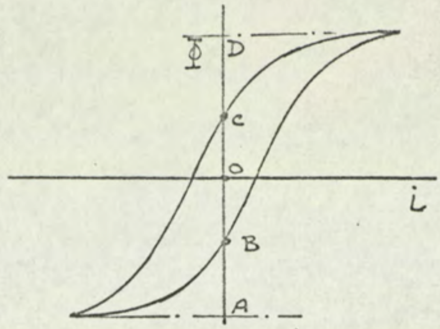

Fig. 5.2

All flux measurements were taken with the flux meter switch set to both normal (P) and reversed (Q) positions to compensate for any meter drift.

Care was taken to ensure that the magnetic characteristics of the sample represented as closely as possible those of the parent material by cutting the ring sample from one end of the load loss dynamometer secondary, and giving it to the same heat treatment. By doing so the sample had a high ratio of radial thickness to outside diameter causing a drop in circumferential flux density with increasing radius. The testing of such samples has been investigated by Hughes[11] and his correction factor is used here. The required flux density at the mean diameter, D_m, is slightly less than the measured mean flux density. The magnetic intensity, H, at diameter D_m is calculated from the geometry of the sample and the value of flux density, B at the same diameter is obtained by using the correction factor K', Fig. 5.3, based on Hughes's paper and applicable to this particular ring sample.

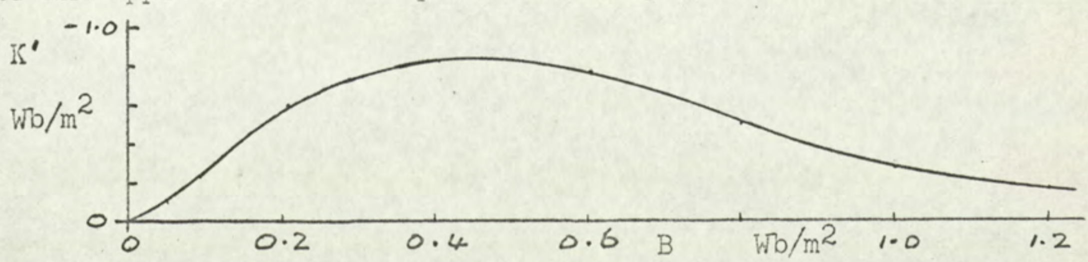

Fig. 5.3 Flux Density Correction Factor for the Ring Sample Tested

For example, if the measured $B = 0.707\ Wb/m^2$
then from Fig. 5.3 $K' = 0.0065\ Wb/m^2$

giving the value of B at
diameter D_m $= 0.707 - 0.0065 = 0.7\ Wb/m^2$

5.2.2 The B/H Curve

This is the curve joining the extremities of a large number of B/H loops, Fig. 5.4. In order to reduce errors due to meter drift, the mean of four fluxmeter deflections was taken. For example in the determination of the flux change DA, Figs. 5.2. the current was switched from I_1 to $-I_1$ and $-I_1$ to I_1 for both positions of the fluxmeter changeover switch, PQ. I_1 was increased in steps from zero to 76.5 Amps (40,000 $\bar{A}/m$) and reversed several times at each step to produce the "cyclic state" of magnetisation.

5.2.3 The B/H Loop

One B/H loop for a high value of peak flux density of 1.44 Wb/m^2 was obtained by completing the loop between 4.26 and -4.26 Amp, Fig. 5.5. Compensation for meter drift was afforded by taking the mean of two curves.

5.3 The Influence of Temperature

5.3.1 Secondary Resistivity

The resistivity of the secondary iron was determined by the manufacturers of the dynamometer , and is shown in Fig 5.6. Over the temperature range 25°C to 150°C the resistance between potential electrodes (spaced 13.95cm.) was expressed as

$$R = 0.000142\ (1 + 0.0053t + 0.00001t^2)$$

The dimensions of the sample were 10.0" x 0.501" x 0.501"

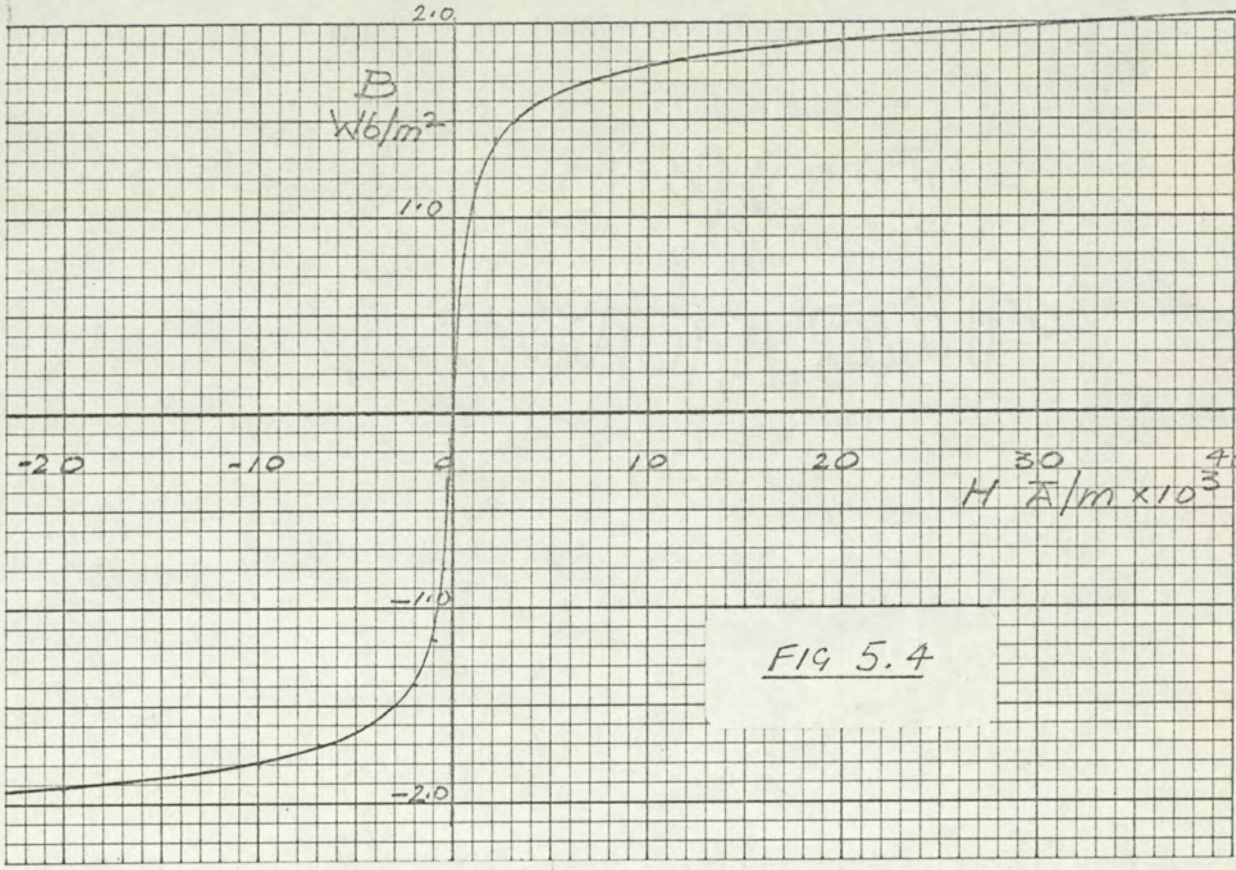
2.0
B
Wb/m²
1.0
-1.0
-2.0
-20
-10
0
10
20
30
40
H A/m x10³

FIG 5.4

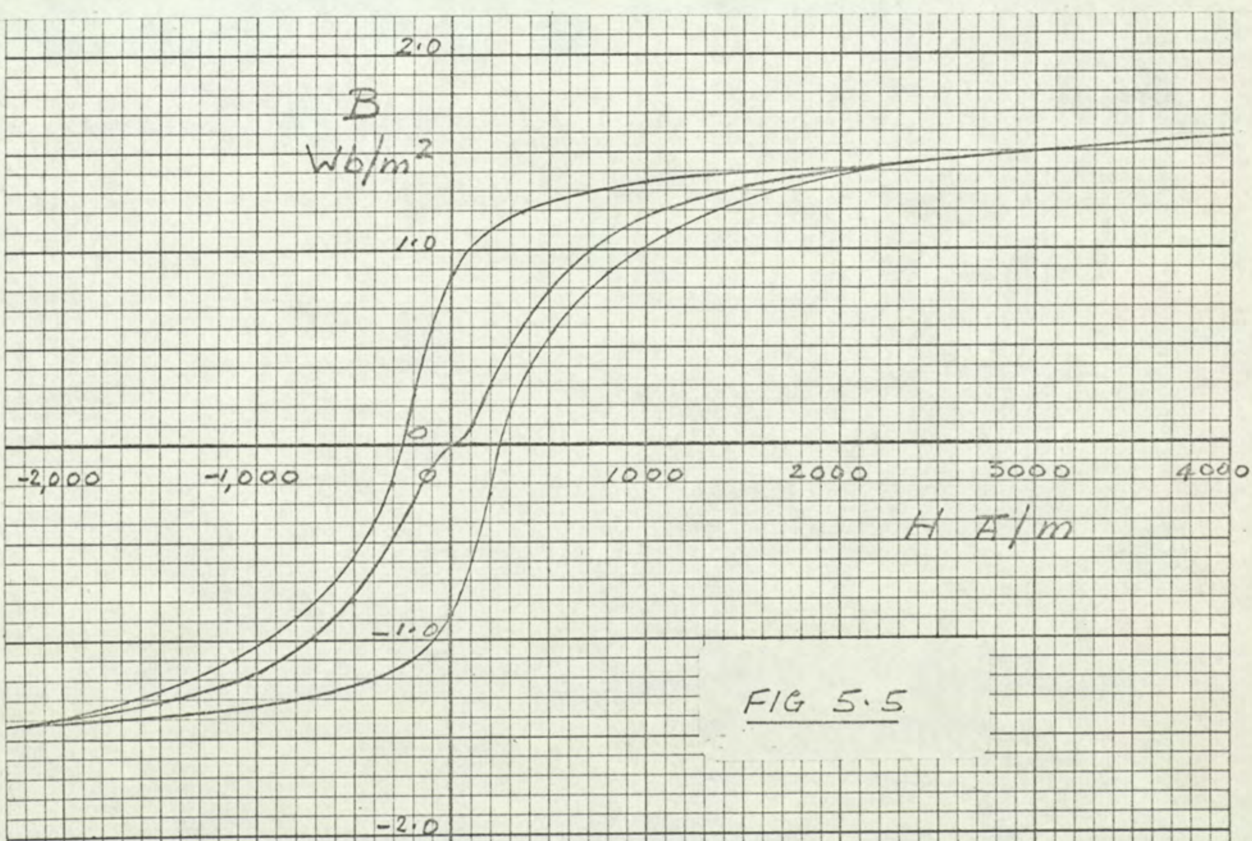
2.0
B
Wb/m²
1.0
0
-1.0
-2.0
-2,000
-1,000
0
1000
2000
3000
4000
H A/m

FIG 5.5

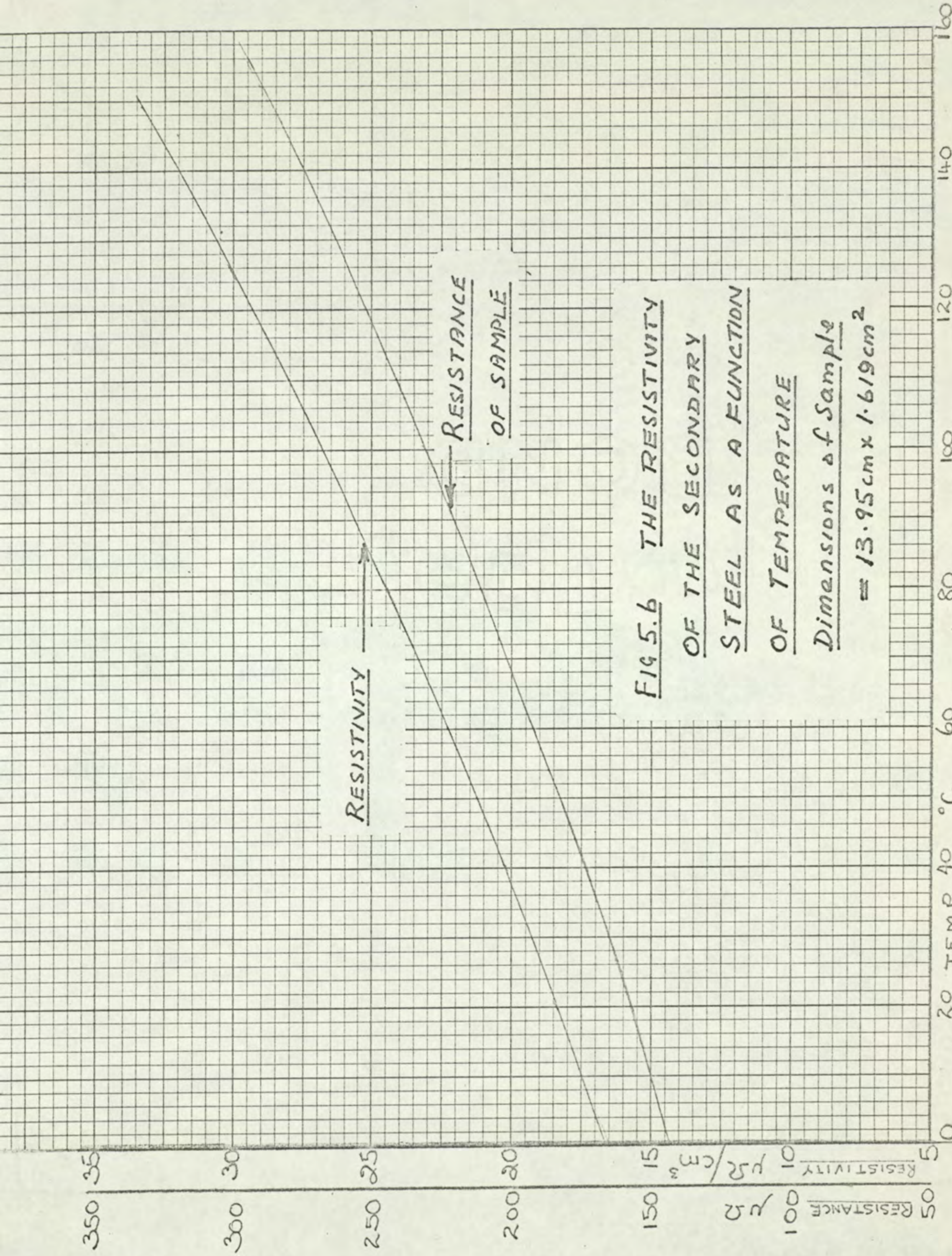

Fig 5.6 THE RESISTIVITY OF THE SECONDARY STEEL AS A FUNCTION OF TEMPERATURE
Dimensions of Sample = 13.95cm x 1.619cm²
RESISTANCE OF SAMPLE
RESISTIVITY
TEMP °C
0 20 40 60 80 100 120 140 160
RESISTIVITY μΩ/cm³
5 10 15 20 25 30 35
RESISTANCE μΩ
50 100 150 200 250 300 350

FIG. 5.6.

5.3.2 Pole Face Loss

The measured input power to the experimental load loss dynamometer was found to very considerably with temperature, Fig.5.7. For this reason investigations into the effects of other parameters were undertaken after the secondary had reached a steady temperature.

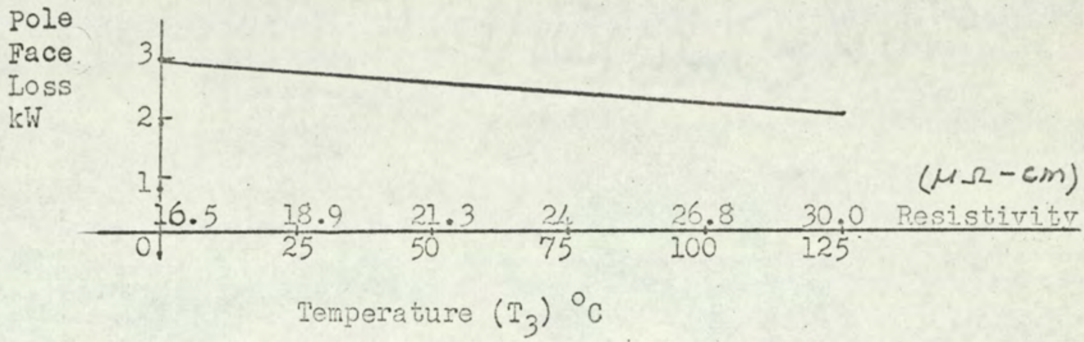

Fig. 5.7 Variation of Pole Face Loss with surface temperature for a primary current of 25 Amp.

Experimental procedure for this test was in accordance with Section 5.8.4

5.4 Primary Current Balance

During the initial tests the three primary currents were found to be unequal, partly due to the three phase variac producing a slight voltage asymmetry. The degree of unbalance was not unduly high, I_B and I_C being within 2% of I_A, the reference current. The importance of phase sequence losses caused by the current unbalance was ascertained by controlling the three currents with three series rheostats. When the primary currents were equalised the change in loss was negligible. It is therefore concluded that a current unbalance of 2% will not adversely affect the experimental results.

5.5. The Magnetisation Curve of the Experimental Load Loss Dynamometer

The magnetisation curve for the experimental machine was obtained by

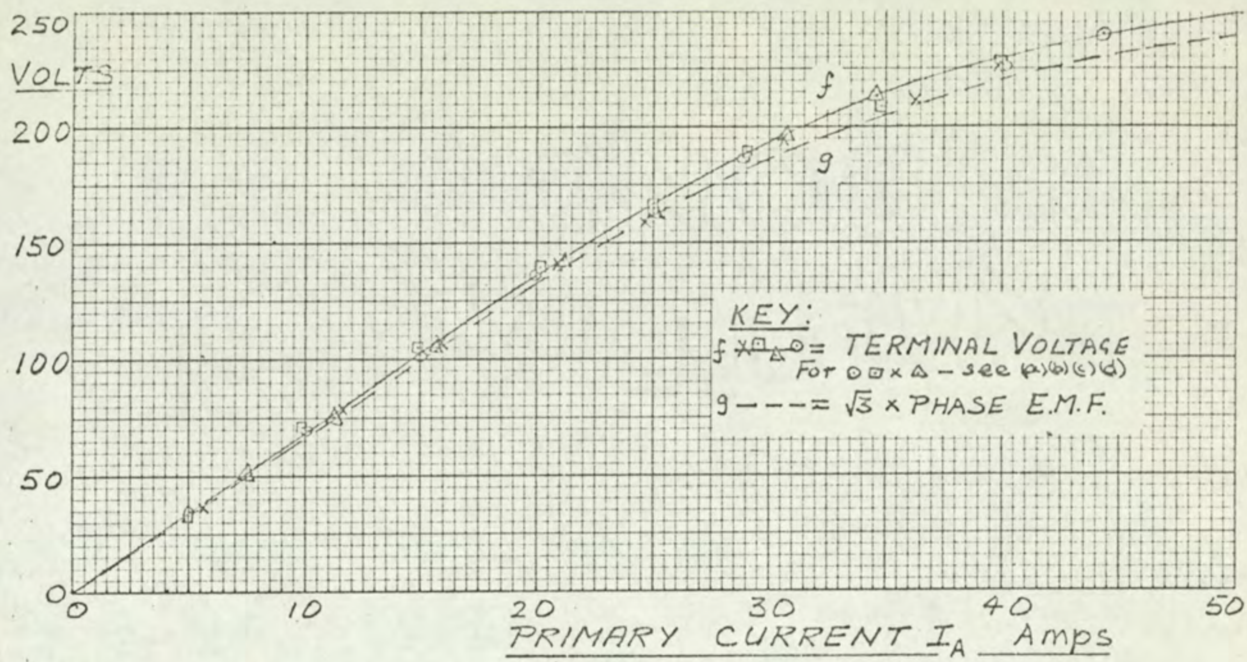

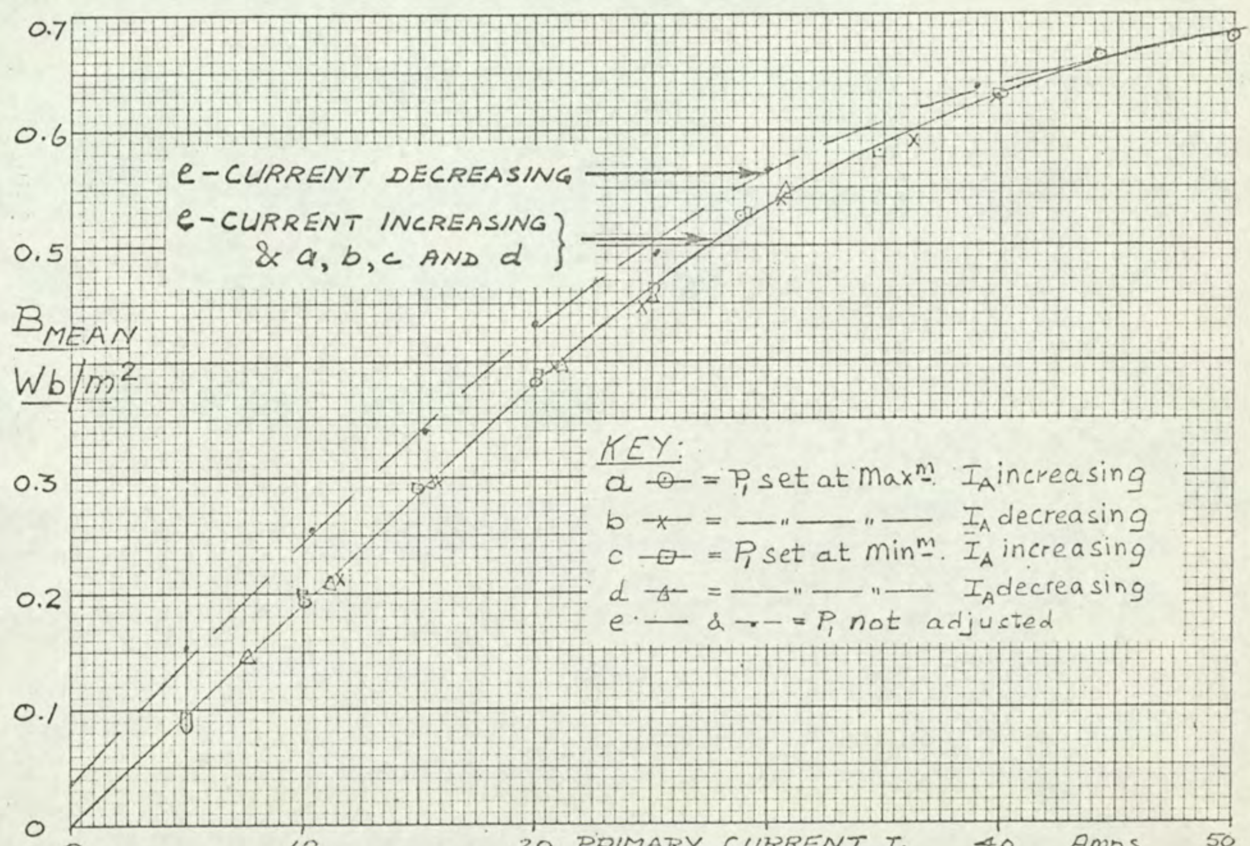

FIG. 5.8. MAGNETISATION CURVES FOR THE EXPERIMENTAL MACHINE

recording the e.m.f. induced in the single turn full pitched primary search coil over a range of primary current. Before taking measurements the secondary was demagnetised by slowly reducing the primary m.m.f. at a very low slip speed. A low (but variable) slip speed was obtained without alteration to the circuit or supply system by reducing the syncage terminal voltage until pole slipping occurred. Zero search coil e.m.f. indicated complete demagnetisation. Fig 5.8(e) shows that

(i) for this machine there is considerable hysteresis if the stator is held stationary throughout the test.

(ii) the curve is linear over $\frac{2}{3}$ of the normal working range (0 - 30 A)

(iii) Rotation of the stator reduced hysteresis to negligible proportions curves (a) to (d).

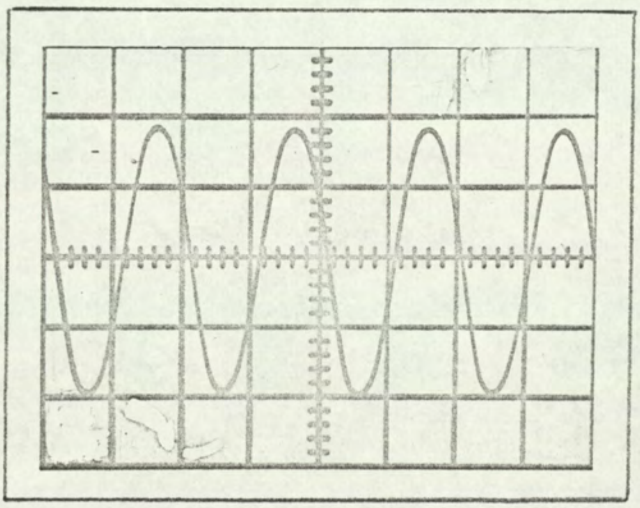

The Primary Search Coil E.M.F. when

I_A = 29 amp

Coil pitch = 180°E

These results were taken during the secondary hysteresis investigation The experimental procedure is detailed in Section 5.10.4.

5.6 Calibration of the Drive Motor

The complete analysis of the losses in the dynamometer, discussed in section 5.11, required an accurate assessment of the mechanical shaft input. The Syncage was therefore calibrated against a swinging frame d.c. dynamometer feeding a resistance load, Fig. 5.9(a).

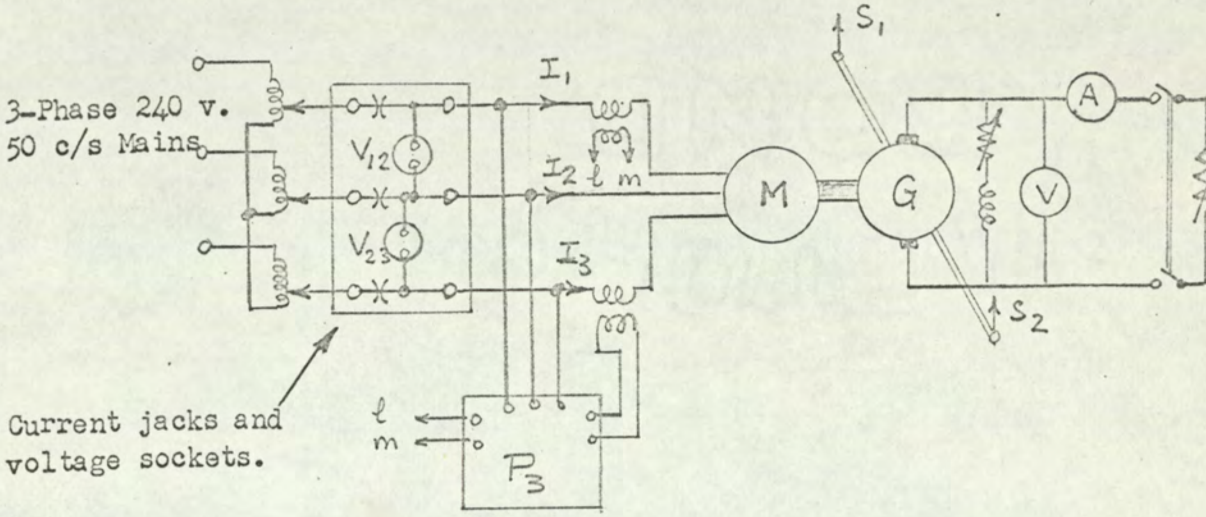

P_3 = 3 phase Wattmeter, previously calibrated.
S_1,S_2 = Salter spring balances, calibrated in place; radius of each Torque arm = 1.00ft.

Fig. 5.9(a) The Circuit Arrangement Used for the Syncage Calibration

The Syncage stator temperature was maintained close to its normal working value, temperature measurements being made by the resistance method for the copper primary winding and by thermometer for the primary core. The flow diagram, Fig. 5. 9(b), charts the subdivision of the various losses in the machine set. The Syncage output, P_4, equals the d.c. dynamometer windage loss plus the power indicated by the torque arm.

Because the accuracy in measuring the windage and friction losses in the d.c. dynamometer was poorer than desired, errors were minimised by taking the mean of two different measurements : -

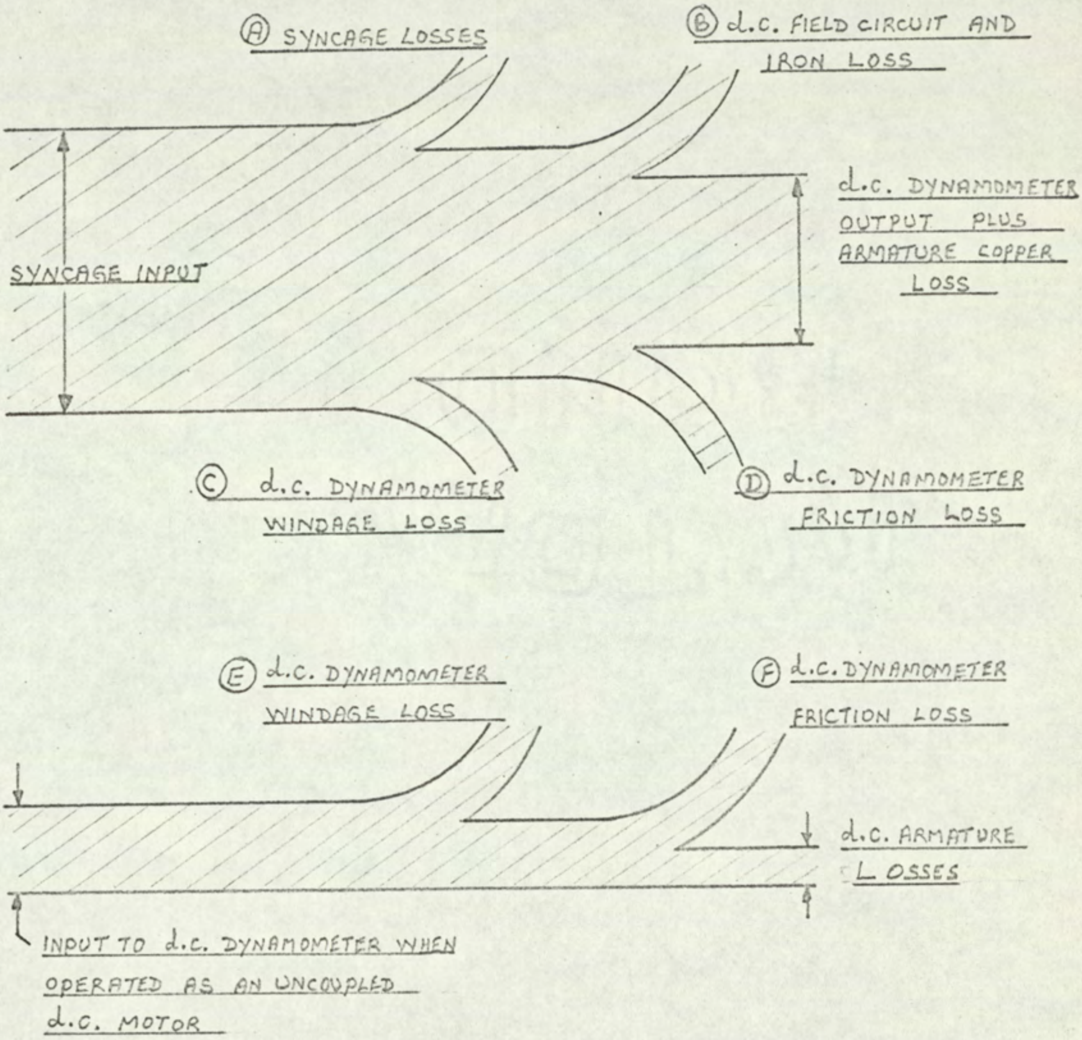

Fig. 5.9(b) Separation of Losses in the Syncage Calibration Test.

(a) With the d.c. dynamometer unexcited and open circuited, the syncage input was measured with the machines (i) coupled and (ii) uncoupled. On the assumption that the syncage losses do not alter significantly between (i) and (ii) the difference in input power gives the windage and friction losses in the dynamometer (= C + D, Fig.5.9(b))

By measurement : C + D = 0.08 kW

(b) With the machines uncoupled the light load loss curve of the dynamometer, operating as a shunt motor, was obtained (Fig. 5.10, overleaf).

Extrapolation to zero gave E + F = 0.066 kW.

The mean Windage and friction loss

$$= \tfrac{1}{2}(\ (C + D) + (E + F)\ )$$

$$= 0.07 \text{ kW}$$

The friction torque (including viscous drag) was obtained with the d.c. dynamometer unexcited on open circuit :

At 1500 r.p.m. the d.c. dynamometer friction loss,

$$F = 0.04 \text{ kW}$$

$$\therefore E = 0.07 - F$$

$$= 0.03 \text{ kW}$$

∴ The syncage output $P_4 = \dfrac{2\,N(S_1 - S_2)}{33000}\,0.746 + 0.03$ kW

$$P_4 = 0.213\,(S_1 - S_2) + 0.03 \text{ kW at 1500 r.p.m.}$$

The family of calibration curves is shown in Fig. 5.11a. The power input includes the power loss in the instruments. The calibration at 240v (drawn through about 20 carefully measured values over the range zero to 135% full load) differs markedly from the manufacturers calibration of this particular machine, which was subsequently disregarded. The difference may be due to changes in bearing friction with age, and in working temperature. Tests on the experimental synchronous load loss dynamometer become meaningful with the new syncage calibration (e.g. Fig.5.12), thereby confirming its accuracy. The limits of accuracy are estimated in section 5.12.

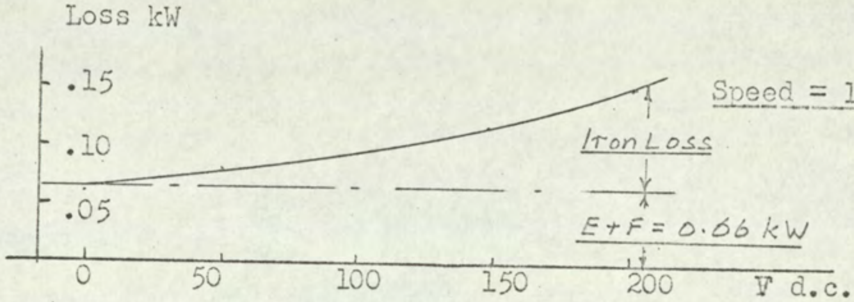

Fig. 5.10 Light Load Loss Curve of the D.C. Dynamometer

5.7 Torque Measurements on the Experimental Machine

The torque on the secondary member was measured at 0.5m radius by a weighing scale reading 0-1kg in 10-gm divisions. A flexible link from the torque arm exerted a downward pull on one pan, kilogram weights being added to the other pan, as required, Figs. 2.6

At the outset of this investigation it was considered that the power losses would be generated in the secondary member of the load loss dynamometer by a mechanical/electrical energy conversion process. The requisite mechanical power, being the product of the torque, T, on the secondary member and the synchronous speed ω of the machine, should be independent of the measuring equipment. Initial tests revealed that for a constant primary current, and constant total input power T varied considerably with

(i) The position of the pointer of the Avery balance, (total angular movement of dynamometer secondary = 1.6°Mech. for full

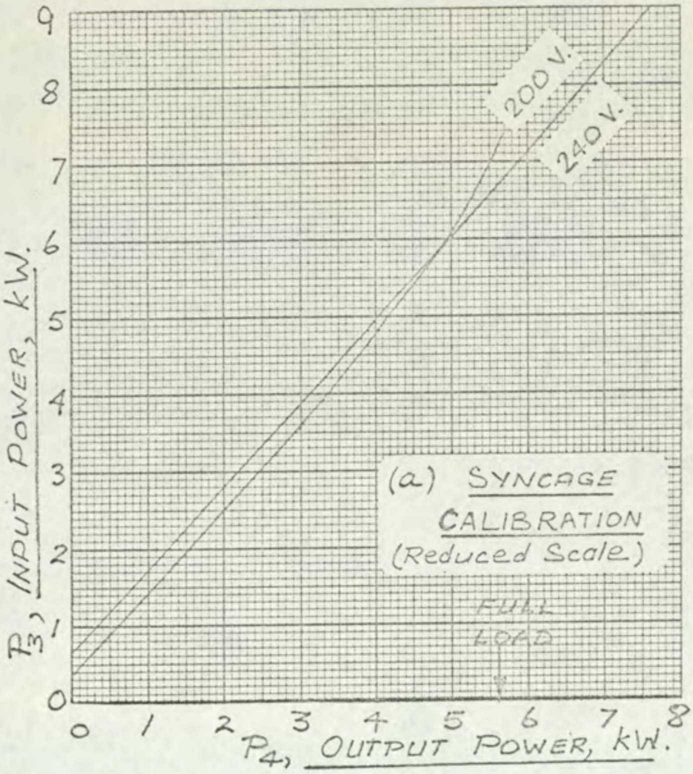

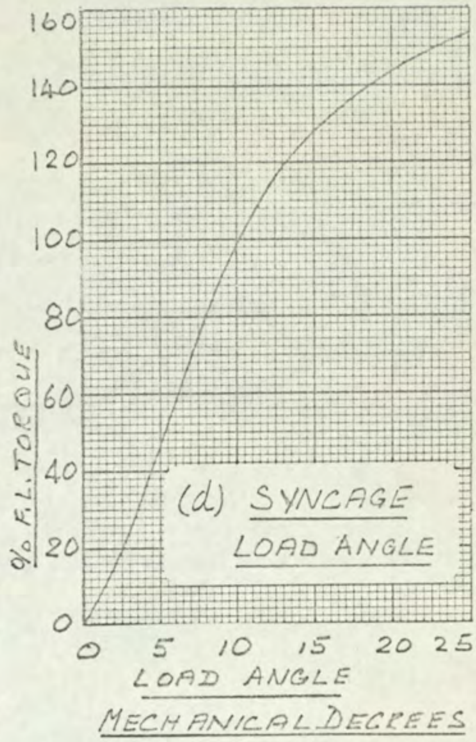

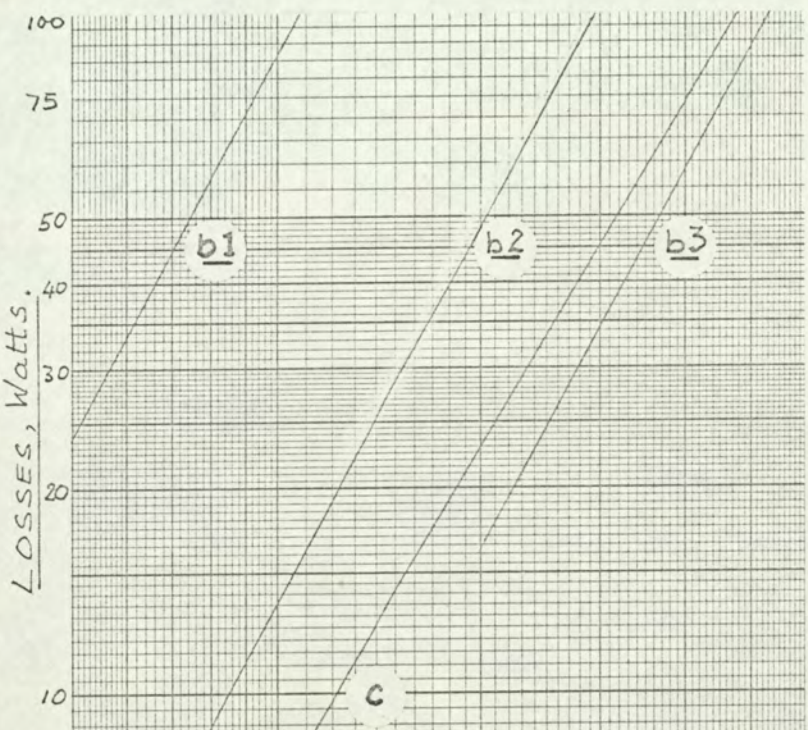

(b) LOSSES IN THE THREE PHASE WATTMETER

b1: 150-V, 10-A. Scale × 0.4

b2: 150-V, 25A × 1

b3: 300-V, 50A × 4

(c) LOSSES IN THE DYNAMOMETER PRIMARY CIRCUIT

FIG. 5.11

THE EXPERIMENTAL MACHINE SET.

CALIBRATION CURVES

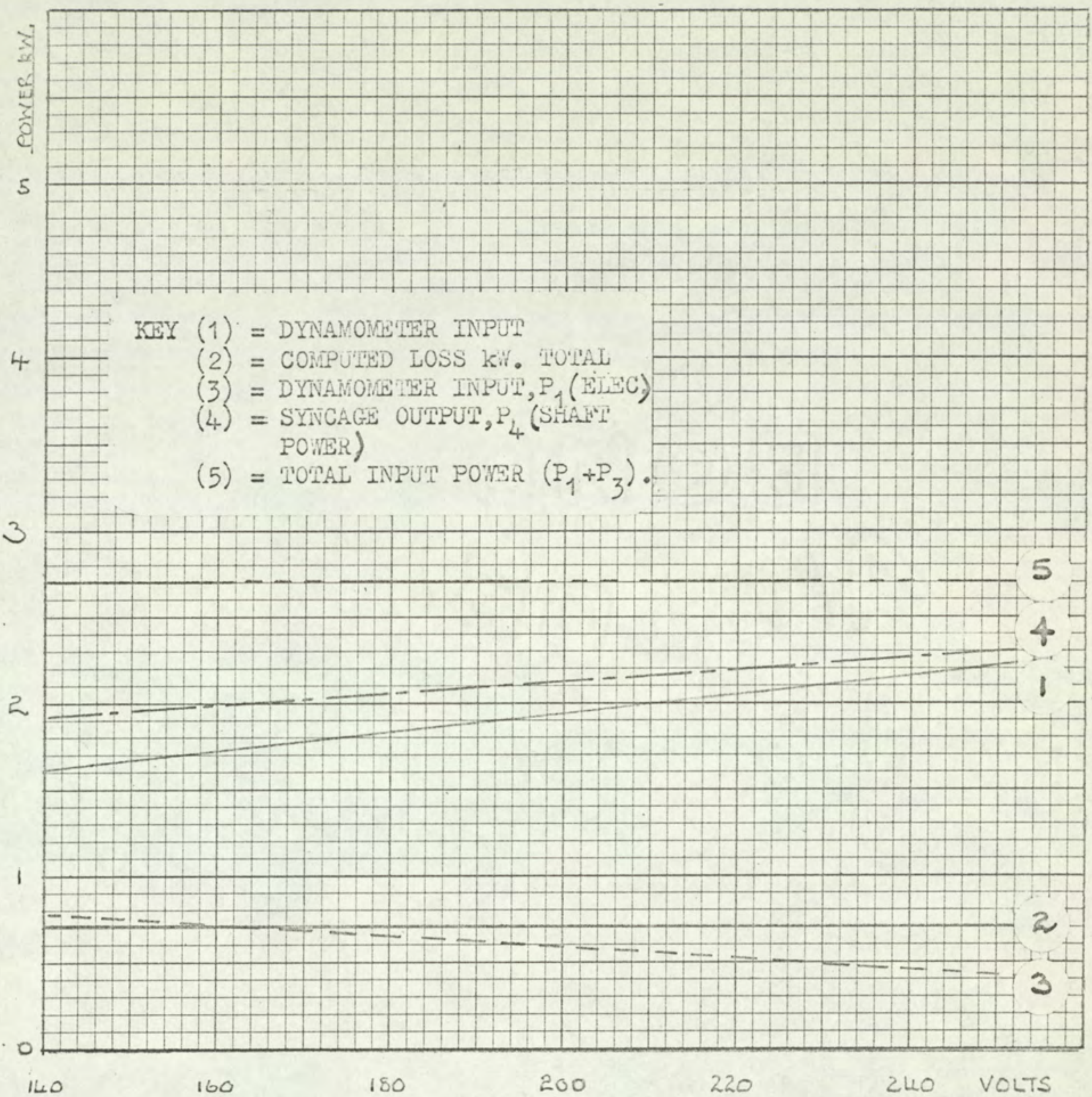

Fig. 5.12. Variation of Power Input to the Experimental Machine with Motor Line Voltage.

Primary current, = I_A = 20 Amp.

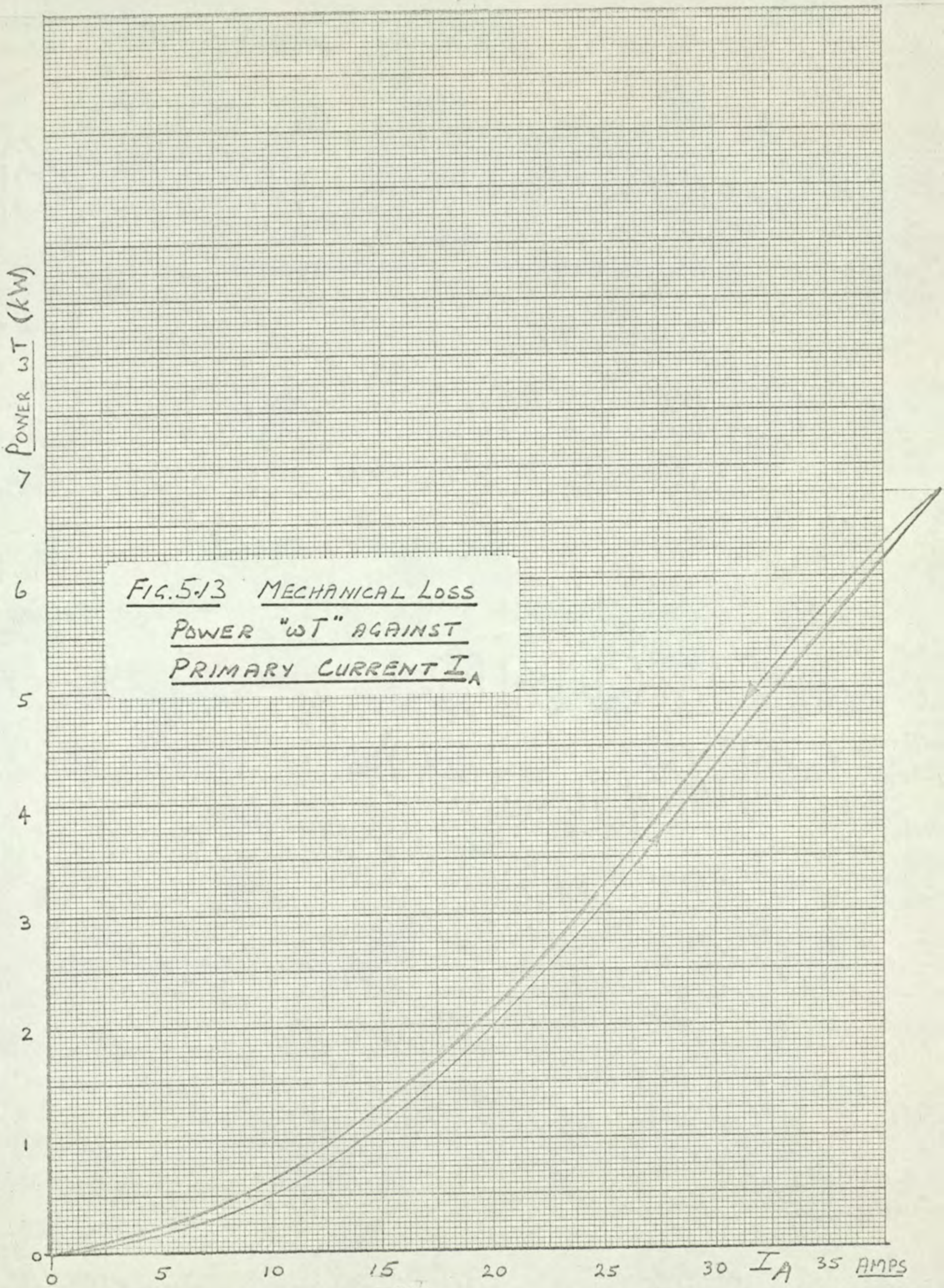

FIG. 5.13 MECHANICAL LOSS POWER "ωT" AGAINST PRIMARY CURRENT I_A
POWER ωT (kW)
0
1
2
3
4
5
6
7
0
5
10
15
20
25
30
35
I_A
AMPS

scale deflection of the balance).

(ii) The syncage terminal voltage, i.e. with a change in the syncage load angle or torque angle, Fig. 5.12.

(iii) Pole Face temperature.

(iv) The electromagnetic history of the load loss dymamometer (Fig.5.11

The reason for the change of T with the various parameters (i) to (iv) is discussed later (sections 5.10).

These fluctuations prompted deeper investigations into the method of measurement. In consequence a method of "loss separation" was used, despite the intrinsic inaccuracy of a "difference" method of calculation. The use of trunnion bearings caused the dynamometer bearing friction torque and viscous drag torques to be included in the measured torque. Since the brushes are mounted on the bedplate the brush friction torque is not included. The power "ωT" therefore equals the difference between P_4 and the load loss dynamometer windage and brush friction losses. This relationship between ωT and P_4 is confirmed by the variable voltage test, Fig 5.12 and the loss/slip test, section 5.9.2.

Using the loss figures of section 5.8.1. we can write

$$\omega T = P_4 - 0.12 \text{ Watts at 1500 r.p.m.} \qquad (5.1)$$

At 1500 r.p.m. P_4 is determined from the calibration curve (Fig 5.11) but under any other non-calibrated condition P_4 can be ascertained simply by measuring the torque and assessing the appropriate windage and friction losses. If $\omega < 25$ rad/sec.(Mech) the friction losses are reduced in proportion to the speed and the windage loss to some power of the speed (e.g. speed^2), the precise value of the index being unimportant because of the small magnitudes involved.

The torque arm has been used in this test to determine the mechanical losses of the dynamometer at low voltage and in tests at other speeds, reported later, to calibrate the syncage drive in situ.

5.8 The Separation of Losses in the experimental machine

The losses in the machine set were subdivided under the various headings indicated in Fig. 5.15. This section describes how all these losses were determined experimentally. Before each test the dynamometer was allowed to reach working temperature at rated speed with a primary current of about 15 Amps., and then demagnetised in the manner described in section 5.5

5.8.1 Windage and Friction Losses

The shaft input to the unexcited dynamometer in Table 5.1 is the sum of the windage loss and friction loss. With the brushes raised the shaft input fell by 0.10 kW.

From the measured torque and the calibrated syncage output power the friction loss was calculated directly, the windage loss by subtraction, as follows :

Table 5.1 Dynamometer Mechanical Losses

Primary current = 0

Syncage Terminal Voltage	V_{12} (v)	240	230	220
Syncage Input Power	P_3 (kW)	0.85	0.75	0.69
Syncage output power	P_4 (kW)	0.20	0.20	0.20
Spring Balance Pull	F (kg)	0.100	0.100	0.105

P_4 can be read from the calibration curve to within ± 0.01 kW

The Windage + Brush Friction + Bearing Friction = P_4 = 0.20 kW

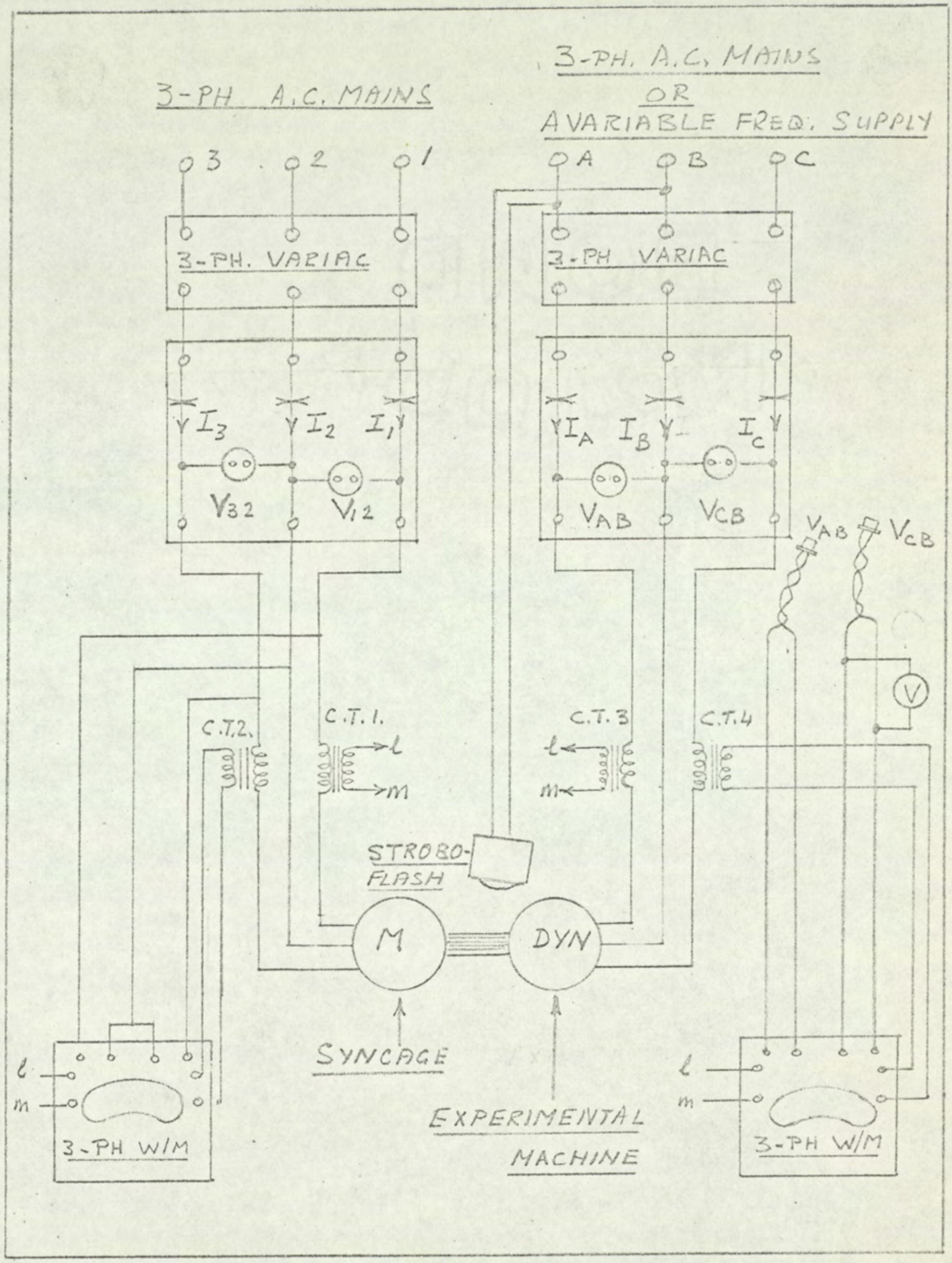

FIG. 5.14. CIRCUIT USED FOR LOSS TESTS AND SLIP TESTS

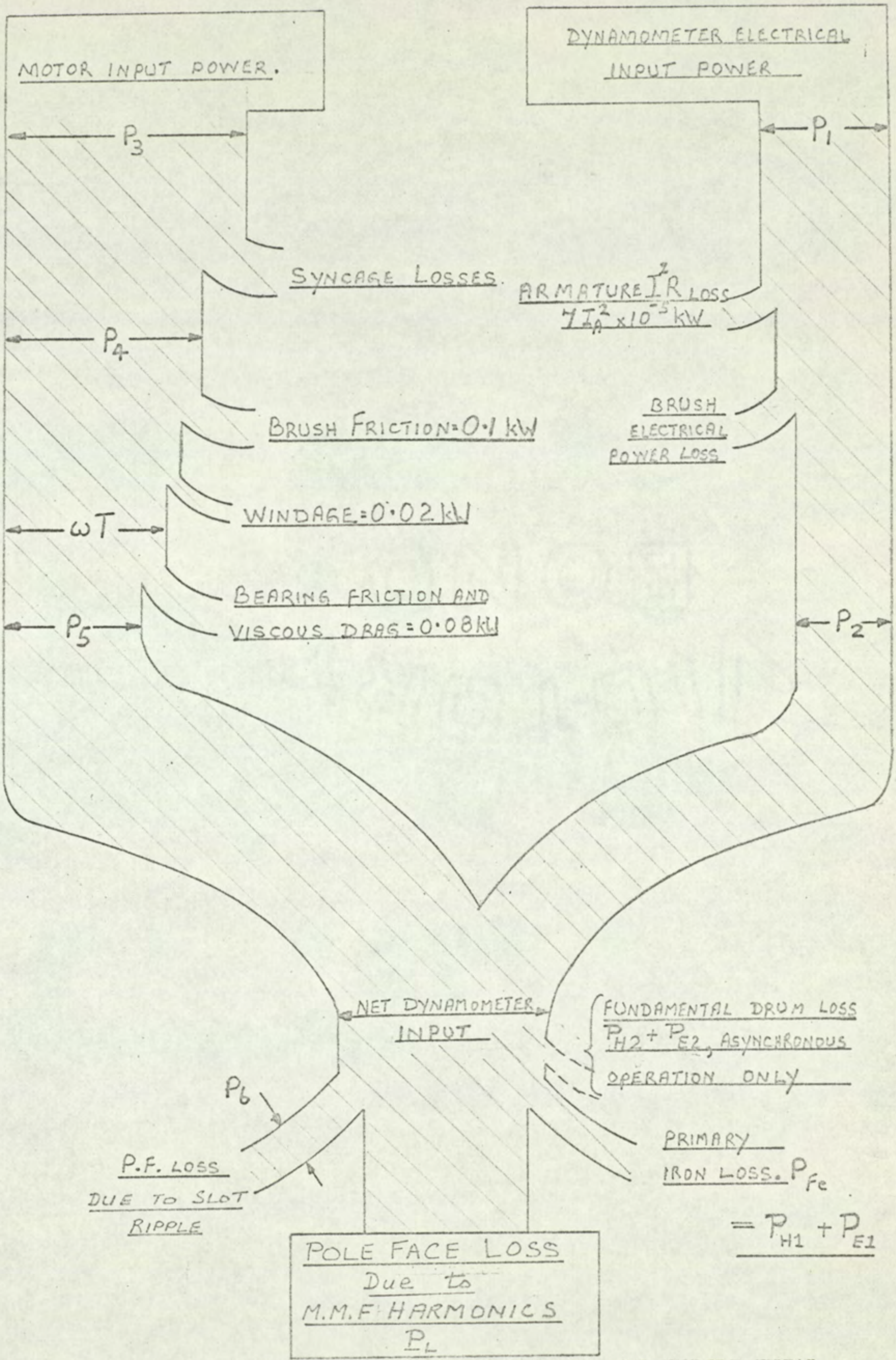

FIG. 5.15. THE SEPARATION OF THE LOSSES IN THE EXPERIMENTAL MACHINE SET.

The Mean Bearing Friction (including viscous drag, equation 4.2)

$$= \omega T = 0.771F = 0.771 \times \frac{0.305}{3} = 0.078 \text{ kW}$$

Brush Friction (by test) $\approx$ 0.10 kW

$\therefore$ Windage (by subtraction) = 0.02 kW

5.8.2 Primary Circuit Losses

The copper loss in the primary winding and the brush loss were quite small, the winding and slip rings being grossly over-rated (section 4.2 (ii)(1)). The winding resistance of each phase, indicated by the "Ducter" ohmmeter, was recorded at ambient temperature and after the secondary had reached a steady surface temperature of 100°C; the brush loss is calculated from manufacturer's data. The total primary circuit loss is given in Table 5.2 and plotted in Fig.5.11(c)

The Average Winding Resistance

Cold $R = 0.0183$ ohms/phase at 20.0°C.

Hot $R = 0.0210$ ohms/phase at a secondary temperature of 100°C

$\therefore$ The primary copper loss when star connected is

$= 3 \times I^2_A \times 0.0210 \times 10^{-3}$ kW

$= 6.3\ I^2_A \times 10^{-5}$ kW (hot)

The Brush Volt-Drop

The manufacturer's curves relate the volt drop between brush and slip ring to current density. Each brush is 16 mm. x 20 mm. in section, type CM3H.

$\therefore$ Total brush area per slip ring $= 2 \times \dfrac{16 \times 20}{25.4 \times 25.4} \simeq 1.0$ sq.in

Total brush loss $= 3 \times I_A \times (\text{volt drop}) \times 10^{-3}$ kW

Table 5.2 Primary Circuit Losses

Line current	Amp.	10	20	40	60		
Current density	A/sq.in	10	20	40	60	80	100
Volt drop	volts	0.260	0.305	0.325	0.340	0.350	0.360
Brush loss	kW	0.008	0.018	0.039	0.061		
Copper loss	kW	0.006	0.025	0.100	0.227		
Total	kW	0.014	0.043	0.139	0.288		

5.8.3 Iron Losses

These comprise :

(a) The loss in the pole face due to (i) the m.m.f. harmonics P_L (ii) The slot ripple, P_6, and (b) the primary iron loss, P_{Fe}. The primary iron loss was assessed experimentally by testing asynchronously - ref. sections 5.9.1. and 5.9.2. The slot ripple loss in the solid secondary was calculated in Appendix 12.6 using Gibbs[9] method. The only remaining loss is the armature current generated component of the secondary surface loss. This is obtained by subtracting the above losses from the total power supplied to the dynamometer.

5.8.4. Experimental Procedure

After checking the appropriate zero readings the syncage was started on reduced voltage and on no-load. Judicious increase of syncage voltage to 240V ensured the correct positioning of the dynamometer standing flux relative to the secondary, the syncage pulling into synchronism at a predetermined rotor position.

The dynamometer current was then adjusted to a suitable value to allow the temperatures to stabilise. Oscillograms of the primary search coil

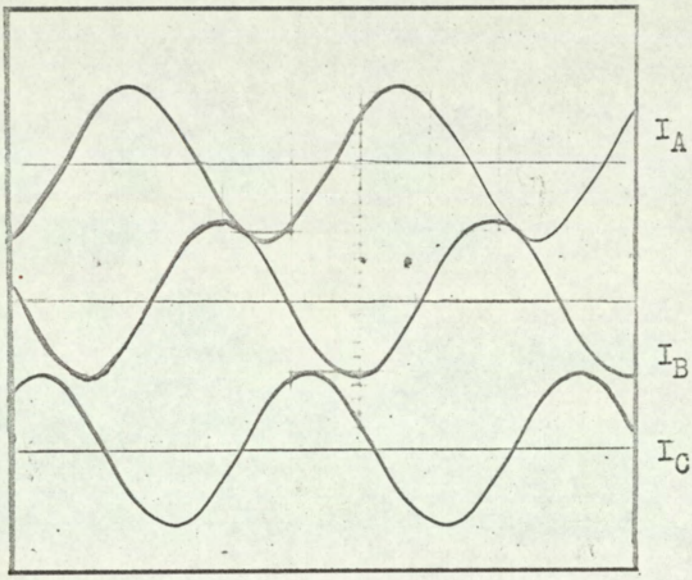

Fig. 5.16. PRIMARY CURRENT WAVEFORMS

I_A = 30.0 Amp.

e.m.f.(Section 5.5) and the three line currents (Fig.5.16) were taken.

The primary current balance was checked.

For the initial tests a surface temperature of 55 to 60°

(outer shell $\triangleq$ 45°C) was considered suitable, since this temperature could be approached fairly quickly and easily from either cooler or hotter conditions.

For the later tests, when the machine was overloaded, it was considered more suitable to stabilise the air gap surface temperature at 100°C. All other measurements were recorded with the surface temperature as near as possible to 100°C and in no case outside the range 95-105°C. Instrument readings are recorded section 5.11. and the losses separated by the method outlined below. The nomenclature is given Fig. 5.15

(1) P_1, P_3 measured.

(2) $P_2 = P_1$ - Primary circuit and meter losses Ref. Fig.5.11. (b) and (c).

(3) P_4 read from syncage calibration Fig.5.11.(a)

(4) $P_5 = P_4$ - Mechanical losses (0.2.kW at 1500 r.p.m.)

(5) P_{Fe} read from Fig. 5.25 at 50 c/s, 100°C.

At other frequencies and temperatures P_{Fe} is determined by slowly rotating the secondary core as described in section 5.10.4

(6) P_6 read from Fig.5.28 at 50c/s.

At other frequencies P_6 is calculated by the method given in Appendix 12.6

(7) The net dynamometer input is then $P_2 \pm P_5$.

(8) The unwanted iron losses are $P_6 + P_{Fe}$

(9) The Required Pole Face loss due to the m.m.f. harmonics is therefore :-

$$P_L = (P_2 + P_5) - (P_6 + P_{Fe})$$

Alternating method using the Torque Arm

Applying the argument of paragraph 5.7 and realising that T includes bearing drag only, at any speed N the gross shaft input power to the dynamometer is :

$P_4 =$ (indicated torque $\times\,\omega$) + brush friction loss + windage loss.

$$\text{i.e. } P_4 = \omega T + 0.1\ \frac{N}{1500} + 0.02\left(\frac{N}{1500}\right)^2 \qquad (5.2)$$

The net shaft input power (which supplies the electrical losses) is:

$P_5 = P_4$ - brush friction loss - windage loss - bearing friction loss

$\quad =$ (indicated torque $\times\,\omega$) - bearing friction loss

$$\left.\begin{aligned} \text{i.e. } P_5 &= P_4 - 0.18\ \frac{N}{1500} - 0.02\left(\frac{N}{1500}\right)^2 \\ &= \omega T - 0.08\ \frac{N}{1500} \end{aligned}\right\} \qquad (5.3)$$

5.9 Asynchronous Operation

The aim of this test series, in which the standing flux was allowed to rotate very slowly at a known speed, was (i) to investigate the changes in torque mentioned in section 5.7 and (ii) to assess the primary core loss.

5.9.1 Loss/slip curves at constant primary current

The additional nomenclature is given in Figs. 5.14 and 5.15. Under asynchronous conditions the load loss dynamometer behaves as a solid secondary induction motor, in either the motoring or generating

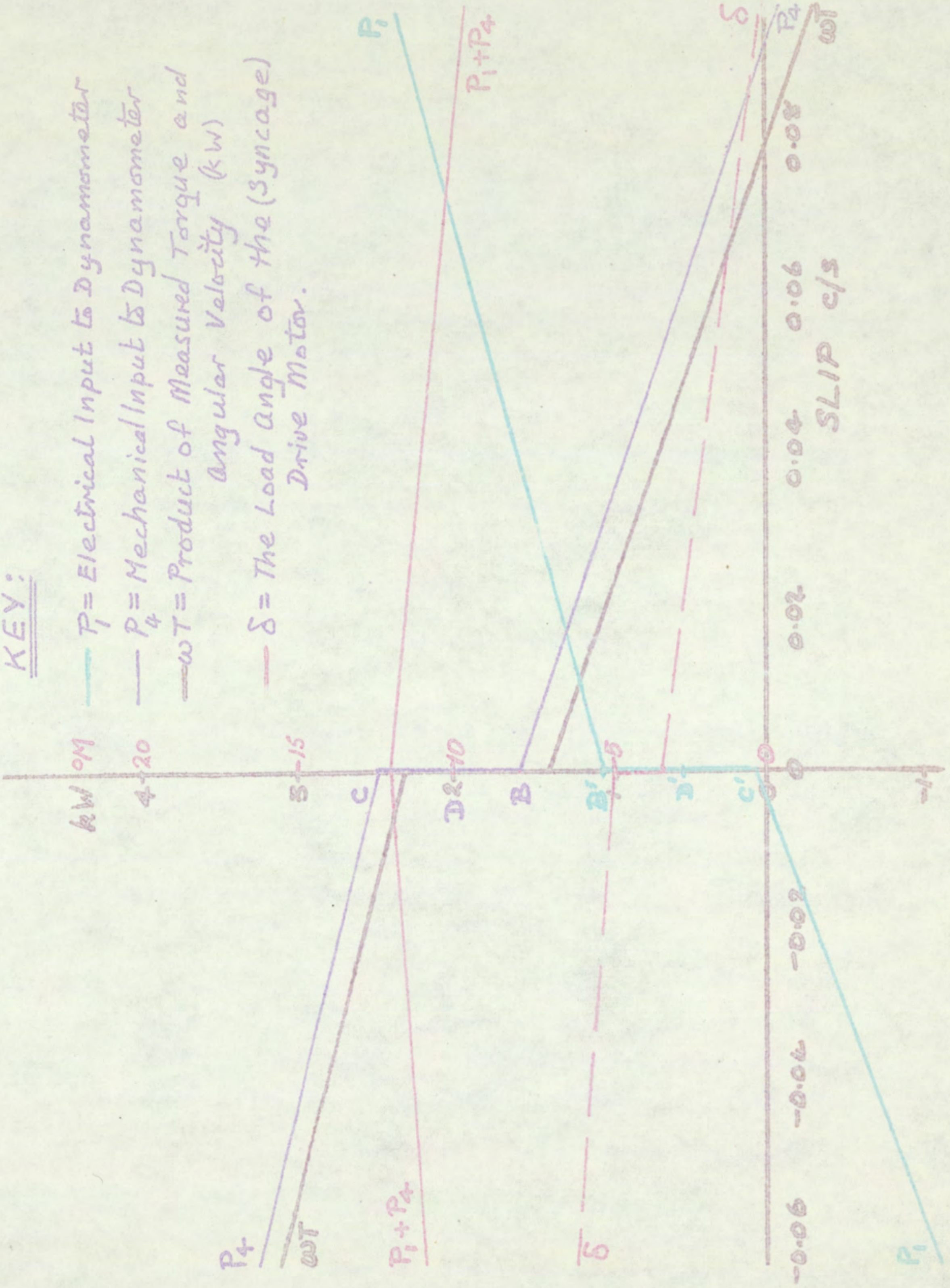

FIG. 5.17. THE ASYNCHRONOUS TEST

Primary Current = 20 Amp 50 c/s

mode, depending on whether the slip ($s = (f_1 - f_{syncage})/f_1$) is positive or negative. The test series was performed with the dynamometer supplied from the a.c. mains and the syncage from a variable speed d.c. motor - alternator set. This arrangement made it possible to transmit power in either direction through the system. In passing through synchronism (s becoming positive) the net dynamometer input power increased and the shaft input decreased by an equal amount, Fig. 5.17. Both the slip speed and the change in syncage load angle at zero slip were measured by the stroboscope triggered from the dynamometer supply. When the syncage output had been reduced to point B, the secondary fundamental remanence torque had reached its maximum value. Further reduction of P_4 (by increase of the d.c. motor excitation) resulted in a fall in shaft speed causing the standing flux to rotate very slowly past the dynamometer secondary. Slip frequency currents induced by the rotating fundamental flux produced a fundamental shaft torque restoring the mechanical power approximately to its former level at a new rotor speed.

Under these conditions the slip was positive, the fundamental torque acting on the secondary in the direction of the slip speed (i.e. in the same direction as the fundamental primary rotating m.m.f.) thereby reducing the measured torque, Fig. 5.17. The reaction torque acts on the primary against the direction of the fundamental rotating m.m.f. i.e. in the direction of rotation and therefore supplements the shaft torque. Further increase in slip will eventually cause the syncage to regenerate.

Conversely, on reducing the d.c. motor excitation synchronism is lost at point C and the dynamometer behaves as an induction generator having negative slip, the fundamental primary torque reverses and the shaft torque increases. The results are similar to those of the "Linke Test" discussed by Rawcliffe and Menon[12] on a slip ring induction motor with an open-circuited secondary. In such tests (which are considered in more detail in section 5.13) the primary a.c. input power P_1, and the shaft input power, P_4, suddenly change by twice the magnitude of the fundamental hysteresis power associated with the secondary remanence torque. The value of shaft input power at the mid point of its "step" was confirmed by Rawcliffe and Menon to be the sum of the friction and harmonic frequency losses. It is important to note however that they considered the space harmonics in the primary field negligible. Their results cannot be applied to our experimental machine tests here without considering the nature of loss caused by the space harmonics. Furthermore their sV^2 test is also inapplicable here since the load loss dynamometer secondary cannot be open circuited.

The results of the loss/slip tests on the experimental machine should only differ from those of reference 12 by virtue of the exaggerated harmonic m.m.f. losses in the experimental machine. These are shown in section 12.7 to have the nature of a mechanical loss. From tests conducted by the author on a slip ring induction motor it was concluded that the primary iron loss is supplied via the primary winding not via the shaft. The evidence available at this stage therefore, in the load loss investigation, indicated that

(i) the step B C (= B^1 C^1) is twice the fundamental hysteresis power.

(ii) the mid point D^1 of B^1 C^1 on the a.c. input curve P_1 is the sum of the primary iron loss and the primary circuit losses. Further evidence

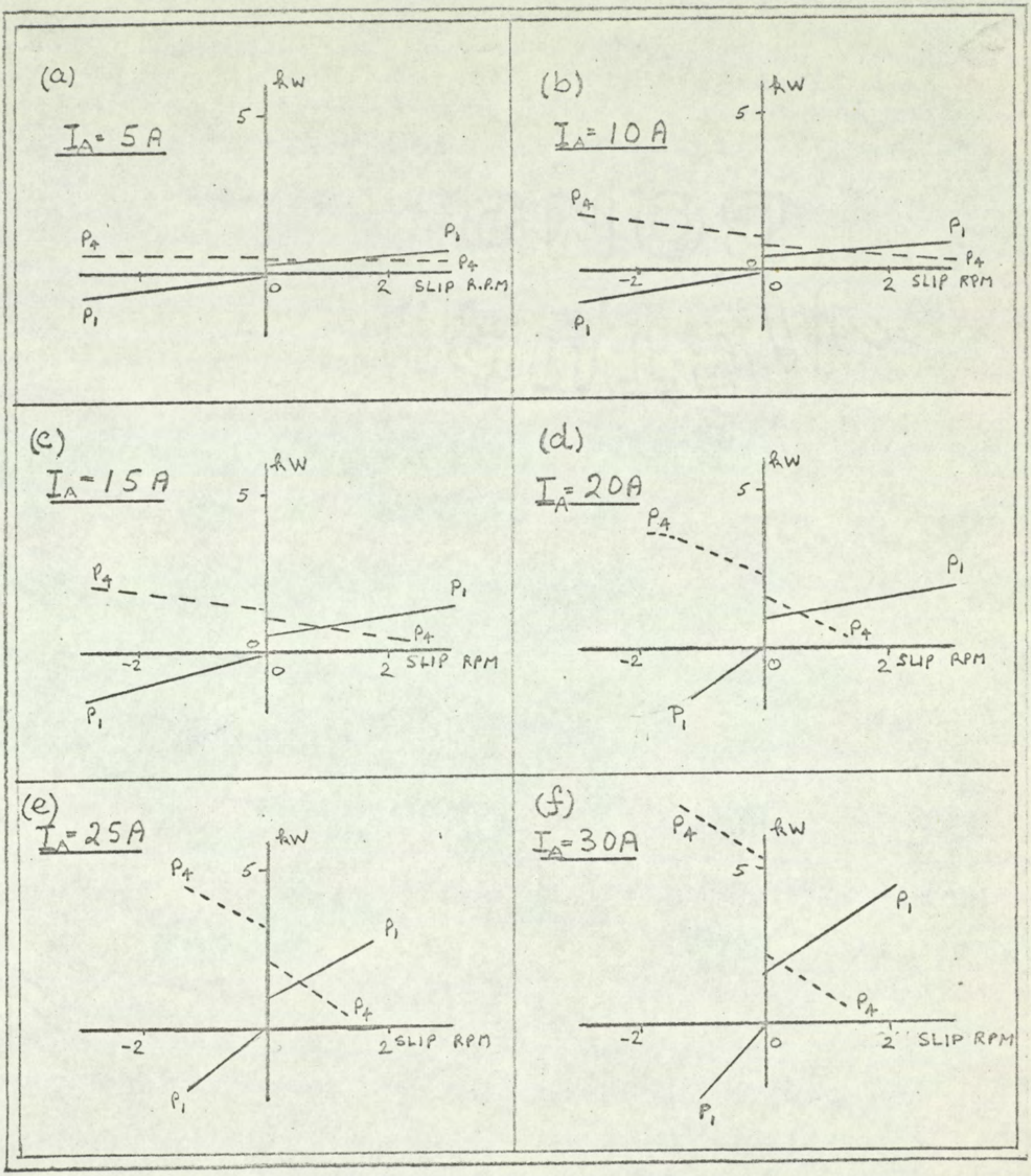

The variation of mechanical input power, P_4, and the electrical input power, P_1, as the shaft speed passed through synchronous value (slip = 0).

Fig. 5.18 The Asynchronous Test Series on the Experimental Machine in support of this theory can be found in sections 5.10.3.

(iii) The mid point D of BC equals the losses supplied by mechanical shaft power i.e. friction, windage, m.m.f. harmonic, and slot ripple losses.

5.9.2. Primary Current Variation

The above test was repeated for a range of constant values of primary current from 5 to 30 Amp. Fig. 5.18(a) to (f). The advantage of keeping the current constant for each test was that the m.m.f. losses could then be assumed constant. The primary standing flux (and primary search coil e.m.f.) consequently changed slightly with slip as the dynamometer power input and power factor changed, Fig.5.17, thereby altering the primary core loss slightly. However the curves of power and e.m.f. were reasonably linear and were therefore extrapolated to the zero slip axis to enable the values of B, B^1, C ... etc. to be determined for each current value. Care was taken to ensure a reasonably constant temperature on the secondary surface (between 50 and 70°C). Both wattmeters were read simultaneously and their average readings over the time interval required for slip measurement recorded. (Points B, B^1, C, C^1 were eventually retaken at 100°C)

The fundamental secondary hysteresis power P_{h2}, and the primary iron loss P_{Fe}, were then estimated from these results :

$$P_{h2} = \text{average of } \tfrac{1}{2}\,BC \text{ and } \tfrac{1}{2}\,B^1C^1$$

$$\underline{P_{h2} = \tfrac{1}{4}\,(BC + B^1C^1)}$$

$$\text{AND} \quad P_{Fe} \; \underline{= \tfrac{1}{2}(OC^1 + OB^1) \text{ minus the primary circuit losses.}}$$

5.9.3 Comments

In each of the above slip tests (Fig.5.18) the dynamometer input P_1

passed through or close to the origin (OC^1 = zero), indicating a primary core loss equal to the fundamental secondary hysteresis power. This unusual result was treated with considerable suspicion. The Primary iron loss was therefore examined more closely (see 5.10 and 5.11) before the above method of calculation was adopted. When operating synchronously, the syncage load angle increased with dynamometer excitation, Fig. 11 d, thereby causing a small but noticable remanence torque to exist. The operating point A moved from the mid point of BC to an indeterminate position just above A, the measured torque giving no direct indication of the surface loss. The variation of torque with relative movement of secondary and primary mains field is now considered in more detail in the next section.

5.10 Fundamental Secondary Hysteresis

Further investigation was made into the hysteresis phenomena of the standing (fundamental) flux in order to explore

(i) The fluctuations in measured torque, and

(ii) The apparent equality between the primary core loss and the fundamental hysteresis power. Tests on the experimental machine with torque arm removed were made (i) over a range of primary current at rated frequency, and (ii) over a range of frequency at constant current. Loss/slip curves, also taken on a standard slip ring induction motor were used to verify that work by previous authors [12] on stator fed induction machines was equally valid when the machines were rotor fed at non-rated frequencies with the stator short circuited.

5.10.1 Rated Frequency and Constant Current.

For a constant primary current of 12 amp the power inputs P_1 and P_4 were determined as the angular position of the secondary was gradually changed w.r.t. the standing field. All readings were taken with the drum locked in its new position and with standing flux stationary. This entailed waiting a few seconds while the flux moved to its new position. Special care was taken to avoid recoil loop effects.

The angular position of the secondary, θ_2 was considered positive when the secondary was rotated in the same direction as the shaft rotation, (equivalent to a positive slip). θ_2 was measured relative to the frame of the set. The syncage load angle was thereby compensated for and did not enter into the measurement of θ_2. As θ_2 decreased at constant current P_2 fell gradually from its initial value at A^1(Fig. 5.19) to a lower value at E^1 and remained constant until the rotation was reversed. P_2 then increased along $C^1 F^1$ to a maximum value $F^1 B^1$. This maximum value OB^1 was maintained until the direction of rotation was reversed. When this happened P_2 decreased along such a curve as B^1G^1.

FIG 5.19

HYSTERESIS TEST

f = 50 c/s

I = 20 A.

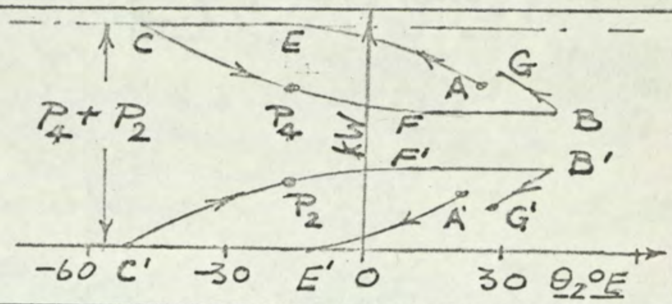

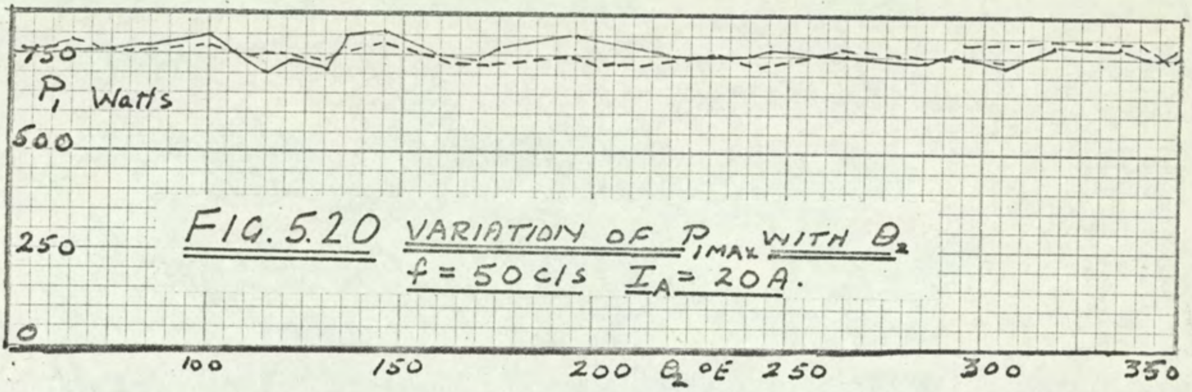

FIG. 5.20 VARIATION OF P_{1MAX} WITH θ_2

f = 50 c/s I_A = 20 A.

The shaft input P_4 followed a similar curve, AECFBG. Changing θ_2 only altered the distribution of loss between P_2 and P_4, the total dynamometer iron loss, $P_2 + P_4$ being unaffected.

The ordinates OB^1, OC^1, OB and OC were equal to those ordinates so labelled on the Power/Slip curves of Fig. 5.17. Obtaining the ordinates this way is much simpler than by the asynchronous test. This method therefore became part of the standard procedure. The repeatability of the results was checked and found to be reasonably satisfactory over a wide range of θ_2 - Fig. 5.20. Fluctuations in the graph were probably caused by mechanical movement of the secondary clamping equipment (which has since been reconstructed) and by mains voltage fluctuations.

The variation in secondary remanence power over a wide range of primary current is shown in the log-log graph of Fig. 5.27, plotted from the results tabulated in section 5.11.1. Analysis is beyond the scope of this thesis.

5.10.2. Variation with Frequency

The asynchronous tests of section 5.9 indicated that the remanence power P_{h2} equalled the primary iron losses at 50 c/s. A change in synchronous frequency, f_1, might be expected to alter this parity since :

The secondary remanence power, $P_{h2} \propto f_1$

The primary hysteresis loss, $P_{h1} \propto f_1$

The primary eddy current loss, $P_{e1} \propto f_1^{\ 2}$

The secondary fundamental eddy current loss, P_{e2} = zero since synchronous operation was maintained at all frequencies.

The pole face losses are proportional to some power of frequency.

Assuming that the primary eddy current and hysteresis losses are of the same order, any reduction in frequency would therefore be expected to cause a greater drop in primary iron loss than in the secondary remanence power. Should this be the case OC' would become negative between f_1 = zero and 50 c/s. The converse would apply on increasing the synchronous frequency.

Experimental investigation followed the procedure outlined in the previous section except that only the points B, B', C and C' were recorded. The supply frequency to both machines increased in steps from 10 to 60 c/s. $P_{1\ max}$, P_{1min}, P_{3max}, P_{3min} are tabulated in sections 5.11.2.

A hysteresis loop was taken at 40 c/s as a spot check on the validity of this approach (Fig. 5.21.)

The torque arm was then attached and used to calibrate the motor for the particular values of speed and P_3 previously noted.

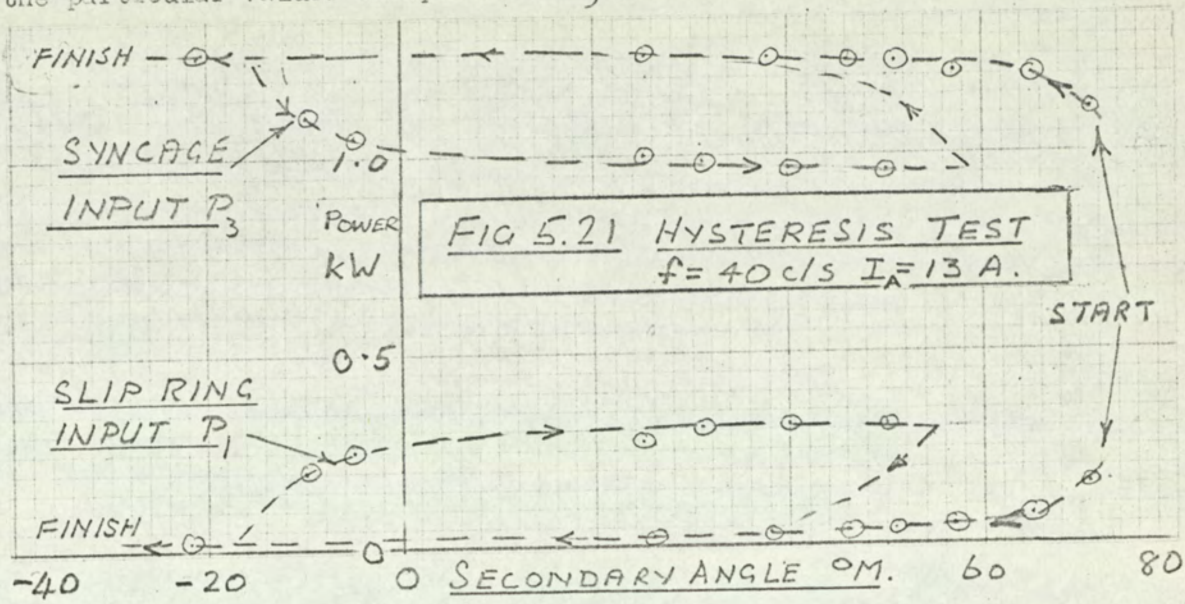

P_5 was then calculated from eqn. 5.3. The measurements so obtained contain sufficient information for the calculation of the pole face loss. Graphs of derived results germane to this section are plotted overleaf in Figs. 5.22 and 5.23. Note that the intercept OC' (= P_{1min}) did not become negative. The slopes of the log-log graphs reveal that :

(a) $P_{h2} \propto f_1^{1.07}$

(b) $P_{fe} \propto f_1^{1.06}$

Proportionality (a) confirms that $P_{h2} \propto f_1$ and proportionality (b) indicates that the primary hysteresis loss is much greater than the eddy current loss. This may be due to the flux density being well below saturation ($B_{mean} \doteq 0.4$ Wb/m^2). The proportionality (b) would also indicate why OC' did not become negative. Direct comparison with the asynchronous test is not possible because these tests were performed at a higher surface temperature using a refined method of measurement.

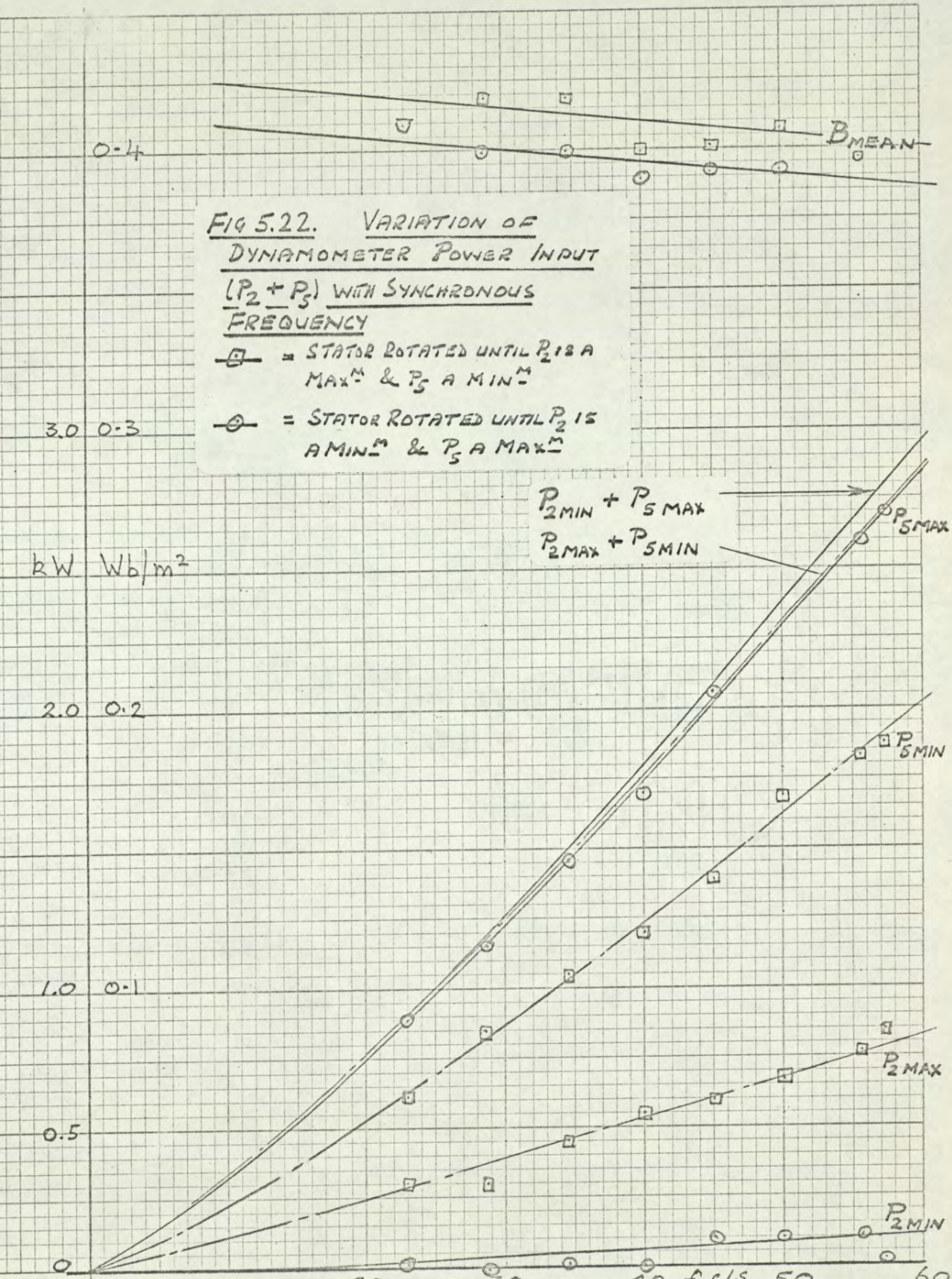
Fig 5.22. Variation of Dynamometer Power Input ($P_2 + P_5$) with Synchronous Frequency
= Stator rotated until P_2 is a Max^m & P_5 a Min^m
= Stator rotated until P_2 is a Min^m & P_5 a Max^m
B_{MEAN}
$P_{2MIN} + P_{5MAX}$
$P_{2MAX} + P_{5MIN}$
P_{5MAX}
P_{5MIN}
P_{2MAX}
P_{2MIN}
kW Wb/m^2
3.0 0·3
2.0 0·2
1.0 0·1
0.5
0·4
0
10
20
30
40
50
60
f c/s

FIG. 5.22

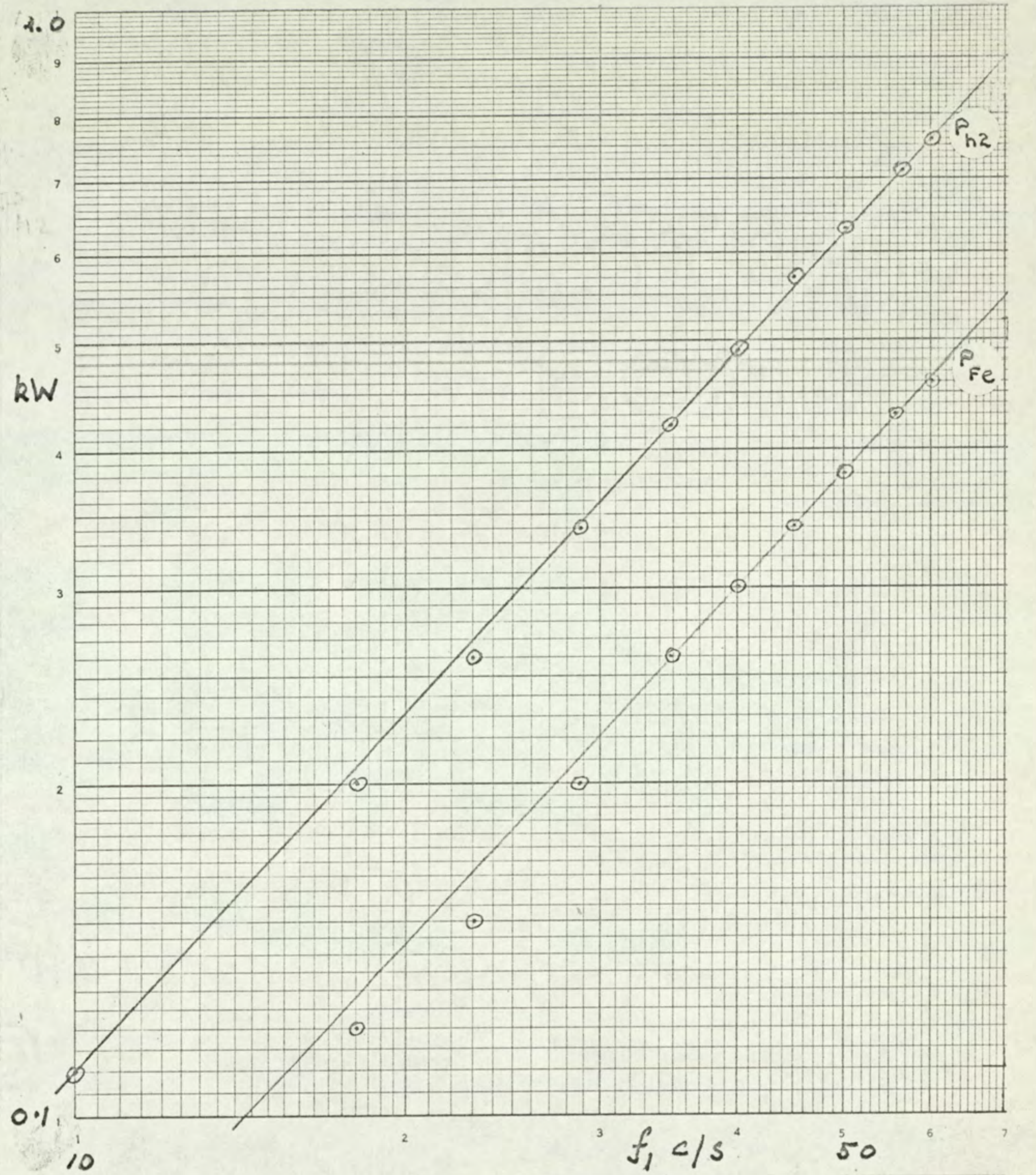

FIG. 5.23. SECONDARY HYSTERESIS AND PRIMARY IRON LOSS — VARIATION WITH FREQUENCY (20 AMP, 70°C)

5.10.3. Hysteresis with a Stationary Secondary

It is now possible to comment on the preliminary tests where the power 'ωT' obtained from the torque measurement was plotted against primary current, Fig. 5.13. The higher torques obtained on reducing the primary current, I_A compared to those on increasing I_A are due to

(i) conventional ferromagnetic hysteresis, whereby a higher value of standing flux exists when the current is reduced. This is indicated by the rotor search coil e.m.f.,

and (ii) the change in the division of remanence power P_{h2} between P_4 and P_2, dependent on both the magnetic and mechanical history of the machine. **Whilst the required loss power, the mean of OB and OC, cannot be measured directly, OB and OC can be measured and hence their average is easily found.**

5.10.4 Hysteresis with the secondary rotated

After demagnetising the machine, the primary current I_A was increased to set value carefully avoiding recoil loops. P_2 max. and P_4 min were obtained in the manner described in section 5.10.2, the rotation of the secondary being performed very slowly to avoid fluctuations in I_A. The test was repeated over the current range 0 to 130% of rated value for both increasing and decreasing values of current.

The complete test was then repeated with the reverse secondary rotation to obtain P_{2min} and P_{4max}. The results are plotted in Figs. 5.22 and 5.23.

5.10.5 Conclusion

The remanence power Ph2 is only important in its bearing upon the calculation of primary core loss. P_{h2} itself does not constitute any additional loss at synchronism (see section 5.13). The validity of the slip test in predicting P_{h2} and P_{Fe} is reconsidered.

In experimental machine the primary iron is being driven through a static magnetic field. The question arises as to whether the primary iron loss of the rotating mass is supplied by mechanical shaft power (as for an excited d.c. generator on open-circuit) or by electrical power (as for a transformer). If by the former both the remanence power and the primary iron loss calculations would be considerably modified. However, previous experiments [12] with rotor fed induction motors indicate otherwise. These induction motors had open-circuited stator windings whereas the model machine has effectively a short-circuited stator. Although a short-circuited secondary was not expected to affect the losses under synchronous conditions it was considered important to obtain experimental confirmation. The experimental evidence given in section 5.13, confirms Rawcliffe and Menon's work at the rated frequency of 50 c/s and demonstrates its validity at other frequencies, and with the secondary winding shorted. The primary core loss in the experimental machine will therefore be determined by rotating the secondary core in each direction and calculating the mean slip ring input less the primary circuit losses :

$$P_{Fe} = \tfrac{1}{2}(P_{2max} + P_{2min}).$$

The design value of core loss $\simeq$ 7% of the experimental value calculated in appendix 12.4. Better correlation between design and test was not expected. The design value was calculated from the dynamometer manufacturer's own established design data for the practical design of synchronous machines manufactured in the same works as the model machine, but in view of the assumptions made in Appendix 12.4 the experimental value ofprimary iron loss is more reliable than the design value. The former will therefore be used in the pole face loss calculations, by referring to the graph of primary iron loss against B_{mean}, Figs. 5.25 or 5.26. The apparent equality between the primary iron loss and secondary hysteresis power in the slip test is attributed to experimental error in extrapolating the various curves.

5.11. Pole Face Loss Measurements and Calculations

5.11.1 Rated Frequency, Constant Temperature

The appropriate maximum and minimum values of power input were obtained by the method of section 5.10.4 with a supply frequency of 50 c/s and surface temperature of 100°C. The test divides into 4 sections according to the direction of movement of the stator, and the electromagnetic history of the dynamometer :-

(a) Current increasing from the demagnetised state.
Secondary adjusted until $P_1 = max^m$.

(b) Current decreasing from 45 amp,
Secondary adjusted until $P_1 = max^m$.

(c) Current increasing from the demagnetised state,
Secondary adjusted until $P_1 = min^m$.

(d) Current decreasing from 45 amp.
Secondary adjusted until $P_1 = min^m$.

The measured values of current and power are plotted in Figs. 5.8(a to d) and 5.24.

The determination of the surface loss caused by the rotating space harmonics in the primary m.m.f. waveform, performed in accordance with section 5.8.4., is illustrated by the following typical calculation for a B_{mean} of 0.5 Wb/m^2 (I_A increasing from zero). Measurement errors were minimised by using where possible data extracted from the appropriate graphs and not directly from tables of instrument readings.

Typical Calculation

$$B_{mean} = 0.5 \text{ Wb/m}^2, \quad I_A \simeq 25 \text{ Amp.}$$

(i) The determination of the primary iron loss

From Fig. 5.25,

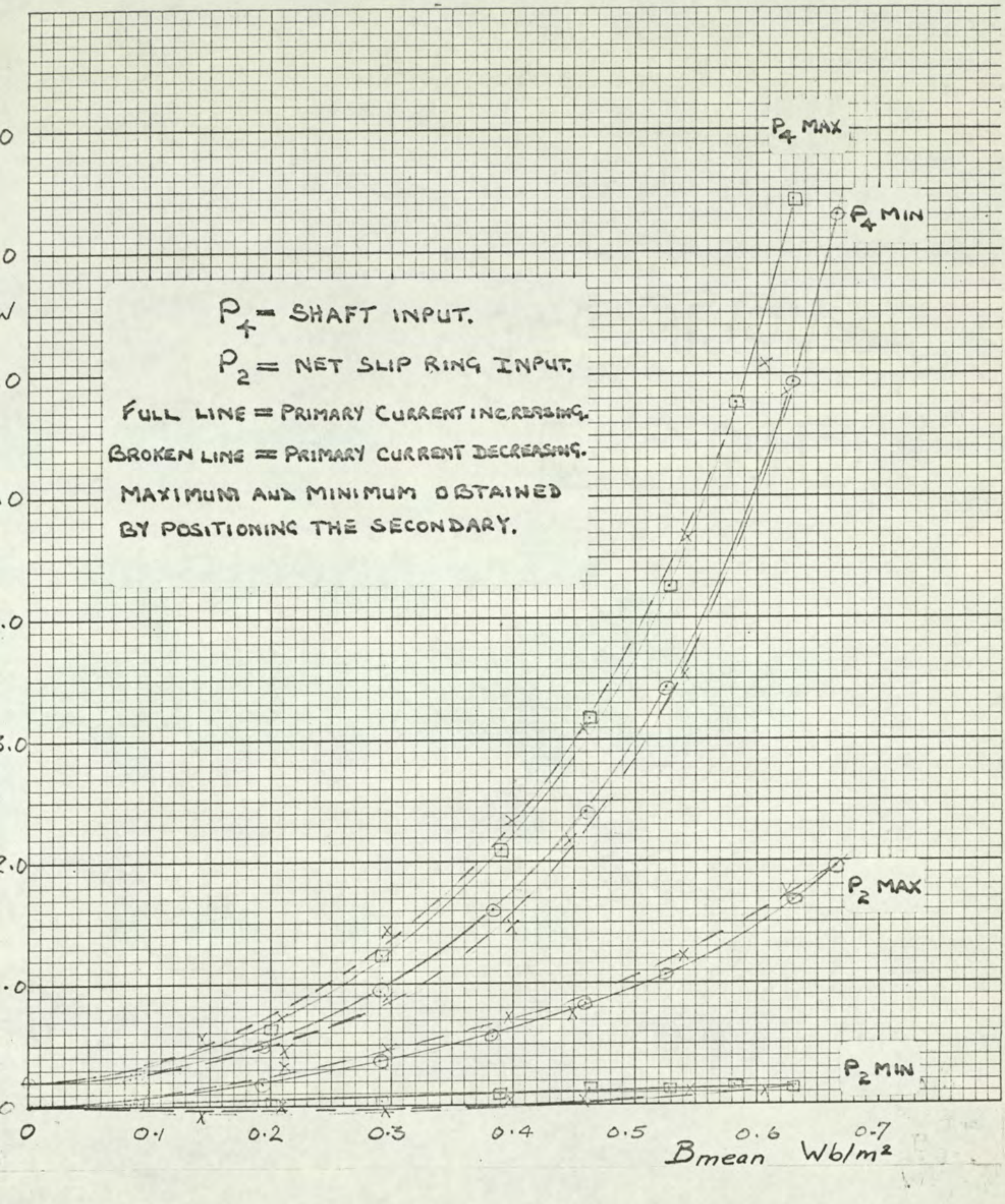

FIG 5.24. VARIATION OF DYNAMOMETER INPUT POWER WITH B_{mean} AT 50 C/S

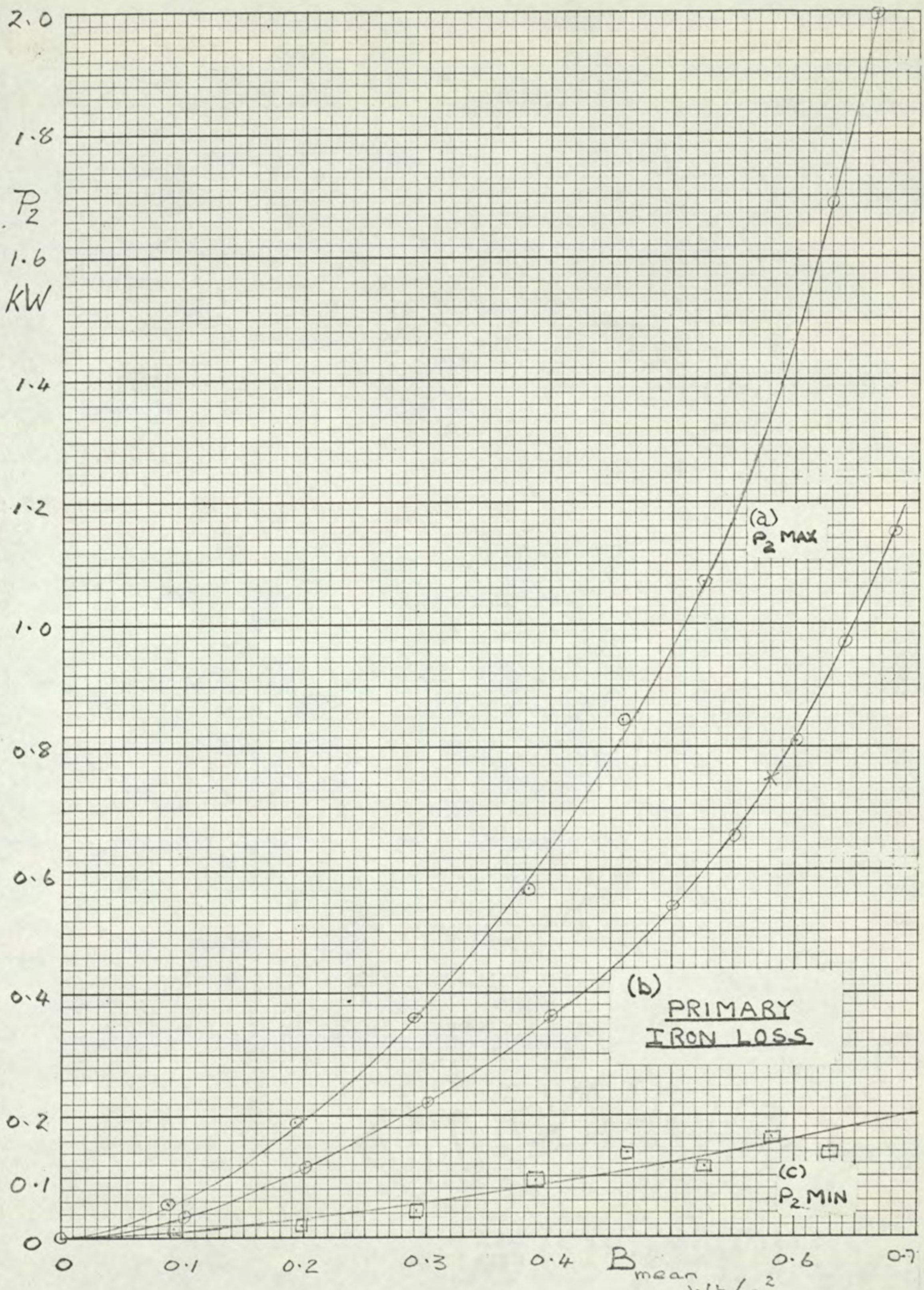

Form No. 8845 FIG 5.25. MEASURED PRIMARY IRON LOSS AS A FUNCTION OF B_{MEAN}

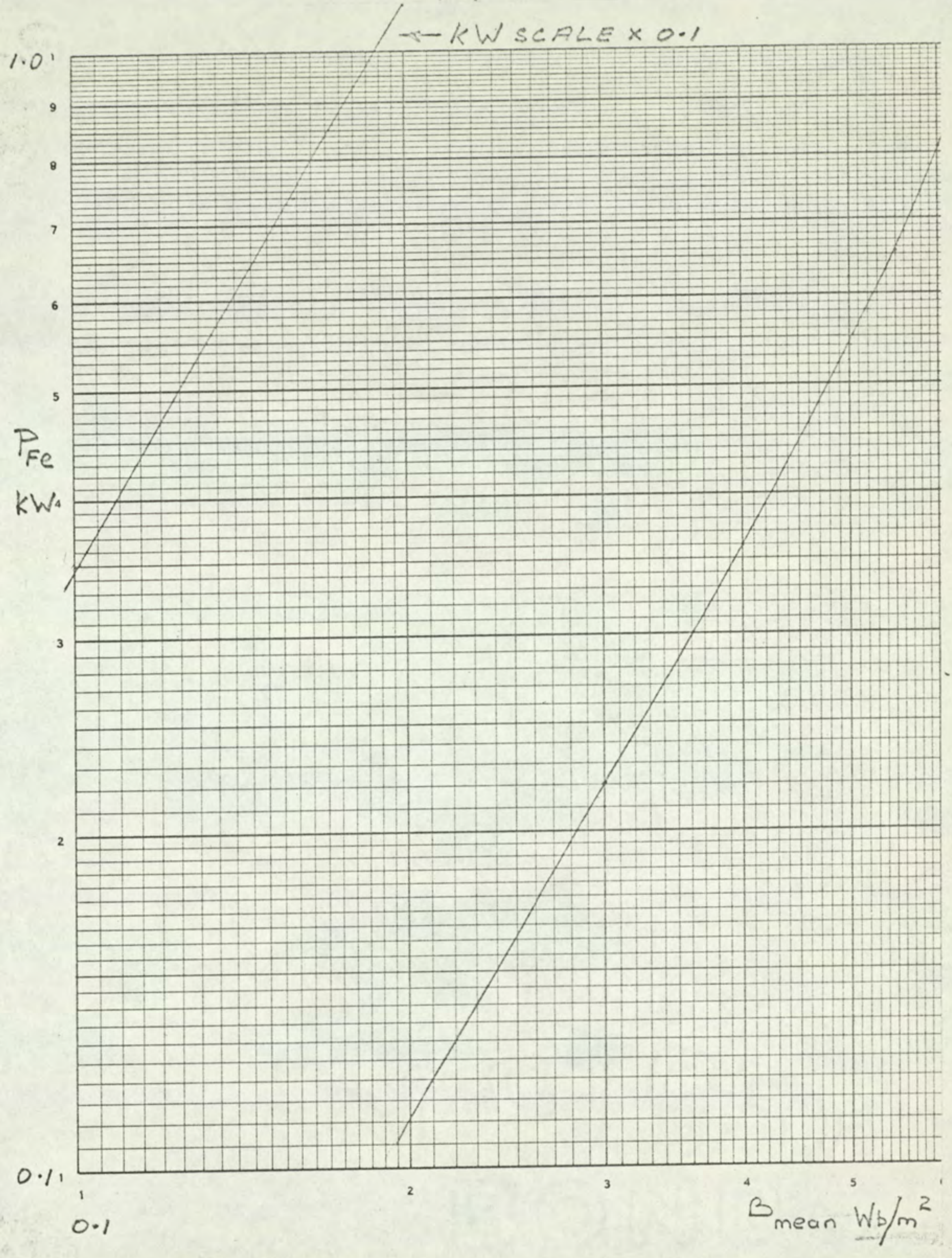

FIG. 5.26. MEASURED PRIMARY IRON LOSS AS A FUNCTION OF B_{mean} (Log - Log)

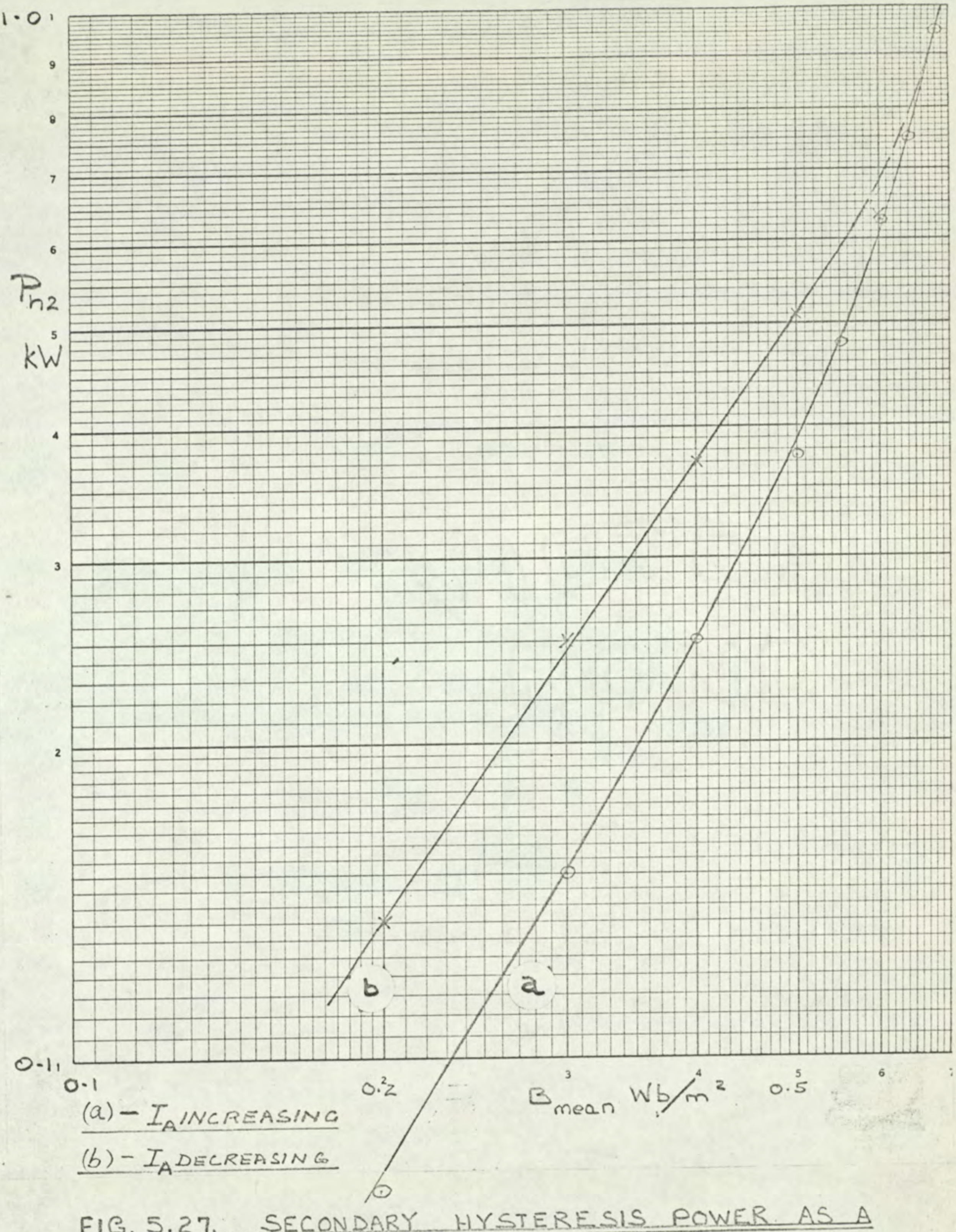

FIG. 5.27. SECONDARY HYSTERESIS POWER AS A FUNCTION OF B_{mean}.

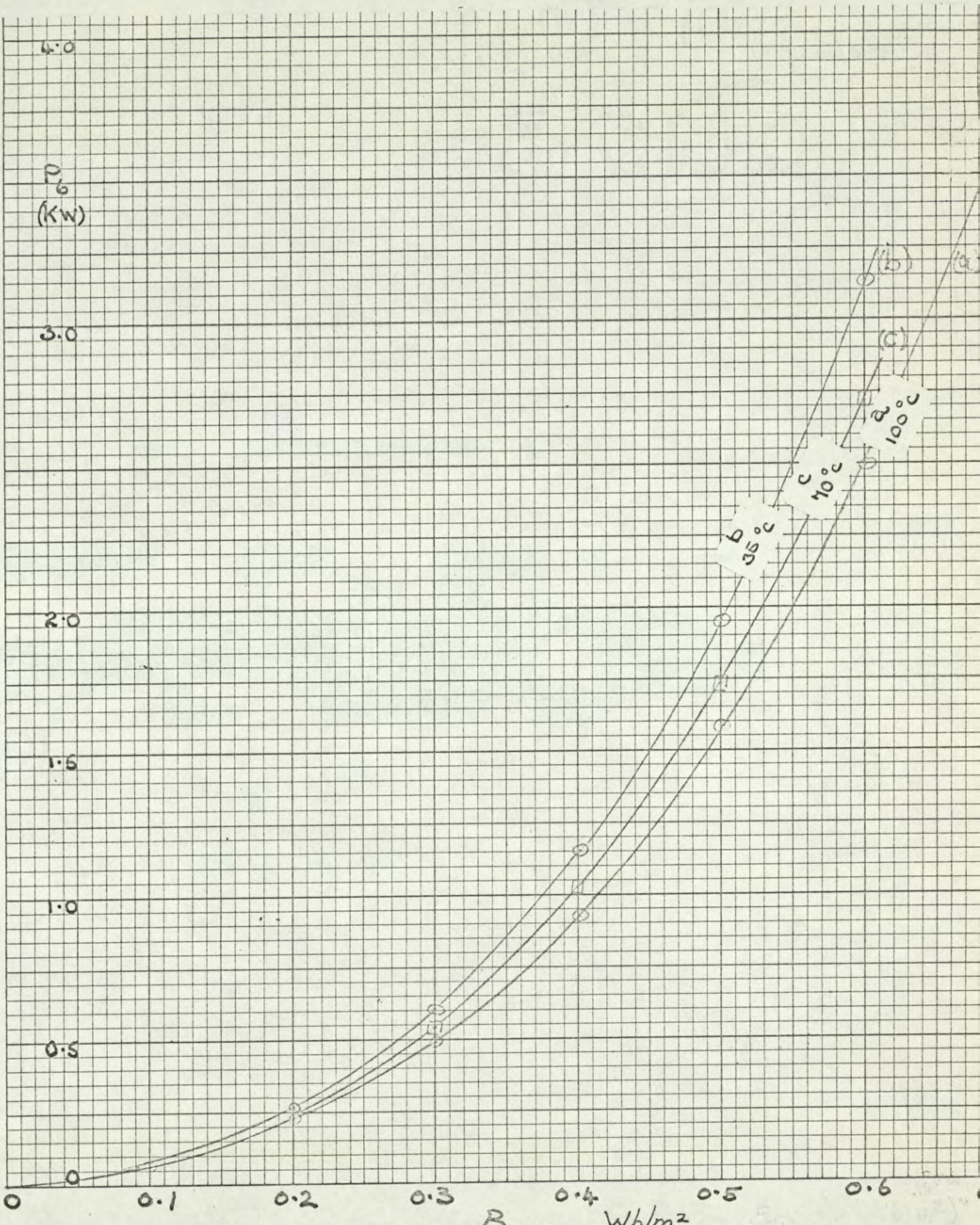

FIG. 5.28. THE CALCULATED POLE FACE LOSS DUE TO THE SLOT OPENINGS.

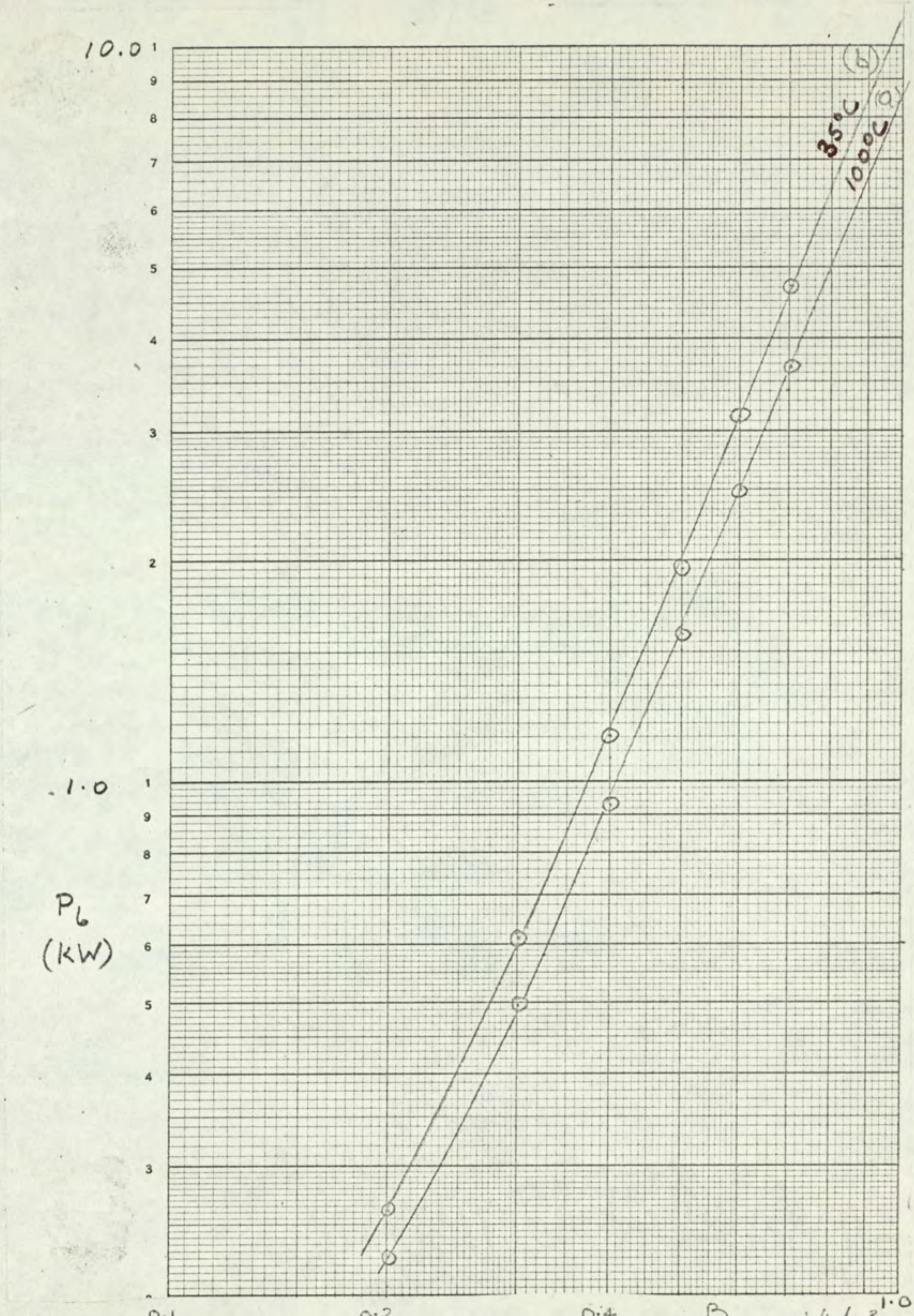

FIG. 5.29. POLE FACE LOSS DUE TO SLOT RIPPLE AS A FUNCTION OF B_{mean}.

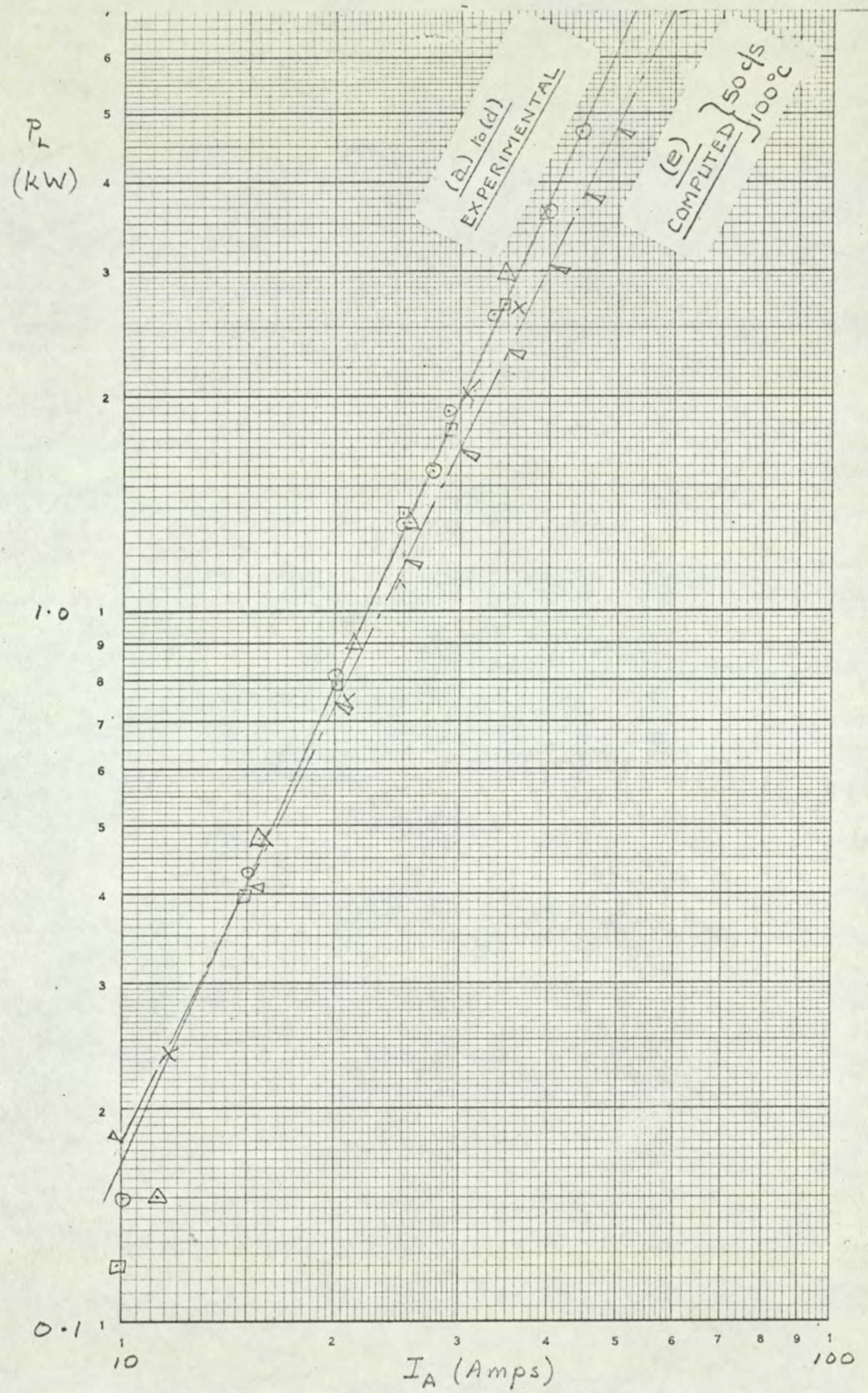

FIG 5.30. VARIATION OF M.M.F. LOSSES WITH ARMATURE CURRENT.

$P_{2max} = 0.96$ kW ⎫⎧ = measured P_1 minus primary

$P_{2min} = 0.122$ kW ⎭⎩ circuit loss and meter loss, Fig. 5.11(c))

$\therefore P_{Fe} = \frac{1}{2}(P_{2max} + P_{2min}) = 0.54$ kW

This point is now plotted on Figs. 5.25 and 5.26

(ii) <u>Determination of the remanence power</u>

From Fig. 5.24 (full lines)

P_4 max = 3.66 kW

P_4 min = 3.00 kW

$\therefore P_{h2} = \frac{1}{4}(P_{2max} - P_{2min} + P_{4max} - P_{4min}) = 0.375$ kW

This point is now plotted on Fig. 5.27

(iii) From Fig. 5.28 the slot ripple loss is

$P_6 = 1.58$ kW

Using the curves of P_{2max} and P_{4min} the net shaft input power is

$P_5 = P_4 - 0.2 = \qquad = 2.80$ kW

$\therefore$The net dynamometer input $= P_2 + P_5 = 3.76$ kW

The unwanted iron losses $= P_{Fe} + P_6 = 2.12$ kW

$\therefore$The m.m.f. harmonic loss $= 3.76 - 2.12 = 1.64$ kW

From Fig. 5.8(a), $I_A = 27.5$ Amps.

This point is now plotted on Fig. 5.30

It is evident from Fig. 5.30 that the experimental value of the surface loss caused by armature reaction m.m.f. harmonics is independent of the electromagnetic history of the dynamometer.

5.11.2 <u>Variation of Frequency at constant temperature and constant current</u>

Measured values of P_1 and P_4 were recorded in a similar manner to the previous section for a surface temperature of 70°C and a primary current of 20 amps. The measured and derived results were obtained in the manner described in section 5.10.2. The dynamometer input powers P_2 and P_5

were then calculated and plotted on Fig. 5.22. These tests were actually performed on stator No. 1 to whilst search coils were being fitted in the surface of stator No. 2. changing the stator made negligible difference to the dynamometer input power.

For specific values of frequency new values of P_2 and P_5 were obtained from the graphy (thereby reducing measurement and error) and then P_{Fe} and P_{h2} calculated as before.

The slot ripple loss was calculated for each frequency in Appendix 12.6 over a range of B_{mean}. To reduce experimental error Bmean was taken as the average of two values read from Fig. 5.22.

The sum of P_{2max} and P_{5min}, the net dynamometer input, is considered to be slightly more accurate than $P_{2min} + P_{5max}$ (section 5.12 (vi)) and therefore the former is used in column 10, rather than an average of both. The ultimate value of m.m.f. loss is plotted in Fig. 5.31.

5.11.3. Variation with Temperature

Measured values of minimum and maximum input power were again recorded in the manner described above with a supply frequency of 50c/s and a primary current of 25A. A time interval of at least one hour was allowed between all readings for the surface temperature to stabilise. Derived results are plotted additively in Fig. 5.32.

The slot ripple loss obtained from Fig. 5.28 is also shown.

The m.m.f. harmonic loss, obtained by graphical subtraction, is plotted to a base of surface resistivity in Figs. 5.33 and 5.34 (log-log scale)

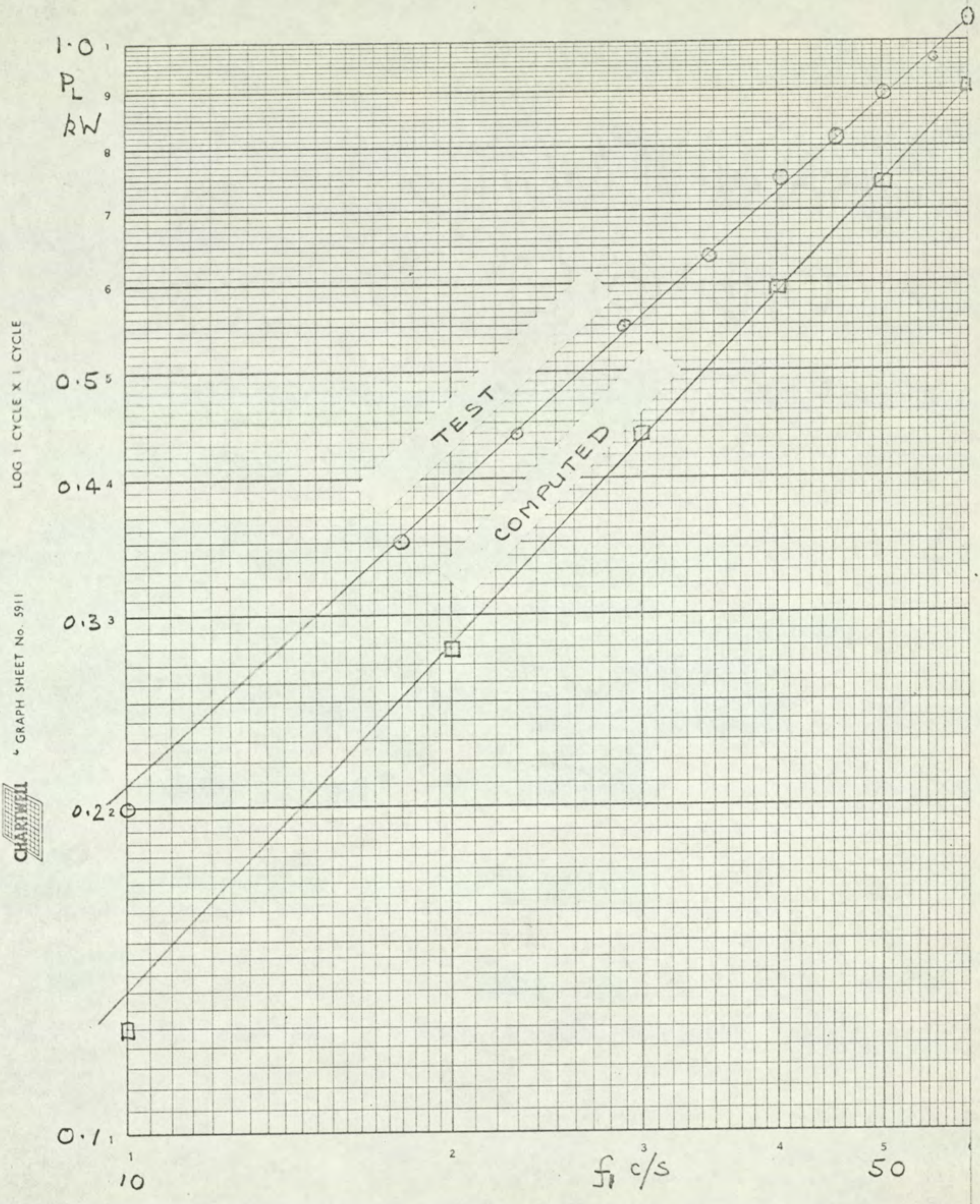

FIG. 5.31 POLE FACE LOSS DUE TO M.M.F. HARMONICS IN THE LOAD LOSS DYNAMOMETER. VARIATION WITH FREQUENCY (20A 70°C).

FIG 5.32. LOSS SUMMATION IN THE EXPERIMENTAL MACHINE.

Variation with Temperature. $I_A = 25A, 50\%$

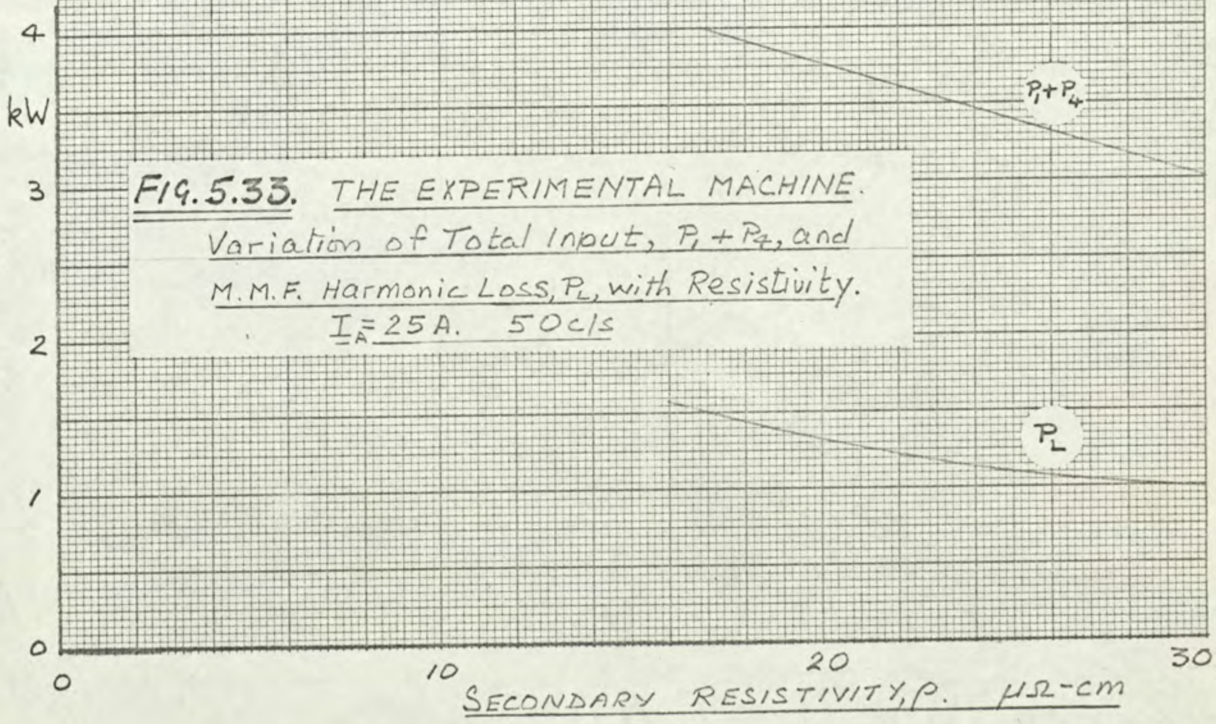

FIG. 5.33. THE EXPERIMENTAL MACHINE.

Variation of Total Input, $P_1 + P_4$, and M.M.F. Harmonic Loss, P_L, with Resistivity.

$I_A = 25A$. 50c/s

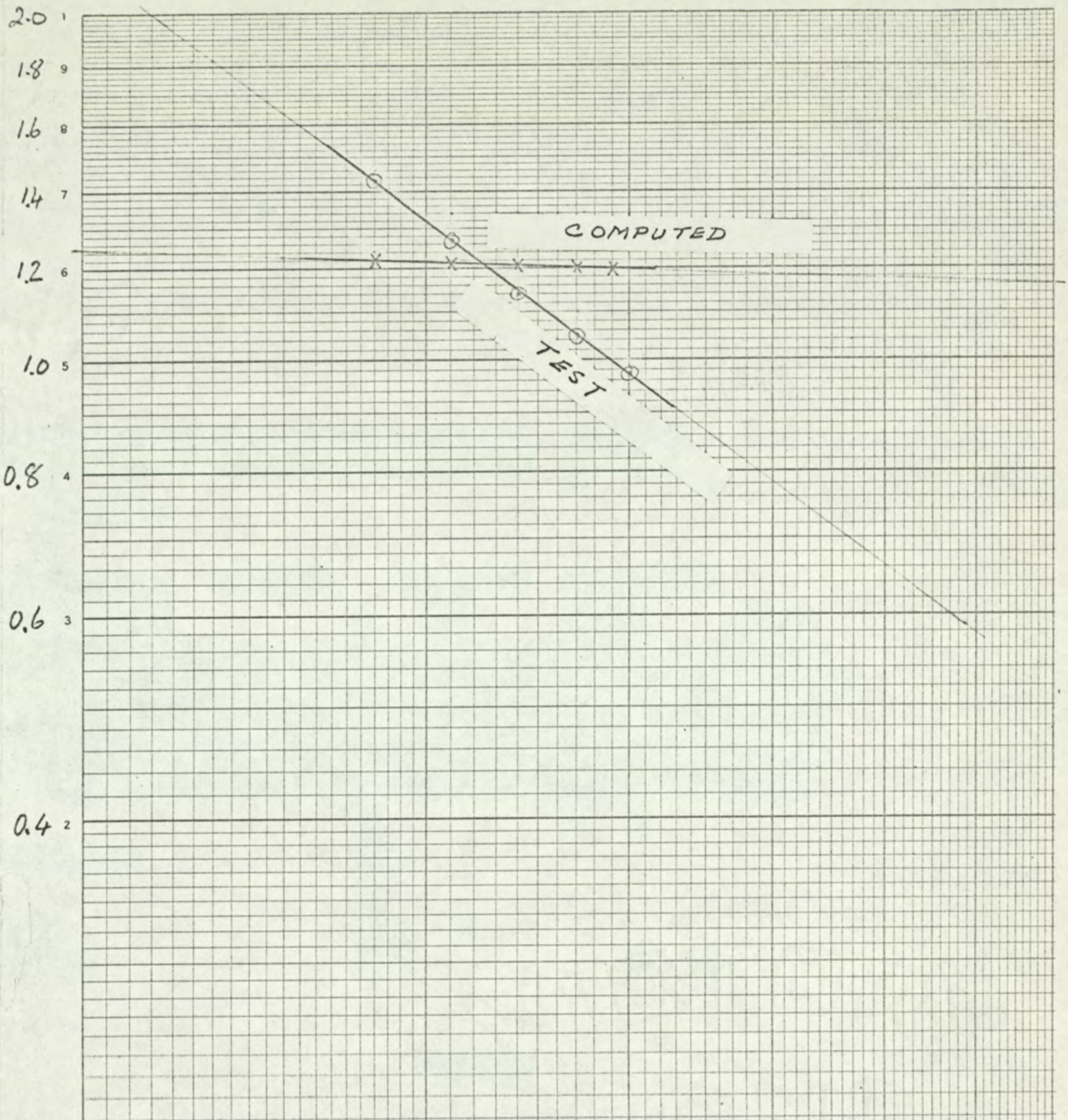

FIG. 5.34. VARIATION OF M.M.F. HARMONIC LOSSES, P_L, WITH WITH RESISTIVITY (25 AMP 50c/s)

5.12. Limits of Error

Errors occuring in electrical measurements have been broadly divided into random errors and systematic errors.[37]

Random errors in the measurements taken on the experimental synchronous load loss dynamometer have been minimised by taking the ... precautions outlined below for each test, by repeating readings, and by drawing the best curve through several plotted points. Random errors are difficult to calculate since they depend on such factors as irregular fluctuations in supply voltage and frequency, temperature variation of the pole face during readings, changes in ambient temperature and personal errors of judgement.

The supply voltages were adjusted so that selected quantities, usually I_A and V_{12}, were set on particular scale divisions. The pole face temperature was maintained within the limits prescribed in the relevant results sections above. It was considered unnecessary to compensate the measured values for variations in mains frequency at this stage. The deviation from 50 c/s was usually much less than 1%; since the pole face loss is proportional to frequency (Fig.5.31) the error introduced will also be less than 1%.

Systematic errors have also been minimised by careful calibration of the various measuring devides and using indicating instruments of substandard grade provided with mirrors and knife edge pointers. For the connections to the various search coils, the resistance of leads was minimised by using gold plated plugs and sockets, silverplated switch contacts, and silver slip rings. The leads were so placed as to minimise errors due to stray magnetic fields. The limits of error in the final loss figure are calculated below for the centre of the armature current range of section 5.11.1.

(i) <u>The shaft power P_4</u>

It is estimated that the error in obtaining P_4 from the calibration curve for the syncage driving motor is $\pm$ 3% at the mid range ($P_4 \simeq 3$kW), and better at higher loads. The otherwise large percentage error at very low values of P_4 is reduced considerably by the high accuracy of measuring the motor input P_3 with the shaft uncoupled. For this condition the error in P_4 is zero and in P_3 is $\pm$ 0.013 kW (about $\pm$ 2% of the indication) - which is only slightly worse than the reading error in using the calibration curve itself.

(ii) <u>The Electrical Powers, P_1 and P_2</u>

P_1 is read on the three phase wattmeter for which the reading error is $\pm \frac{1}{2}$ watt times the scale factor and the calibration error is $\pm \frac{1}{2}$%. During the rated frequency tests of section 5.11.1 the wattmeter P_1 read 193 Watts x 5 for an armature current I_A of 25.0 amps. From this value of P_1 must be subtracted the meter losses and the primary circuit losses i.e. with a wattmeter scale factor of 5/1000 kW

$$P_1 = \left(193 \pm 0.5 \pm \left(\frac{0.5}{100} \times 193\right)\right) 5/1000 \text{ kW}$$

From Fig. 5.11(b) the meter losses $= 0.965 \pm 0.0075$

$= 0.073 \pm 0.006$

From Fig. 5.11(c) The circuit losses $= 0.066 \pm 0.002$

$\therefore$ Total losses $= 0.139 \pm 0.008$

$P_2 = 0.826 \pm 0.016$ kW or $\pm$ 1.9%,

say $\pm$ 2%

The limits stated above for the meter losses are calculated by a similar process to that for P_1. Those for the circuit losses are estimated by taking limits of error for the specified brush voltage drop as $\pm$ 5%, the current as $\pm \frac{1}{2}\%$, and the armature resistance as $\pm$ 1%

(iii) Primary Iron loss

Since the primary circuit losses are approximately constant for both $P_{2\ max.}$ and P_{2min} it is more convenient to express the errors in watts than to convert to percentages. For the typical calculation suppose the limits on P2 to be $\pm$ 0.016 Watts (as above). To this must be added an error of $\pm$ 0.001 in the reading of Fig. 5.25.

Now the primary iron loss $P_{Fe} = \frac{1}{2}(P_{2max} + P_{2min})$

$$\therefore P_{fe} = \tfrac{1}{2}(0.96 \pm 0.016 \pm 0.001 + 0.122 \pm 0.016 \pm 0.001)$$

$$= \tfrac{1}{2}(1.082 \pm 0.034)$$

$$= 0.541 \pm 0.034 \quad \text{or} \pm 6.3\% \text{ (mid range)}$$

(iv) The remanence Power

The reading error on Fig. 5.24 is $\pm$ 0.005 kW.

The measurement error on P_4 at mid-range is $\pm$ 3%

$\therefore$ In the typical calculation section 5.11.1(ii)

$$P_{h2} = \tfrac{1}{4}(0.96 \pm 0.017 - (0.122 \pm 0.017) + 3.66 \pm 0.11 \pm 0.005 - (3.00 \pm 0.09 \pm 0.005))$$

$$= \tfrac{1}{4}(1.498 \pm 0.244)$$

$$= 0.375 \pm 0.061 \quad \text{or} \quad \pm 16\%$$

(v) The dynamometer mechanical losses

At the zero end of the syncage calibration curve the error in P_4 is taken as $\pm$ 0.015 (ref. sub-section (i) above). When the dynamometer is demagnetised the windage and friction losses equal P_4 and are therefore measured to within $\pm$ 0.015 kW.

Therefore in the typical example above

$$P_{5max} = P_4 - (0.2 \pm 0.015)$$

$$= 3.66 \pm 0.115 - 0.2 \pm 0.015 = 3.46 \pm .13 \text{ or } \pm 3.8\%$$

Similarly $P_{5min} = 2.80 \pm 0.11$ or $\pm 3.9\%$

(vi) <u>The total secondary power input P .</u>

Taking the percentage errors in P_{Fe}, P_2 and P_5 respectively to be $\pm$ 6%, $\pm$ 2% and $\pm$ 4% at mid-range, and using the expression below quoted from p.174 of Buckingham and Price [37], the percentage error in the secondary power input, P, is now calculated :

$$P = P_2 + P_5 - P_{Fe}$$

$$= 0.96 + 2.80 - 0.54 = 3.22 \text{ kW}$$

From ref. 37

$$\frac{dP}{P} = \frac{P_{Fe}}{P}\cdot\frac{dP_{Fe}}{P_{Fe}} + \frac{P_2}{P}\cdot\frac{dP_2}{P_2} + \frac{P_5}{P}\cdot\frac{dP_5}{P_5}$$

$$= \frac{0.54}{4.30}\cdot\frac{6}{100} + \frac{0.96}{4.30}\cdot\frac{2}{100} + \frac{2.80}{4.30}\cdot\frac{4}{100}$$

$$= 5.1/100$$

i.e. the error in P is about $\pm$ 5% at mid range.

(vii) **<u>The armature current generated component of pole face loss</u>, P_L**

Subtracting the slot ripple loss P_6 from P above leaves P_L .

The method of calculating P_6 gives reliable results on practical synchronous machines. However the validity of extending this method to the exceedingly small gap/slot pitch ratio of the experimental machine has not been proven. Errors much larger than those arising in the various steps in the calculation above may occur and it is therefore considered inexpedient to quote any limit of error on P_6. Since P_6 and P_L are of the same order, an error of $\pm$ 20% say, on P_6 would increase considerably the limits of error on P_L by ± 0.3 kW to $\pm$ 25%

5.13 Induction Motor Loss/Slip Curves.

Because the secondary remanence torque of the experimental load loss dynamometer has a disturbing influence on the measured torque, the pole face loss is determined experimentally by the separation of the losses. This necessitated the accurate measurement of the primary iron loss. A paper published by Rawcliffe and Menon[12] suggested that a variable speed test would provide a suitable method of determination. In such a test the rotor speed is varied over a wide range by means of a variable speed motor whilst the stator frequency and flux per pole are kept constant. The experimental machine differs from the open circuited slip ring induction motors of reference 12 in that (i) its secondary is solid, and therefore short circuited, and (ii) its primary iron loss almost equals its standstill secondary hysteresis loss. In order to establish that the results of reference 12 could be applied to the experimental machine it was considered expedient to perform some slip tests on a standard rotor-fed slip-ring induction motor at various synchronous frequencies with the secondary member both shorted and open circuited.

Since this test programme departs distinctly from the main investigation and does not directly involve the load loss dynamometer, the experimental details of these slip tests are omitted, attention being concentrated on the nature of the phenomenon under examination and on the ultimate conclusions.

Let P_{h1} = Stator hysteresis loss at all speeds when stator fed.

P_{h2} = Rotor hysteresis loss at all speeds when rotor fed.

P_{e1} = Stator eddy current loss at all speeds when stator fed.

and P_{e2} = Rotor eddy current loss at all speeds when rotor fed.

The above are also the respective losses at standstill when the power is fed to the other member, assuming constant flux per pole.

Let T_{h1}, T_{h2} = Hysteresis or remanence torques in Nm.

and ω_1 = Synchronous speed in r.p.s.

It has been shown [12] that the losses in an open circuited rotor of a stator fed induction motor are $sP_{h2} + s^2P_{e2}$ and furthermore that

$$\text{the mechanical power produced} = \frac{1-s}{s} \times \text{losses} = (1-s)(P_{h2} + sP_{e2})$$

$$= P_{h2} \text{ just before the machine looses synchronism.}$$

It therefore follows that the hysteresis torque

= Mechanical power $\div$ the relative angular velocity

$$T_{h2} = \frac{sP_{h2}}{s\omega_1} = P_{h2}/\omega_1$$

There is no rotor iron loss at synchronism but there is a transference of power due to the hysteresis or remanence effects. The above expression shows that for a given flux per pole the hysteresis torque is constant at all speeds with the exception of synchronous speed where it changes from + T_{h2} to − T_{h2} as the spedd passes positively through the synchronous value. When the machine is rotor-fed with the stator on open circuit this change in hysteresis torque at synchronism is reflected in a reduced primary (rotor) - power input and an increased mechanical power input, the losses being unaffected, Fig. 5.35.

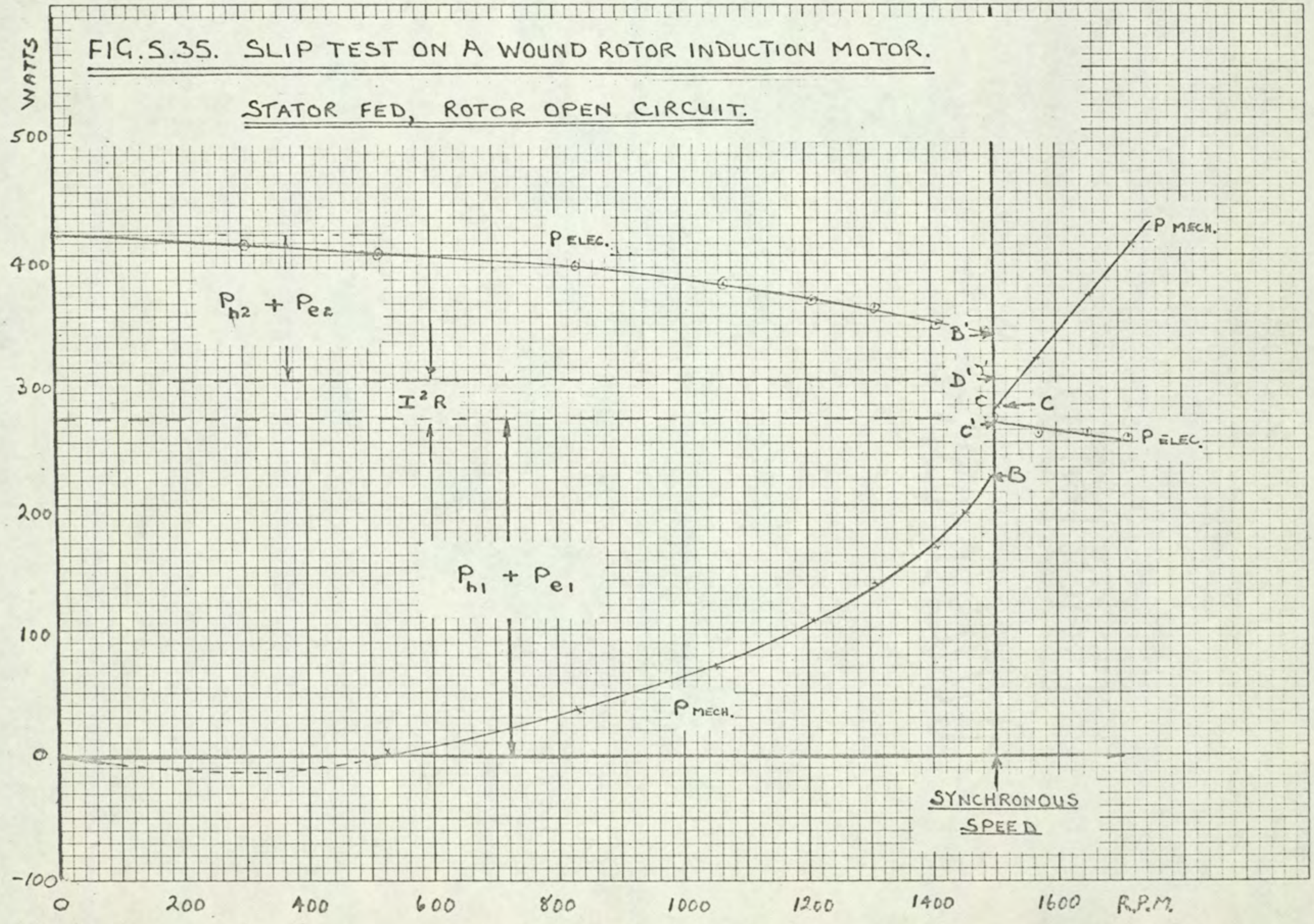

FIG. 5.35. SLIP TEST ON A WOUND ROTOR INDUCTION MOTOR.

STATOR FED, ROTOR OPEN CIRCUIT.

At the mid point 'D' of this change B'C' Fig. 5.35 there is no secondary remanence torque and therefore no remanence power and no secondary eddy current loss. The electrical power supplied neglecting stray losses should therefore be the total primary loss

$= P_{h1} + P_{e1} +$ Copper loss.

At standstill the rotor loss is a maximum and equals the electrical input minus OD', i.e. $P_{h2} + P_{e2}$. When rotor fed, suffices 1 and 2 are interchanged and the electrical brush loss included in the measured electrical input.

From the aforementioned tests performed on a 16 h.p. slip ring induction motor it is concluded that in a 3-phase induction machine excited via its rotating primary winding :

(i) that, in confirmation of previous work [12], the loss/slip test is a valid means of assessing the stator hysteresis power.

(ii) that the primary iron losses (excluding surface and pulsation losses) are supplied electrically by electrical-electrical energy conversion.

(iii) that the above two clauses are valid(a) at non rated frequences, and (b) when the secondary is shorted.

and (iv) that the electrical power input/slip curve does not necessarily pass through the origin.

6. COMPARISON OF MEASURED AND PREDICTED LOSSES.

6. COMPARISON OF MEASURED AND PREDICTED LOSSES

6.1 Introduction

The losses measured on the experimental load loss dynamometer recorded in the previous chapter for a range of armature current, synchronous frequency, and secondary resistivity are compared with the losses computed from the modified eddy current coupling theory of chapter 3 in section 6.2

In section 6.3 the loss measured on the short circuit test on each of several large synchronous machines is also compared with that predicted by the same theory, Tables 6.11 and 6.13, and also Appendix 12.8.

In the absence of a computer programme the comparisons with the methods of Kuyper[1] and Barello[2] are more onerous and are therefore restricted to two cases,(section 6.4.) An estimate of permeability is necessary before proceding with these calculations. Section 8.1 suggests that μ_r varies between 500 and 1500. Chalmers[6] states that a value of μ_r equal to several hundred is most appropriate. For reasons given in section 8.1 μ_r is taken as 1000. These calculations account for peripheral flux leakage, negligible in the experimental machine because of the unusually short air gaps, but not negligible in production machines where the gap approaches half a slot pitch. For these machines the predicted loss computed by the modified eddy current coupling theory, which ignores peripheral flux leakage, must be reduced - especially for the slot harmonic terms. The reduction factor K_L used in section 6.3.1 (iii) is derived in Appendix 12.2.3.

The three methods of calculation are compared in Section 6.5

6.2 The Experimental Machine

The variation of the pole face loss due to m.m.f. harmonics with a few selected parameters is shown in Figs. 5.31 to 5.34 on each case the predicted loss is computed by the modified eddy current coupling theory of section 3.7.1. using the constants K_1 and m in equation 3.13 applicable to the secondary iron. The validity of the theory in predicting changes in surface loss has been tested for three variables only on the experimental machine :-

(i) Armature (primary) current from 5 to 50 A, Fig. 5.30.

(ii) Frequency from 10 to 60 c/s , Fig. 5.31 and

(iii) resistivity from 18 to 30 $\mu\Omega$ - cm., Fig. 5.33

The effects of other variables (on production machines) is discussed in section 6.3

The comparison between the measured and predicted m.m.f. harmonic losses, P_L, is summarised in Table 6.1.

Table 6.1. Parameter Changes in the Experimental Machine

Columns 2 and 3 tabulate the slope 'a' of the various log - log graphs.

Test/Fig.	Variable	Comparison bet. theory and test.		
		Slope 'a'		Magnitude of Loss.
		Theory	Test.	
1/5.30	Primary Current I_A	2.05	2.25	within 20%
2/531	Primary Frequency f	1.06	0.91	within 15% at 60 c/s 60% at 10 c/s
3/534	Secondary Resistivity ρ	-0.036	-0.75	within 20%

The "theory" is that of chapter 3, and the corresponding indices were found from successive computer runs. From Test 1 the empirical relationship,

$$P_L \propto I_A^{\,2.25}$$
$$\propto F^{\,2.25}$$

is in fairly good agreement with chapter 3 ($\propto F^{2.05}$) and with both Kuyper and Barello ($\propto F^2$, section 2.4.2).

From Test 2

$$P_L \propto f^{0.91}$$

also agrees fairly well with chapter 3 ($\propto f^{1.06}$) with Kuyper ($\propto f^{1.0}$) and with Barello ($\propto$ f $\div$ (a function of α))

From Test 3,

$$P_L \propto \rho^{-0.75}$$

It is difficult to assess by inspection of Kuyper's equation any relationship between loss and secondary resistivity. Barello's indicates that the loss is proportional to $\rho^{-0.5}$ which is approaching the test result.

The modified eddy current coupling theory in section 3.8. predicts an index between -0.3 and -0.9 for practical machines depending upon the value of normalised speed for the predominant harmonics, which is well below the maximum torque point ($n/n_m = 1$). For the experimental machine n/n_m is about unity for the predominant harmonics, and above unity for the fifth.

<u>At the peak torque point</u>, the loss $\propto$ $T_m \times n$, since $\frac{T}{T_m} = 1$

i.e. $W_h \propto DF^2Lphn/g$ (6.1)

Above the peak torque point, the index of n/n_m varies between zero and -0.5, Fig. 3.5. For an index of -0.2, corresponding to $n/n_m = 3$, typical for the lowest harmonic orders of the experimental machine we get :

$$W_h \propto \left(\frac{n\,D^{3.18}\,F^{0.824}}{\rho\,g^2\,(ph)^{2.18}}\right)^{-0.2} \times \frac{F^2 phDL}{g} \times n$$

or $$W_h \propto D^{0.36} F^{1.84} L\, p^{1.44} h^{1.44} \rho^{0.2}\, n^{0.8} g^{-0.6} \qquad (6.2)$$

i.e. the loss is predicted to increase with resistivity.

In the experimental machine for which n/n_m varies from 0.1 to 10 the modified eddy current coupling theory therefore suggests that W_{TOT} varies as $\rho^{-0.85}$ to $\rho^{0.4}$ depending upon the n/n_m vâlue of the predominant harmonics. The measured value of -0.75 suggests that the machine is not operating near to the peak torque point and that the theoretical value of n_m has been underestimated.

6.3 Production machines

Before designing the experimental machine a preliminary investigation was undertaken with a wide range of large salient pole synchronous machines and turbo alternators. The stray load loss of each was compared with the loss predicted using the modified eddy current coupling theory with ingot iron parameters which underestimates by about 15% the predictions using mild steel parameters. The work is summarised in Tabular form in appendix 12.8. It is presented not as conclusive evidence but as an indication that the theoretical predictions are of the right order.

A more detailed investigation has been undertaken with selected machines to illustrate where possible the effects of parameter changes and a means of accounting for the pole shoe profile in salient pole synchronous machines.

Computer "print ups" illustrate salient steps in the evolution of the computer programme. In most computations insignificant harmonic orders are not required on the print-up , in which case a note appears to that effect.

6.3.1 60-MVA Synchronous Compensator

(i) Computations

The machine data is given on a typical computer data sheet in Table 6.2. The gap quoted is constant for $10^{o}M$ on either side of the pole centreline. From this point to the pole tip, the pole shoe is chamfered in a straight line, where the gap = g_2 (Fig. 12.2.1). Several computer-runs were carried out for this machine in order to determine the pole face loss and the effect of (i) increasing the number of slots per pole per phase, (ii) including the slot width factor (iii) increasing the slot width and (iv) changing the pole shoe material :

Table 6.3	Uniform gap equal to g_1; ingot iron parameters
Table 6.4	" " " g_2; " " "
Table 6.5	as per 6.3 but s/p/p increased from 5 to 6.
Table 6.6	" " " " " " 5 to 7.
Table 6.7	" " with slot width factor included
Table 6.8	as per 6.7 with slot opening increased to $\frac{1}{2}$ slot pitch
Table 6.9	as per 6.7 but using mild steel parameters.

(ii) The Pole Profile

The first method of accounting for the pole profile is the mathematical one developed in appendix 12.2 and the second the graphical one described below.

For the above machine the peripheral flux leakage factor is calculated in Table 6.10. using equation 12.2.5. The pole face loss is :

$$P_L{}^1 = P_L K_L (2\beta_1 \frac{g_1}{g_2} + \beta_2)$$

where $2\beta_1 = 22^oM/60^oM = 0.367$

$\beta_2 = 20^oM/60^oM = 0.333$

$$P_L{}' = 44.5\,(0.367\,\frac{0.748}{1.11} + 0.333)$$

$$= 44.5\,(0.247 + 0.333)$$

$$= 25.4\ \text{kW}$$

Table 6.2. Computer Data Input Sheet

		POLE FACE LOSS		
LABEL: = cr. lf. cr. sp^{45} REF.DATE. cr. lf. cr. bl.			REF.	1E
			DATE:	6/4/64
A 0	P	Pole pairs		3
A 1	NS	Synchronous Speed	r.p.m.	1000
A 2	Z	Conductors/slot		2
A 3	Y	Parallel paths/coil side		1
A 4	C	Parallel paths/phase		2
A 5	I	Total phase current	Amps.	2670
A 6	S/P/P	Slots/pole/phase (q)		5
A 7	PITCH	Per unit pitch	p.u.	0.8
A 8	SPREAD	Spread	deg.	60
A 9	D	Rotor diameter	ins.	61.5
A 10	G	Effective air gap	ins.	0.748
A 11	L	Rotor Length	ins.	106.2
A 12	RHO	Rotor iron resistivity	μΩ-cm	30
A 13	A13	Parameter		1
A 14	KMAX	Highest term required	(h ∓ 1)6	15
A 15	SLOT	Slot width (b)	ins.	0.866
A 16	REF.	Cross reference number		105

TABLE 6.3. M/C. REF: 1E 6/4/64

LOSS DUE TO HARMONICS IN MMF WAVEFORM

PPRS	NS	Z	Y	C	I	A13	KMAX
3.000	1000	2.000	1.000	1.000	2670	1.0	15

S/P/P	PITCH	SPREAD	D	G	L	RHO
5.0000	.80000	60.000	61.500	.74800	106.20	30.00

CF	CT	CN	PROG
.36045/ 05	.27146/-03	.23599/ 05	7

K	H	KPH	KDH	T/TM	N/NM	KW	KW TOT
1.0	5.00	.00000	.20000	.000	.000	0000	.0000
1.0	7.00	.58779	.14945	.659	.179	22.98	22.98
2.0	11.0	.95106	.10946	.368	.069	14.60	37.58
2.0	13.0	.58779	.10223	.148	.021	1.402	38.98
3.0	17.0	.58779	.10223	.082	.011	.6831	39.66
3.0	19.0	.95106	.10946	.087	.012	1.732	41.39
4.0	23.0	.58779	.14945	.049	.006	.6385	42.03
5.0	29.0	.95106	.95668	.176	.026	191.8	233.8
5.0	31.0	.95106	.95668	.141	.020	134.9	368.8
10	59.0	.95106	.95668	.026	.003	13.79	382.9
10	61.0	.95106	.95668	.023	.003	11.40	394.3

PROGRAMME PRINTS IF KW GREATER THAN 0.01KWTOT

6/4/64

TABLE 6.4 LOSS DUE TO HARMONICS IN MMF WAVEFORM

PPRS	NS	Z	Y	C	I	A13	KMAX
3.000	1000	2.000	1.000	1.000	2670	1.0	15

S/P/P	PITCH	SPREAD	D	G	L	RHO
5.0000	.80000	60.000	60.800	$\boxed{1.1000}$	106.20	30.00

CF	CT	CN	PROG
.36045/ 05	.18249/-03	.52866/ 05	7

K	H	KPH	KDH	T/TM	N/NM	KW	KW TOT
1.0	5.00	.00000	.20000	.000	.000	.0000	.0000
1.0	7.00	.58779	.14945	.413	.080	9.691	9.691
2.0	11.0	.95106	.10946	.199	.031	5.319	15.01
2.0	13.0	.58779	.10223	.073	.009	.4652	15.48
3.0	17.0	.58779	.10223	.040	.005	.2230	15.70
3.0	19.0	.95106	.10946	.042	.005	.5664	16.26
4.0	23.0	.58779	.14945	.024	.003	.2055	16.47
5.0	29.0	.95106	.95668	.088	.012	64.33	80.80
5.0	31.0	.95106	.95668	.070	.009	44.79	125.6
10	59.0	.95106	.95668	.012	.001	4.318	130.0
10	61.0	.95106	.95668	.011	.001	3.535	133.5

PROGRAMME PRINTS IF KW GREATER THAN 0.01KWTOT

TABLE 6.5

C/2A
14/4/64

LOSS DUE TO HARMONICS IN MMF WAVEFORM

PPRS	NS	Z	Y	C	I	A13	KMAX
3.000	1000	2.000	1.000	1.000	2170	1.0	15

S/P/P	PITCH	SPREAD	D	G	L	RHO
6.0000	.83333	60.000	61.500	.74800	106.20	30.00

CF	CT	CN °	PROG
.35154/ 05	.27146/-03	.23599/ 05	7

K	H	KPH	KDH	T/TM	N/NM	KW	KW TOT
1.0	5.00	.25882	.19718	.896	.408	19.66	19.66
1.0	7.00	.25882	.14529	.413	.080	2.513	22.18
2.0	11.0	.96593	.10173	.348	.064	11.69	33.87
2.0	13.0	.96592	.09195	.194	.030	3.822	37.69
4.0	23.0	.96593	.09195	.049	.006	.6135	38.36
4.0	25.0	.96592	.10173	.039	.005	.5115	38.87
6.0	35.0	.96593	.95614	.107	.015	94.42	133.3
6.0	37.0	.96592	.95614	.088	.012	69.40	202.7
12	71.0	.96594	.95614	.015	.002	6.622	209.5
12	73.0	.96592	.95614	.014	.002	5.605	215.1

PROGRAMME PRINTS IF KW GREATER THAN 0.01KWTOT

TABLE 6.6

C/3A
14/4/64

LOSS DUE TO HARMONICS IN MMF WAVEFORM

PPRS	NS	Z	Y	C	I	A13	KMAX
3.000	1000	2.000	1.000	1.000	1890	1.0	15

S/P/P	PITCH	SPREAD	D	G	L	RHO
7.000	.80952	60.000	61.500	.74800	106.20	30.000

CF	CT	CN	PROG
.35721/05	.27146/-03	.23599/ 05	7

H	KPH	KDH	T/TM	N/NM	KW	KW TOT
5.00	.07473	.19551	.551	.131	1.024	1.024
7.00	.50000	.14286	.587	.147	13.31	14.33
11.0	.98883	.09744	.347	.063	11.58	25.91
13.0	.73305	.08645	.153	.022	1.586	27.49
19.0	.82624	.07224	.055	.007	.3526	27.92
41.0	.95557	.95582	.071	.009	53.62	82.16
43.0	.95558	.95582	.060	.008	41.11	123.3
83.0	.95557	.95582	.010	.001	3.580	126.9
85.0	.95558	.95582	.009	.001	3.104	130.0

PROGRAMME PRINTS IF KW GREATER THAN 0.01KWTOT

TABLE 6.7

C/A/1E 22/7/65

LOSS DUE TO HARMONICS IN MMF WAVEFORM

PROGRAMME ACCOUNTS FOR SLOT WIDTH AND PRINTS IF KW EXCEEDS 0·01KWTOT

PROG 8

PPRS	NS	Z	Y	C	I	A13	KMAX
3·000	1000	2·000	1·000	1·000	2670	-1·0	10

S/P/P	PITCH	SPREAD	D	G	L	RHO	SLOT
5·0000	·80000	60·000	61·504	·74800	106·20	30·000	·86600

CF	CT	CN
·36045@+05	·27148@-03	·23594@+05

K	H	KPH	KDH	KBH	T/TM	N/NM	KW	KW TOT
1·0	5·00	·00000	·20000	·99293	·000	·000	·0000	·0000
1·0	7·00	·58779	·14945	·98617	·654	·177	22·18	22·18
2·0	11·0	·95106	·10946	·96606	·359	·067	13·31	35·49
2·0	13·0	·58779	·10223	·95278	·143	·020	1·226	36·71
3·0	17·0	·58779	·10223	·92008	·077	·010	·5415	37·26
3·0	19·0	·95106	·10946	·90078	·080	·010	1·293	38·55
4·0	23·0	·58779	·14945	·85667	·043	·005	·4116	38·96
5·0	29·0	·95106	·95668	·77811	·146	·021	96·23	135·2
5·0	31·0	·95106	·95668	·74903	·112	·015	59·86	195·1

H	FH	FH9	TM	N	NM	T
5·00	·167@-04	·391@-04	·381@-12	1200	·172@+11	·238@-18
7·00	·446@+03	·279@+03	·378@+03	857·1	·484@+04	·247@+03
11·0	·330@+03	·211@+03	·324@+03	1091	·164@+05	·116@+03
13·0	·159@+03	·107@+03	·889@+02	923·1	·456@+05	·127 +02
17·0	·117@+03	·812@+02	·634@+02	1059	·105@+06	·488@+01
19·0	·178@+03	·119@+03	·163@+03	947·4	·903@+05	·130 +02
23·0	·118@+03	·817@+02	·868@+02	1043	·196@+06	·377 +01
29·0	·880@+03	·522@+03	·610@+04	1034	·498@+05	·888@+03
31·0	·792@+03	·474@+03	·528@+04	967·7	·630@+05	·591 +03

TABLE 6.8. C/A/1J 27/7/65

LOSS DUE TO HARMONICS IN MMF WAVEFORM

PROGRAMME ACCOUNTS FOR SLOT WIDTH AND PRINTS IF KW EXCEEDS 0.01KWTOT

PPRS	NS	Z	Y	C	I	A13	KMAX	PROG 8
3.000	1000	2.000	1.000	1.000	2670	1.0	10	

S/P/P	PITCH	SPREAD	D	G	L	RHO	SLOT
5.0000	.80000	60.000	61.504	.74800	106.20	30.000	1.0996

CF	CT	CN
.36045@+05	.27148@-03	.23594@+05

K	H	KPH	KDH	KBH	T/TM	N/NM	KW	KW TOT
1.0	5.00	.00000	.20000	.98862	.000	.000	.0000	.0000
1.0	7.00	.58779	.14945	.97776	.651	.176	21.70	21.70
2.0	11.0	.95106	.10946	.94562	.354	.065	12.56	34.27
2.0	13.0	.58779	.10223	.92454	.139	.020	1.127	35.39
3.0	17.0	.58779	.10223	.87307	.074	.010	.4679	35.86
3.0	19.0	.95106	.10946	.84301	.076	.010	1.075	36.94
5.0	29.0	.95106	.95668	.65765	.128	.018	60.23	97.48
5.0	31.0	.95106	.95668	.61521	.095	.013	34.34	131.8

TABLE 6.9 C/B/1E 29/10/65

LOSS DUE TO HARMONICS IN MMF WAVEFORM PROG MS-1L

PROGRAMME ACCOUNTS FOR SLOT WIDTH AND PRINTS ALL TERMS

PPRS	NS	Z	Y	C	I	A13	KMAX	REF
3.000	1000	2.000	1.000	1.000	2670	-1.0	10	105.000

S/P/P	PITCH	SPREAD	D	G	L	RHO	SLOT
5.0000	.80000	60.000	61.504	.74800	106.20	30.000	.86600

CF	CT	CN
.36045@+05	.27148@-03	.91186@+04

K	H	KPH	KDH	KBH	T/TM	N/NM	KW	KW TOT
1.0	5.00	.00000	.20000	.99293	.000	.000	.0000	.0000
1.0	7.00	.58779	.14945	.98617	.723	.208	24.55	24.55
2.0	11.0	.95106	.10946	.96606	.446	.077	16.51	41.06
2.0	13.0	.58779	.10223	.95278	.195	.025	1.679	42.74
3.0	17.0	.58779	.10223	.92008	.111	.012	.7782	43.52
3.0	19.0	.95106	.10946	.90078	.110	.012	1.777	45.30
4.0	23.0	.58779	.14945	.85667	.063	.006	.5998	45.90
4.0	25.0	.00000	.20000	.83204	.000	.000	.0000	45.90
5.0	29.0	.95106	.95668	.77811	.167	.020	110.3	156.2
5.0	31.0	.95106	.95668	.74903	.130	.015	69.40	225.6
6.0	35.0	.00000	.20000	.68722	.000	.000	.0000	225.6
6.0	37.0	.58779	.14945	.65473	.015	.001	.0474	225.6
7.0	41.0	.95106	.10946	.58720	.012	.001	.0414	225.7
7.0	43.0	.58779	.10223	.55242	.006	.000	.0055	225.7
8.0	47.0	.58779	.10223	.48151	.004	.000	.0029	225.7
8.0	49.0	.95106	.10946	.44565	.005	.000	.0085	225.7
9.0	53.0	.58779	.14945	.37375	.003	.000	.0025	225.7
9.0	55.0	.00000	.20000	.33798	.000	.000	.0000	225.7
10	59.0	.95106	.95668	.26745	.012	.001	.4708	226.2
10	61.0	.95106	.95668	.23294	.010	.001	.2609	226.4

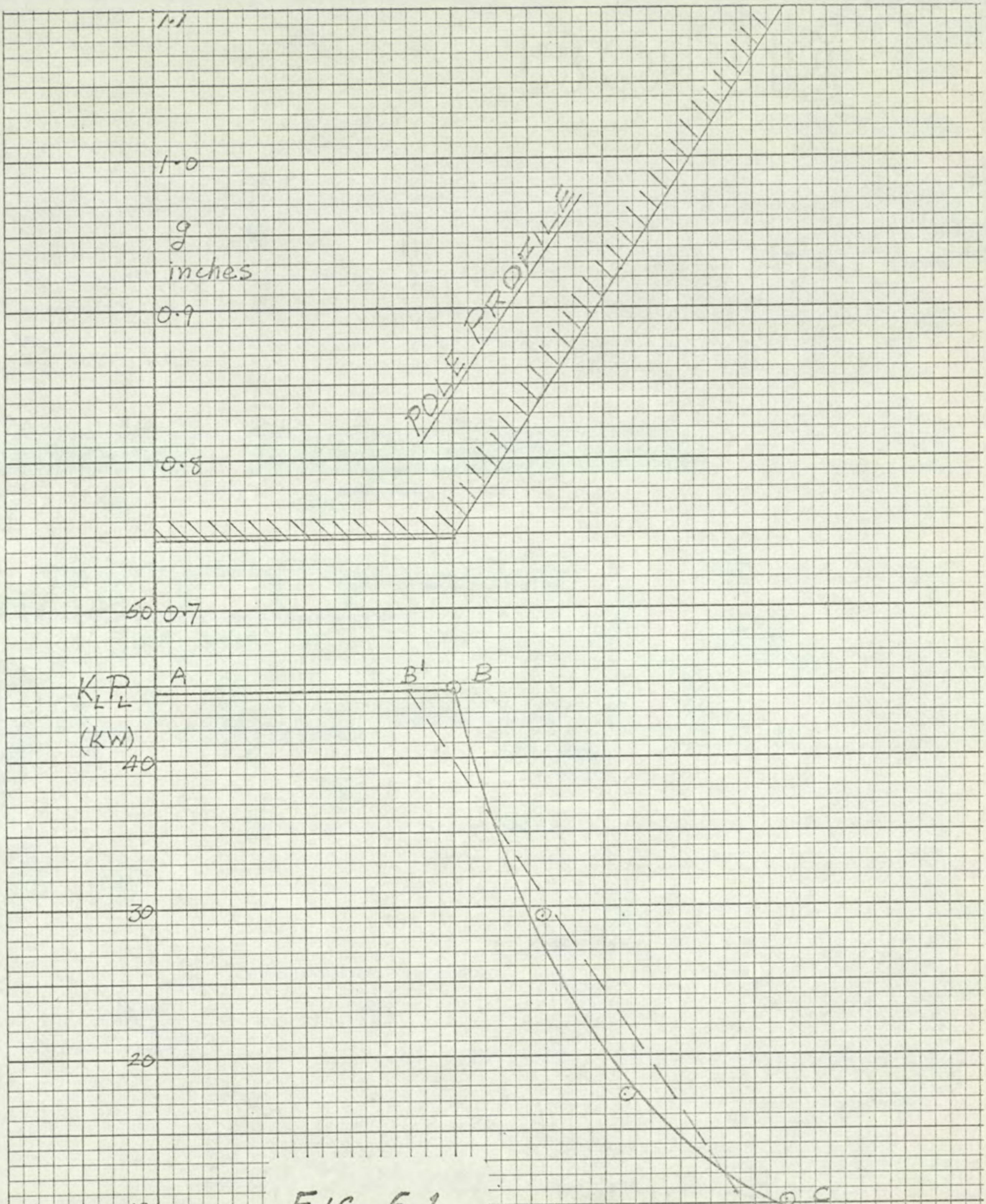
1·1
1·0
g
inches
0·9
0·8
0·7
POLE PROFILE
50
40
30
20
10
0
$K_L P_L$
(KW)
A
B'
B
C
C'
D
0
10
20
θ_2 °M

FIG. 6.1

Table 6.10 The Effect of Peripheral Flux Leakage.
Machine Ref: 105 Table 6.9
P_L = Computed Loss in kW, K_L = Reduction Factor From Fig.12.2.4

h	hp =3h	g = 0.748" g/D_o= 0.012 (Table 6.9)			g = 0.84" g/D_o= 0.013			g = 0.925" g/D_o= 0.015			g = 1.1" g/D_o= 0.017		
		P_L	K_L	P_LK_L	P_L	K_L	P_LK_L	P_L	K_L	P_LK_L	P_L	K_L	P_LK_L
7	21	24.55	0.78	19.1	19.68	0.74	14.6	16.0	0.67	10.7	11.15	0.62	6.90
11	33	16.51	0.57	9.4	12.69	0.51	6.5	9.87	0.42	4.15	6.23	0.35	2.18
13	39	1.68	0.47	0.8	1.26	0.41	0.5	0.96	0.32	0.3	0.58	0.26	0.15
17	51	0.78	0.31	0.2	0.56	0.26	0.1	0.43	0.16	0.07	0.26	0.14	0.04
19	57	1.78	0.25	0.4	1.28	0.21	0.3	0.97	0.114	0.11	0.61	0.08	0.05
23	69	0.60	0.16	0.1	0.44	0.13	0.1	0.35	0.065	0.02	0.23	0.05	0.01
29	87	110.3	0.08	8.8	80.0	0.06	4.8	60.5	.025	1.51	36.9	0.02	0.67
31	93	69.4	0.07	4.9	49.7	0.05	2.5	37.9	0.012	0.45	23.4	0.01	0.23
59	177	0.47	-	-	0.33	-	-	0.24	-	-	0.14	-	-
61	183	0.26	-	-	0.18	-	-	0.14	-	-	0.08	-	-
Totals:		226		44.5	166		29.4	127		17.3	79.7		10.2
Sub-Totals Belt :		46		29.8	36		22.1	19		15.3	191		9.3
Slot :		180		13.7	130		7.3	108		2.0	60.6		0.9

The second method uses a graph of loss per unit surface area against pole periphery. The loss is calculated for discrete increments in gap length over the shaped portion of the pole. The computer programme does not include the peripheral flux leakage factor K_L. Therefore each harmonic loss figure in the computer print-up must be multiplied by the corresponding value of K_L, as in Table 6.10. Computations for four values of g between g_1 and g_2 (inclusive) yield four points on a graph of W_{TOT} against pole angle, Fig. 6.1. The loss in all 6 poles, taken as the mean height of the curve multiplied by the pole arc/pole pitch ratio of 0.7, is 22.6 kW - about 11% lower than method one.

(iii) <u>The Flux Leakage Factor</u> K_L

The factor K_L is based on the widely accepted premise that eddy current losses vary as the square of the flux,(i.e. $W_h \propto (\phi ac)^2{}_h$) Fig. 12.2.4. The modified eddy current coupling equations suggest another relationship between loss and flux :

Section 3.6.1. states :

$$\phi \propto \frac{W_h}{H}$$

Furthermore, $$H_m \propto W_h^{1/2m}$$

hence : $$\phi \propto W_h^{1-1/2m}$$

$$\therefore W_h \propto \phi^{2m/(2m-1)}$$

when m = 0.794 $\underline{W_h \propto \phi^{2.7}}$

In using the index 2.7 instead of 2, K_L would be reduced by $(\phi_i / \phi_o)^{2.7/2.0}$

However in view of the widely accepted index of 2 , more recent work by James[38] on eddy current couplings in which an index nearer to

2(namely 2.4) was measured, and the assumptions upon which K_L is based it was decided in the first instance to take

$$K_L = \left(\frac{\phi_i}{\phi_o}\right)^2$$

and evaluate K_L for any particular machine from the family of curves plotted in Appendix 12.2.2 Fig. 12.2.4

6.3.2 Changes in Main Machine Dimensions

Because of the high indices involved, as the frame size increases the loss increases at a greater rate than the D^2L product and the effect of a relatively large gap in reducing the loss may be swamped, so that the harmonic m.m.f. loss becomes an increasing proportion of the total load loss. From this point of view, a long machine is better than a short one.

From tests on practical machines it is very difficult to assess the effect of changing one machine parameter only, since a change in unit rating usually entails a change in several parameters. Occasionally a second machine which differs in only one major aspect from its predecessor is tested. The data on three such machines; made available by industry, is tabulated below. Machines reference C and D differ only in core length, A and B in gap length. B is actually machine A with its gap increased. This also applies to E and F in Table 6.13. Both A and E originally had a particularly high stray load loss which was reduced by turning a few mm. off the pole shoes.

In many other cases the rotor is also grooved thereby making it impossible to assess the effect of an increase in gap alone.

Table 6.11

Comparison of Measured and Calculated Losses

			A	B	C	D
1.	Machine Reference Cross Reference		A 1.2330	B 1.4025	C 330/1	D 200331
2	MVA Rating		1.5		3.4	2.15
3.	Pole pairs	p	2		2	2
4.	Synchronous speed	N_s r.p.m.	1800		1500	1500
5.	Effective Conductors per slot	Z/Y	2		10	16
6.	Parallel paths per phase	C	4		1	1
7.	Total phase current	I amp	2460		179	113
8.	Slots/pole/phase	q	9		6	
9.	Pitch	p.u.	0.815		0.778	
10.	Spread	deg.	60		60	
11.	Rotor diameter	D mm	682	686	865	
12a.	Actual air gap	g mm	9.0	7.0	7.5	
12b.	Effective air gap	g_1 mm	9.99	7.95	8.9	
13.	Slot width	b mm	10.5		18	
14.	Slot pitch	λ_s mm	20.4		38.5	
15.	Active rotor length	L mm	490		1020	640
16.	Rotor iron resistivity	ρ $\mu\Omega$-cm	21		25.4	
17.	Chamfered Periphery/pole pitch	β_1	0.13		0	
18.	Parallel-gap periphery/pole pitch	β_2	0.35		0.7	
19.	Ampere-conductors/mm		65		47.6	
20.	$g/(D + 2g)$		0.012	0.010	0.0085	
	Computed Loss (mmf harmonics only)					
21.	Belt harmonic terms	kW	0.43	0.70	3.6	2.2
22	Slot harmonic terms	K_L "	0.1	0.1	0.3	0.3
23.	Slot harmonic terms	W_{slot} "	0.18	0.34	4.4	2.8
24.	Slot harmonic terms	$K_L W_{slot}$ "	0.02	0.03	1.3	0.8
25.	Total	$K_L W$ kW	0.45	0.73	4.9	3.0
26.	CHANGE (Reduction in Loss)		0.3 kW		40%	
27	Total stray load loss measured on short circuit test	kW	10.5	11.5	28.3	19.4
28	CHANGE		1.0 kW		32%	
	Calculated tooth pulsation loss (Gibbs)	kW	1.1	1.9	Change in length = 40%	
	Change		0.8 kW			
	Measured iron loss on open circuit test	kW	10	11		
	CHANGE	kW	1 kW			

For all machines the rotor surface was ungrooved.

The peripheral flux leakage factor for the first pair of belt harmonics ($\simeq$ 0.94) has not been included.

In Table 6.11 machines A and B are identical apart from their respective air gaps of 9 and 7 mm. The values of gap tabulated account for the effects of armature slotting in the usual way by Carter coefficients. This was suggested by Laurenson[7] in his recent paper on tooth pulsation loss.

Increasing the gap reduced the measured load loss on the short circuit test by 1 kw (or 10%) which is of the same order as the change in computed loss (0.3 kW). These results together with Fig.12 of Richardson's paper (which shows that the 'short circuit loss minus the end winding loss' to be proportional to g^2) give support to the theoretical prediction of the change in loss width g. The change in calculated tooth pulsation loss (using Gibbs' formula) of 0.8 kW, which compares favourably with the change in measured value, is also included. Incidentally the calculated surface losses due to these two different phenomena are roughly the same order of magnitude.

Machines C and D have the same endwinding construction and differ only in that the length of machine C(and therefore its computed loss,) has been decreased by about 40%. The measured loss on short circuit has also decreased in the same proportion, but is greater in magnitude than the computed figure since it includes all the stator supplementary losses which are difficult to separate with any degree of confidence.

For Machines E & F, Table 6.13, the components of stray loss have been estimated by the manufacturers.

The calculated m.m.f. harmonic loss is compared with the measured loss in Table 6.13, K_L is not included. The machine details appear in Table 6.12.

Table 6.12 Computer Data Sheet

POLE FACE LOSS DUE TO M.M.F. HARMONICS

DATA - FRACTIONAL SLOT, 3-PHASE WINDINGS

				E	F		
LABEL:- cr. 1f. cr. sp[45] REF. DATE. cr. 1f. cr. bk			REF.	50 MVA 260646/1	50 MVA 26064/1		
			DATE.	13/11/64	/ /	/ /	/ /
A 0	PPRS	Pole pairs		3	3		
A 1	NS	Synchronous speed	r.p.m.	1000	1000		
A 2	Z	Conductors/slot		72	72		
A 3	Y	Parallel paths/coil side		18	18		
A 4	C	Parallel paths/phase		3	3		
A 5	I	Total phase current	amp	2620	2620		
A 6	S/P/P	Numerator ϕ		11	11		
A 7	S/P/P	Denominator ϕ		2	2		
A 8	PITCH	Per unit pitch	p.u.	0.787878	0.787878	0	0
A 9	D	Rotor diameter	ins.	64.8	64.3		
A10	G	Effective air gap	ins.	0.6	0.85		
A11	L	Stator length	ins.	110	110		
A12	RHO	Rotor iron resistivity		24.7	24.7		
A13	A13	Integer Parameter*		1	1	1	1
A14	K	Highest term required 6(h±1)		12	12		
A15	SLOT.	Slot width (b)	ins.	0.84	0.84		
A16	REF.	Cross reference No.		145	147		

FOOTNOTES * To print k, h, k_{ph}, k_{dh}, T/T_m, T, KW, KW TOT: A13 > 1
To princt complete data: A13 < 1

ϕ A6 and A7 must be prime to each other. e.g. for $5\frac{1}{2}$ S/P/P A6 = 11, A7 = 2

The slot harmonic terms are expected to produce little loss in view of the large (slot pitch / gap) ratio of 3.3. They are excluded from the analysis but are included in the Table 6.13 for interest.

Table 6.13 Breakdown of Losses for Two 50 MVA machines

Machine Reference No. Cross References Air gap.	E 260646/1 0.6"	F 260646/1 0.85"	Ratio E/F 1/1.4
Calculated m.m.f. loss (a) Belt & slot (b) Belt	120 38	60 25	2.0 1.5
Measured s/c Loss	314	259	
Estimated losses : Stator winding d.c. Cu loss Core end loss + tooth loss + total slot eddy loss + circulating loss, by calc^{n}.	132 75 207	132 68 200	
Total pole face, by subtraction	107	59	1.8

The m.m.f. harmonic losses computed by the modified eddy current coupling theory (excluding peripheral flux leakage) are of the right order of magnitude. Multiplication by K_L, which is not worthwhile until all the other stray losses can be assessed accurately, will reduce the slot terms by about 90% (see Fig.12. 2.3). The ratio of E/F will then be nearer the value on the bottom row determined by the summation of losses. Although the whole analysis is dependent upon the validity of the methods used to calculate the other short circuit losses, which are based on the industrial experience of the particular manufacturer, it serves to illustrate the practical difficulties in verifying any theoretical loss formulae. The last row also includes any short circuit slot ripple loss.

In table 6.13 the computed cylindrical rotor loss has been multiplied by the fractional pole pitch. Pole contour has been accounted for graphically (ref. section 12.2) but no account has been taken of the variation in the summated harmonic magnitude from pole centre to pole tip (see chapter 7). The E/F ratios in the top and bottom rows satisfy the proportionality : $W \propto \frac{1}{g^{1.7}}$

6.4 Other methods of Calculation

The predicted m.m.f. harmonic loss in the pole faces of two machines using the methods of Kuyper[1] and Barello[2] are compared with that obtained using the eddy current coupling theory (Table 6.17).

The two machines are :-

i. The 60 MVA, 6 pole synchronous compensator ref. 1E Tables 6.7 and 6.9.

and

ii. The experimental load loss dynamometer. In the first, the predictions are compared with the stray load loss measured on the short circuit test and in the second with the pole face loss measured in the laboratory.

Some further comments are also made on the methods of Kuyper and Barello. The solutions of Maxwell's field equations by these two authors is outlined in section 3.11 . Their solutions apply to the idealised mathematical model of Fig. 2.7 used for the modified eddy current coupling theory. They differ from the latter inthe attention paid to peripheral flux leakage but not paid to the variation in permeability.

6.4.1 Barello

The formula for the m.m.f. harmonic loss per unit area of pole face derived by Barello is quoted in section 3.11 (equation 3.36)and evaluated below using an assumed value of μ .

The substitution of an analytical expression for permeability in the early stages of Barello's derivation (just after the integration of the field equations - Davies[3] solution) is, unlike Davies' solution, unhelpful. For example :

The constants of integration E_1 and E_2 are found by solving the two simultaneous equations 6.3 and 6.4 (valid when $\sqrt{2}\alpha \gg 2\pi/\lambda$). Their final form is more cumbersome if a substitution for is attempted :

$$E_1 e^{2\pi g/\lambda} + E_2 e^{-2\pi g/\lambda} = \rho J_m \qquad (6.3)$$

and $$E_1 e^{2\pi g/\lambda} - E_2 e^{-2\pi g/\lambda} = -\rho J_m \frac{\mu_0}{\mu} \cdot \frac{\lambda\alpha}{2\pi}(1+j) \qquad (6.4)$$

Davies[3] shows (his eq.7) that when $\sqrt{2}\alpha$ dominates $2\pi/\lambda$ the magnetic intensity, H tends to H_x, where

$$H_x = \frac{\beta + j\gamma}{2j\,\alpha^2} J_z$$

$$= \frac{\alpha(1+j)}{2j\alpha^2} J_z \quad \text{when } \sqrt{2}\alpha \gg 2\pi/\lambda \quad \text{(section 3.4)}$$

Hence $$J_m = \alpha(1+j) H_m$$

Let us take an analytical substitution for μ of the form :

$$\mu^{\frac{1}{2}} H = k_1 H^m$$

Putting $$\alpha^2 = \mu\omega/2\rho$$

and adding 6.3 to 6.4 we get :

$$E = \frac{1}{2\sqrt{2}}\left[\rho^{\frac{1}{2}}\omega^{\frac{1}{2}}k_1^2 H_m^{2m-1} + j\left\{\rho^{\frac{1}{2}}\omega^{\frac{1}{2}}k_1^2 H_m^{2m-1} + \omega\mu_0\lambda H_m/\pi\sqrt{2}\right\}\right]e^{-2\pi g/\lambda}$$

The different indices of H_m make this expression less manageable than one in terms of μ

$$E = \tfrac{1}{2}\rho J_m\left[1 - \frac{\mu_0\lambda\alpha}{2\pi\mu}(1+j)\right]e^{-2\pi g/\lambda}$$

which is used to obtain the loss equation 3.3 6.

When the gap is comparatively large, for example when $\lambda/g < \pi$, some terms in Barello's equations become negligible. This inequality usually applies to terms of order $6q \pm 1$ (slot harmonics), and for these the gap permeance is most important, any such mathematical simplification must be confined to a model which makes a realistic appraisal of the gap profile and not applied to the idealised model used by Barello. The calculations made in this section will therefore be limited to a direct application of Barello's loss equation - equation 3.3 6 section 2.4.2. For convenience in hand calculations, where the values of F_h are available from the computer print-up, an appropriate substitution is made in the numerator of equation 3.3 6 as follows

Using the nomenclature of equation 12.1.1 , appendix 12.1,

$$F_h = 2.70 \quad q \frac{k_{wh}}{h} \cdot \frac{ZI}{2YC}$$

where Z = Conductors per slot

I = Total phase current in amps.

Y = parallel paths per phase.

C = Parallel paths per coil side.

Then, in equation 3.36,

$$N = Zq/Y$$

and $$F_h = 2.70 \left(\frac{k_{wh}}{h}\right) \frac{IN}{ZC} \qquad (6.5)$$

multiplying by the pole surface area of a cylindrical rotor, π DL, equation 3.36 becomes :

$$P = \sum \frac{3.1 \pi D L C^2 F_h^2 \; (6Kf)^{1.5} \times 10^{-8}}{\sqrt{\mu\rho} \left\{ [\sinh A + B\cosh A]^2 + [B\cosh A]^2 \right\}} \qquad (6.6)$$

where $A = 2\pi g h / \lambda_1$

and $B = \dfrac{\alpha}{\mu_r} \cdot \dfrac{\lambda_1}{2\pi h}$

The loss P_B is now calculated first for a 60 MVA synchronous compensator, and second for the experimental load loss dynamometer. The numerator of the first machine, which has salient poles, is also multiplied by the pole arc/pole pitch ratio.

Example 1

Machine ref 1E. The main dimensions and F_h are tabulated in Tables

6.7 and 6.9, pole arc/pole pitch ratio = 0.7.

Taking Barello's suggested value of $\mu_r \rho = 3 \times 10^{-4}$ and noting that $\rho = 30 \times 10^{-8}$ Ω-m we get

$$\mu_r = 1000$$

and $\sqrt{\mu_r \rho} = 0.0173$

hence

$$\alpha = \left\{\pi \times 10^3 \times \frac{4\pi}{10^7} \cdot \frac{6K \times 50}{30 \times 10^{-8}}\right\}^{1/2}$$

$$= 1980\sqrt{K}$$

$$\lambda_1 = \frac{\pi D}{p} \times 0.0254 = \frac{\pi \times 61.5 \times 2.54}{3 \times 100} = 1.64 \text{ m.}$$

$$g/\lambda_1 = 0.0748/6.45 = 0.0116$$

$$A = 2\pi h \times 0.0116 = 0.0728h$$

$$B = \frac{1980\sqrt{K} \times 1.64}{1000 \times 2\pi h} = 0.516\sqrt{K}/h$$

$$P_{Bh} = 0.7 \times \frac{3.1\pi \times 61.5 \times 106.2 \times 2.54^2 \times 10^{-4} \times 300^{1.5} \times F_h^2 K^{1.5} \times 10^{-8}}{0.0173\left\{[\sinh A + B\cosh A]^2 + B^2\cosh^2 A\right\}}$$

or

$$P_{Bh} = 0.124\, F_h^2 K^{1.5} \times 0.7/\left\{[\sinh A + B\cosh A]^2 + B^2\cosh^2 A\right\}$$

The loss is now calculated in Table 6.14.

Example 2. The Experimental Machine

The principal dimensions and tabulated values of F_h are given in Table 3.5. Keeping μ_r at 1000 and putting $\rho = 27 \times 10^{-8}\,\Omega\,m.$ (at 100°C) we get

$$\mu_r \rho = 2.7 \times 10^{-4}$$

and $\sqrt{\mu_r \rho} = 0.0164$

hence

$$\alpha = \sqrt{\pi \mu . 6Kf_1/\rho}$$

$$= \left\{\pi \times \frac{4\pi}{10^7} \times 10^3 \times \frac{6K \times 50}{20 \times 10^{-8}}\right. = 2430\sqrt{K} \quad m^{-1}$$

$$g/\lambda_1 = 0.000305/0.456 = 0.00067$$

$$A = 2\pi h\, g/\lambda_1 = 0.0042h$$

$$B = \frac{\alpha \times \lambda_1}{\mu_r \times 2\pi h} = \frac{2430\sqrt{K} \times 0.456}{1000 \times 2\pi h} = 0.176\sqrt{K}/h$$

Subst. in equation 6.6 to give :

TABLE 6.14.

Barello's method of calculation for machine ref. 1E - 60 MVA.

K	h	F_h	$K^{1.5}$	*	A	B	chA	shA	BchA	(d+e)	$(d+e)^2$	e^2	g+l	loss
					.0728h	$\frac{0.516\sqrt{K}}{h}$								$P_B = \frac{b}{m}$
			a	b $\times 10^3$			c	d	e	f	g	l	m	kW
1	5	0	1	0	-	-	-	-	-	-	-	-	-	0
	7	446	1	24.6	0.508	0.074	1.17	0.560	0.086	0.646	0.418	0.007	0.425	59
2	11	330	2.83	38.1	0.801	0.067	1.34	0.888	0.090	0.978	0.960	0.008	0.968	41
	13	159	2.83	8.82	0.945	0.056	1.49	1.10	0.083	1.183	1.40	0.007	1.407	6.3
3	17	117	5.19	7.38	1.24	0.053	1.89	1.58	0.100	1.69	2.86	0.010	2.87	2.6
	19	178	5.19	20.4	1.38	0.047	2.11	1.76	0.100	1.86	3.46	0.010	3.47	5.9
4	23	118	8	13.8	1.67	0.045	2.75	2.55	0.124	2.67	7.15	0.015	7.17	1.9
	25	0	8	0	1.82	-	-	-	-	-	-	-	-	0
5	29	880	11.2	1080	2.21	0.040	4.22	4.55	0.169	4.72	22.3	0.029	22.33	49
	31	792	11.2	870	2.36	0.037	5.2	5.1	0.193	5.3	28.2	0.037	28.24	31
													TOTAL	196.7

* $b = 0.124\, F_h^2\, K^{1.5}$

TABLE 6.15. Kuyper's method of calulation for machine ref. 1E

K	h	Using Fig. 3.8: $\frac{hgp}{D} = 0.0365h$	R_1	$6KhF_h^2R_1$	Loss $= 9.85 \times (c) \times 10^{-6}$	Using Fig. 3.7: μ_r	g/λ_h	$\sqrt{\frac{6Kf_1\lambda_1^2}{\mu_r \rho h^2 \times 10^9}}$	R_1	Loss kW $\frac{(d)\times(l)}{(c)}$
		(a)	(b)	(c)	(d)	(e)	(f)	(g)	(l) ϕ	(m)
1	5	0.183	0.52	0	0	250	0.06	0.207	0.55	0
	7	-	-	-	-	250	0.08	0.148	0.33	28
	7	0.256	0.34	29.5	29	1000	0.08	0.074	0.22	19
2	11	0.402	0.18	26	26	1000	0.13	0.067	0.066	9.5
	13	0.475	0.135	5.3	5.2	1000	0.15	0.057	0.045	1.7
3	17	0.621	0.08	3.2	3.2	1000	0.20	0.053	0.018	0.7
	19	0.694	0.054	5.9	5.8	1000	0.22	0.047	0.012	1.3
4	23	0.840	0.03	2.3	2.3	1000	0.27	0.045	0.007	0.5
	25	0.914	0.022	0	0	1000	0.29	0.041	*	*
5	29	1.06	0.012	81	80	1000	0.34	0.040	*	*
	30	1.13	0.009	53	52	1000	0.36	0.037	*	*
			TOTAL = 204.2					for μ_r = 1000, TOTAL =32		
5	29					10	0.34	0.4	0.012	80
	30					10	0.36	0.37	0.008	46

Multiplying by the ratio: pole arc / pole pitch of 0.7, we get:

$$\text{Total Loss} = 0.7 \times 9.85 \times 10^{-6} \sum_{K=1}^{5} (hF_h)^2\, 6K\, R_1 / h$$

$$= 0.7 \times 9.85 \times 10^{-6} \times 204.2 \times 10^5$$

$$= 141 \text{ kW} \quad \text{(using Fig.3.8.)}$$

Belt harmonic loss = 67 x 0.7

= 47 kW (using Fig. 3.8.)

or 32 x 0.7 = 22 kW (using Fig.3.7.)

ϕ indicates that R_1 is near a maximum.
* indicates that R_1 is outside the plotted range.

$$P_{Bh} = \frac{0.00215 \; F_h^2 \; K^{1.5}}{[sh A + B ch A]^2 + B ch A^2}$$

The results of this calculation, performed in like manner to example 1. above are tabulated in Table 6.17.

6.4.2. Kuyper

(i) Loss Prediction

Kuyper's Formula for pole face loss due to primary m.m.f. harmonics, equation 3.41 section 3.11 is modified to include k_{bh} :

$$P_K = \sum_{K=1}^{\infty} \{A_1^2 \times 10^{-9} \times Lp\}\left\{\frac{f_{hr} R_1}{h}\left(\frac{k_{bh} \; k_{dh} \; k_{ph}}{k_{b1} \; k_{d1} \; k_{p1}}\right)^2\right\} \quad \text{kW} \quad (6.7)$$

$A_1 = \frac{\pi}{4} F_1$; f_{hr} and F_1 are defined in section 3.2 (v)and (vii) resp.

Substituting for A_1, f_{hr} and F_1 we get :

$$P_K = \sum_{k=1}^{\infty} \{1.5\sqrt{2}\, NIq\, k_{w1}\, k_{b1}\}^2 \times 10^{-9} \times Lp \times \frac{6Kf_1 R_1}{h}\left(\frac{k_{wh} \; k_{bh}}{k_{w1} \; k_{b1}}\right)^2 \quad \text{kW} \quad (6.8)$$

For convenience in hand calculations, where F_h is available from the computer print-out, the substitution :

$$A_1^2\left(\frac{k_{wh} \; k_{bh}}{k_{w1} \; k_{b1}}\right)^2 = h^2 A_h^2 = h^2 \left(\frac{\pi}{4} F_h\right)^2$$

gives

$$P_K = Lp\, f_1 \times 10^{-9} (\pi/4)^2 \sum_{K=1}^{\infty} F_h^2 \times 6Kh \times R_1 \quad (6.9)$$

In view of the difficulty in selecting suitable values for μ_r, and (to a lesser extent) ρ, Kuyper proposes a pessimistic estimation of the loss (i.e. a high value of R_1) occuring with the worst combination of factors. The maximum value of R_1, plotted by Kuyper against a quantity which is independent of ρ and μ_r, is redrawn in Fig. 3.7 section 3.11 Further work (section 10.1.) will presumably bring about a revision of this pessimistic philosophy as the state of the art advances.

The loss calculations of the previous section are now repeated using equation 6.9.

Example 1. Machine Ref 1E, Tables 6.7 and 6.9

The expression for the pole face loss caused by the armature m.m.f. harmonics stated as equation 6.9 is :

$$P_K = Lpf_1 \times 10^{-9} \times \left(\frac{\pi}{4}\right)^2 \sum_{K=1}^{\infty} (hF_h)^2 \times \frac{6K}{h} \times R_1$$

where $h = 6K \pm 1$
L is in inches

In the following calculations the resistance factor R_1 is taken from Figs. 3.7 and 3.8 in turn.

$$L_{pf_1} \times 10^{-9} \times (\pi/4)^2 = 106.2 \times 3 \times 50 \times 10^{-9} \times \pi^2/16$$
$$= 9.85 \times 10^{-6}$$

For Fig. 3.8 :

$$hgp/D = 0.748 \times 3h/61.5$$
$$= 0.0365h$$

For Fig. 3.7:

$$\rho = 30 \times 10^{-6}$$
$$\lambda_1 = \frac{\pi D}{3} \times 2.54 = 164 \text{ cm}$$
$$g/\lambda_1 = 0.0116 \text{ and } g/\lambda_h = 0.0116h.$$

The loss is now calculated in Table 6.15

Example 2. The Experimental Machine

The main dimensions and "F_h" of the experimental machine are taken from Table 3.5.

$$Lpf_1 \times 10^{-9} \times (\pi/4)^2 = 9.85 \times 2 \times 50 \times 10^{-9} \times \pi^2/16$$
$$= 0.607 \times 10^{-6} \text{ inch-sec units.}$$

For the method using Fig. 3.8 :

$$hgp/D = 0.012 \times 2h/11.42 = 0.0021h$$

NB If $h < 47$, hgp/D lies outside Kuyper's range and is not calculable .
The loss for the 47th and 49th harmonics is quoted below Table 6.16.

The calculation using Fig.3.7, Table 6.16, requires the following data :

TABLE 6. 16. Kuyper's method of calculation for the experimental load loss dynamometer.

R_1 is determined from Fig. 3.7

I_A = 29.8 A, 50 c/s

ρ = 27$\mu\Omega$ - cm (100°C)

K	h	$\frac{\lambda_1}{h}\sqrt{\frac{f_{hr} \times 10^{-9}}{\mu\rho}}$	g/λ_h = 0.00067h	R_{11}	Loss kW
1	5	0.030	0.0034	8*	0.66
	7	0.027	0.0047	7.5*	0.48
2	11	0.020	0.0074	4.5	0.34
	13	0.016	0.0087	3.1	0.20
3	17	0.0155	0.011	2.1	0.15
	19	0.014	0.013	1.7	0.102
4	23	0.013	0.015	1.3	0.08
	25	0.012	0.017	0.95	0.054
5	29	0.0115	0.019	0.7	0.040
	31	0.011	0.021	0.55	0.028
6	35	0.0105	0.023	0.5	0.025
	37	0.010	0.025	0.45	0.021
7	41	0.010	0.027	0.4	0.019
	43	0.009	0.029	0.3	0.012
8	47	0.009	0.031	0.28	0.010
	49	0.009	0.033	0.25	0.008
			Total for 1st 16 terms		2.201

Using Fig. 3.8. $P_{K\ (h = 47)}$ = 0.04 kW (R_1 = 1.0)

$P_{K\ (h = 49)}$ = 0.03 kW (R_1 = 0.9)

* estimated by extrapolation

From Fig. 5.6 $\rho = 27 \times 10^{-6}\ \mu\Omega$-cm at 100°C

$\lambda_1 = 29\pi/2 = 45.6$ cm

$g/\lambda_1 = 0.0305/45.6 = 0.000\,67$

$g/\lambda_h = 0.00067h$

The harmonics, for which g/λ_h lies within the range plotted in Fig. 3.8, are $h \geqslant 11$, whence

$g/\lambda_h = 0.0074$

(ii.) Permeability

Using Kuyper's graphs of the resistance factor R_1 for a particular machine, a value of permeability can be found. The examples below show that this value is unrealistic and inconsistant.

Example 3.

Consider the 7th harmonic of a turbo alternator (e.g. machine reference CEGB/K). The relevant data is :

$g = 1.5''$

$D = 37''$

$p = 1$ pair

$\rho = 27.5\ \mu\Omega$ - cm

For the 7th harmonic,

$g/\lambda_7 = 1.5 \qquad = 0.09$

and $f_7 = 6Kf_1 \qquad = 300$ c/s

From Fig. 3.7 when $g/\lambda = 0.09$, R_1 has a maximum value of 0.3

and $\sqrt{\dfrac{f\lambda^2 10^{-9}}{\mu_r \rho}} = 0.35$

Solving this equation for μ_r :

$$\mu_r = 300\left(\frac{37\pi}{7} \times 2.54\right)^2 \times \frac{10^{-9}}{27.5 \times 10^{-6} \times 0.1225}$$

(cm units)

$$= 300 \times 1780 \times 10^{-3}/3.38$$

$$= \underline{160}$$

This value is considered impractical for the reasons given in Section 8.1.

Example 4.

Consider the example given by Kuyper in line 3 of his Table 3. In the test described a machine was operated at its rated speed of 3600 rpm with direct current applied to the armature winding connected in open delta.

The relevant machine details are :

$$\rho = 20\ \mu\Omega\text{-cm}$$

$$D = 20''$$

$$g = 0.375''$$

$$\lambda_1 = 20\pi$$

$$g/\lambda_1 = \tfrac{3}{8} \times \frac{1}{20\pi} = 0.006$$

For the first triplen harmonic, which Kuyper tabulates in line 3,

$$h\frac{gP}{D} = 3 \times \tfrac{3}{8} \times 1/20 = 0.056$$

The corresponding value of R_1 lies outside the range published by both Kuyper and Chalmers(Fig. 3.8) but is quoted by Kuyper as :

$$R_1 = 1.6.$$

With $R_1 = 1.6$, and $g/\lambda_3 \simeq 0.02$ the value of μ implied is obtained by reading from Fig. 3.7

$$\sqrt{\frac{f_3 \lambda_3^2 10^{-9}}{\mu_r \rho}} = 0.08$$

Thence

$$\mu_r = f_3 \lambda_3^2\ 10^{-9}/0.0064\rho$$

$$= 4000$$

This value of μ_r, obtained by using R_1 from Fig. 3.8, is obviously too high, supporting Kuyper's recommendation that Fig. 3.7 gives a more realistic estimate of the measured loss. Kuyper repeats the calculation in lines 1 and 2 using Fig. 3.7 giving R_1 values of 0.75 and 1.1. He assumes values of μ_r = 100 and 400 respectively, which the author considers too low. Nevertheless using these values of μ_r, values of R_1 fall below and to the right of the maxima.

6.5 Comparison of Methods

Table 6.17 summarises the calculations made in this chapter using the methods of Kuyper and Barello together with the proposed theory. Whilst it is unrealistic to draw any general conclusion from two sample calculations (which are not necessarily typical) it is evident that all the methods of calculation highlight the partiuularly lossy harmonic terms, and predict a pole face loss of the right order. Kuyper's short method using Fig. 3.8 overestimates the loss in both above examples, his long method with μ_r = 1000 underestimates it.

The peripheral flux leakage factor used with the modified eddy current coupling theory seems to overestimate the reduction of surface loss due to the peripheral leakage of the harmonic fluxes in the air gap.

TABLE 6.17. Comparison of methods.

The harmonic loss in KW is calculated using (1) Kuyper's formula (two methods of finding R_1), Barello's formula and the modified eddy current coupling theory.

K	h	Experimental load loss dynamometer.			60 MVA machine ref. 1E Cross ref. 105				
		Kuyper Fig. 3.7	Barello	E.C.C. ref. A44 (164)	Kuyper Fig. 3.7	Fig. 3.8	Barello	E.C.C. By computer	E.C.C. Including leakage
		$\mu_r = 1000$	$\mu_r = 1000$		$\mu_r = 1000$		$\mu_r = 1000$		
		P_K	P_B	P_L	P_K	P_K	P_B	P_L	$K_L\ P_L$
1	5	0.66	0.20	0.44	0	0	0	0	0
	7	0.48	0.13	0.33	19	29	59	24.6	19.1
2	11	0.34	0.01	0.30	9.5	26	41	16.6	9.4
	13	0.20	0.06	0.20	1.7	5.2	6.3	1.68	0.8
3	17	0.15	0.05	0.14	0.7	3.2	2.6	0.78	0.2
	19	0.10	0.03	0.09	1.3	5.8	5.9	1.78	0.4
4	23	0.08	0.02	0.06	0.5	2.3	1.9	0.6	0.1
	25	0.05	0.02	0.04	0	0	0	0	0
5	29	0.04	0.01	0.03	*	80	49	110.3	8.8
	31	0.03	0.01	0.02	*	52	31	69.4	4.9
6	35	0.03	0.01	0.01					
	37	0.02	0.01	0.01					
7	41	0.02	0.00	0.01					
	43	0.01	0.00	0.01					
Belt		-	-	-			117	46	30
Slot		-	-	-			80	180	14
Total		2.2	0.65	1.69	32	204.2	197	226	44
Total x Pole arc/Polepitch				-	22	143	137	158	31 ∅
Measured value		1.92					-		
Stray load loss on S/C							246		
Stray load loss minus the estimated supplimentary copper loss							146		

* outside the range of plotted data ∅ = 25 kW when poles chamfered.

7. THE DISTRIBUTION OF HARMONIC E.M.F.S AT THE POLE SURFACE

7. THE DISTRIBUTION OF HARMONIC E.M.F.S AT THE POLE SURFACE

7.1 Introduction

In section 2.3 the fluctuations in the predicted armature m.m.f. waveform were shown to be much greater on the direct axis of the m.m.f. wave ($\theta_2 = 0$) than on the quadrature axis ($\theta_2 = \pm 90^\circ E$). The induced electric intensity (E) in the pole member, the current density (J), and the loss ($\int \rho J^2$) will therefore very in magnitude between these two axes. This chapter details the measurement of the induced e.m.f.s. ($= \int_0^L E \, dz$) at the secondary surface (i.e. the pole surface) of the experimental machine by means of search coils. In section 7.4 the results are analysed in conjunction with the theory presented in sections 7.2 and 12.5. The analysis takes into account the troughs in the polarising field opposite the armature slot openings. These have a marked effect on the time variation of the search coil voltages, increasing the magnitude and quantity of high order harmonics, Oscillograms A1 to F5, section 7.4.1.

The first pair of m.m.f. harmonics (for which K = 1) and the first slot ripple harmonic all induce 300 c/s e.m.f.s. in the secondary and cannot therefore be separated empirically. They were isolated from the other harmonics by using a narrow band pass filter and from each other by applying the theory given in Appendix 12.5.

The analysis in practical machines is complicated further by the varying displacement between the m.m.f. waves and the pole shoe (section 2.3). This is avoided here by using an experimental model having magnetic symmetry and a uniform air gap.

7.2. The Search Coil Array

Two groups of search coils were laid in fine axial grooves cut approximately 0.005" deep with a 0.005" circular saw blade, Fig. 7.1 (a). The first group contained six 0.0025" diameter resin insulated wires spaced 1/5th of a fundamental pole pitch apart, the second group contained eight wires spaced 1/7th, i.e. the groups spanned a fundamental pole pitch and were full-pitched to either the 5th or 7th m.m.f. harmonic. These wires were formed into search coils by soldering a common bus rail at one end of the secondary core and a screened multicore cable at the other, care being taken to avoid pick-up from stray fluxes, Fig. 7.1 (b). The e.m.f.s induced in a selected search coil could be investigated by the switching arrangement of Fig. 7.2. Gold plated plugs and sockets and a silver plated selector switch were used to minimise contact resistance. The 5 coils pitched $\lambda_1/10$ (or $\pi/5^c$) were labelled 51 to 55 and those pitched $\pi/7$, 71 to 77. Coils 53 and 74 were used for most tests as they had the same axis.

7.3. Theory

An expression for the e.m.f. induced in a very short pitched search coil on the secondary surface is now derived in terms of its angular position relative to the inducing m.m.f. wave by considering the rate of change of flux-linkages.

7.3.1 General Expression for the Primary M.M.F.

E.M.F.s are induced in the secondary of the experimental machine due to (i) the changes in the air gap flux density caused by the primary slot openings and (ii) the rotating primary m.m.f. harmonics. The variation in flux density due to the slot openings, already referred to in section 5, is analysed in Appendix 12.6 into a slowly decaying Fourier series. Both

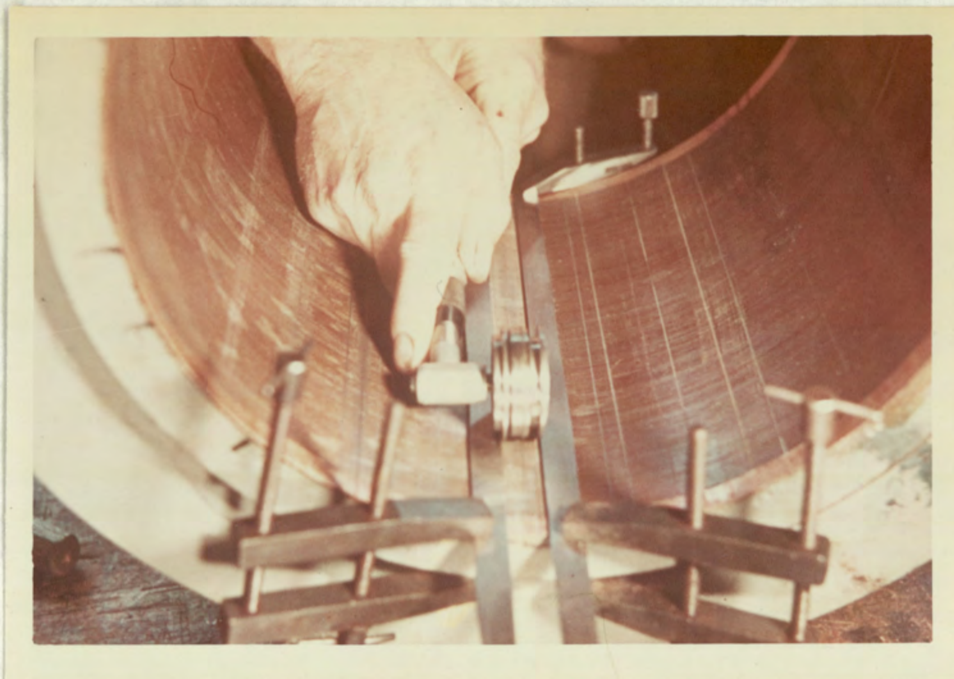

FIG. 7.1(a) CUTTING THE 0.006" WIDE GROOVES FOR THE SEARCH COILS.

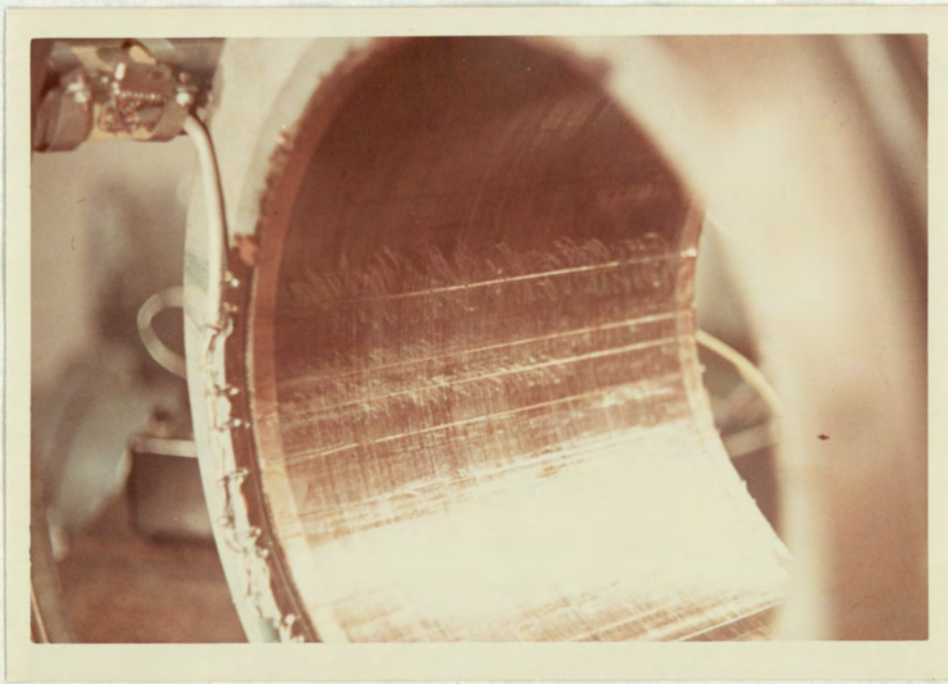

FIG. 7.1(b) THE SEARCH COIL ARRAY.

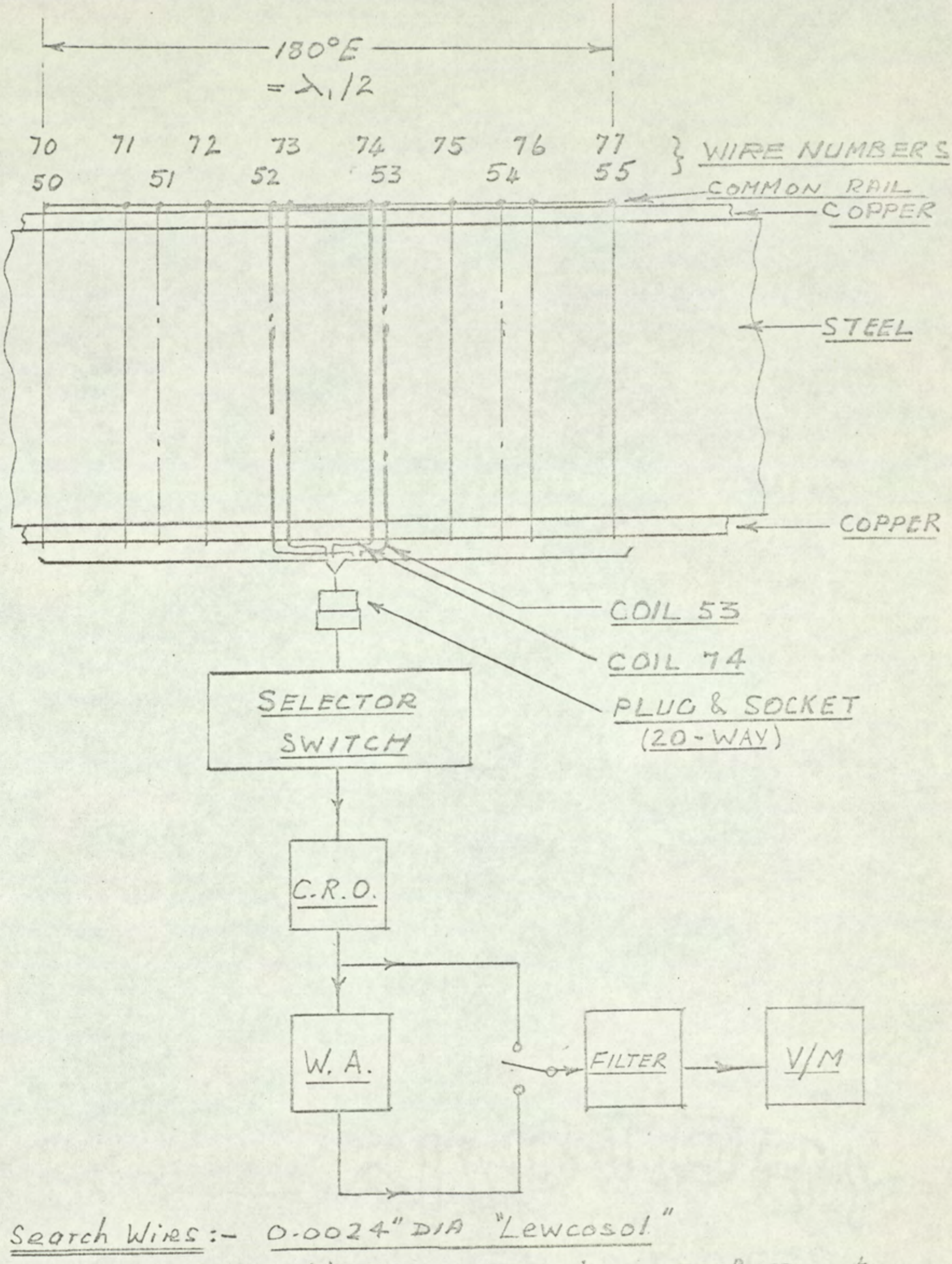

Search Wires :- 0.0024" DIA "Lewcosol"
coil 53 uses wires 52 & 53 etc.
set in 0.006 in. sq. grooves using an
Unsaturated Polyester Resin

FIG. 7.2 THE SEARCH COIL ARRAY

the frequency and the wavelength, of the first pair of slot ripple harmonics are shown to equal that of the qth pair of m.m.f. harmonic terms ($q = S/P/P$) A resultant e.m.f. can therefore be obtained by vector addition.

The problem is analysed initially by considering these 300 c/s e.m.f.'s to the exclusion of all higher orders, even though the higher order terms may in practice alter the effective permeability. A smooth cylindrical secondary is also assumed, such as an unslotted turbo-alternator rotor or the secondary of the experimental machine, i.e. we assume that the air-gap is uniform and the pole arc is 180°E. When balanced sinusoidal currents flow in the practical 3-phase integral slot winding (having 60° phase bands and represented by AA', BB' and CC', (Fig. 7.3) the rotating m.m.f. waves are established. These may be expressed mathematically in terms of the primary space angle θ_1 by equation 3.1, section 3, viz :

$$F = \frac{6\sqrt{2}}{\pi} (NI_{RMS})\, q \left(K_{w1} \cos(\theta_1 - \omega_1 t) + \ldots + \frac{1}{h} + K_{wh} \cdot \cos(h\theta_1 \mp \omega_1 t) + \ldots \right)$$

The fundamental wave rotates at synchronous speed, its direct axis being coincident with the axis of that phase coil carrying maximum current (Fig. 7.3). The velocity of these rotating m.m.f. waves with respect to the secondary is obtained by subtracting from the speed of each the relative speed of the secondary. Therefore by making the substitution, $\theta_2 = \theta_1 - \omega_1 t$ in equation 3.1 we get the Fourier series for the m.m.fs. appearing at the secondary surface :

$$F = F_1 \cos\theta_2 + F_5 \cos(5\theta_2 + 6\omega_1 t) + \ldots \quad F_h \cos(h_2 + (h \pm 1)\omega_1 t) \tag{7.1}$$

where $h = 6K \mp 1$

and $F_h = \dfrac{F_1 K_{wh}}{h\ K_{w1}} = \dfrac{6\sqrt{2}\ NIq.}{h} \dfrac{K_{wh}}{K_{w1}}$

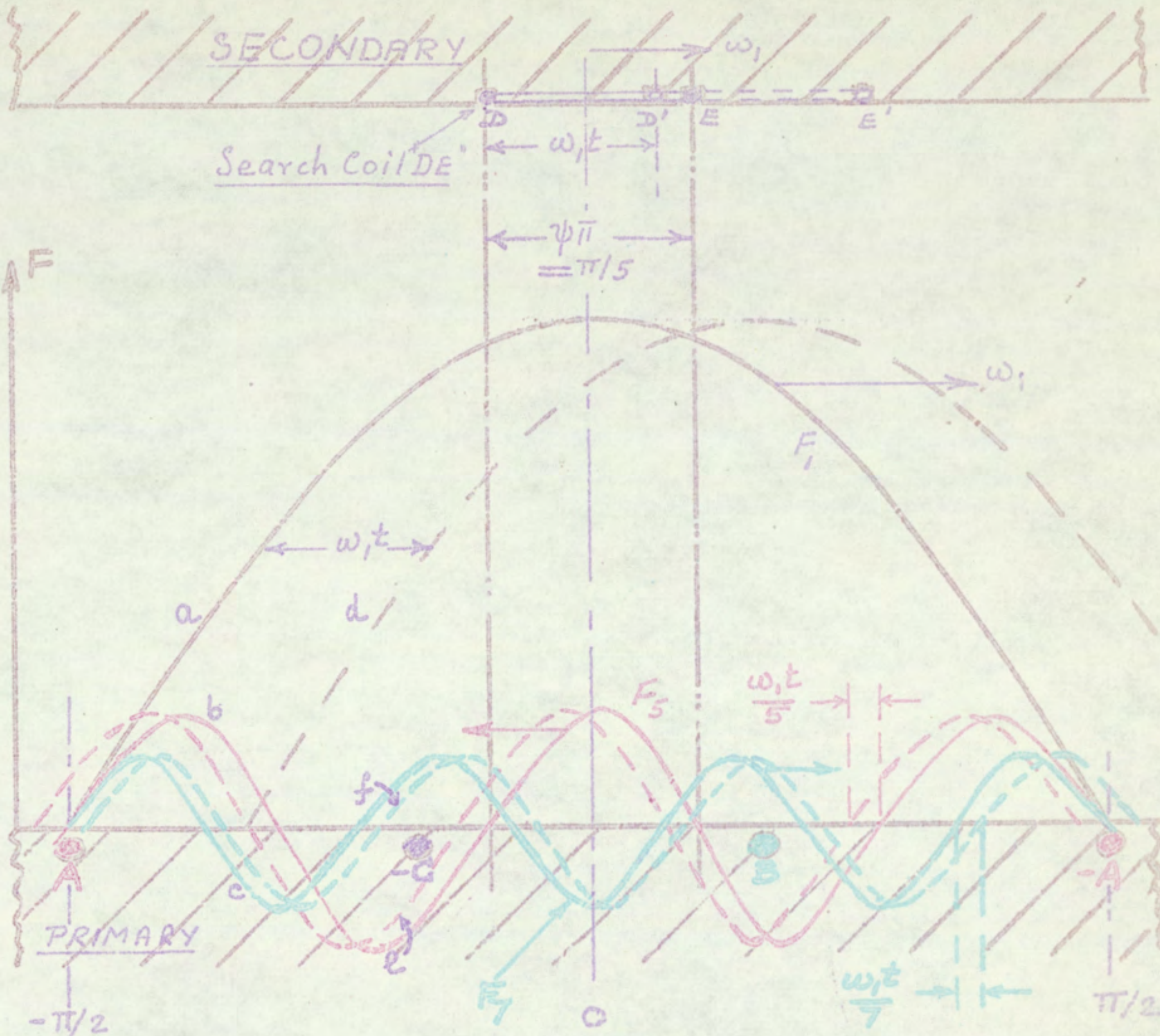

Curves a, b & c: Position of Fundamental, & 5th and 7th Harmonics Respectively, when $\omega_1 t = 0$

d, e & f: Ditto, when $\omega_1 t = 30°E$

All curves are shown relative to the primary and apply to the Experimental Machine which has a full-pitched winding with 1 s/p/p.

FIG 7.3 THE HARMONIC M.M.F.S

PROBLEM NO. A1
DATE: 28/1/64
HARMONICS IN MMF WAVEFORM

K	H	KPH	K_{DH}
1.0	5.00	1.0000	1.0000
1.0	7.00	-1.0000	1.0000
2.0	11.0	-1.0000	1.0000
2.0	13.0	1.0000	1.0000
3.0	17.0	1.0000	1.0000
3.0	19.0	-1.0000	1.0000
4.0	23.0	-1.0000	1.0000
4.0	25.0	1.0000	1.0000
5.0	29.0	1.0000	1.0000
5.0	31.0	-1.0000	1.0000
6.0	35.0	-1.0000	1.0000
6.0	37.0	1.0000	1.0000
7.0	41.0	1.0000	1.0000
7.0	43.0	-1.0000	1.0000
8.0	47.0	-1.0000	1.0000
8.0	49.0	1.0000	1.0000
9.0	53.0	1.0000	1.0000
9.0	55.0	-1.0000	1.0000
10	59.0	-1.0000	1.0000
10	61.0	1.0000	1.0000
11	65.0	1.0000	1.0000
11	67.0	-1.0000	1.0000
12	71.0	-1.0000	1.0000
12	73.0	1.0000	1.0000

Table 7.1. Change in sign of k_{ph} for the Experimental machine having a full-pitched winding with 1 S/P/P

At the direct axis $\theta_2 = 0$ and therefore :

$$F_{da} = F_1 + (F_5 + F_7)\cos 6\omega_1 t + \ldots + (F_{6K-1} + F_{6K+1})\cos 6k\omega_1 t \qquad (7.$$

At the quadrature axis $\theta_2 = \pi/2$, hence:

$$\begin{aligned} F_{qa} &= 0 + F_5\cos(6\omega_1 t + \pi/2) + F_7\cos(6\omega_1 t - \pi/2) + \\ &\quad + F_{11}\cos(12\omega_1 t - \pi/2) + F_{13}\cos(12\omega_1 t + \pi/2) \\ &\quad + \ldots\ldots \quad F_h\cos(6K\omega_1 t \pm h\pi/2) \\ &= -1(F_5 - F_7)\sin 6\omega_1 t + (-1)^2(F_{11} - F_{13})\sin 12\omega_1 t + \ldots \\ &\quad \ldots + (-1)^K(F_{6K-1} + F_{6K+1})\sin 6K\omega_1 t \end{aligned} \qquad (7.3$$

i.e. at the direct axis all the harmonic m.m.fs. are added algebraically whereas at the quadrature axis they are subtracted. It must be remembered that the harmonic m.m.f. F_h may be positive or negative depending on the signs of its component winding factors. This point is now illustrated by considering the harmonic winding factors of the experimental machine, Table 7.

7.3.2 The Experimental Machine - Harmonics

In contrast to the full pitched infinitely distributed winding of Fig. 2.5, which produces a maximum m.m.f. fluctuation at the direct axis, the full pitched integral winding of the experimental machine produces a minimum fluctuation. This is found by changing the signs of the coefficients in equation 7.3. in accordance with Table 7.1. The sum of each 6K - 1 term and the corresponding 6K + 1 term will be a maximum at the direct axis and a minimum at the quadrature axis:-

$$F_{qa} = F_1\left\{-\left(\frac{k_{w5}}{5} + \frac{k_{w7}}{7}\right)\sin 6\omega_1 t + \left(\frac{k_{w11}}{11} + \frac{k_{w13}}{13}\right)\sin 12\omega_1 t \right.$$
$$\left. - - - - - (-1)^K\left(\frac{k_{wh}}{h} + \frac{k_{w(h+2)}}{h+2}\right)\sin 6K\omega_1 t\right\} \qquad (7.4)$$

where k_{wh} = the modulus of the winding factor

and h = 6K - 1, not 6K ∓ 1.

In appendix 12.5.1 equations describing the e.m.f.s induced in the secondary search coils are derived in terms of the alternating flux densities caused by the m.m.f. harmonics. These equations show that at the direct axis the induced e.m.f.s e_h and e_{h+2} are 180° out of phase and that this phase difference is reduced by $2\theta_2$ at any point displaced $\theta_2{}^\circ$E from the direct axis. The quadrature axis e.m.f.s are therefore in phase.

7.3.3 Experimental Machine - M.M.F. Waveform

The analysis of Appendix 12.5 shows that the m.m.f. fluctuation is not necessarily a maximum at the direct axis as implied in section 2.3. The position of maximum fluctuation depends upon the magnitude and sign of each harmonic winding factor, or, fundamentally, upon the actual shape of the m.m.f. waveform and the way this waveform changes in time relative to the pole surface.

This change in the m.m.f. waveform was illustrated for a full pitched infinitely distributed winding in Fig. 2.5., section 2.3. It is repeated here for a practical winding having 1 s/p/p. The m.m.f. wave relative to the primary is plotted for three instants in time in Fig. 7.4. It is evident that a small fluctuation occurs at the direct axis but not evident at the quadrature axis. By taking 12 equal increments in time, curves 1 to 13 Fig. 7.5, the time variation of the direct axis and quadrature axis m.m.f.s can be plotted. The m.m.f. fluctuation at the direct axis, curve (a) Fig. 7.5., is much smaller than at the quadrature

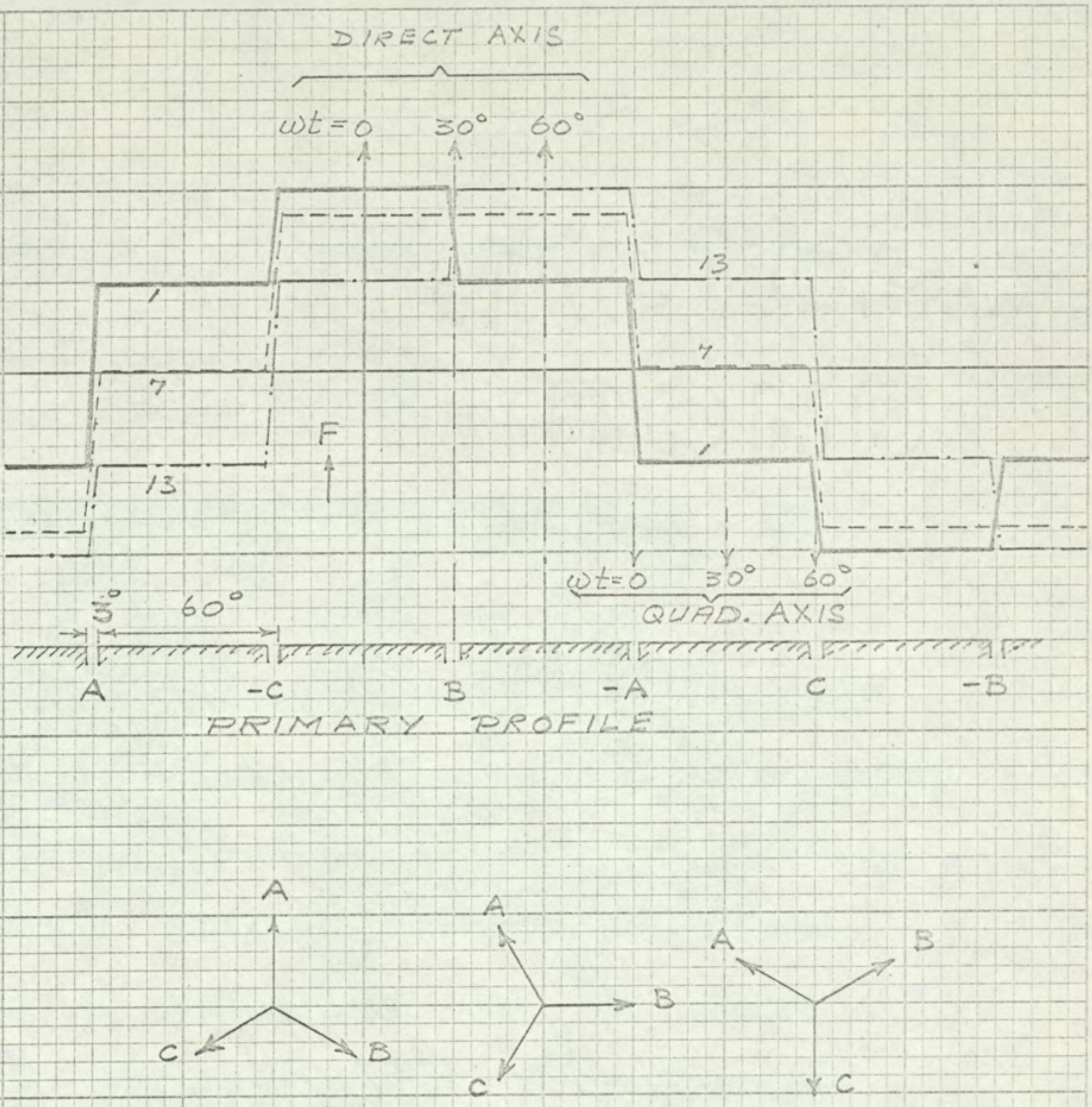

CURVE 1	CURVE 7	CURVE 13
$\omega t = 0°$	$\omega t = 30°$	$\omega t = 60°$

Curve 1 shows the Impressed M.M.F., F, Produced by the Primary Winding, as a Function of the Angular Displacement Along the Primary Circumference at one instant in time: $t = 0$.

Curves 7 and 13 show how F changes in space after discrete intervals of time.

Curves 2 to 6 and 8 to 12 are shown in Fig 7.5.

The Arrowheads indicate the M.M.F. axes for 1, 7 & 13.

FIG. 7.4 M.M.F. WAVEFORMS IN THE EXPERIMENTAL MACHINE

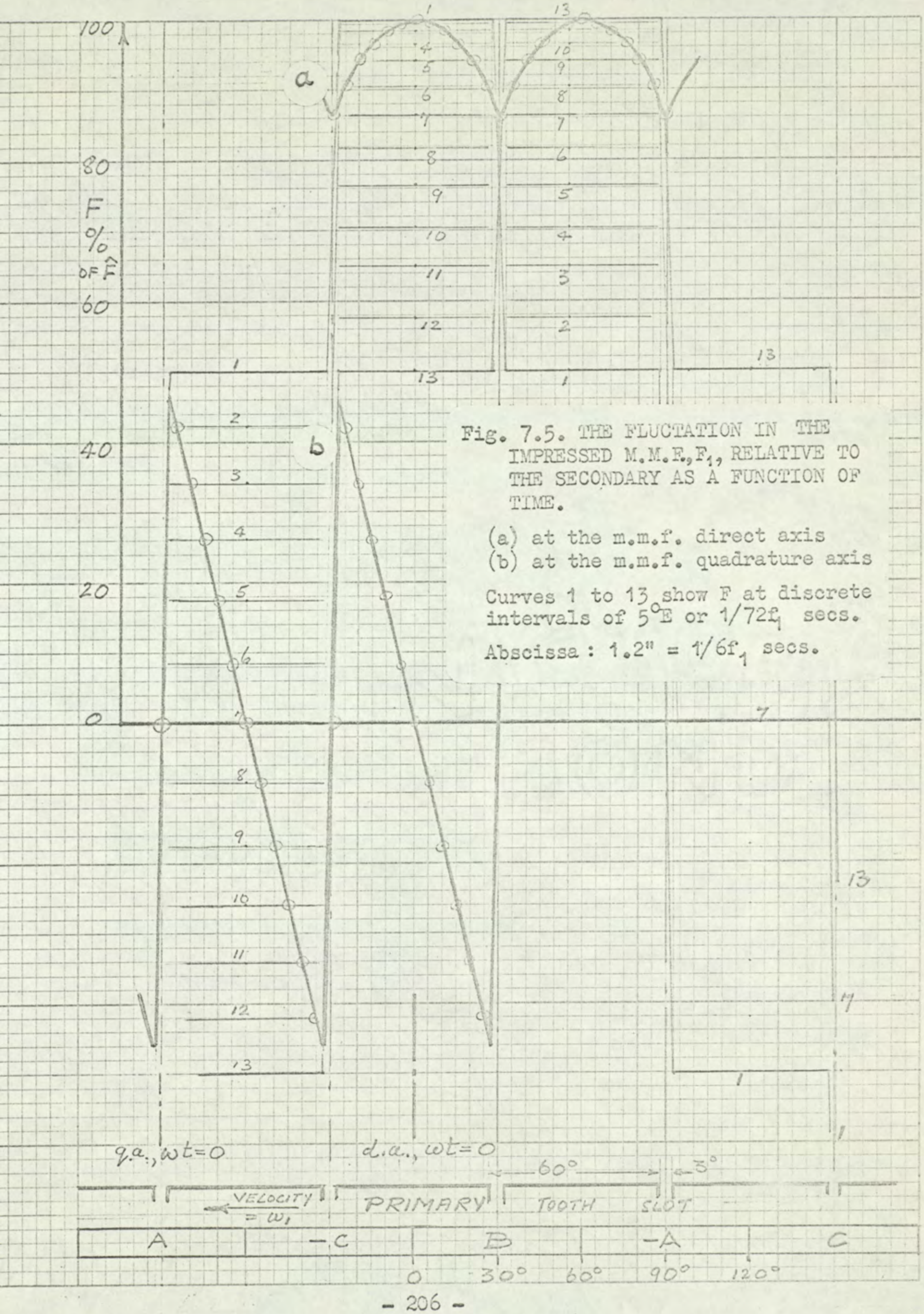

Fig. 7.5. THE FLUCTATION IN THE IMPRESSED M.M.F., F_1, RELATIVE TO THE SECONDARY AS A FUNCTION OF TIME.

(a) at the m.m.f. direct axis
(b) at the m.m.f. quadrature axis

Curves 1 to 13 show F at discrete intervals of 5°E or $1/72f_1$ secs.

Abscissa : 1.2" = $1/6f_1$ secs.

axis, curve (b), and confirms the conclusion drawn from the harmonic synthesis in section 7.3.2. that the direct axis m.m.f. is greater than the quadrature axis m.m.f. The d.a. fluctuation is similar to that of Fig. 2.5., i.e. the low number of armature conductors has little influence on the d.a. fluctuation. On the other hand the q.a. fluctuation is very different to that of Fig. 2.5., the influence of the small number of armature conductors situated below the narrow slot openings being considerable.

7.4 Experimental Results

The variation in search coil e.m.f. over a pole pitch was found by swinging the secondary in its trunnion bearings. All readings for a given search coil pitch were thereby obtained using one coil eliminating any error due to differences in coil construction. Coils numbered 53 and 74 were selected because they were coaxial (Fig. 7.2)

7.4.1 The Waveforms of the Induced E.M.F.s.

Oscillograms of the induced e.m.f.s in coil 74 are shown below (A 1-5, C 1-5, E 1-5). The point on the polarising wave and the primary current is indicated. Oscillograms B 1-5, D 1-5, F 1-5 show the corresponding flux-linkage waveforms obtained using an integrating amplifier.

The most striking feature is the influence of the primary slot openings causing sharp peaks of e.m.f.. Unfortunately this distortion together with an unknown degree of armature reaction foils any serious attempt to correlate the oscillograms with the m.m.f. waveform fluctuations of Fig.7.5. The waveform obtained with the primary unexcited is explained below.

The slight change in the waveform of successive cycles is due to rotor deformations mainly at the slot openings. Repetition occurs every 12 cycles after one complete revolution of the rotor.

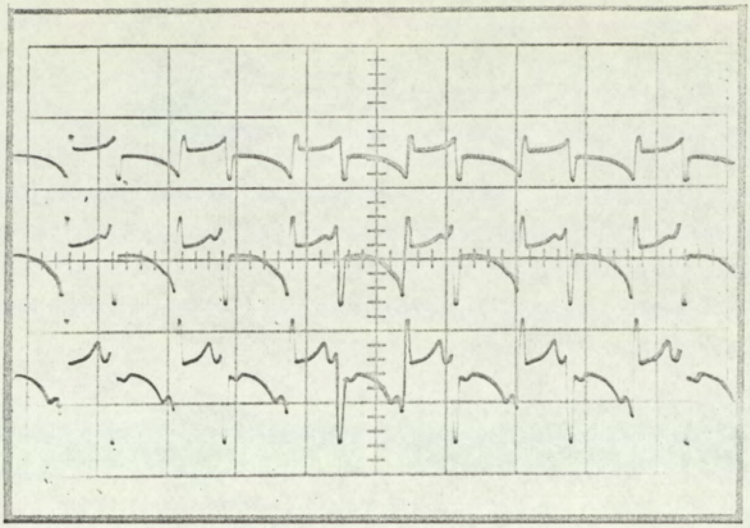

A1 10

A2 20

A3 30

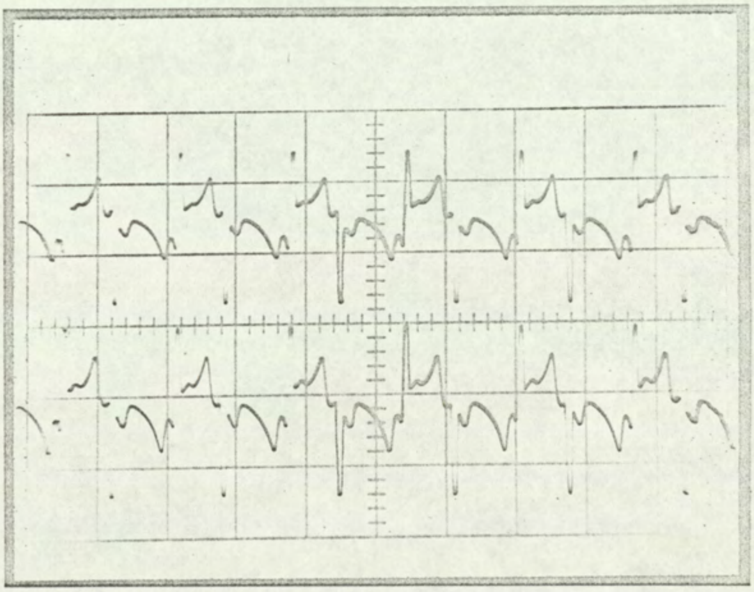

A4 40

A5 50

E.M.F. induced in coil 74

Armature phase current indicated in amps.

SEARCH COIL WAVEFORMS - DIRECT AXIS.

B1 10

B2 20

B3 30

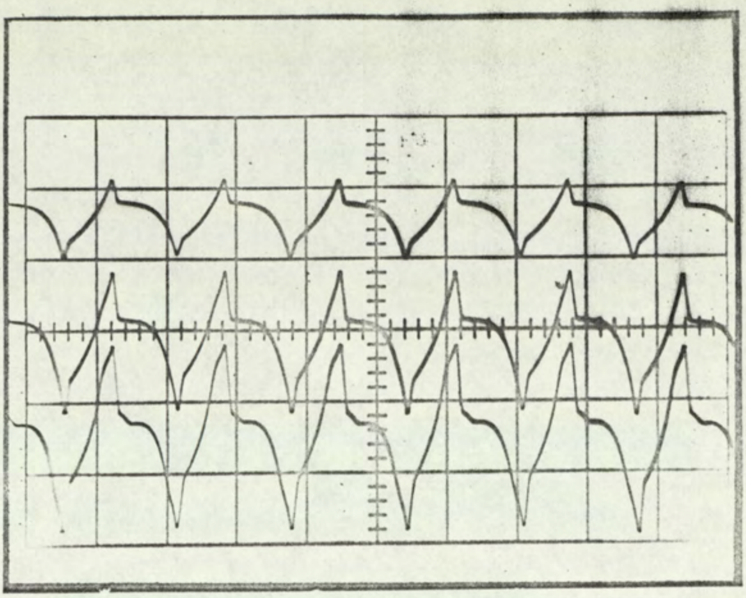

B4 40

B5 50

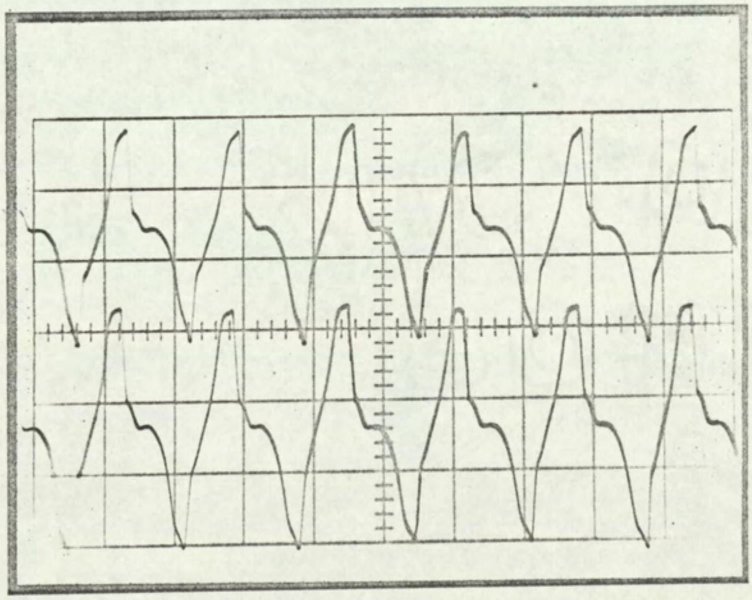

Flux linkage with coil 74
Armature phase current indicated in amps.

SEARCH COIL WAVEFORMS - DIRECT AXIS.

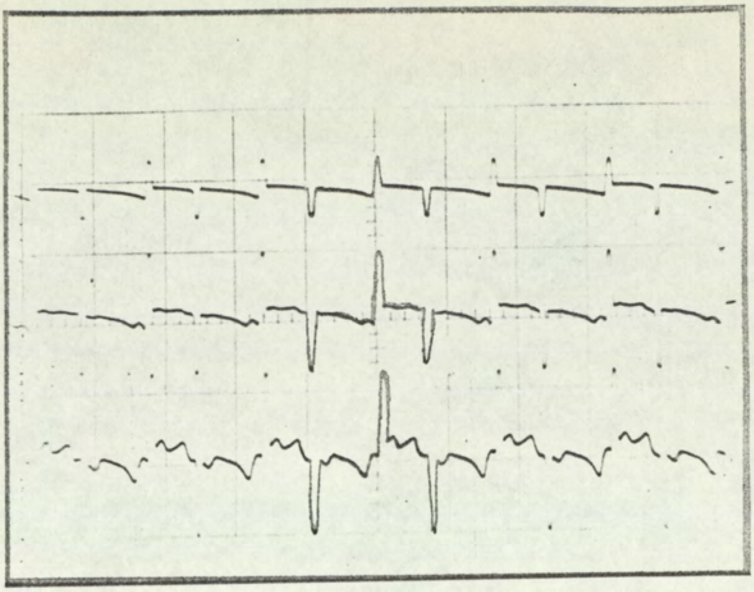

C1 10

C2 20

C3 30

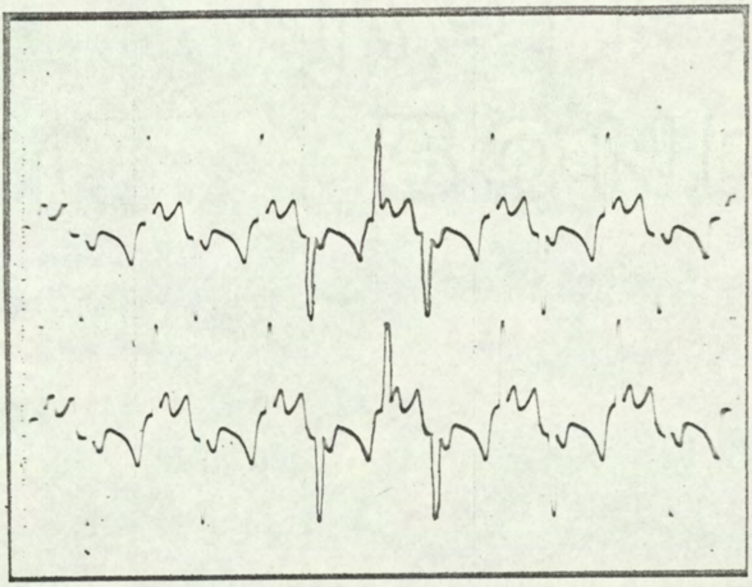

C4 40

C5 50

E.M.F. induced in coil 74

Armature phase current indicated in amps.

SEARCH COIL WAVEFORMS.

MIDWAY BETWEEN DIRECT AND QUADRATURE AXES.

D1 10

D2 20

D3 30

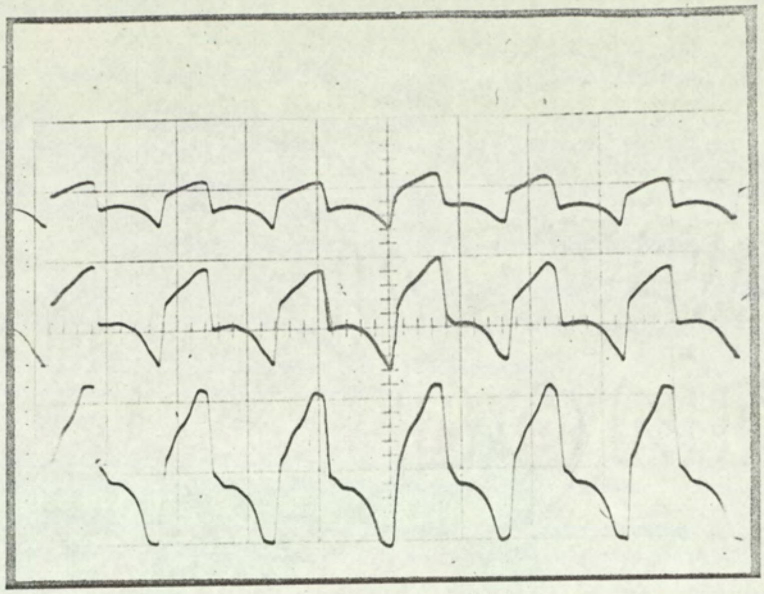

D4 40

D5 50

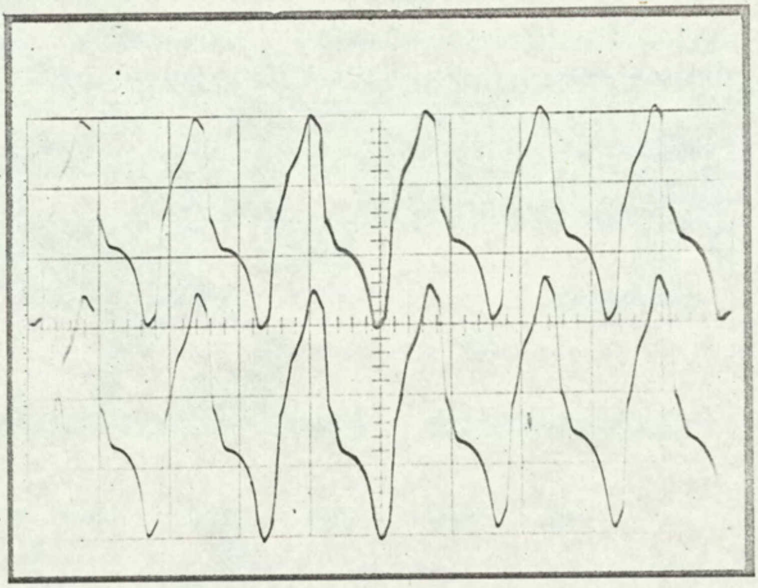

Flux linkage with coil 74

Armature phase current indicated in amps.

SEARCH COIL WAVEFORMS.

MIDWAY BETWEEN DIRECT AND QUADRATURE AXES.

E1 10

E2 20

E3 30

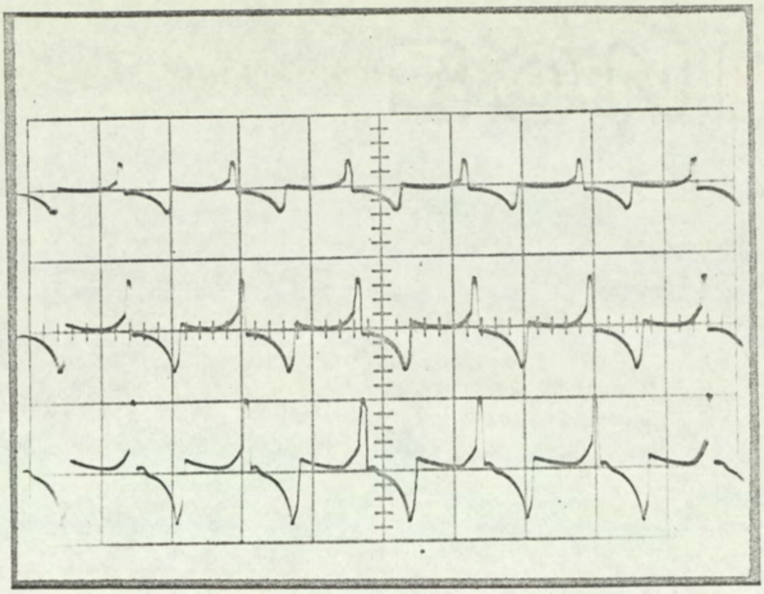

E4 40

E5 50

E6 50
(Output of Filter)

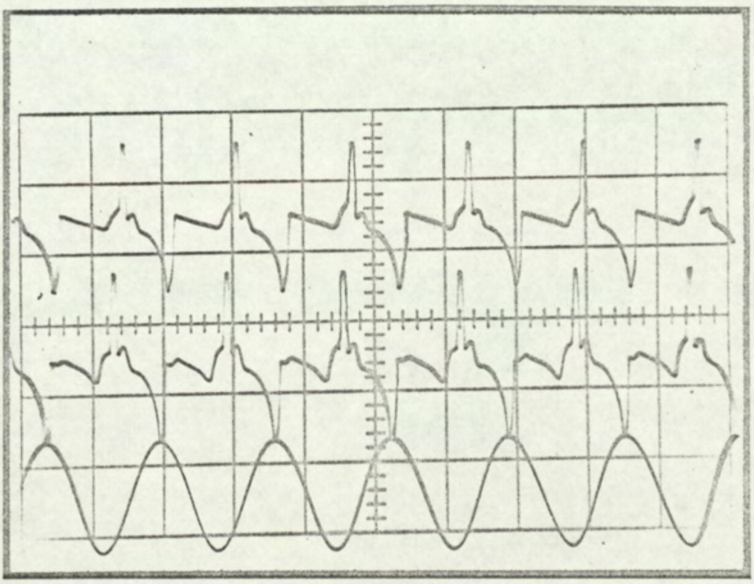

E.M.F. induced in coil 74

Armature phase current indicated in amps.

SEARCH COIL WAVEFORMS - QUADRATURE AXIS.

F1 10

F2 20

F3 30

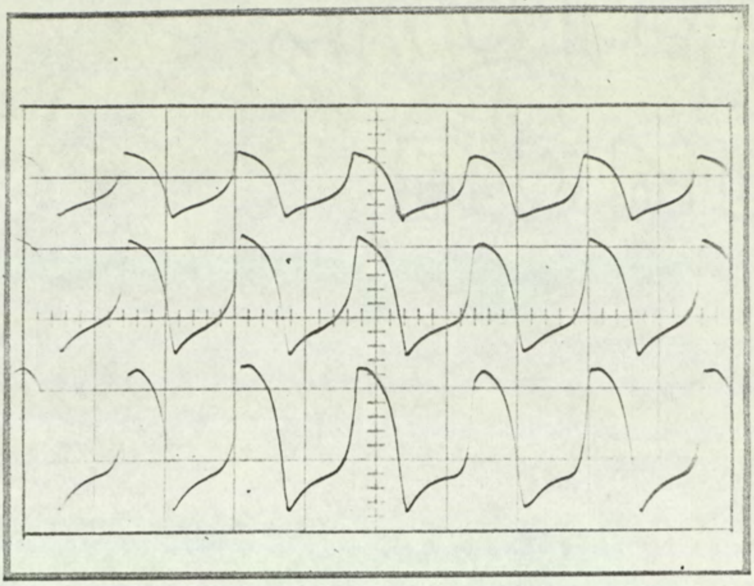

F4 40

F5 50

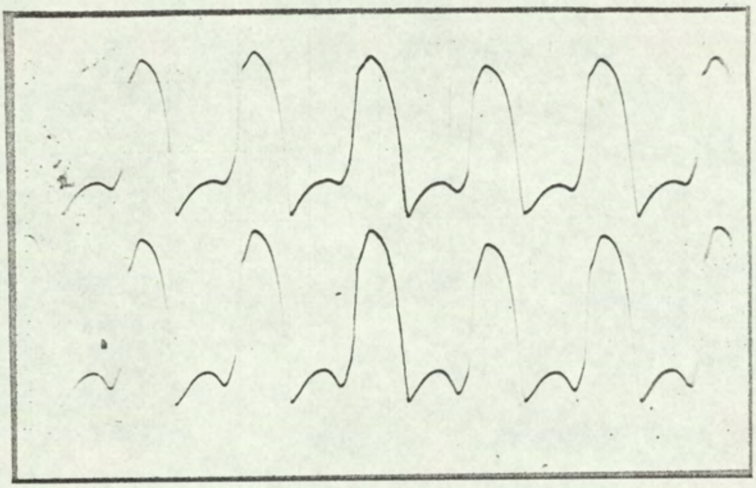

G1 0

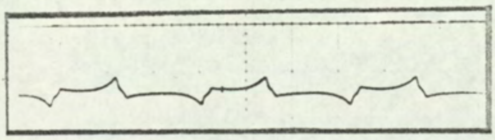

F1 to F5: Flux linkage with coil 74

Armature phase current indicated in amps.

G1 : E.M.F. induced in coil 74 due to the remanent D.C. field.

SEARCH COIL WAVEFORMS - QUADRATURE AXIS.

The change in amplitude and shape of the oscillograms in each set with primary current is attributed to magnetic saturation.

7.4.2 The Calibration of Waveforms.

For the e.m.f., the vertical sensitivity = 0.5 v/cm.

For the flux densities, the vertical sensitivity = 2 v/cm.

From the Tektronix Type - O amplifier Manual p 4 - 4, the output voltage of the integrator is

$$e_o = - \frac{1}{C_i R_f} \int e_s dt = - \frac{\phi}{C_i R_f}$$

i.e. the flux linking the search coil,

$$\phi = - C_i R_f \ e_o$$

and the average flux density,

$$B_{av} = \frac{- C_i R_f \ e_o}{A_1 / h_1}$$

where A_1 = fundamental pole pitch x length

$= \pi DL/2p = 0.057 \ m^2$

and h_1 = the harmonic order for which the search coil is full-pitched.

$\therefore \quad B_{av} = 17.5 \ C_i R_f e_o h_1$

With $R_i = 0.2 \ M\Omega$, $C_f = 0.001 \mu F$, and $h_1 = 7$

$B_{av} = - 17.5 \times 0.2 \times 0.001 \times 7 \ e_o$

$= - 0.0235 \ e_o \ Wb/m^2$

$\therefore$ The Vertical sensitivity = $0.047 Wb/m^2$ per cm deflection

7.4.3 The Influence of the Slot Openings.

Oscillogram G1 taken with the machine unexcited but not demagnetised is now considered. Fig. 7.6 shows two positions of a secondary search coil relative to a primary slot opening. The flux linkage, which depends on the remanent magnetism

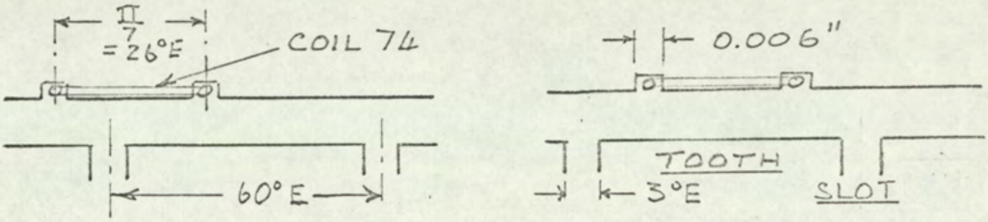

(a) minimum flux linkage (b) maximum flux linkage

Fig. 7.6 SLOT RIPPLE FLUX LINKAGES.

varies between ϕ_a in (a) and ϕ_b in (b), a discrete change occuring each time a slot opening enters or leaves the region beneath the coil, i.e. at intervals of 26° and (60 - 26)°, Fig. 7.7.

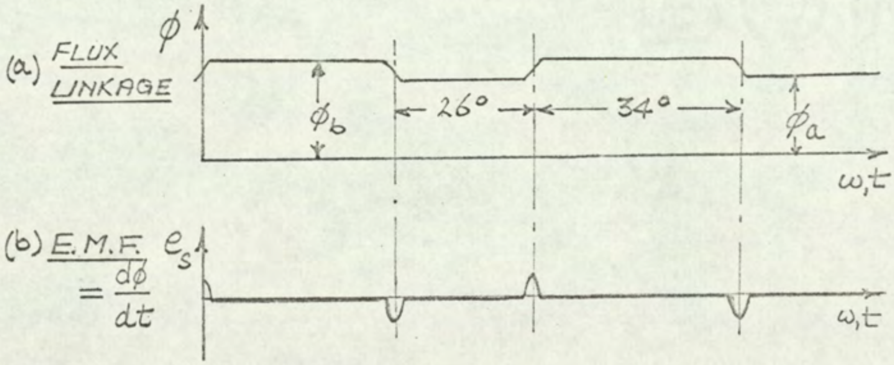

Fig. 7.7 ϕ and e_s for coil 74 with machine unexcited.

The corresponding predicted e.m.f. waveform (b) confirms oscillogram G 1. It may be distorted slightly by the axial groove housing the search coil. If the flux density is not uniform between the two coil sides the horizontal lines of Fig. 7.7 will also be distorted.

7.4.4 The measurement of the 300 c/s e.m.f.s.

In view of the substantial harmonic content of those waveforms, typified by Fig. 7.8, it was decided to limit the present work to the 300 c/s component of the search coil e.m.f.s. i.e., the component attributed to the 5th and 7th m.m.f. harmonics and the 1st slot ripple harmonic.

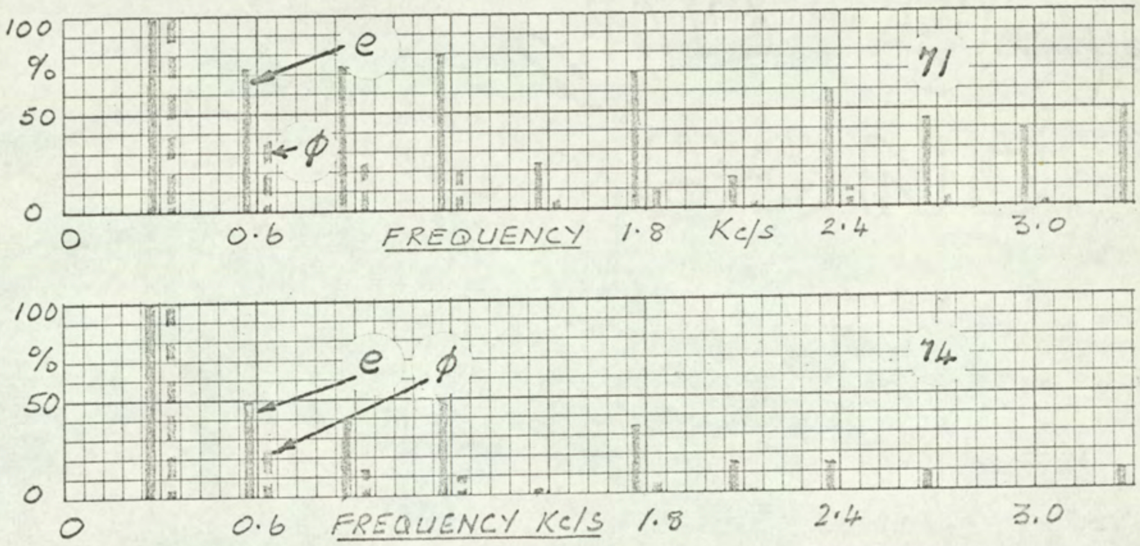

Primary current I_A = 25A

Coil 71 is positioned at $\theta_2 = 90\,^{o}E$ (q.a.)

Coil 74 is positioned at $\theta_2 = 13\,^{o}$

Fig. 7.8 Harmonic Analysis of Coils 71 and 74.

The search coil e.m.f. e_s, was passed through a narrow band-pass filter having unit gain (Fig. 7.9.) and recorded on a valve voltmeter. Random fluctuations in secondary remanence torque were avoided by adopting the following procedure for each reading:

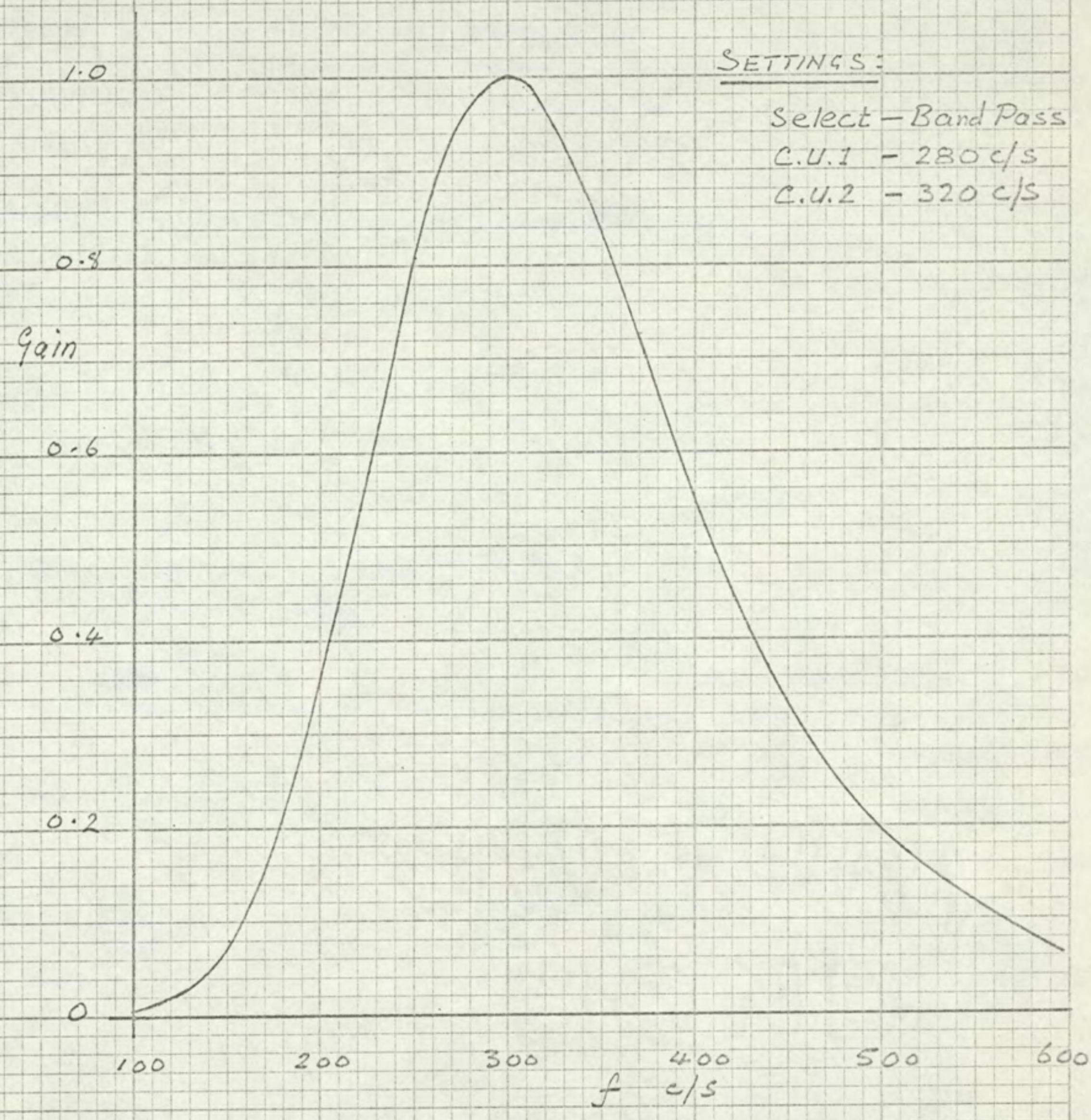

FIG 7.9 RESPONSE CURVE FOR CAWKELL FILTER

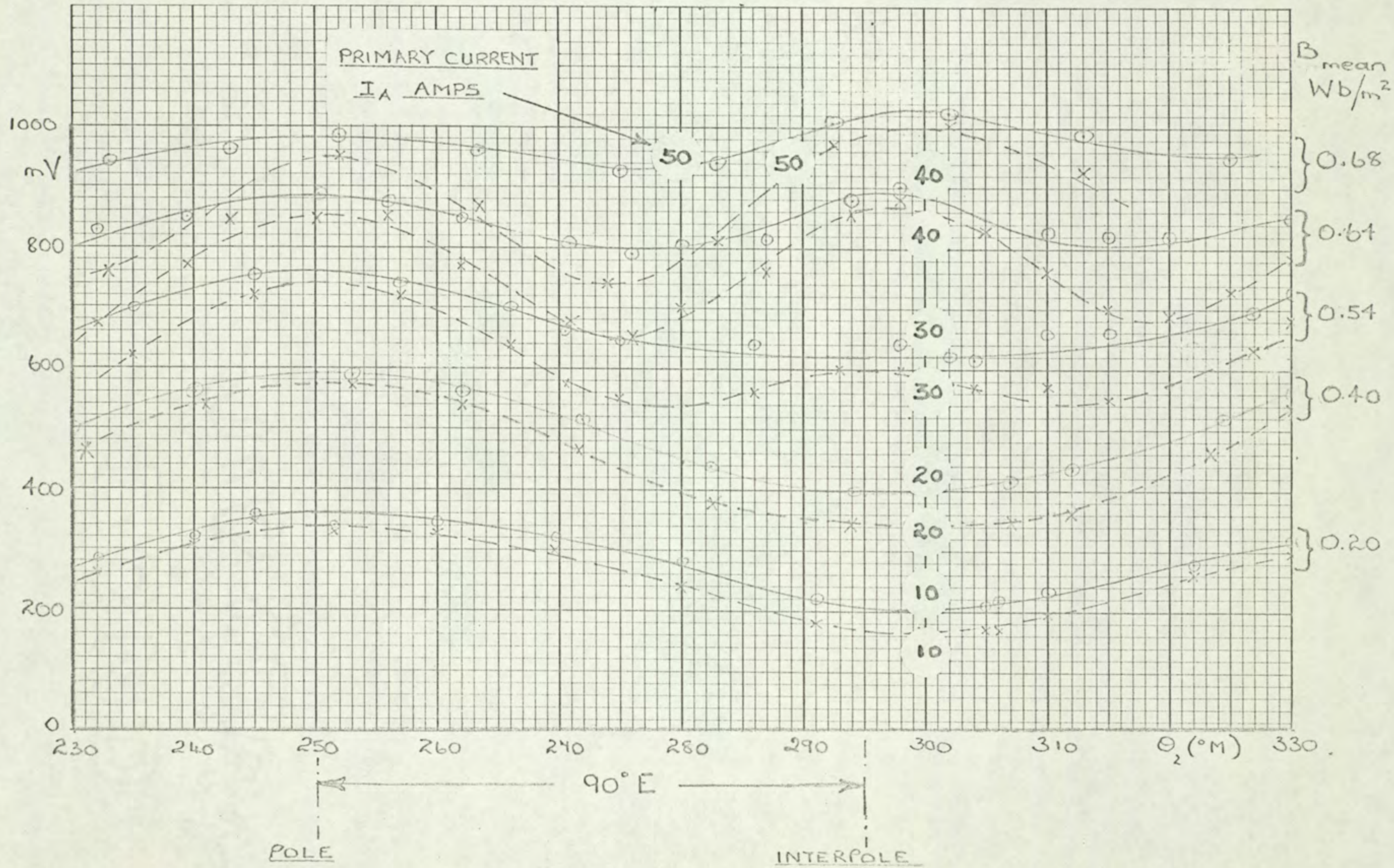

FIG. 7.10. THE E.M.F.S INDUCED IN THE SEARCH COILS OF THE EXPERIMENTAL MACHINE FOR STATED VALUES OF PRIMARY CURRENT AND B_{mean}

(i) The temperature was set by adjusting the primary current, I_A, and allowing time to stabilise.

(ii) With the secondary clamped, I_A was reduced to zero and then increased to the required setting without overshooting.

(iii) Readings of Θ, e_s, I_A and surface temperature were were recorded as quickly as possible.

To avoid errors due to mains frequency drift, the filter gain was adjusted to unity before each set of readings, using a signal obtained from the harmonic analyser (Fig. 7.2). The results are plotted in Fig. 7.10.

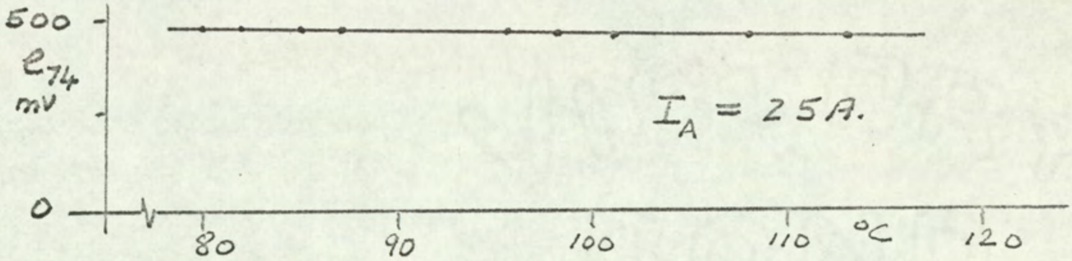

Fig. 7.11 Search Coil E.M.F. e_{74} against surface temperature

Two other tests showed that (i) the search coil e.m.f., e_s, was independent of temperature over a wide range - Fig. 7.11, and (ii) the remanence torque has a small effect on e_s and - Fig. 7.12. Fig. 7.12 was obtained by modifying the above procedure and selecting a value of primary current which would maintain the secondary surface temperature constant at a reasonable value. The secondary was then rotated in one direction and (with the secondary clamped and conditions steady) e_s recorded for small increments in Θ.

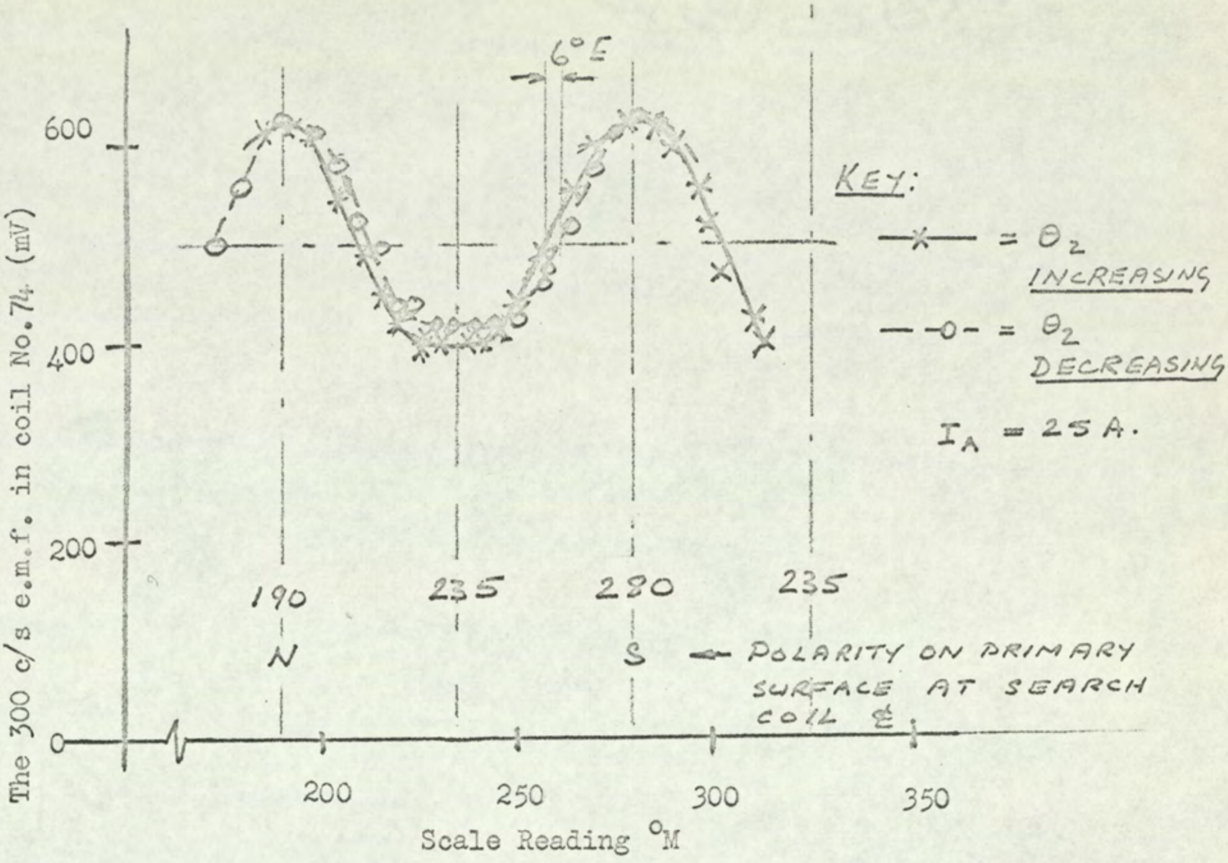

Fig. 7.12. The Effect of Remanence Torque

7.4.5 The Analysis of the 300 c/s e.m.f.s.

It is shown in Appendices 12.5 and 12.6 that the e.m.f. induced in the search coils of the experimental machine at 300 c/s contains 4 components; two produced by the m.m.f. wave and two by the slot openings. This section develops a method of separating these components.

Corresponding components in each pair have the same wavelength, either $\lambda_1/5$ or $\lambda_1/7$. (equation 12.5.12 C and D) and therefore the same pitch factors. The two m.m.f. harmonics are in antiphase at the direct axis but in phase at the quadrature axis. Conversely the two slot ripple harmonics are in phase at the direct axis but in anti-phase at the quadrature axis. The 5th harmonic e.m.f.s of each pair are phase displaced by a small angle $\delta - \delta_R$. These four components are difficult to separate with any degree of confidence because so many assumptions are introduced to simplify the arithmetic in the initial analysis.

For the m.m.f. harmonics it is assumed that the harmonic flux density, B_h, is proportional to the harmonic m.m.f., F_h, i.e. that the demagnetising ampare-turns at the common rotor frequency are proportional to F_h. With these assumptions the proportion contributed by the 5th and 7th harmonics is estimated in Appendix 12.5.2 and summarised in Table 7.2 below.

TABLE 7.2

Point on the polarising wave.	d.a.		q.a.	
Coil pitch - electrical radians	$\pi/5$	$\pi/7$	$\pi/5$	$\pi/7$
- mm.	46	33	46	33
component attributed to 5th m.m.f. harmonic (arbitrary units)	100	90	100	90
component attributed to 7th m.m.f. harmonic	41	51	41	51
component attributed to 5th & 7th m.m.f. harmonics	59	39	141	141
Ratio : d.a. value/ q.a. value (=a)	0·42	0·28		

Let b = the ratio of the 300 c/s d.a. component of the slot ripple e.m.f. to the 300 c/s q.a. component.

From Appendix 12.6.6:

$b \;=\; 3.7$ for the $\pi/5$ - pitched coil

and $b \;=\; 8.6$ for the $\pi/7$ - pitched coil.

<u>Notation</u> In separating the components of the search coil e.m.f. a double subscript notation is introduced whereby the first number refers to the harmonic order for which the coil is full pitched and the second to the harmonic order of the inducing field. A single subscript will indicate the measured value, d or q the appropriate axis, and R the slot ripple component.

Using the above ratio the unknown components can be expressed in terms of two parameters U and V which are evaluated from the test results. Solution of the resulting simultaneous equations will give some indication of the harmonic e.m.f. and flux density levels.

Let U = the total e.m.f. at the quadrature axis due to the harmonic m.m.f.s.

and V = the total e.m.f. at the quadrature axis due to the slot ripple flux density

Then, at the quadrature axis, for the coils pitched $\pi/5$:

$$e_{55} + e_{57} = U$$

$$\text{and} \quad e_{5R} = V$$

At the direct axis:

$$e_{55} - e_{57} = aU$$

$$\text{and} \quad e_{5R} = bV$$

The summation of these two equations gives the measured values of the e.m.f.s, e_{5d} and e_{5q} respectively. If $\delta - \delta_R$ is negligibly small the summation is arithmetic:

$$aU + bV = e_{5d}$$

$$U + V = e_{5q}$$

from which

$$U = (e_{5d} - be_{5q})/(a - b)$$

$$V = (ae_{5q} - e_{5d})/(a - b)$$

and $e_{55} = (a - 1) U/2$

i.e. $$e_{55} = \frac{1 + a}{2a - 2b} (e_{5d} - be_{5q}) \tag{7.5}$$

and $$e_{57} = \frac{1 - a}{2a - 2b} (e_{5d} - be_{5q}) \tag{7.6}$$

substituting for (a) and (b) quoted above for the coil pitched

$\pi/5$ gives:

$$e_{55} = - 0.22 (e_{5d} - 3.7 e_{5q}) \tag{7.7}$$

For the coils pitched $\pi/7$:

$$e_{75} - e_{77} = U \text{ and } e_{75} - e_{77} = aU \text{ etc.}$$

Putting $a = 0.28$ and $b = 8.6$,

equation 7.6 becomes:

$$e_{77} = \frac{0.72}{2(-8.32)} (e_{7d} - 8.6 e_{7q})$$

$$= 0.0433 (8.6 e_{7q} - e_{7d}) \tag{7.8}$$

The peak 5th and 7th harmonic flux densities, B_5 and B_7, are calculated from equations 12.5.6 and 7. They are plotted in Fig. 7.13 against the primary current. The theory assumes $B_h \propto F_h$, i.e. that C_5 in the equation: $B_7 = C_4 B_5$ (12.5.4)

is constant and equals $F_7 / F_5 = 5/7$. Clearly once B_5 has been calculated from the measured results B_7 is found. In order to test

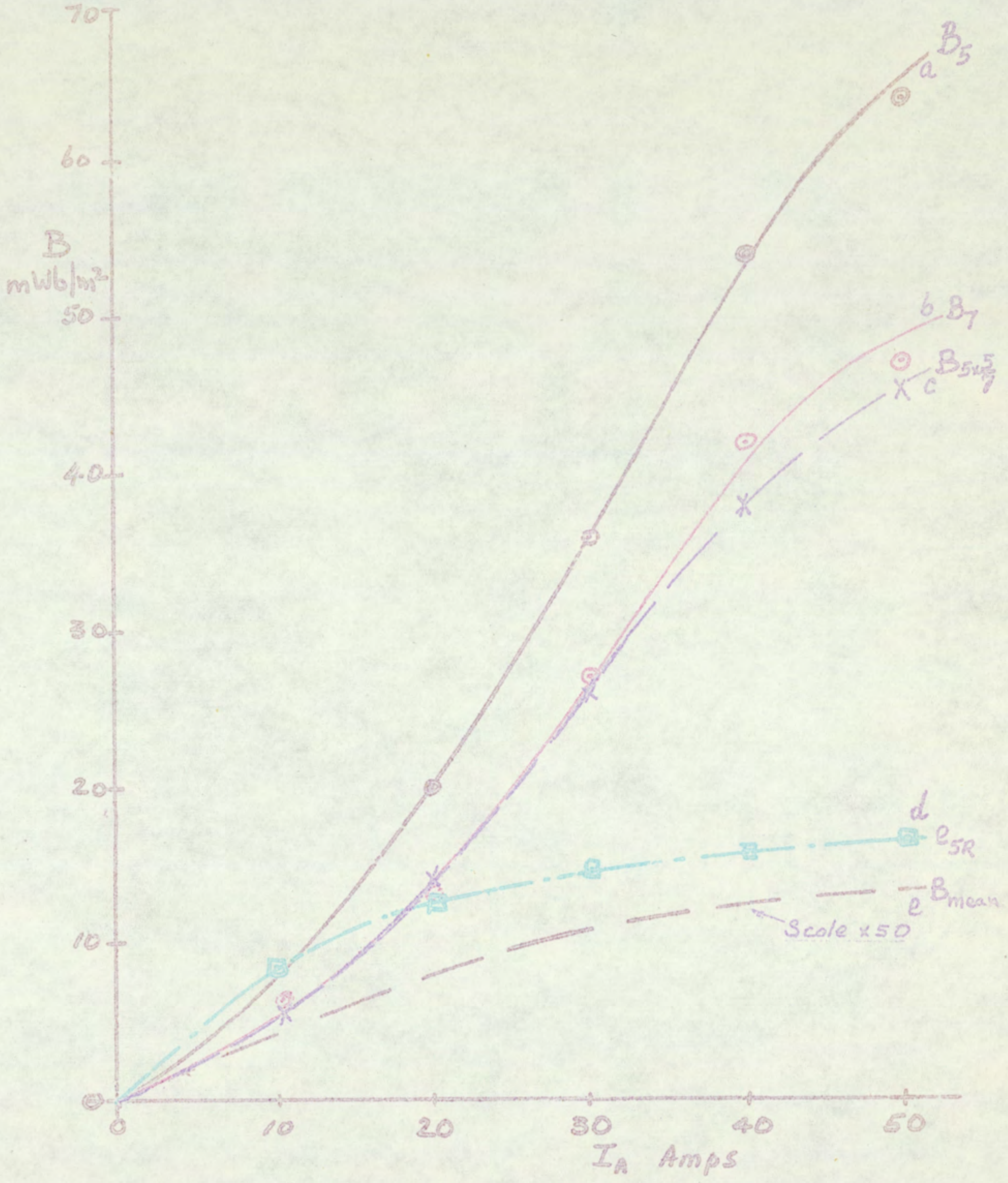

<u>KEY</u>: a b&c: The 5th and 7th m.m.f. harmonic Flux Densities:— a–using coil 53, b–using coil 74, c–curve a $\times \frac{5}{7}$.

d: The 1st harmonic <u>slot ripple</u> e.m.f. (wavelength $= \lambda_1/5$).

e: <u>B_{mean}</u> – using the Primary Search Coil.

<u>FIG. 7.13 THE ANALYSIS OF THE SEARCH COIL E.M.F.S</u>

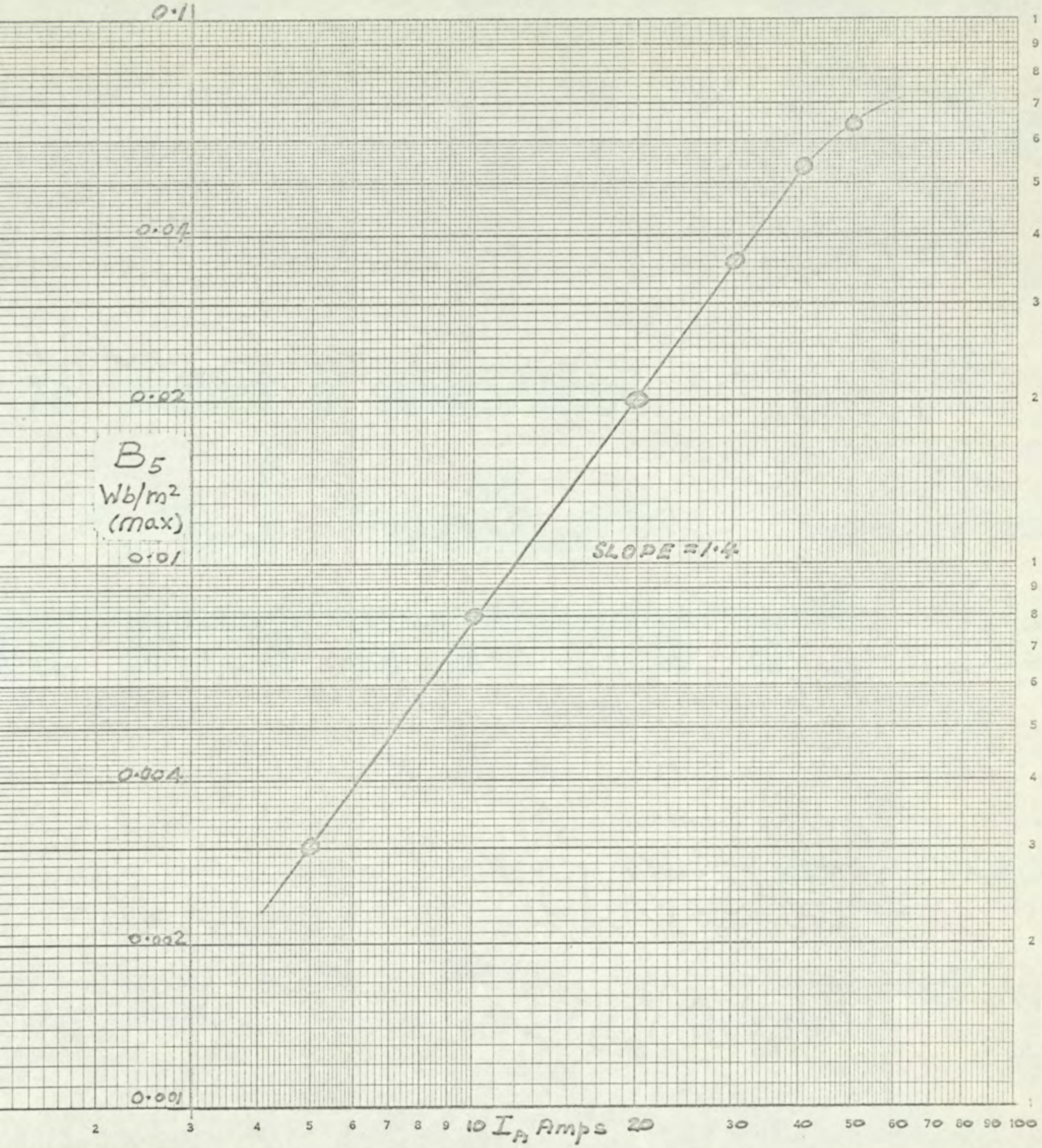

FIG. 7.14. THE 5TH HARMONIC M.M.F. FLUX DENSITY, B_5, AS A FUNCTION OF PRIMARY CURRENT, I_5. Obtained from the measured 300 c/s e.m.f. (Log – Log Scale).

this assumption B_7 was calculated twice using the results of two coils having unequal pitch, curves (b) and (c) Fig. 7.13. The close proximity of these two curves verifies this part of the theory.

7.4.6 Calculation of The Harmonic Flux Densities.

This example typifies the calculation of B_5 and B_7 from Fig. 7.10 when $I_A = 30A$

$$e_{5q} = 0.64 \text{ V. R.M.S.}$$

$$e_{5d} = 0.76 \text{ V. R.M.S.}$$

substituting in equation 7.7 gives:

$$e_{55} = 0.22\ (\ 3.7 \times 0.64 - 0.76\ ) = 0.354 \text{ v.}$$

The peak value of the e.m.f. in a full pitched coil is related to the peak flux density by equation 12.5.6, Appendix 12.5:

$$e_{h1} = 6\,\omega_1 \frac{L\,D}{h_1\,p} B_h \qquad \text{volts R.M.S.}$$

where h = harmonic order

and π/h_1 = coil pitch

For the experimental machine, the R.M.S. value of e_{h1} is measured,

$$\therefore\ B_h = \frac{\sqrt{2}\ e_{h1} \times 2 \times h_1}{6 \times 2\pi \times 50 \times 0.29 \times 0.25} = 0.0206\ h_1\ e_{h1}$$

Using the double subscript notation:

when $h_1 = 5$, $B_5 = 0.103\ e_{55}$ for coils 51 to 55

and when $h_1 = 7$, $B_7 = 0.144\ e_{77}$ for coils 71 to 77.

$\therefore$ When $I_A = 30A$, $B_5 = 0.103 \times 0.354 = 0.036\ Wb/m^2$ (max)

It is interesting to compare B_5 with the value of normal d.c. flux density.

When $I_A = 30$ A, $B_{mean} = 0.535$ Wb/m^2

$\therefore B_1 = 0.535\sqrt{2} = 0.756$ Wb/m^2

i.e. B_5 is about 1/20th of B_1.

Now the m.m.f. F_1 is 5 times F_5 (equation 3.1). Also the normalised slip N_5/N_{m5} is much greater than 1 (Table 3.5), indicating that the harmonic armature reaction is much greater than half of F_5 (Reference 4 section 2.7) Therefore the flux component of F_5 is less than half F_5 i.e. less than 1/10th of F_1 indicating that B_5 and e_5 are of the right order but perhaps smaller than expected.

7.4.7. Calculation of slot ripple e.m.f.

The slot ripple flux densities and e.m.f.s. are not plotted but the above example is extended to facilitate a comparison between the slot ripple e.m.f. obtained by the analysis of the experimental results using section 7.4.5 and the value obtained theoretically using appendix 12.6.6.

From Section 7.4.5.

At the quadrature axis the total slot ripple e.m.f. induced in the $\pi/5$ pitched coil is

$$e_{5R} = V = (a\,e_{5q} - e_{5d}) / (a - b)$$

$$= (0.42 \times 0.64 - 0.76) (-3.28)$$

$= 0 \cdot 15$ Volts.

and in the $\pi/7$ pitched coil is

$$e_{7R} = (0 \cdot 28 \times 0 \cdot 60 - 0 \cdot 74) / (0 \cdot 28 - 8 \cdot 6)$$

$= 0 \cdot 069$ Volts.

From Appendix 12.6.6, at the Quadrature Axis:

$$e_{5R} = 6\omega_1 \, LDb_1B_1 \times 0 \cdot 0212 / p\sqrt{2} \qquad \text{Volts R.M.S.}$$

and $$e_{7R} = 6\omega_1 \, LDb_1B_1 \times 0 \cdot 0094 / p\sqrt{2} \qquad \text{Volts R.M.S.}$$

From Table 12.6.2,

$$b_1 = 77 \cdot 9/960 \cdot 9 = 0 \cdot 081$$

From section 7.4.6, When $I_A = 30$ amp.

$$B_1 = 0 \cdot 756 \text{ Wb/m}^2$$

and $$\frac{6\omega_1 LD}{p\sqrt{2}} = \frac{1}{0.0206}$$

$$\therefore \quad e_{5R} = 0.081 \times 0.756 \times 0.0212 / 0.0206 = 0.063 \text{ volts}$$

and $$e_{7R} = 0.063 \times 0.0094 / 0.0212 = 0.028 \text{ volts}$$

Whilst it is encouraging that the experimental and theoretical values are the same order of magnitude, the large difference between them suggests that the analysis of this complex problem has been oversimplified.

7.5 Summary.

This chapter has demonstrated the importance of examining the fundamental nature of the armature reaction m.m.f. waveform. The point on the pole face where the fluctuation in this waveform is a maximum may be ascertained by studying a progression of such waves. Alternatively a method of harmonic synthesis may be used provided all the important harmonics are included, together with the sign of their winding factors.

The technique used to separate the harmonic components of the search coil e.m.f.s. is believed to be sound in principle but is complitcated by the presence of the slot openings. In view of this complication and some rather sweeping assumptions the degree of corroboration between theory and experiment for the 300 c/s induced e.m.f.s. is encouraging. No attempt has been made to correlate the search coil waveforms with the m.m.f. fluctuations of Fig. 7.5 since the reaction of eddy currents and the influence of the slot openings will cause the actual flux linkage pattern to be very different to one obtained by integrating the appropriate m.m.f. waveform. The quantity of harmonics present is considerable and these vary in magnitude across the pole face, Fig. 7.8. The effect of magnetic saturation in reducing the 300 c/s component is evident from the waveforms and also from Fig. 7.13 and 7.14. The flux waveforms also become less peaky above a primary current of 30 amps due to saturation.

The shape of Fig. 7.13 would appear to follow that of the magnetisation curve. For example below a flux density of 0.7 Wb/m^2 the Log-log graph of Fig. 7.14 shows that B_5 changes with I_A in an orderly manner:

$$B_5 \propto I_A^{1.4}$$

over the same range of primary current the B - H curve for the secondary iron has the form:

$$B \propto H^{1.6}$$

The similarity between these two relationships suggests that a substitution for μ based on the unsaturated part of the magnetisation curve might be more applicable to this problem.

8. DISCUSSION

8 DISCUSSION

8.1. Some Comments on the substitution for permeability

8.1.1. Saturation

The three methods [1.2.3] of predicting surface loss discussed in this work all assume that the high frequency of induced surface currents (equal to integer multiples of 300 c/s) results in a low depth of penetration of flux. An assumed exponential decay of the electromagnetic quantities with distance, y, into the secondary (pole) member forces the surface flux density well into the region of magnetic saturation. In the eddy current coupling theory the surface flux density is therefore considered to be high enough for the power-law relationship between B and H to apply. The simplification of the mathematical expressions derived from Maxwell's field equations by this substitution for μ has led to comparatively simple formulae involving only the machine parameters. These formulae account for the reaction of the pole face current density on the inducing field, a requirement which has been stressed by previous authors (e.g. ref. 7). The substitution avoids using either a numerical method (expensive in terms of computer-time) or a single value of μ . Since μ varies in space and time, the substitution of a single numerical value has doubtful validity, whereas an analytical substitution is more realistic, especially if it is made before solving Maxwell's equations and when there is no superposed d.c. flux. The pole face loss problem where the eddy currents are produced by an alternating m.m.f. superposed on a direct m.m.f. is discussed later. First, consider the validity of the substitution expressed by equation 3.13

applied to an eddy current coupling or a solid rotor induction motor:

$$\mu^{1/4} H = k_1 H^m \qquad (3.13)$$

This expression for μ allows direct substitution in equation 3.8. The use of this substitution in our problem is claimed to be justifiable on the grounds that

(a) the graph of log $\mu^{1/4}$H against log H is linear over a larger range of H than that of log B against log H.

(b) the drum flux density lies within this saturated region.

(c) eddy current coupling performance characteristics based on equation 3.13 can be predicted with reasonable accuracy.

The logarithmic graph of Fig. 3.3. indicates that the above substitution could be used to represent the mild steel of the experimental machine over the range H = 600 to 30,000 A/m ($B=0.95$ to $2.0 Wb/m^2$). In this case the values of k_1 and m (which have been used in the computer programme for pole face loss) substituted in equation 3.13 give eq. 3.2:-

$$\mu^{1/4} H = 0.769\, H^{0.794} \qquad (3.2)$$

Equations 3.13 and 3.2 may be expressed in terms of B and H alone by making the usual substitution $B = \mu H$:

$$B = 0.35\, H^{0.176} \quad \ldots\ldots\ldots\ldots\ldots \quad (8.1)$$

$$\text{or } B = k_1^4\, H^{4m-3} \quad \ldots\ldots\ldots\ldots\ldots \quad (8.2)$$

Mathematically, 3.2 and 8.1 are identical. Equation 8.1 suggests that the slope of the log B/log H graph should be 0.176 at high flux densities. This is untrue. The measured slope over the linear range of Fig. 3.3 is actually 0.124 and is valid over a much smaller range of

H. (1,600 to 30,000) A more accurate relationship for the saturated region is obtained by measuring the slope over this range, giving:

$$B = 0.55 \ H^{0.124} \ . \ . \ . \ . \ . \ . \ . \ . \ . \ . \ . \ . \ (8.3)$$

Fig. 8.1 shows the graphs of equation 8.1 and 8.3 plotted on the same linear paper as the B/H magnetisation curve and a B/H loop. The considerable difference between the index of H in equations 8.1 and 8.3 is due to the drawing of straight lines through points which actually have a slight curvature. The effect of curvature is masked by plotting Log $\mu^{1/4}$H against Log H because:

(a) the curvature is very slight
(b) As H falls, μ increases thus extending the apparent linear range.
(c) The cramped scale of the logarithmic paper at higher flux densities minimises the gap between plotted points and the assumed straight line, giving a false sense of accuracy.

The index of H in eqn. 8.1, obtained by taking the small difference between two larger numbers (4m-3), is very sensitive to errors in the measurement of m. This extension of the linear range is to be expected: any graph of μ^{ℓ}H against H will always be more linear than B against H if $0 < \ell < 1$. As ℓ is reduced, the graph changes from a B/H curve when $\ell = 1$, to a straight line when $\ell = 0$. This point is illustrated by taking the particular case of the experimental machine by measuring k_1' and m using equations 8.2 and 8.3:

$$k_1' = \sqrt[4]{0.558} = 0.864 \ (\text{cf. } k_1 = 0.769)$$

$$\text{and } \ m' = \frac{3 + 0.124}{4} = 0.781 \ (\text{cf. } m = 0.794)$$

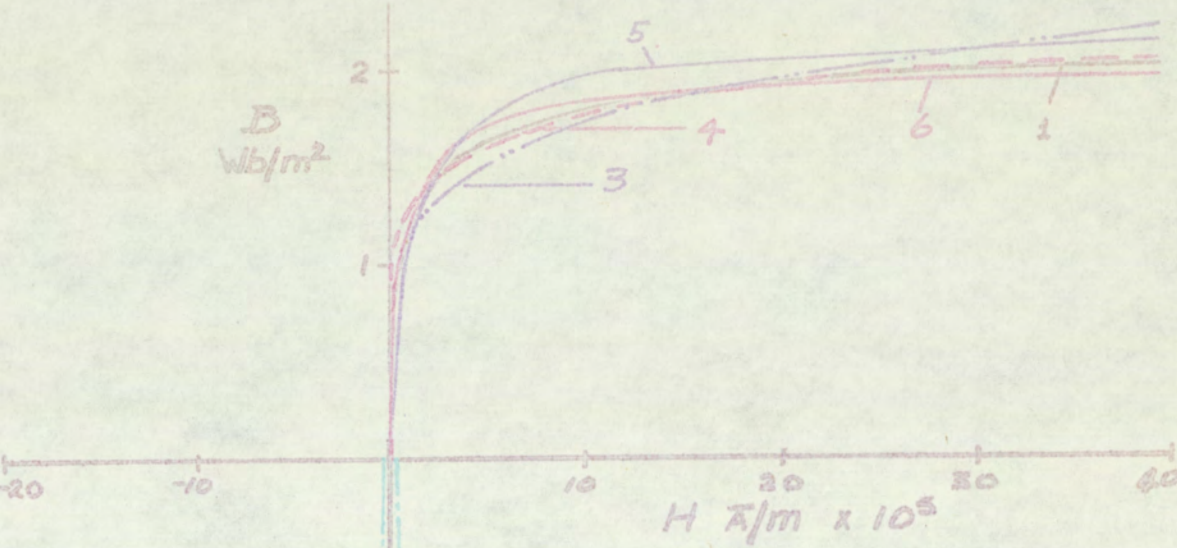

KEY:

1. The Measured Curve using the Toroid
2. The Measured Loop ——"——"——
3. By Taking the Slope of Log $\mu^{1/4}H$/Log H Graph — $B \propto H^{0.176}$ ($\mu^{1/4}H = 0.77\,H^{0.79}$)
4. By Taking the Slope of Log B/Log H Graph — $B \propto H^{0.124}$
5. By Frahlich's Formula: $B = H/(543 + 0.452H)$
6. Ditto: $B = H/(337 + 0.504H)$

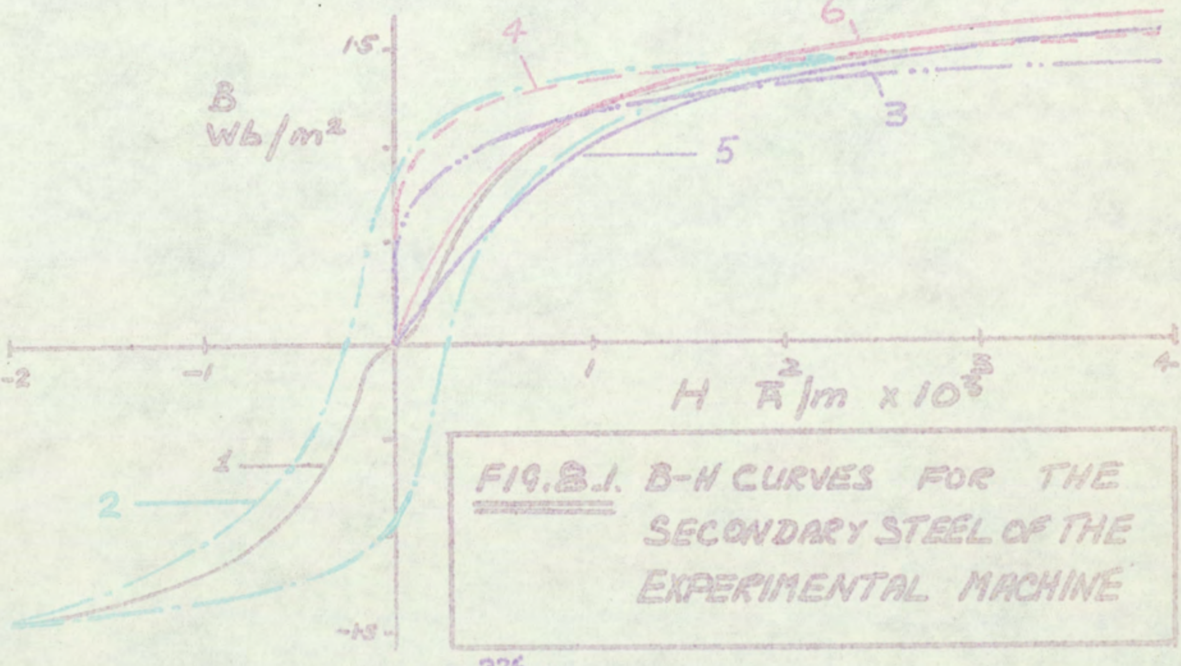

FIG. B.1. B-H CURVES FOR THE SECONDARY STEEL OF THE EXPERIMENTAL MACHINE

This calculation indicates that m is too sensitive for engineering applications. Equations 3.2 and 8.3 describe two quite distinct magnetisation curves for which the magnitudes of m differ by only 1.6%. This produces a difference in the magnitudes of index (4m-3) of 30% i.e. a very small error in the calculation of m makes a considerable difference to the calculated quantities in the eddy current coupling theory, the indices of which are also obtained by taking the difference of two large quantities involving multiples of m. A particular example is equation 3.24. In Fig. 8.1., the difference between the calculated B/H curve (curve 3) and the measured magnetisation curve (curve 1) indicates the degree of approximation introduced by Davies' substitution for μ . Such approximation is masked by the deceptive juggling of the indices of μ and H. As far as the iron is concerned it is the actual relationship between μ and H that is important, the suitability of the substitution therefore depends on the proximity of curves 1 and 3.

8.1.2. The complete range of Flux Density

Under alternating conditions equation 3.13 will be valid only for that limited part of the cycle for which the medium is saturated. Furthermore because of the influence of eddy currents the maximum flux density in some regions will not even reach the knee of the magnetisation curve (see B. James' Thesis ref. 38). It would appear then that a different substitution for μ may be necessary for some parts of the cycle and in some regions of the iron.

The hysteresis loop has been plotted on Fig. 8.1 (corrected for flux meter drift and calibration errors) for a fairly high value of B_{max}(=1.44 Wb/m^2). The shape of this loop is not expected to alter greatly for other cyclic variations having greater peak flux densities. Now the proposed substitution for μ, eqn. 3.13, is not intended to follow the cyclic variations of B and H around the loop, as an elliptical substitution might, but to follow some mean curve. In doing so considerable errors are bound to be introduced, see Fig. 8.2.

Returning to Fig. 8.1, curve 4 (described by equation 8.3) follows the B/H loop very closely over the whole range of decreasing values of $|H|$, but not when $|H|$ is increasing between 0 and 2000 A/m. Neither curve 3 nor curve 4 describes precisely the variation of B with H over the complete range ($-2,230 < H < 2,230$) and in this respect there is little to choose between them. The empirical magnetisation curve(curve 1) is exact, but curve 3 is mathematically superior.

Another substitution for permeability can be expressed in terms of the well known Frohlich's equation:

$$B = \frac{H}{a + bH} \tag{8.4}$$

i.e. $\quad = (a+bH)^{-1}$

This substitution, which has been used in Maxwell's equations to give a numerical solution to the eddy current loss problem is now considered. A qualitative assessment of the suitability of Frohlich's equation has been carried out by finding the two values of a and b which satisfy equation 8.4 at two given points

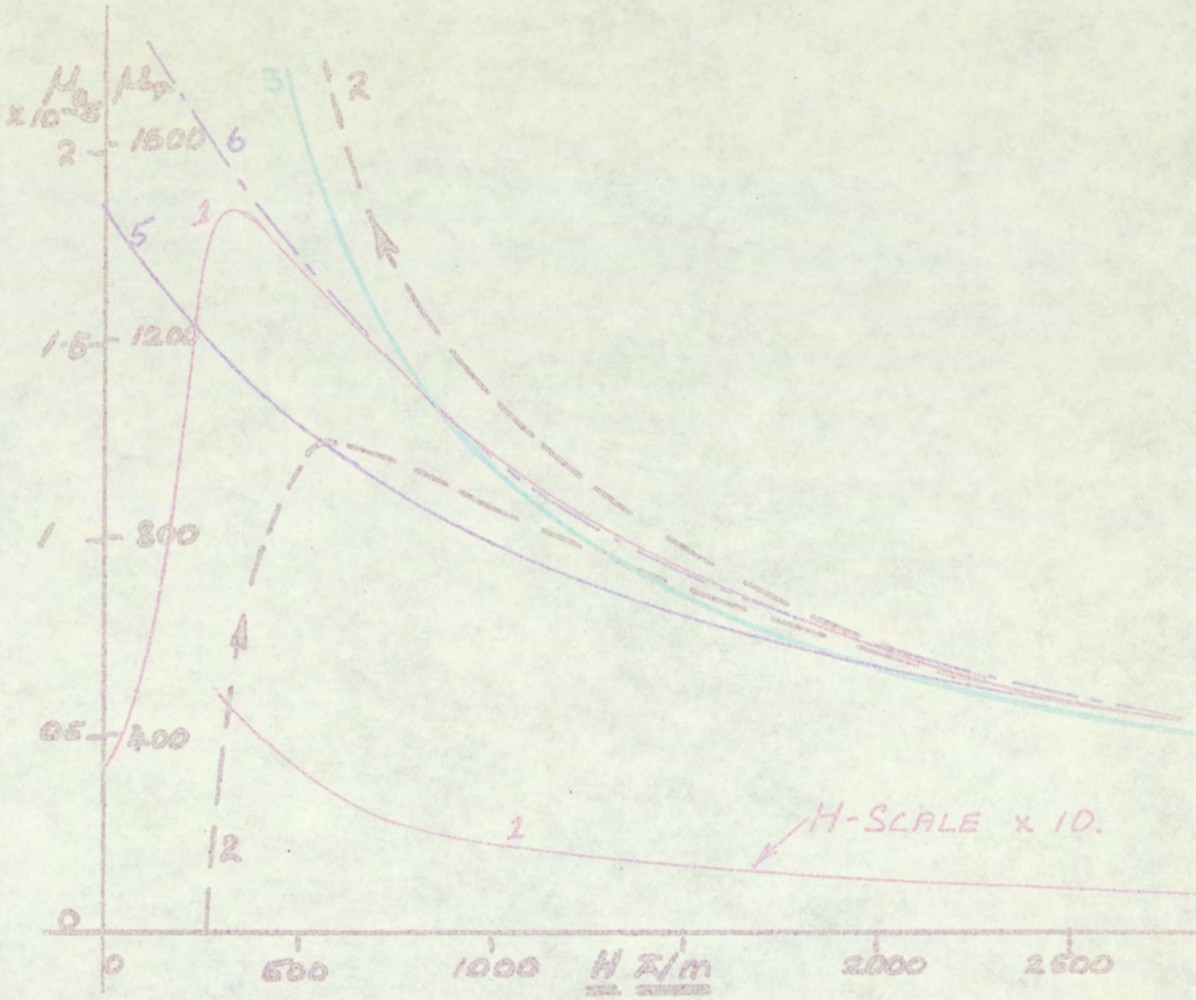

KEY:

1 —— = μ/H using the measured B/H curve

2 — — = μ/H using the measured B/H loop

3 —— = μ/H using $\mu^{1/4} H = 0.77\, H^{0.79}$ (Ref. 3)

5 —— = μ/H using FROHLICH : $B = \dfrac{H}{543 + 0.452H}$

6 —·— = μ/H using FROHLICH : $B = \dfrac{H}{337 + 0.504H}$

These numbers correspond to those used in Fig 8.1 — curve 4 is not plotted.

FIG. 8.2. EMPIRICAL AND ANALYTICAL CURVES OF PERMEABILITY against MAGNETIC INTENSITY FOR THE SECONDARY STEEL

on the B/H curve.

The resulting equation for B is:

$$B = H\,(543+0.452\,H)$$

This is plotted in Fig. 8.1 (curve 5). By selecting two other points on the B-H curve the equation of curve 6 is obtained:

$$B = H\,(337+0.504\,H)$$

Both curves indicate that Frohlich's substitution is unsuitable at high flux densities ($B > 1.6$ Wb/m^2 approx. $H > 4{,}000$ $\overline{A}$/m approx.) because they depart farther from the measured curve than do curves calculated by Davies' method. When $H \to \infty$, Frohlich's substitution gives $\mu \to 0$ and $B \to$ constant: $B \to 2.21$ for curve 5 and $B \to 1.99$ for curve 6.

At the lower flux densities both calculated Frohlich curves lie closer to the empirical curve but the associated permeability is very different from the empirical value (Fig. 8.2).

Frohlich's substitution assumes (incorrectly) for mild steel that the permeability is a maximum $(=\frac{1}{a})$ when H=0.

i.e. for curve 5, $\mu_{(H=0)} = 1.84 \times 10^{-3}$, i.e. $\mu_r = 1{,}470$

for curve 6, $\mu_{(H=0)} = 2.97 \times 10^{-3}$, i.e. $\mu_r = 2{,}360$

whereas for the empirical curve, $\mu_{(H=0)} = 0.4 \times 10^{-3}$, i.e. $\mu_r = 318$, indicating an error in μ of the order of 400 to 700%. The importance of this error, which is much less than that involved in using the substitution defined by equation 3.2, is assessed in terms of the results of the theory taken as a whole. Other factors have yet to be considered.

To summarise, it is possible to choose a and b such that the calculated value of B is close to the measured value over a limited range.

If, for example, a and b are chosen to give good correlation over the knee of the curve, Frohlich's substitution is much less accurate at higher flux densities than is Davies'.

Since it is impossible to find a single simple mathematical function relating permeability, μ, to a high alternating magnetic intensity, H, for material exhibiting hysteresis a best compromise solution must be found. The graphs indicate that Frolich's equation is a reasonable compromise applicable to unsaturated regions (around knee of the curve) but to cover a wide range of H an equation of the form B= (Const) $H^{(const)}$ could well be preferable. A more accurate substitution could probably be obtained by putting $B \propto H^{2m}$ for $0 < H < 500$ $(0 < B < 0.9)$ (ref. section 7.5) and

$$\propto H^{4m-3} \text{ for } 500 < H < 30{,}000 \quad (0.9 < B < 2.0)$$

If this is done, a discontinuity is introduced and the beauty of Davies' substitution is lost.

8.1.3. Variation of B_x with y

Variation of permeability throughout the depth of the drum presents another problem. The permeability will increase with y, as B decreases above the knee. The flux will therefore tend to penetrate deeper into regions of higher permeance.

In section 3.4 the solution of the diffusion equation[3] assuming constant μ yields the expression for H_x. Multiplying by μ gives:

$$B_x = \frac{\mu J_m e^{-\beta y}}{2\alpha^2} \sin(\omega t - 2\pi x/\lambda - \gamma y + \phi). \text{ (real part)}$$

i.e. as y increases, $B_{xmax} \propto \mu e^{-\beta y}$

$$\propto \mu e^{-\alpha y} \quad (if \sqrt{2}\alpha \gg \tfrac{2\pi}{\lambda})$$

$$\propto \mu e^{-\sqrt{\mu}\sqrt{\omega/2\rho}\cdot y}$$

$\therefore$ if ω and ρ are constant,

$$B_{xmax} \propto \mu e^{-const\sqrt{\mu}\cdot y}$$

Assuming that the surface flux density is above the knee of the magnetisation curve, μ at the surface will be low and B_x will decrease slowly from A, Fig. 8.3. As B_x decays μ increases, increasing the rate of decay, i.e. B_x decays at a rate which gets progressively greater until the point P is reached, where μ is a maximum. Beyond point P, B_x decays less rapidly to give the resultant curve APQ. Such a path could be obtained by drawing an infinite number of decay curves such as AA', BB' etc. in Fig. 8.3 each for a value of permeability appropriate to the thin layers AB, BC etc. This procedure is illustrated later in Table 8.1, it is a very crude approximation to the method of finite differences, but is included for its simplicity. The selection of an "appropriate value of permeability" presents a difficult problem.

Similar flux density distributions to Fig. 8.3 have been achieved at the University of Aston both by final year under-graduates using a solid iron toroid[39] under the author's supervision (1966) and by other research workers in the Electrical Machines Research Centre.

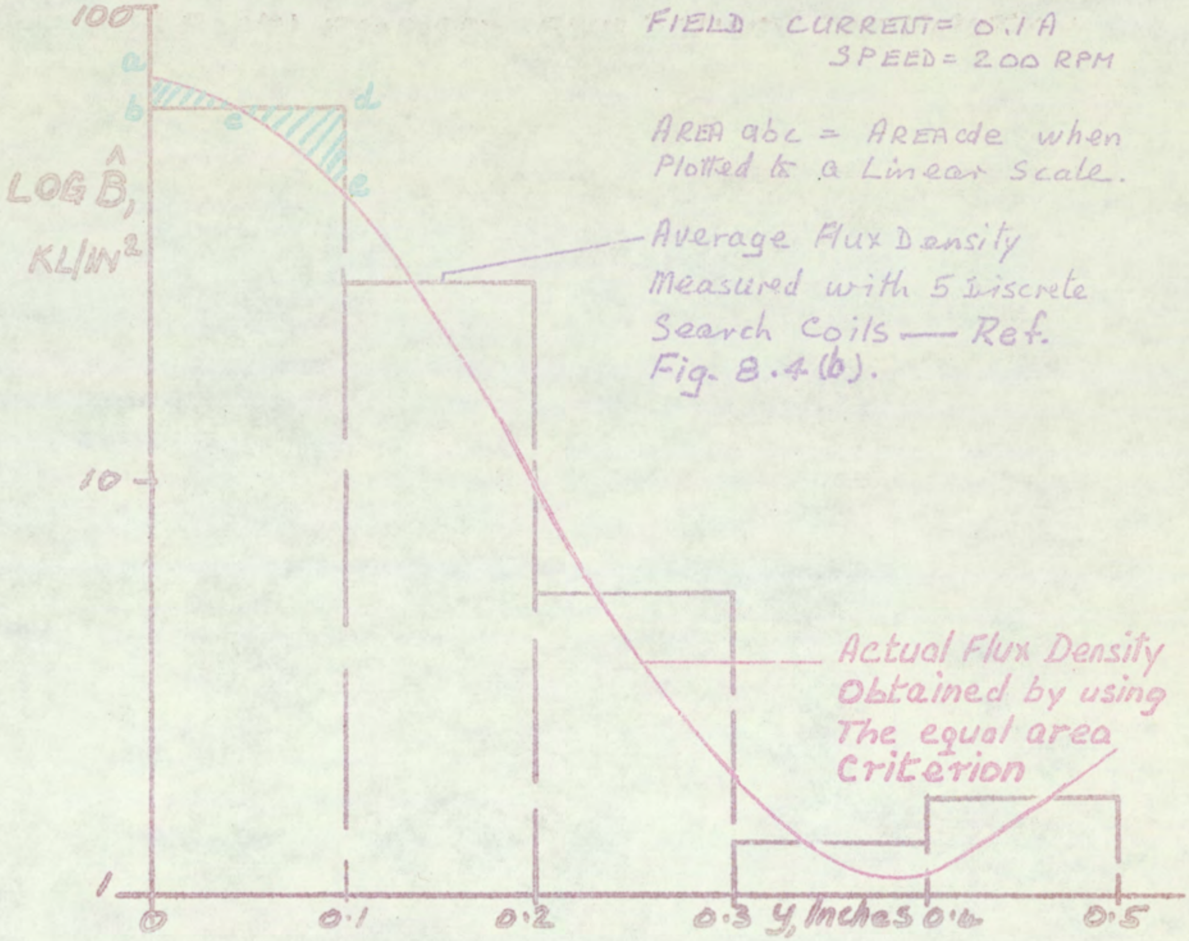

FIG 8.4(a) PROPOSED FLUX DENSITY DISTRIBUTION FOR EDDY-CURRENT COUPLING OF REF. 3.

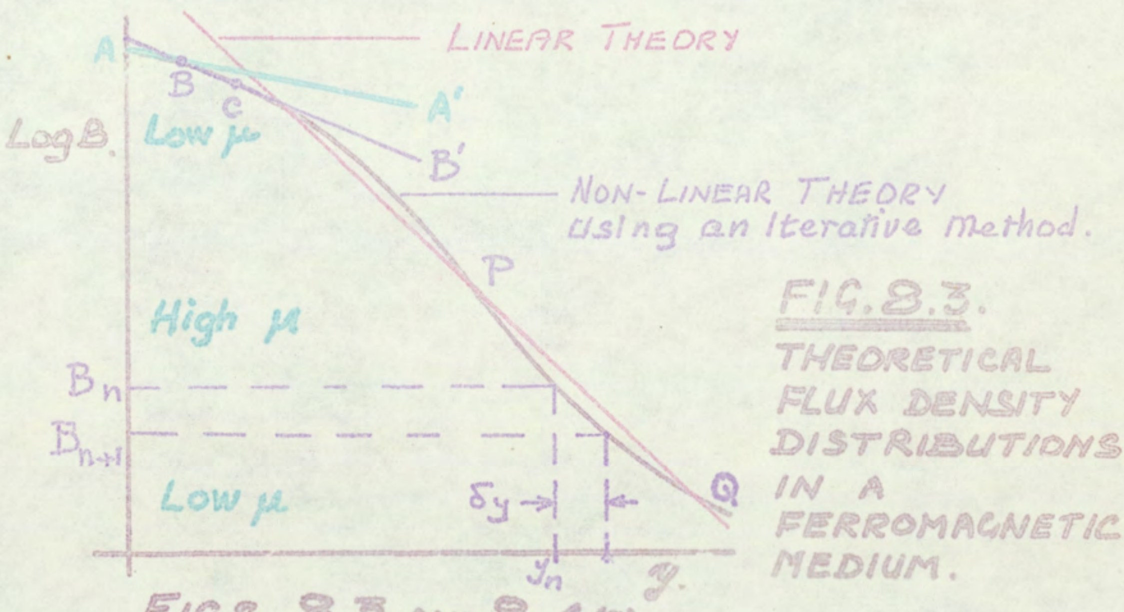

FIG. 8.3. THEORETICAL FLUX DENSITY DISTRIBUTIONS IN A FERROMAGNETIC MEDIUM.

FIGS. 8.3 AND 8.4(a)

FLUX DENSITY DISTRIBUTION IN DRUM IRON AS A FUNCTION OF DEPTH.

(MEASURED WITH 5 DISCRETE COILS. THE MEAN DENSITY HAS BEEN PLOTTED AT THE CENTRE OF THE APPROPRIATE SECTION)

FIELD CURRENT = 0.1A

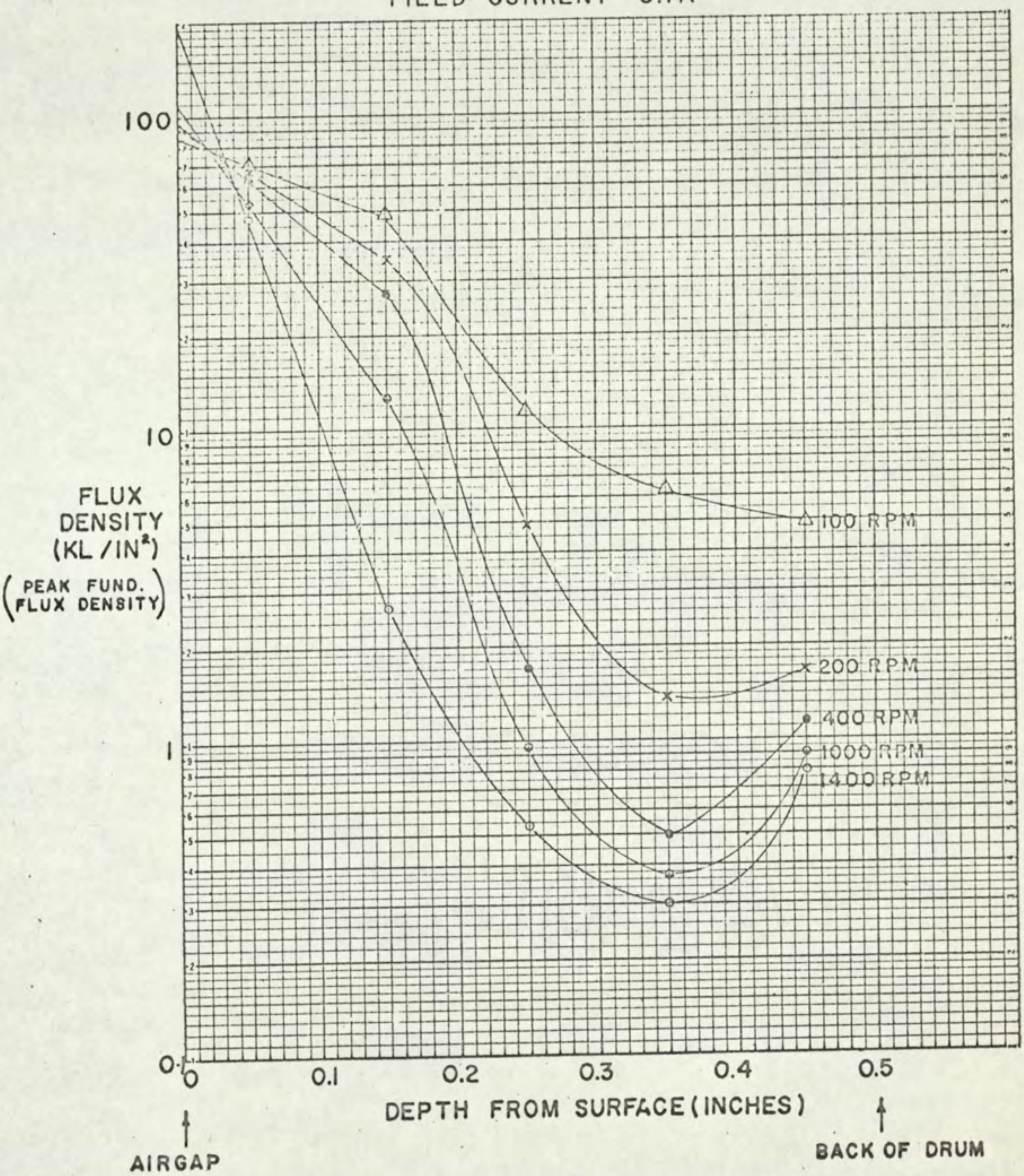

FIG. 8.4.(b)

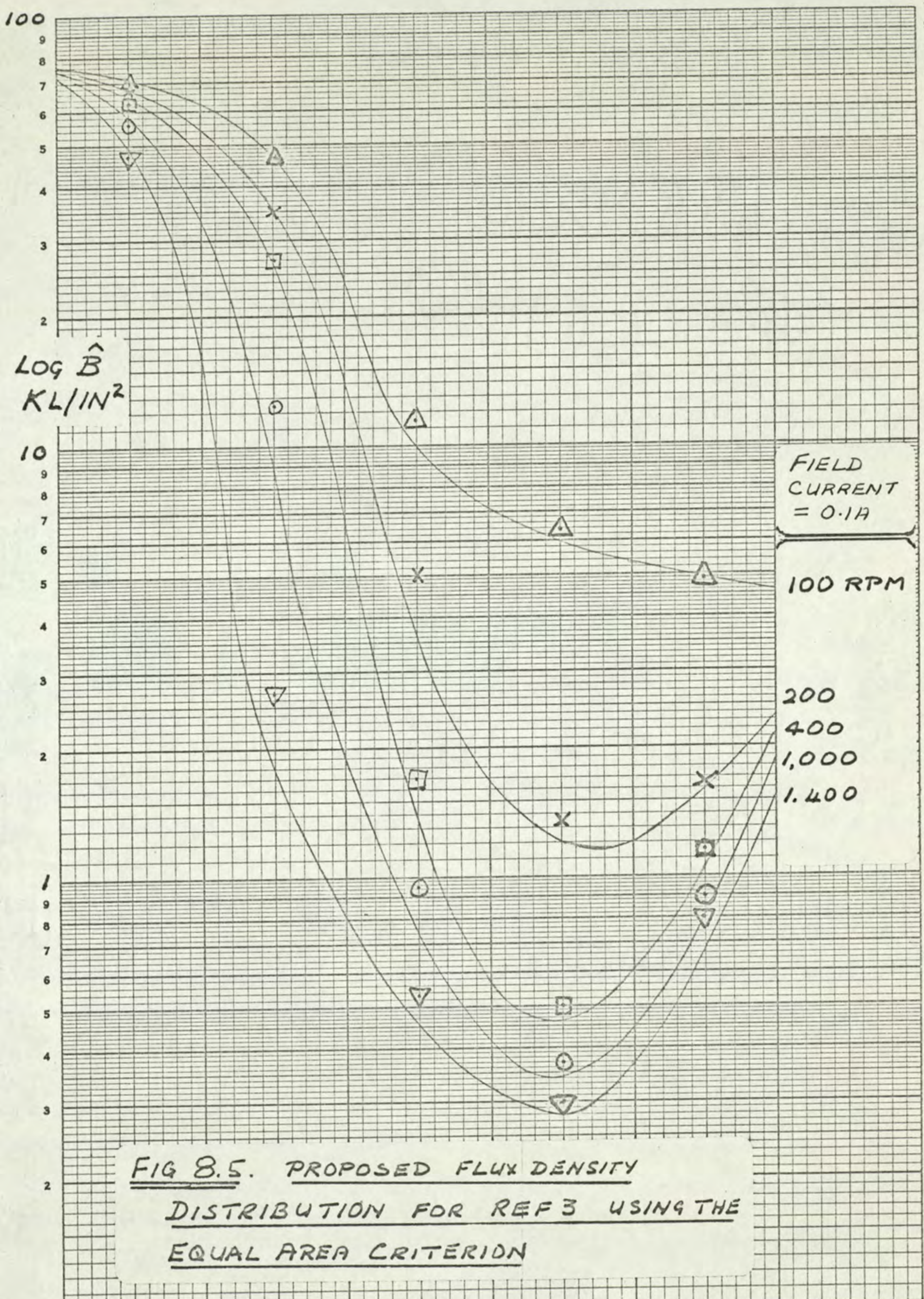

FIG 8.5. PROPOSED FLUX DENSITY DISTRIBUTION FOR REF 3 USING THE EQUAL AREA CRITERION

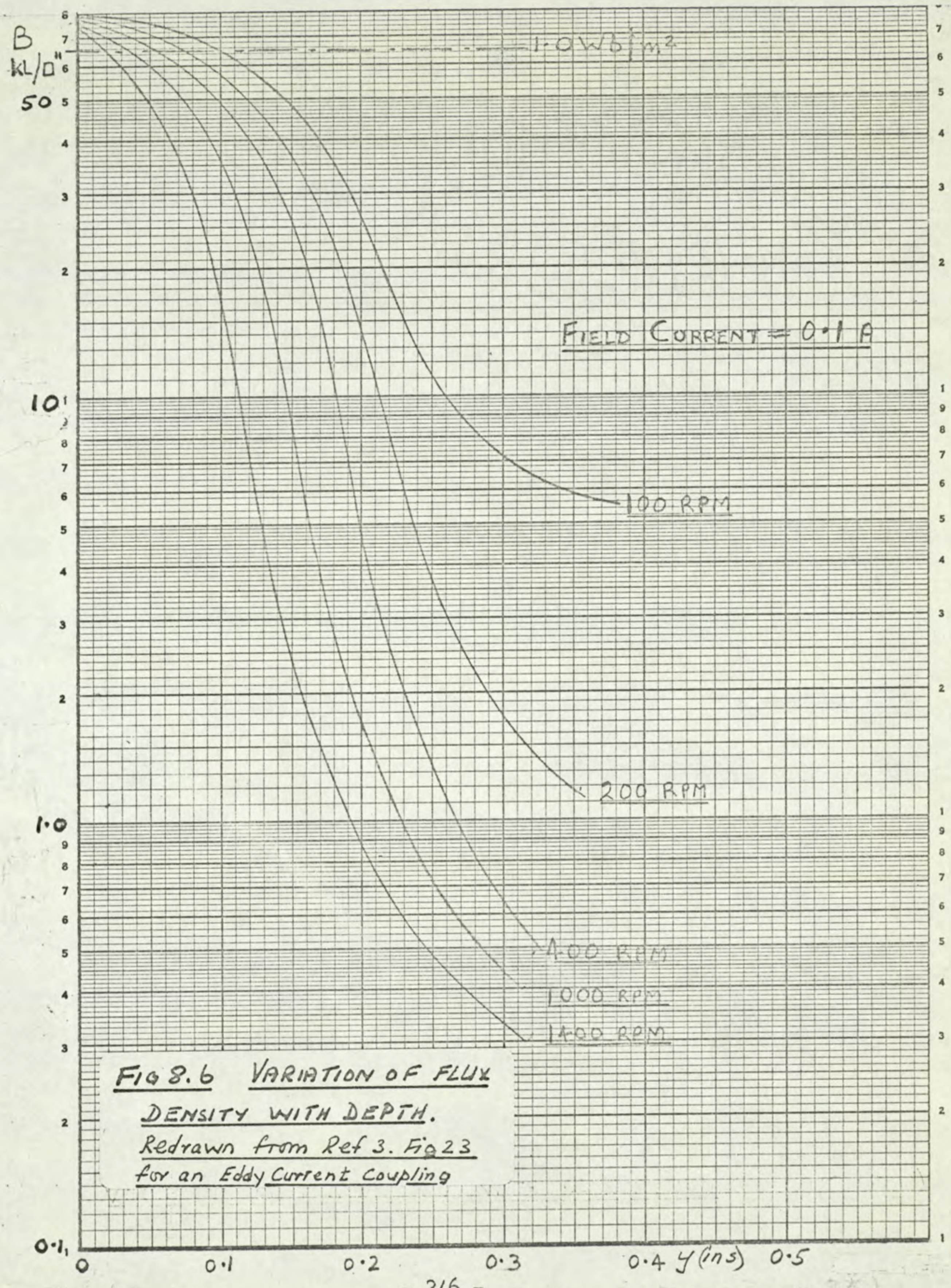

FIG 8.6 VARIATION OF FLUX DENSITY WITH DEPTH.
Redrawn from Ref 3. Fig 23
for an Eddy Current Coupling

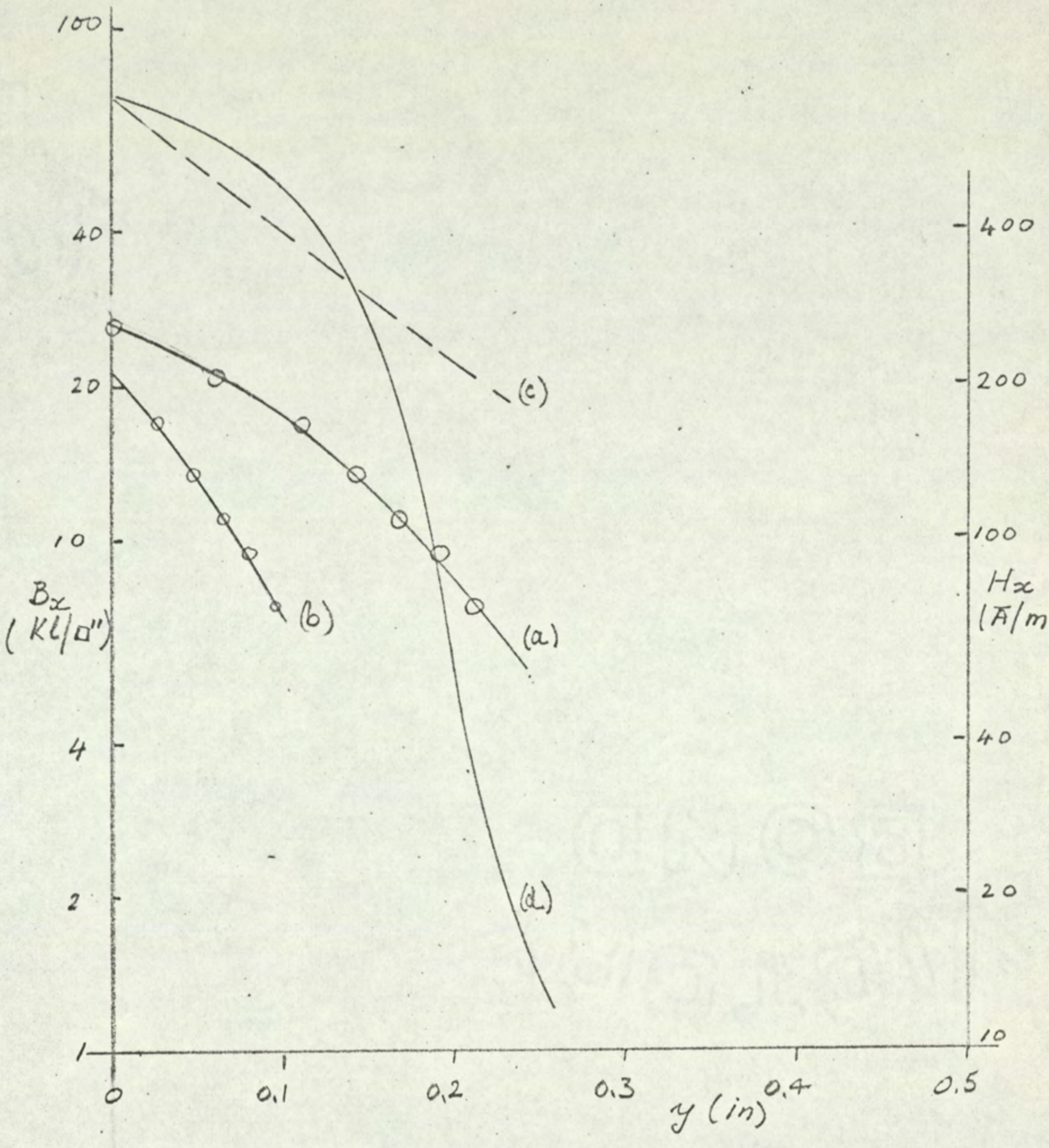

(a) = CALCULATED H_x FROM MEASURED B_x & μ FOR 100 R.P.M.

(b) = DITTO FOR 1400 R.P.M.

(c) = CALCULATED B_x FROM TABLE 8.1. } 400 R.P.M.

(d) = MEASURED B_x

FIG. 8.7 DISTRIBUTION OF B_x AND H_x WITH DEPTH y FOR THE EDDY-CURRENT COUPLING OF REF. 3

As a further illustration of this theory Fig. 23 of Davies[3] paper on eddy current couplings (below) has been redrawn. The points plotted in ref. 3. were originally obtained by measuring the e.m.f.s induced in search coils of equal area embedded in the iron. Each e.m.f. will therefore be a measure of the total flux linking the search coil. A horizontal line drawn through each point would indicate either the total flux or average value of peak flux density over the area enclosed by that particular search coil, Fig. 8.4(a) The graph should therefore be plotted as a hystogram. A smooth curve may now be drawn across this hystogram taking care to ensure that the $\int Bdy$ for each section of the curve is as nearly as possible the same as that for corresponding section of the hystogram, Fig. 8.4(a) Note that the shaded areas abc and def are not equal on log-linear paper.

The family of curves in Fig. 23 of reference 3 has been redrawn in Fig. 8.5. using the equal area criterion. Some similarity of shape in the member curves of such a family might be expected. On this supposition the irregularities in the family are attributed to experimental error and it is redrawn in Fig. 8.6 as the best family of curves making the least discrepancy with Fig. 8.5. The middle curve (400 r.p.m.) is redrawn on Fig. 8.7 and compared with a calculated curve derived in section 8.1.5. The two outer curves have been plotted on linear paper in Fig. 8.8. Whilst illustrating the difficulty of drawing the B_x/y curves on linear paper with so few points, they bring into true perspective the trivial increases in B_x at the back of the drum, which are probably due to currents flowing at the outer drum periphery.

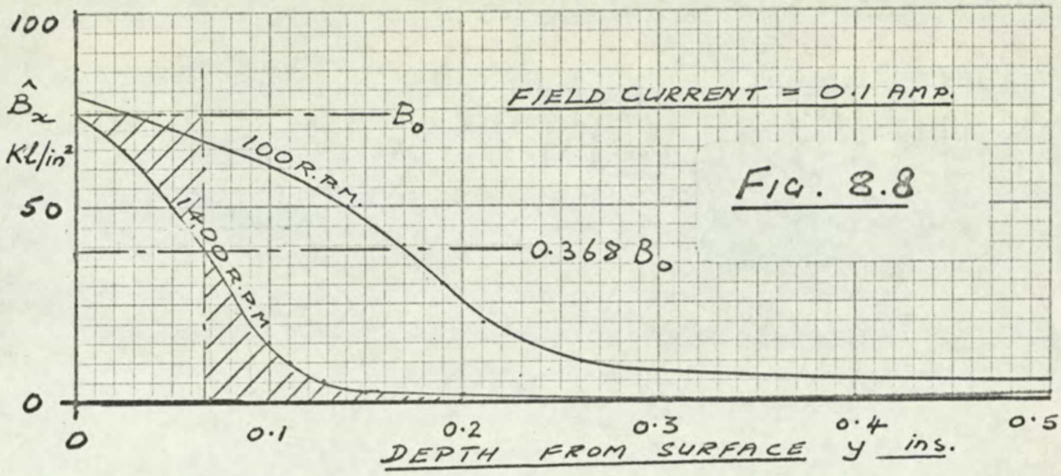

An alternative explanation of the variation B_{xmax} with depth in terms of the instantaneous power and instantaneous value of stored energy is suggested in chapter 10.

The conclusion of this analysis (albeit over-simplified) is that the maximum flux density neither decays exponentially with depth, nor reaches the high surface values that previous authors such as Kuyper[1] and Davies[3] have supposed. The resultant flux path is governed by two opposing influences: that of minimum reluctance - which tends to draw flux away from the surface, and that of the eddy current m.m.f. - which has the opposite effect.

8.1.4. The Variation of H_x with depth

It is interesting to consider the distribution of the magnetic intensity H_x throughout the drum depth, which should be different to the B_x distribution in view of the changing permeability. The following exercise refers to the curves previously analysed, Figs. 8.4 to 8.6. The values of H, are read off the empirical magnetisation curve of ref. 3. which is reproduced is Fig. 8.9.
The resulting H_x distribution, shown in Fig. 8.7, approaches more closely the theoretical exponential curve, (which would be a straight line on the log/linear paper used.)

CURVES RELATING FLUX DENSITY (B) AND MAGNETIC FIELD STRENGTH (H) WITH μ

Full Line = Ingot Iron
Broken line = Mild Steel
M.K.S. Units

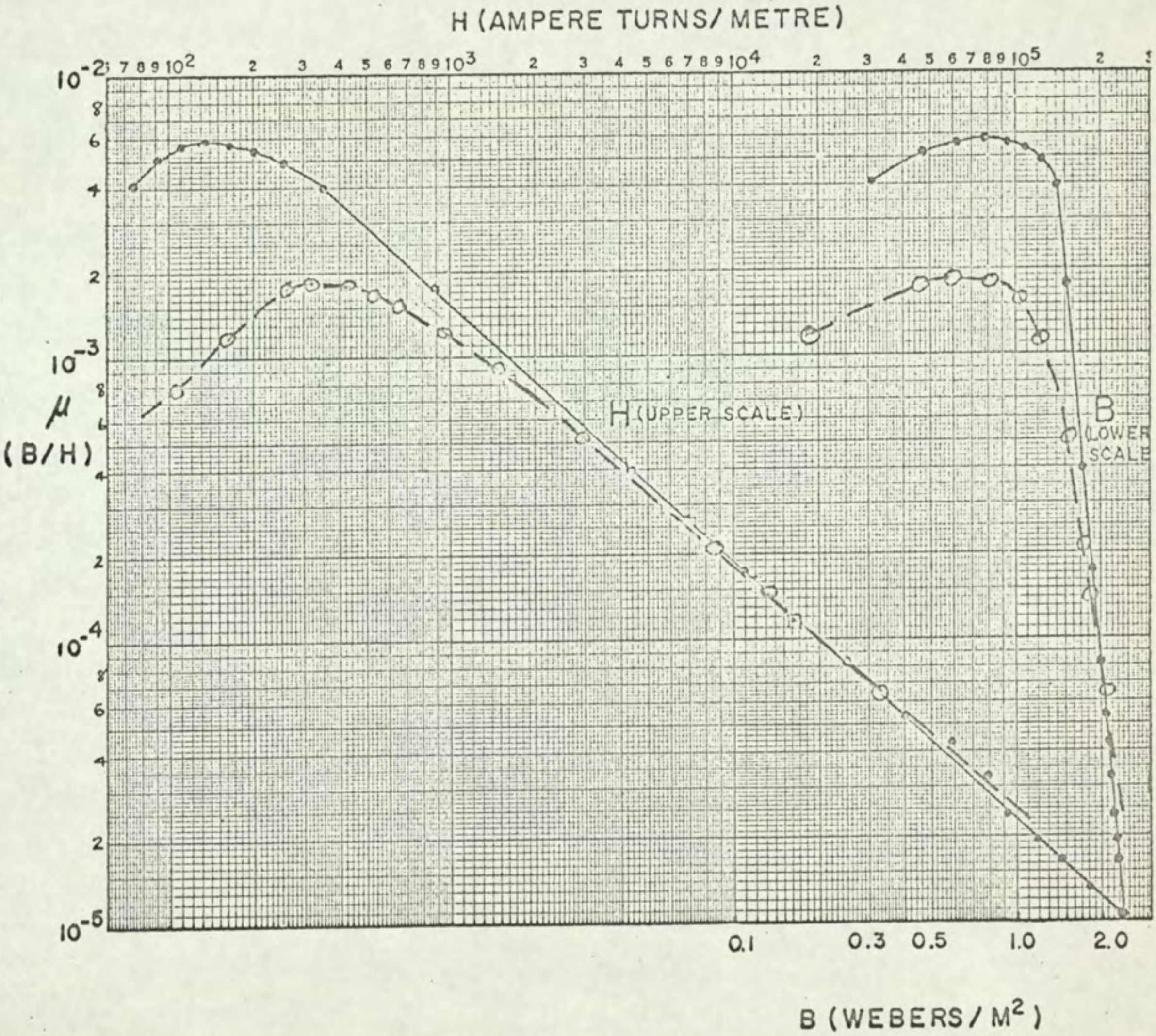

FIG. 8.9.

The assumptions made in plotting this H_x distribution from that of B_x must be noted. It is assumed that the d.c. magnetisation curve also relates alternating magnetic quantities, that the effects of other harmonics on the degree of saturation (and the value of μ) is negligible.

The value of μ used in converting B_x to H_x is that corresponding the peak value of B_x. Some other value of μ corresponding to the average or r.m.s. B_x might be more applicable. This could be achieved by transforming B_{mean} into H_{mean}, say, and then multiplying by $\pi/2$.

With the limited amount of experimental data available from reference 3. (5 points over a depth of ½"), further analysis of this particular family of curves could be misleading. The validity of the new curves is confirmed by work on other iron specimens at University of Aston.

8.1.5. The Calculated B_x distribution

In section 8.1.3. an iterative method of predicting the B_x/y distribution was suggested. This method is now explored using the results presented in reference 3. Fig. 23, (reproduced in sec. 8.1.3, Fig. 8.4.b.) in terms of peak fundamental flux density.

Let B_n = the peak flux density at any depth y,

B_{n+1} = " " " " " a depth y + dy,

and n = o when y = o.

Then, using the expressions in section 8.1.3. and assuming μ is constant over the thin layer "dy" we can write:

$$B_{n+1} = B_n \, e^{-\alpha \, dy}$$

where $\alpha = (\mu \omega / 2 \rho)^{\frac{1}{2}}$

Assuming some surface value, B_o, μ is read off the empirical magnetisation curve for ingot iron, Fig. 8.9, and B_1 calculated. The new value of B_1 is then used to calculate B_2 in the same way, and so on. A few steps in the calculation, using the assumed surface value of B at 400 r.p.m. are shown in Table 8.1. The calculated B_x distribution is shown by the dotted line in Fig. 8.7. The calculated curve bears no resemblance to the empirical one, the reason being that the permeability is almost constant over this range of B_x. It is therefore concluded that either the experimental values of search coil e.m.f.s. are erroneous, and should be much greater, bringing B_o above the knee of the curve, or other factors are involved.

When the diffusion of B_x into the iron is not exponential, the classical depth of penetration "d", becomes meaningless. For example consider the average value of permeability over the depth "d" for the 1400 r.p.m. condition, Fig. 8.6.

At the surface $B_x = B_o = 73\ \mathrm{Kl/m^2}$ $(1.1\mathrm{Wb/m^2})$

$\therefore$ At the depth d, $B_x = 0.368\ B_o = 27\mathrm{Kl/in^2}$ $(0.42\mathrm{Wb/m^2})$

From Fig. 8.6, when $B_x = 0.368\ B_o$ the measured depth of penetration is

$$d = 0.084$$
$$= 2.13\ \mathrm{mm}$$

Using $\alpha^2 = \mu\omega/2\rho = 1/d^2$ we can now obtain a value for the average permeability:

$$\mu = \frac{2\rho}{\omega d^2}$$

or

$$\mu_r\mu_o = \frac{2\rho}{2\pi f d^2}$$

Table 8.1 The Calculated B_x distribution

Let $B_{n+1} = B_n\, e^{-\alpha dy} = B_n\, e^{-dy/\alpha}$

where $d = \sqrt{2\rho/\mu\omega}$

take dy = 1/20 of the expected value of d.

= 0.020 mm

and N = 400 r.p.m.

then $d = \sqrt{(11.2\text{x}10^{-8}\text{x}2/\mu\ \text{x}2\pi\text{x}\frac{N}{10})}$

$= \dfrac{3 \times 10^{-5}}{\sqrt{\mu}}$

n	B_n Wb/m^2	μ $=\mu_u\mu_o$ From Fig.8.9	d $=\frac{3}{10^5\mu^{0.5}}$ mm	y = nd mm	$\frac{dy}{d}$ $=\frac{0.02}{d}$	-dy/d	B_{n+1} Wb/m^2	B_{n+1} Kl/m^2	y inches
-1							1.15	74	0.008
0	1.15	$52\text{x}10^{-4}$	0.416	0.02	0.0484	0.953	1.1	71	
1	1.1	$53\text{x}10^{-4}$	0.412	0.04	0.0485	0.953	1.05	68	0.016
⋮	⋮	⋮	⋮	⋮	⋮	⋮	⋮	⋮	⋮
26	0.342	$43\text{x}10^{-4}$	0.457	0.52	0.0438	0.957	0.327	21.1	0.205
27	0.327	$42\text{x}10^{-4}$	0.463	0.54	0.0463	0.958	0.314	20.3	0.213

since $f = \frac{pN}{60}$

$= N/10$, (the eddy current coupling having 12 poles)

and $\rho = 13\,\mu\Omega$-cm (at about $30^{o}C$) we get,

$$\mu_r = \frac{10\rho}{\pi N d^2 \mu_0}$$

$$\therefore \quad \mu_r = \frac{10 \times 13 \times 10^{-8}}{\times 1400 \times 2.13 \times 2.13 \times 10^{-6} \times 4 \times 10^{-7}}$$

$$\therefore \quad \mu_r = 63$$

or $\mu_r \mu_o = 7.9 \times 10^{-5}$

over the range of B_x considered, the value of μ, read from Fig. 8.9 is mostly greater than 4×10^{-3}

i.e. the value of μ calculated from the measured depth of penetration is quite erroneous, by the order of 50.

Conversely the depth of penetration calculated from the known value of μ (from Fig. 8.9) is much less than the measured depth, d.

e.g. for the 1400 r.p.m. condition:

$\mu \geqslant 4 \times 10^{-3}$

and $d = (2\rho/\mu\omega)^{\frac{1}{2}}$ metres

$\therefore \quad d \leqslant (2 \times 13 \times 10^{-8} \times \frac{10}{4} \times \frac{1 \times 1}{\pi \times 14}$ mm

$\leqslant 0.27$ mm.

which is about 1/7th of the measured value.

It is interesting to note that the alternative concept of considering all the flux to be enclosed within the depth of penetration (see section 10.1.2) gives much better correlation with the empirical value of 'd' measured from Figs. 8.6 or 8.8. In Fig. 8.8, for instance, the shaded areas each side of a vertical line drawn at $B_x = 0.368\ B_o$ are almost equal, indicating that the total flux equals that contained approximately in a surface layer depth d, having a flux density equal to the r.m.s. value of B_o

i.e. $\phi_{ac} = \frac{B_o}{\sqrt{2}} \times L \times d \simeq \int_0^{\infty} 0.707 B_o L dy.$

It would appear therefore that an empirical value of d forms a reasonable basis for analysis, providing the insertion of the requisite search coils does not severely alter the disposition of the electro-magnetic quantities in the iron. This idea has also been suggested by B. James[38] (M.Sc. Thesis, University of Aston, to be submitted in 1968,). James also points out that the penetration depth at the point for which $B = 0.368B_o$ does not vary with frequency according to the classical formula,

$d = (\rho/\mu\pi f)^{\frac{1}{2}}$

For example, in Fig. 8.6 the depth is halved when the frequency is increased 14 times (100 to 1400 r.p.m.). Closer examination indicates that an orderly relationship between d and f may exist ($d \propto e^{-0.8f}$). Further work with more readings per unit depth is necessary before any such relationship could be claimed.

8.1.6. The Value of Permeability in the Pole Face Loss Problem

For a smooth pole surface the problem of selecting a suitable substitution for permeability is complicated by

(i) the existence of the normal d.c. field, not present in the interdigitated eddy current coupling.

(ii) The superposition of harmonic m.m.f.s whose space phase angle varies (in pairs) over 360° between one fundamental m.m.f. centre line and the next one.

(iii) the harmonics introduced by the armature slot openings and (iv) Variation in magnetic properties due to rolling, cold working, and imperfect annealing.

The question of rotational hysteresis is not easily solved since the sinusoidal rotating harmonic waves, normally associated with rotational hysteresis, cannot be considered in isolation either from each other for from the normal d.c. field. The synthesised surface flux density fluctuation is basically an alternating function and not a rotating one (Fig. 2.5). Consider first the effects of the normal d.c. field on one harmonic term. Suppose the alternator excitation is decreased from its maximum value to produce the d.c. flux density (B_{mean}) at P on Fig. 8.10. The peak to peak value of the harmonic m.m.f., $F_{\phi h}$) is represented by CD.

B_1 = Flux density due to normal d.c. field.
$PQ_1R_1S_1$ and $PQ_2R_2S_2$ = loops due to a superposed a.c. field.

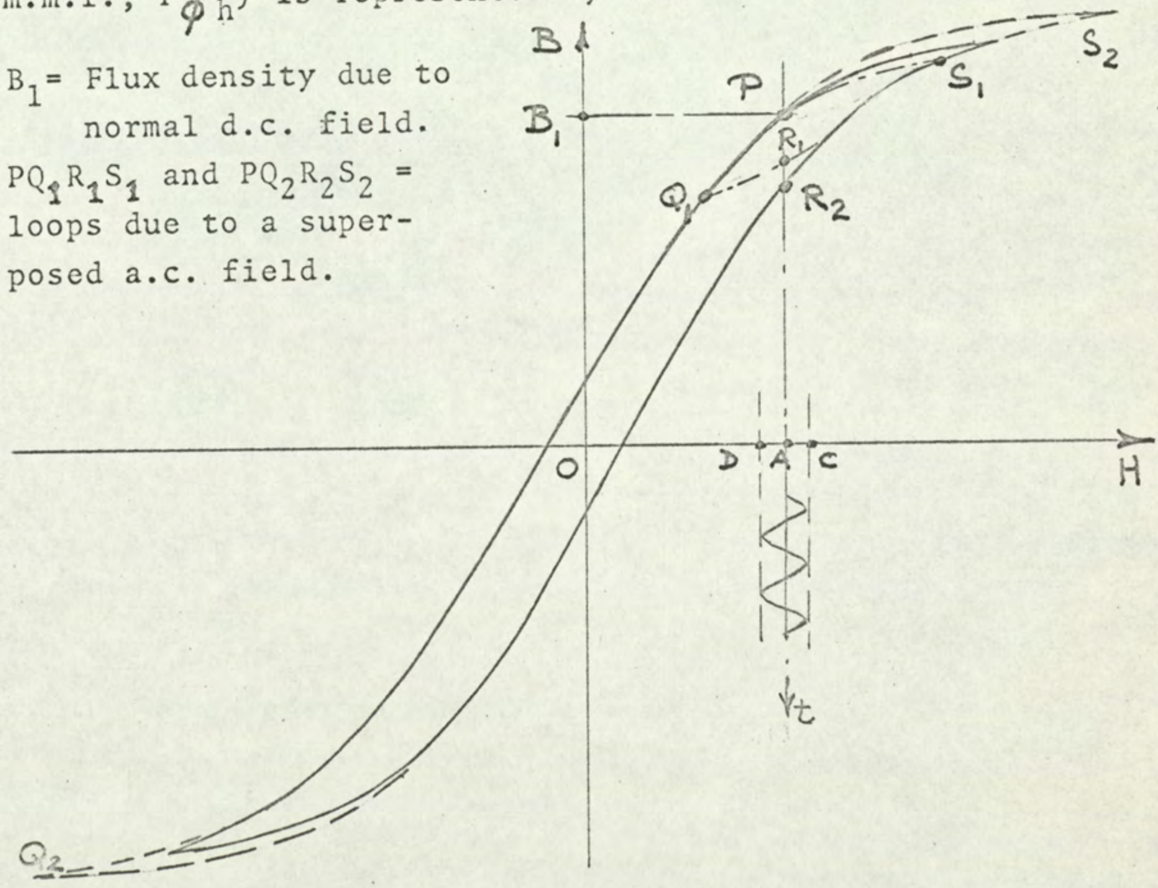

FIG. 8.10 The B-H Loop for the Pole Steel

The recoil loop produced by CD would be quite small providing the harmonic and the d.c. fields share the same flux path. This is not so. The normal d.c. flux passes through the pole body, the harmonic flux through a thin surface layer. The depth of this layer in practice has been shown above (in section 8.1.3) to vary with the flux contained therein, the flux density remaining "around the knee" of the magnetisation characteristic of the pole steel.

The flux should penetrate deeper into the pole during the rise in the instantaneous value of the m.m.f. from A to C; and less deep during the fall from C to D.

The change in flux density would then be smaller on the positive swing of the harmonic ripple than on the negative swing. It is hazardous to try and estimate without further experimental evidence whether the magnitude of this change in flux density follows the small recoil loop $PQ_1R_1S_1$, or the large loop $PQ_2R_2S_2$ which goes further into saturation.

The inclusion of all the harmonic terms complicates the problem still further since the fluctuations in penetration depth will also depend on the peaky nature of the m.m.f. ripple (c.f. Figs. 2.5 and 7.5).

The actual depth of penetration decreases as the rate of change of flux increases, though not necessarily according to the classical formula - Section 8.1.5. It follows that the alternating component of flux produced by the m.m.f. ripple wave should penetrate less deeply into the pole steel on the "peaky" half cycle than on the other half cycle. The depth of penetration will then vary in time, and, since the ripple waveform changes with distance from m.m.f. direct axis (Fig. 7.5), with space. The problem is therefore very complex.

On the subject of hysteresis loss, the conclusion drawn in section 2.4.5 from previous work (in particular that by Aston and Rao[15]) was that alternating hysteresis loss is a negligible proportion (a few %) of the eddy current loss. Rotational hysteresis is considered negligible (see above).

8.1.7. Recommended Substitution for Permeability

The above discussion leads to the follow conclusions:

(1) B_x does not decay exponentially, nor is it expected to do so; H_x ($=B_x/\mu$) very nearly does.

(2) The surface flux density is not as high as some authors have suggested. It is commonly near the knee of the magnetisation curve.

(3) The complexity of the B-H relationship prohibits precise mathematical treatment. A realistic substitution for μ should approximate fairly closely to the real value of μ as it changes in both time and space, but above all give meaningful results.

(4) In view of (3) a substitution for μ such as that proposed by Frolich, would appear to be more appropriate than one obtained by plotting $\mu^{1/4}H/H$ above the knee. Nevertheless, where loss calculations are not required to a high degree of accuracy, the excessive use of computer time is uneconomic and the best compromise between the simplicity of the ultimate formula and mathematical precision may indeed be to adapt a substitution of the form $B = aH^b$ (i.e. $\mu^{1/4}H = k_1H^m$), justified by the results it gives in practice.

An analytical or empirical substitution could be made in Maxwell's equations which would then be solved by numerical methods. Even so the effects which alternating hysteresis and the d.c. field have on the value of μ may have to be excluded from the analysis at present. In this thesis such numerical methods have been avoided in order to justify pragmatically the modified eddy current coupling thoery, in which an analytical substitution for μ is made after integration of the field equations.

For curve 1 B=constant
if $H \neq 0$

For curve 2 $\mu^{\frac{1}{4}}H = 0.769H^{0.794}$

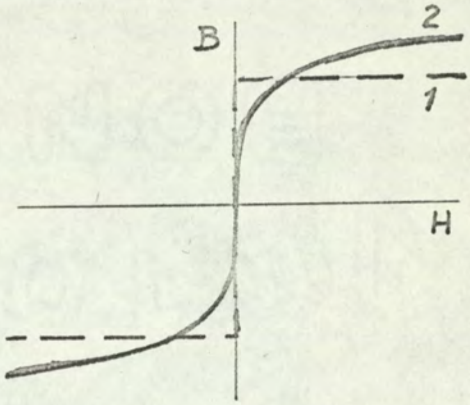

FIG. 8.11

The rectangular B/H curve of Fig. 8.11, curve 1, adopted by previous authors such as Angst[29], is considered a poorer approximation than the logarithmic curve, (2) for three reasons. Curve 2 is a better overall shape, there are no discontinuities, and complete saturation in each direction is unrealistic.

The effect of the main field will cause the harmonic flux density to change along some recoil loop. If the recoil loop was small, then a single-valued substitution for μ would be possible. Section 8.1.6. suggests that large recoil loops are probable because the flux penetration varies to permit the resultant flux density to remain near the knee of the magnetisation characteristic on both positive and negative half cycles. In which case either a logarithmic substitution or Frohlich's substitution might be permissible. In either case the values of B and H will be correct at two points in the first quadrant, where the analytical and empirical curves intersect. (Fig. 8.1.)

These curves have been discussed in section 8.1.2. For the secondary steel of the experimental machine the analytical curve obtained from a logB/log H graph (curve 4, Fig. 8.1)lies closer to the empirical curve for decreasing values of H than does the analytical curve obtained from the $\log\mu^{\frac{1}{4}}H/\log H$ graph (curve 3). On the other hand curve 3 lies nearer the centre of the loop and could be considered a better compromise. Between curves 3 and 4 the change in index m, is only 2% whereas the change in the plotted characteristic is considerable. This not only illustrates the sensitivity of m, but also the fact that considerable change in the slope of the graph of log B against log H above the knee may not affect m very much, although it may affect the k_1 considerably. The main object of the theory is to forecast the effects of changes in machine parameters. For this reason an error in k_1 is less important than an error in m since k_1 only affects directly the coefficient in the normalised speed equation and not the indices of the machine parameters.

For this reason the computations using indices obtained from the equation $\mu^{1/4} H = K_1 H^m$ is considered to yield a permissible approach to the problem at the present state of the art. Since the pole material is not expected to saturate heavily it might be better to determine the relationship between $\mu^{1/4} H$ and H over the working region. Bratoljic takes the function: $\mu H = 4000 \text{ arsinh}(H)$ (H in $\bar{A}$/cm) to define the permeability in "the relevant region of moderate saturation and uses this function to evaluate his test results.

He also correctly points out that in the short circuit test, (when the losses are usually measured) the normal d.c. field is of minor importance. In his thoery the losses are shown to depend only on the square root of $\sqrt{\mu}$ and moreover to increase with μ for low order harmonics and to decrease for high order harmonics so that there is a degree of compensation if μ is wrongly chosen.. The normal d.c. field which changes with load conditions presents such a complex problem that a practical analysis would presumably have to depend on test results to a considerable extent.

8.2 The Experimental Load Loss dynamometer

In view of the difficulties encountered in separating the losses in the model machine the correlation between theory and experiment is most encouraging.

The ability to swing the secondary frame on trunnion bearings proved invaluable in measuring the limits of remanence torque, and subsequently the primary iron loss. The latter agreed closely (within 6%) with the value calculated from the sheet steel manufacturer's curves in Appendix 12.4. The technique used in separating the measured values is based on the conversion of mechanical and electrical source power into the loss power. It has been shown elsewhere[12] that for a conventional (wound stator) induction motor with an open circuited secondary the energy dissipated in primary iron loss at synchronism comes from an electrical power source. Experiments on a rotor fed induction motor have indicated that the same is true for the experimental load loss dynamometer which has a shorted secondary.

Regarding the m.m.f. harmonic loss, it is argued in appendix 12.7 that the ratio

$$\frac{\text{electrical source energy}}{\text{mechanical source energy}} = \frac{1}{h}$$

for any harmonic order $h(=6K\mp 1)$. Further, that the direction of electrical power flow is away from the source for the $6K - 1$ harmonics and towards the source for the $6K + 1$ harmonics. Consequently the power dissipated as m.m.f. harmonic loss comes almost entirely from the mechanical power source. The error in assuming the net electrical power to be zero is shown to be quite small, and has been neglected. The power source appropriate to each of the remaining losses (shown in Fig. 5.15) is unquestionable. So is the magnitude of each, with the exception of the slot ripple loss. The error in calculating this loss by the accepted method[9] may be unusually large because of the unusually large slot opening/gap ratio. On practical machines the prediction is probably within $\pm$ 10%. The results of experimental work being conducted elsewhere in a model machine having a large slot opening/gap ratio should facilitate reassessment of the surface losses. The error in measuring the total surface loss (i.e. m.m.f. harmonics and slot ripple harmonics) is estimated at $\pm$ 5%. The other errors mentioned above could easily account for the difference between measured and predicted m.m.f. harmonic losses. This difference is withing 20% at 50 c/s, the predicted value being the lower value.

Of greater importance to the machine designer however is the ability of the theory to predict the effects of changes. The variations in measured and predicted losses with a few easily varied parameters are compared in section 6.2. Here agreement is within 10% for two of the three parameters only (Table 6.1) namely current and frequency. Whilst it is encouraging that the measured value of the loss is within $\pm$20% of the predicted value over the working range of temperature (for which ρ = 18 to 30 $\mu\Omega$-cm). The wide discrepancy in the loss variation with resistivity, suggests a shortcoming in the theory. The cause of the discrepency which is not normally present in practical machines, is the high value of normalised speed, n/n_m. For the predominant harmonics, n/n_m is above unity and this is the major factor in the inability of the theory to predict reasonably accurately the variation of loss with secondary resistivity. i.e. the predicted n_m is too low. A higher value would reduce n/n_m giving a more realistic prediction of the change in loss with frequency. An increase in the value of maximum torque T_m would then be necessary to produce the same loss. An investigation into the satisfactory prediction of the effect of changes in pole resistivity of practical machines has not yet been done. The ability of the theory to predict the effect of changes in armature (primary) current and frequency is assessed by comparing the indices of the logarithmic graphs in Table 6.1. Correlation is considered good in each case since the indices agree respectively to within 10% and 15%. Over the primary current range the measured loss was within 20% of the predicted value. Poorer correlation was obtained when the synchronous frequency was varied - over the frequency range from 20 to 60 c/s. the measured loss was within 30 to 15% of that predicted.

Although better correlation is obviously desired it is concluded that this theory would highlight a bad machine at an early design stage. The m.m.f. harmonic losses calculated using other methods are also of the right order. Kuyper's "long" method (using Fig. 2.8) is more accurate than Barello's. The predicted value using either method is very dependent on the selected value of μ. This puts the onus on the designer, who will presumably select a value based on his experience.

Section 6.2 shows that for the limited number of variables the methods of Kuyper and Barello will predict the effects of changes as accurately as the eddy current coupling theory. For the loss to decrease as μ increases Kuyper's factor R_1 should lie to the left of the peaks of the curves in Fig. 2.8; This was so for the two machines in Table 6.17 but not for Kuyper's own Table III. Therefore a predicted change in loss with pole resistivity in Kuyper's

Table III would be misleading.

8.3 Production Machines

(i) The Flux Leakage Factor

The g/λ_h ratio of practical synchronous machines is much greater than that of the experimental machine. Consequently the peripheral flux leakage (negligible on the latter) is important. Although the flux leakage factor K_L, used in the modified eddy current coupling theory, theoretically underestimates the leakage and produces a pessimistic loss figure, comparison with Kuyper and Barello shows that an optimistic loss figure is obtained (Table 6.17). It is therefore concluded that either K_L or the predicted loss is too low, further that the assumption that eddy current reaction has a small effect on the derivation of K_L for the predominant harmonics is true, otherwise K_L would be even lower.

(ii) The 60-MVA Synchronous Compensator

The stray load loss of this machine measured by the short circuit test is 246 kW. 100 kW of this is estimated supplementary copper loss leaving 146 kW of "other losses" to be divided between clamp plates, end guards, fingers, duct spacers, the pole face loss of 23 - 25 kW due to stator m.m.f. harmonics alone is not an unreasonable proportion and gives rise to confidence in the modified eddy current coupling theory. This figure accounts for the shape of the pole shoe by an analytical and (2) a graphical technique, quite good agreement being obtained between the two.

Both Kuyper's (short) and Barello's methods give a loss figure roughly equal to the 'other losses' and are therefore considered too pessimistic to be realistic. Nevertheless, in common with the e.c.c. theory these methods do highlight lossy harmonic terms. The selection of a larger value of μ reduces the calculated loss of both to a more realistic value.

It is impossible mathematically to obtain manageable expressions for the electromagnetic quantities which account for both peripheral flux leakage and a variable permeability without resorting to numerical solutions. It is also impracticable physically to define μ analytically to account for its variation with depth, time, magnetic intensity and normal d.c. flux density.

(iii) Changes in Main Dimensions

The change in loss with two machine parameters is indicated in Tables 6.11 and 6.13. The short circuit test data on two "lossy" machines A and E before and after increasing the gap, reveal a measure of correlation between theory and practice. The same conclusion is drawn from the comparison of the two machines C & D of different length, Table 6.11.

It has not been possible to demonstrate practically the effects of changing all the design parameters but a theoretical design study on machine C, a 3.4-MVA 4-pole machine, showed a considerable reduction in pole face loss with increase in the slots/pole/phase and with the pole steel resistivity, Fig. 3.6.

These and other methods of reducing the pole face loss are well known. The influence of the winding factor is discussed in the next section, but before leaving machine C, Table 3.4,it should be noted that the magnitude of the predicted belt harmonic loss with full-pitched coils is about 7 times that when they are pitched 78%. Short pitching has a less noticeable effect on the slot harmonic terms since they always have the fundamental winding factors.

8.4 The Surface E.M.F. Distribution

The importance of harmonic synthesis in dealing with the surface e.m.f.s. is demonstrated in chapter 7. Basically the inducing m.m.f. is a non-sinusoidal time-varying pulsation stationary relative to the pole face but varying in magnitude across it. Any treatment of this synthesized m.m.f. variation, onerous in itself, is made more difficult by the presence of surface discontinuities, a non-linear magnetic medium, and the normal d.c. field.

The expression for the surface e.m.f., e_h, of order h in terms of the harmonic flux density, B_h, has been derived in Appendix 12.5. The algebraic signs of the harmonic winding factors are most important when adding e_h terms. The sign and magnitude of these factors depend of course on the winding layout. For example, the full-pitched uniformly distributed winding of Figs. 2.4 and 2.5 has a maximum m.m.f. fluctuation at the direct axis. Richardson[8] draws attention to this phenomenon as well as to the established practice of short pitching to reduce the harmonic m.m.f. losses. The equations of Appendix 12.5 show that the direct axis m.m.f. fluctuation is reduced if the pitch factor lies between 4/5 and 6/7, i.e. if the 5th and 7th harmonic winding factors have opposite signs. Other significant harmonics should also be considered for in a complete synthesis.

The even non-triplen harmonics introduced by fractional slot pitching further increase the number of loss components; the lowest order terms (h = 2,4) may be particularly troublesome because of their high pitch factors. The d.a. fluctuation affects the measured stray load loss more than the actual loss on load. This is because the m.m.f. direct axis and the pole axis are aligned in the s/c test, but not usually aligned on load. As the rotor torque angle approaches unity the quadrature axis m.m.f. fluctuation becomes significant. Here the synthesised slot harmonic component is greater (see Figs. 2.6 and 7.5), but this is counteracted by the larger attenuating affect of the g/λ_h ratio.

Whilst the above comments emphasise the fundamental nature of the m.m.f. harmonic loss problem they point to flaws in the treatment of pole profile (section 3.7.2.) or of axial slotting, which ignores the change in m.m.f. fluctuation across the pole face. The rather unusual variation in the search coil e.m.f.s. of the experimental machine is due to the combined effect of the rotating m.m.f. harmonics, the slot ripple harmonics, and the polarising m.m.f. The magnitude of the first harmonic term, measured using a sharply tuned filter, will depend to some unassessed extent on the presence of higher harmonic orders. Assuming that these 300c/s harmonic e.m.f.s. are proportional to the armature (primary) current, I_A, and the slot ripple e.m.f.s. are proportional to B_{mean}, the latter might be expected to predominate below the knee of the magnetisation curve but not above it. The measured values of the 300c/s e.m.f. components support these expectations. Although these values are not quoted categorically because of the many assumptions made in separating them, they are of the right order of magnitude.

The curves of B_5 and B_7 plotted in Figs. 7.13 and 7.14 compare reasonably well with the corresponding values of B_{mean}. The values obtained for B_y from two separate search coils are corroborative thereby justifying the assumptions made in obtaining them (7.4.5). It is unrealistic to draw comparisons between the oscillograms and the impressed m.m.f. fluctuation plotted in Fig. 7.5 because the impressed m.m.f. is modified by the effects of eddy current reaction.

9. CONCLUSIONS

9. CONCLUSIONS

It is well known that the armature m.m.f. wave varies periodically between two limits spaced at 30 electrical degrees. Hitherto the resultant wave has been considered as a Fourier series of space harmonics of order $6K \pm 1$, the frequency of each pair of harmonic e.m.f.s induced in the poleface being $6Kf_1$. Richardson[8] has pointed out that the amplitude of the resultant $6Kf_1$ wave varies over the pole surface. This thesis extends the theoretical work of Richardson and is supported by measurements of secondary surface e.m.f.s. on the experimental load loss dynamometer. The measurements are summarised in section 7.5 and discussed in section 8.4.

Basically, the change in the armature reaction m.m.f. relative to the pole face is a non-sinusoidal time varying pulsation superposed on a stationary, sinusoidally distributed, d.c. field. The magnitude of the peak pulsation and its displacement from the m.m.f. direct axis depend on the winding design. The peak pulsation will not occur at the armature m.m.f. direct axis if the $6K-1$ and $6K+1$ harmonics tend to cancel there. For example, when the pitch factor is about 0.83 the 5th and 7th harmonics are in antiphase at the direct axis and in-phase at the quadrature axis. They will therefore cause high surface losses when the m.m.f. quadrature axis and the pole axis are aligned. This occurs under normal operating conditions when the power factor is about unity and not under short circuit test conditions. The value of pole face loss obtained from the short-circuit test would then be less than the actual value on load. In Richardson's[8] words :"there is no direct relationship between the value of stray load loss measured on short circuit and that on load."

The surface e.m.f.s on secondary of the experimental machine were constant over a wide temperature range whereas the measured loss decreased as $\rho^{0.75}$. It is therefore deduced that the surface loss is dependent on the induced E_z wave not the J_z wave, i.e. it requires a mechanical power source in confirmation of the theory given in Appendix 12.7.

The predicted loss is calculated from the modified eddy current coupling theory using the computer programmes presented in Appendix 12.3. The theory uses the relationship $\mu^{\frac{1}{4}}H = k_1H^m$ discussed at length in section 8.1.7. It is adopted, not for its close approximation to the empirical B/H curve at working flux densities, but for the simplicity of its substitution in equation 3.13 and its pragmatic validity in the practical design of eddy current couplings.

The theory does not account for the non uniformity of stator and rotor surfaces due to slotting and grooving except that Carter's coefficients have been used to calculate the effective gap. The effects of pole shoe bolts, wedges and damper windings are not included. The work is parallel to that of Kuyper[1] and Barello[2] in that the electromagnetic field quantities in the pole face are assumed sinusoidal and have small depth of penetration. All current paths are assumed axial since the wavelengths of the harmonic terms are small compared to the rotor length. Kuyper and Barello are not limited to the short air gaps used in eddy current couplings, although Kuyper's simplifying assumption regarding the graph of his factor R_1 (Fig.3.8) imposes a 'short gap' limitation in that Fig. 3.8 is claimed invalid for gap to wavelength ratios g/λ_h greater than 0.3. This will often exclude calculations on the slot harmonic terms of large machines, Appendix 12.8. Work on tooth ripple loss[7] also gives the same limiting condition for a 'short' air gap. The loss due to the slot harmonic m.m.f's. is claimed by Richardson[8] to be negligible when g/λ_h exceeds 0.4, in which case Chalmer's[6] extension of Kuyper's graph to twice this value is rather surprising.

Barello shows mathematically in his Appendix VII that assuming μ and ρ are both constant the loss can be obtained by calculating the separate contributions of each term and adding the results in a scalar manner. The methods of predicting the harmonic losses presented in this thesis, and of treating shaped pole pieces, follow Barello in segregating the component fields.

The correlation between the two ways of treating pole chamfer indicate that the approximate algebraic method is suitable for practical purposes. Any inaccuracies in the algebraic method, introduced by assuming that the loss is proportional to $(\text{gap})^2$, are small compared to those incurred by neglecting the variation in the induced e.m.f. across the pole face.

The predicted loss due to each harmonic m.m.f. has been multiplied by a peripheral flux leakage factor, K_L, derived simply in Appendix 12.2.3. This enables the modified eddy current coupling theory to accommodate the larger gap to wavelength ratios of conventional machines but seems to overestimate its effect on reducing the loss. K_L has been omitted from Table 3.3. Its inclusion would cause the increase in the slots/pole/phase to reduce the loss by an amount greater than that tabulated.

Richardson and others have commented on the impracticability of segregating the components of load loss in practical machines. At the present time, the verification of the proposed theory relies mainly on the evidence from the experimental machine. Nevertheless the change in measured short circuit loss on actual machines when one parameter is varied has given encouraging results (section 8.3). Furthermore the predicted loss for the range of production machines in Appendix 12.8. forms a reasonable proportion of the measured short circuit loss.

This thesis does not present an absolute method of calculation, but rather tries to give a clear picture of the relevant machine parameters with a method of predicting the effects of changes. In view of their simplicity, the proposed formulae should be useful to the design engineer since they refer directly to the machine parameters and not indirectly via complex formulae involving trigonometric, exponential or elliptic functions.

Section 3 shows how the pole face loss in a given machine may be controlled by selection of the slots/pole/phase, q, the winding pitch, and the airgap, g, (within limitations imposed by other requirements). Both q and g should be as large as possible. Fractional slotting increases the number of harmonic orders present but may reduce the loss by improved winding factors. No slotting (for example Davies[42] proposed slotless winding for turbo-generators) eliminates the slot harmonic terms and consequently eliminates the pole face loss associated with them.

The slot width factor, k_{bh}, is important calculations on all conventional machines (Appendix 12.2) but especially important in machines with a small gap. In such machines, the slot harmonic m.m.f's have greater significance and are so modified by k_{bh} that the losses associated with them are reduced by 30 to 60%; k_{bh} is also significant in machines other than the synchronous machines discussed here, e.g. induction motors with open slots or with semi-closed slots where the slot mouths saturate on load. In such cases, the second slot harmonic term ($h = 12q \pm 1$) may be important.

The measurements on the experimental load loss dynamometer demonstrates the ability of the theory to predict trends when either the primary (armature) current or mains frequency is varied. The reduction of pole face loss by an increase in pole resistivity is demonstrated practically, but is not confirmed theoretically. The high values of slot opening/gap ratio and remanence torque have been mainly responsible for delaying the loss measurements and expanding the written work (section 8.2). The predicted value of loss at mid-range agrees with the measured value to within the limits of experimental error which were ± 15 to 20%.

All methods of calculation highlight the particularly "lossy" terms and predict losses of the right order of magnitude (section 6.5). Kuyper's "short " method tends to overestimate the loss and leads to anomalous values of μ_r. His long method with $\mu_r = 1000$ tends to underestimate the loss. The disadvantage of the methods used by both Kuyper and Barello is the need to select a suitable value of μ_r. The choice depends to some extent on previous experience, Kuyper tending to use a lower value than Barello. For reasons given in section 8.1.6. a value of $\mu_r = 1000$ is used in this thesis for calculations using either method.

Numerical solutions to the problem of permeability have given theoretical support to both the author's views on flux penetration in the solid member (section 8.1) and to the experimental work of other investigators at the University of Aston. However, until the effects of the superposition of both the normal d.c. field and the other harmonic fields on one harmonic term is known it is questionable whether a numerical approach is really worthwhile.

In view of its complexity the problem of superposed fields is ignored in the theory but examined in the discussion on permeability - section 8.1.7.

This thesis is primarily concerned with extending Davies'[3] eddy current coupling theory to the pole face loss problem and with examining its usefulness in predicting this component of stray load loss in both an experimental machine and a range of practical machines. No fundamental changes have been made to the theory although some suggestions appear in the next chapter. With the exception of the change in loss with resistivity it is concluded that the practical work supports the theory in all aspects examined.

10. SUGGESTIONS FOR FURTHER WORK

10. SUGGESTIONS FOR FURTHER WORK.

All the methods of calculating the component of pole face loss attributed to the armature currents rest on certain simplifying assumptions. In this research programme it was decided to conduct the initial tests on an experimental machine with an oversimplified pole structure closely resembling the mathematical model. This part of the programme is now almost complete. The reasonably close corroboration between predicted and measured results on the experimental machine is most encouraging, and prompts further investigation into the validity of the theoretical assumptions. Changes to the theory and to the experimental machine are suggested in sections 10.1 and 10.2 respectively.

Refinements in instrumentation, incorporating pen recorders for example, would lessen the secondary heating problem and improve the overall accuracy of the experimental machine set.

10.1 Theory

10.1.1. Permeability

With the exception of permeability the method of loss prediction presented in this thesis holds the same basic assumptions as other widely used methods[1,2]. The substitution for the permeability of the pole steel is discussed in section 8.1, and elsewhere by many other authors.

The m.m.f. harmonic loss problem is complicated further by the presence of the standing fundamental flux density wave. The practical importance of d.c. superposition and of the lack of surface saturation on the surface losses in solid ferromagnetic materials should be established before the theory is revised. An investigation of this type would need new apparatus and should first be confined due to a single impressed frequency.

10.1.2. Depth of Penetration

The classical depth of penetration, d, is expressed in terms of permeability, resistivity and frequency.

In a linear theory :

(a) the value of 'd' is very dependent on the value selected for μ (Section 8.1).

(b) the values of the electromagnetic quantities fall to e^{-1} of their surface value at a distance 'd' beneath the surface

and (c) the total flux in the semi-infinite secondary member would equal the flux contained in a surface layer of depth 'd' if the circumferential component of flux density were maintained constant at its surface R.M.S. value +.

In a non-linear theory the meaning of "the depth of penetration" must be clarified since statements (b) and (c) conflict when the surface flux density exceeds a certain value. A useful measure of the flux penetration would be obtained by defining the depth of penetration in terms of statement (c).

The author suggests that the decay of electromagnetic quantities with depth, y, previously assumed to depend solely on ρ, μ and ω may be determined by energy considerations. This suggestion is prompted by circuit theory : in a purely resistive network the

---

+ Davies' expression for 'd' referred to here is $\sqrt{2}$ times that of some other authors (e.g. Chalmers[6]). Davies takes $d = (2\rho/\mu\omega)^{\frac{1}{2}}$

arrangement of the branch currents is such that the power loss is a minimum. In a purely reactive network the rate of exchange of stored energy between the network and the (a.c.) supply is a minimum. The non linear field problem is much more complex; even so it is felt that some natural law governs the loss mechanism ensuring that the degree of flux penetration is such that the rate of change of energy between the armature and the pole is a minimum.

10.1.3. The Armature slot openings

For the slot harmonic terms, the theoretical representation of the harmonic m.m.f. wave as a current sheet of infinitesimal thickness on a smooth armature surface contrasts vividly with reality where conductors are located in slots extending some distance below the armature surface. The consequent disregard of flux leakage across the slot (especially if the slot wedges are well below the armature surface) will result in an overestimation of the pole face loss, for the slot harmonic terms. The effect of slot leakage on the belt harmonic loss will be less marked, and may be considered negligible when there are several slots per pole per phase.

A theoretical treatment might consider a current sheet situated in the armature body, parallel to the gap surface and some appropriate distance below the surface.

10.1.4. The contour of the pole surface

The smooth pole contour, assumed for calculation purposes, also departs markedly from that of the real machine. The present technique of multiplying the cylindrical rotor loss density by the surface area presents a simple practical solution to a complex problem. It does not account for the change in eddy current paths which arise from introducing axial slots, air ducts, or bolt holes.

Eddy current closing paths have been assumed negligibly small since the axial length/harmonic pole pitch ratio is large. Bratoljic's[18] results indicate that by neglecting the current closing paths the loss in the experimental machine is underestimated by 5% for the 5th harmonic term and underestimated by a progressively smaller amount for the higher orders. This percentage is insignificant compared to other errors incurred in the accurate prediction and measurement of the loss in practice.

10.1.5. Miscellaneous Items

Davies' summation of the air gap ampere-turns, F_ϕ, and the armature reaction, F_R, has been scrutinised by James[38] in connection with further research on eddy current couplings at the University of Aston. His findings may promote some changes in the equations for loss prediction (chapter 3) and for search coil e.m.f.s. (Appendix 12.5).

The distribution of surface e.m.f.s has been examined for the first harmonic term only. The mathematical analysis should be developed to include the vectorial summation of all the harmonic e.m.f.s. The loss density at any particular point on the pole face should take into consideration the pole profile, and the load angle.

The predicted variation of loss with secondary resistivity was not verified on the experimental machine. Further investigation is therefore necessary into this important basic machine parameter.

10.2. The Experimental Machine

10.2.1 The Slot Ripple Loss

To overcome the effect of the armature slot openings the provision of suitably designed magnetic slot wedges is strongly recommended. The average permeability of these wedges in the radial direction should match as nearly as possible that of the armature core. In the circumferential direction the permeability should be as low as possible. A resin bonded wedge made from high-μ steel wire Fig. 10.1. or from steel laminae [43] could be considered.

Several turns of high-μ wire wound on an oval former, insulated and bonded with epoxy resin, then machined to size.

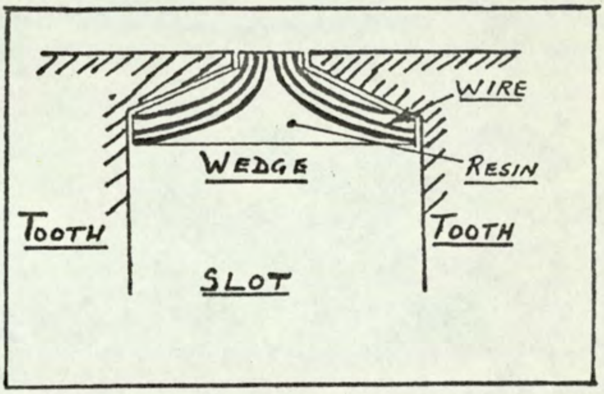

Fig. 10.1 Proposed Design for Magnetic Slot Wedge

The incorporation of magnetic slot wedges in the Aston machine will also provide experimental data on slot ripple loss. Such data would be especially useful since the Aston machine has a sinusoidal fundamental flux density distribution and is therefore more representative of a real machine than the homopolar device used elsewhere [15].

10.2.2. Pole Face Loss Distribution

The measurement of surface electromagnetic quantities could be extended to determine

(i) the induced e.m.f.s of higher order terms,

(ii) the effect on (i) of direct flux saturation

and (iii) the magnitude of the surface currents with particular regard to their closing paths.

The higher frequency e.m.f.s (which have shorter wavelengths) can be obtained by selecting pairs of search wires suitably pitched. The shorter the distance between the search wires therefore, the more noticeable will be the effects of the d.c. field. Alternatively the e.m.f. induced at a particular angle θ_2 from the pole centre could be obtained from a search coil pitched 180 fundamental electrical degrees.

10.2.3. Physical Dimensions

Both the stator bore and stack length of the experimental machine are considered suitable for a laboratory machine-set. No change in these basic dimensions is therefore proposed. However, the predicted loss variation with increase in gap length, g, awaits experimental verification. The second stator can be progressively rebored to provide this data. The gap should be increased in a logarithmic manner at first and ultimately in a manner based on further experience. A suitable progression of gap sizes might be : 0.012, 0.015, 0.019, 0.024, 0.030, 0.036, 0.043, 0.050, 0.010, 0.050, 0.10 inches. The reduction in loss predicted by the modified eddy current coupling theory is shown in Fig. 10.2. The measured results on the experimental machine should be compared with those by Richardson[35] on turbo alternators having 6 to 7½ S/P/P. For these machines the loss decreased as g^4.

The practice of cutting circumferential grooves in the poles of "lossy" machines is well established. The grooves themselves increase the effective air gap making the measurement of loss reduction due to

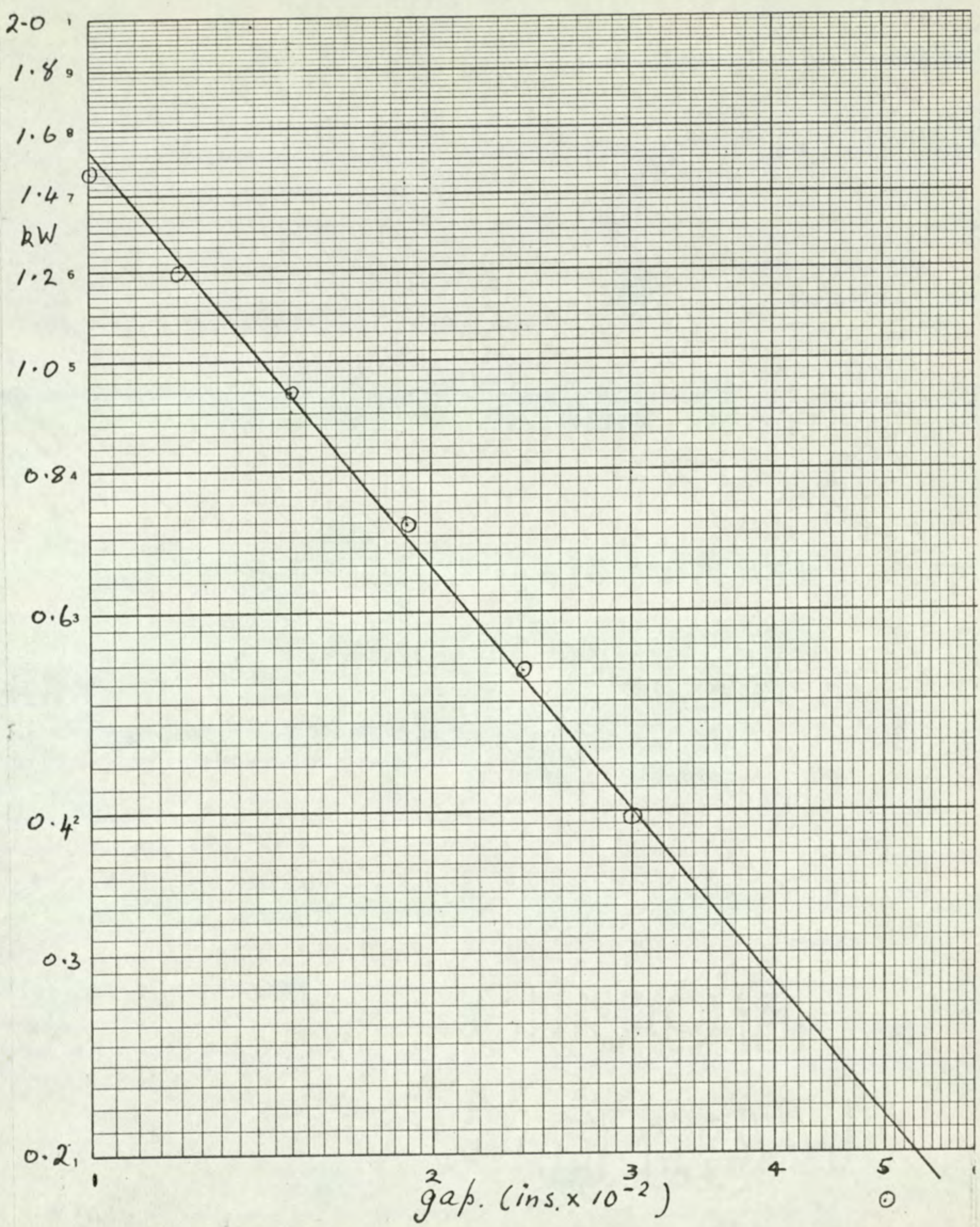

FIG 10.2 PREDICTED LOSS / GAP LENGTH

50 c/s, 25 Amp, 100°C

grooving alone more difficult. Furthermore, grooving is often accompanied by an increase in actual gap length, there being no inter-stage short circuit test measurement to enable the effectiveness of either step to be ascertained. Loss measurements on the experimental machine where the number and depth of the grooves are progressively increased should be included in future test programmes.

In a cylindrical rotor machine, a large proportion of the pole surface consists of cooling ducts and slot wedges. The current investigation is, therefore, incomplete without a theoretical and practical investigation into the effects of axial slots which should be milled in the secondary surface.

11. ACKNOWLEDGEMENTS

11. ACKNOWLEDGEMENTS

For making available considerable design and test data the author would like to thank C.A. Parsons Ltd., Witton Factory; Associated Electrical Industries Ltd., Rugby; The Central Electricity Generating Board, Bankside; and Société Alsthom, France.

The thesis represents part of a programme of research into the armature current generated component of pole face loss in turbo-alternators which is being carried out at the University of Aston under the supervision of Professor E.J. Davies. The Author is indebted to Professor Davies for his continual encouragement and guidance during the progress of the investigation; to Mr. A.L. Bowden, Mr. B. James and other colleagues of the Department of Electrical Engineering and the Department of Mathematics for helpful discussions; and to the technical staff, particularly Messrs. A.L. Stevenson, M.J. Ellett and J.T. Whittle for practical assistance.

Finally the author wishes to express his appreciation to the Department of Electrical Engineering, University of Aston, for the provision of equipment and testing facilities, and for assistance with his departmental duties.

12. APPENDICES

12 APPENDICES

12.1 WINDING FACTORS

12.1.1 The Winding Factors for the Slot Harmonic Terms

It is shown below that the pitch and distribution factors for the slot harmonic terms are numerically equal to those for the fundamental term of a 3-phase integral slot winding with 60^{o} phase belts with 'q' slots/pole/phase and a winding pitch of 's' slots. The fractional pitch is $s/3q$. For the hth harmonic term:

$$k_{ph} = \sin\frac{(hs\pi)}{6q}$$

and
$$k_{dh} = \frac{\sin(h\pi/6)}{q\ \sin(h\pi/6q)}$$

Putting h = 1, the fundamental winding factors will be:

$$k_{p_1} = \sin(s\pi/6q)$$

$$k_{d} = \frac{\sin\pi/6}{q\ \sin(\pi/6q)}$$

Putting $h = 6q \mp 1$, the pitch factor for the slot harmonic term becomes:

$$k_{p(6q \mp 1)} = \sin\{(6q \mp 1)\ \ s\pi/6q\}$$

$$= \sin\{s\pi \mp \frac{s\pi}{6q}\}$$

$$\therefore \left|k_{p(6q \mp 1)}\right| = \sin\{\frac{s\pi\}}{6q} = k_{p_1} \qquad \text{(since s is integral)}$$

Similarly the slot harmonic distribution factor becomes:

$$k_{d(6q \mp 1)} = \frac{\sin(6q \mp 1)\pi/6}{q \sin(6q \mp 1)\pi/6q}$$

$$= \frac{\sin(q\pi \mp \pi/6)}{q \sin(\pi + \pi/6q)}$$

$$\therefore \quad \left| k_{d(6q \mp 1)} \right| = \frac{\sin \pi/6}{q \sin(\pi/6q)} = k_{d1}$$

12.1.2 Slot Width Factor

The stator slot width, b, has a considerable effect on the magnitude of the high order harmonic m.m.f's. and can be accounted for by multiplying each term in the above series by a slot width factor k_{bh} which has the nature of a distribution factor. The m.m.f waveform is assumed to be constant over the width of the tooth and to vary linearly with x across the slot, giving the waveform of Fig. 12.1.1 for each coil. It can easily be shown that[1]:

$$k_{bh} = \frac{D}{bph} \cdot \sin \frac{bph}{D}$$

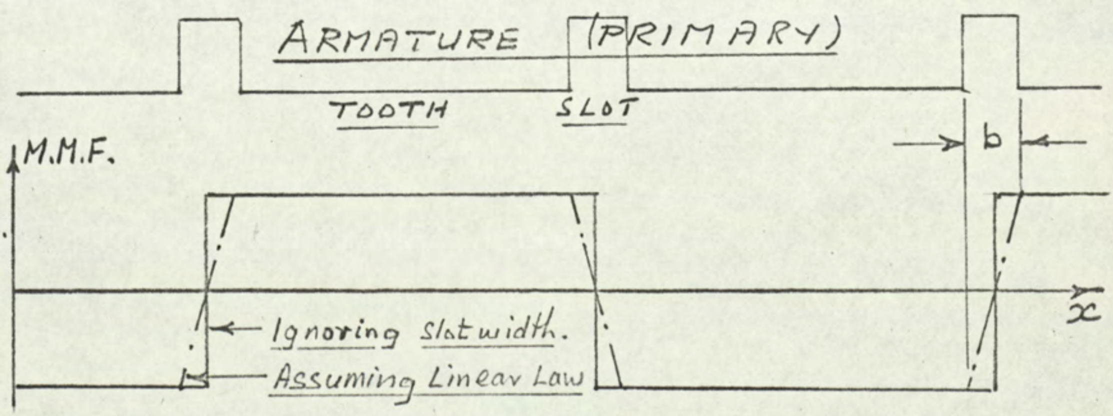

Fig. 12.1.1

The magnitude of the hth harmonic m.m.f will therefore be:

$$F_h = \frac{2.70\ (NI)}{h} \times q\ k_{bh}k_{dh}k_{ph} \quad \text{ampere turns} \quad (12.1.1.)$$

or $\quad F_h = G_o\ k_{bh}k_{dh}k_{ph}/h$

where $G_o = 2.70(NI)q$

and NI = the r.m.s. ampere-turns of a single coil

$= \frac{IZ}{2YC}$ Table 6.11

A family of slot width factor curves is plotted in Fig. 12.1.2 for discrete values of q and for one particular ratio of slot width to slot pitch.

<u>For the slot harmonic term</u>, k_{bh} is practically independent of the number of slots per pole per phase, its value being controlled mainly by the ratio of slot width to slot pitch, (b/λ_s). The above expression for k_{bh} may be expressed in terms of b/λ_s

$$b/\lambda_s = b \div \frac{D}{6qp} = \frac{6bpq}{\pi D}$$

Also to a first approximation, $h = (6q \mp 1) \rightarrow 6q$, as q increases.

i.e. $\quad b/\lambda_s \rightarrow \frac{bph}{D}$

$\therefore \quad k_{bh} \rightarrow \frac{\lambda_s}{\pi b} \cdot \sin(\frac{\pi b}{\lambda_s})$

In fact $k_{b(6q \mp 1)}$ is almost solely dependent on the ratio of slot width to slot pitch (b/λ_s). The curves of Fig. 12.1.2 all have the same basic shape and become superimposed when plotted to a base of h/q (Fig. 12.1.3). The dependency of the slot harmonic k_{bh} on parameter b/λ_s is illustrated by replotting the slot harmonic points of Fig. 12.1.3 to a base of b/λ_s (Fig. 12.1.4).

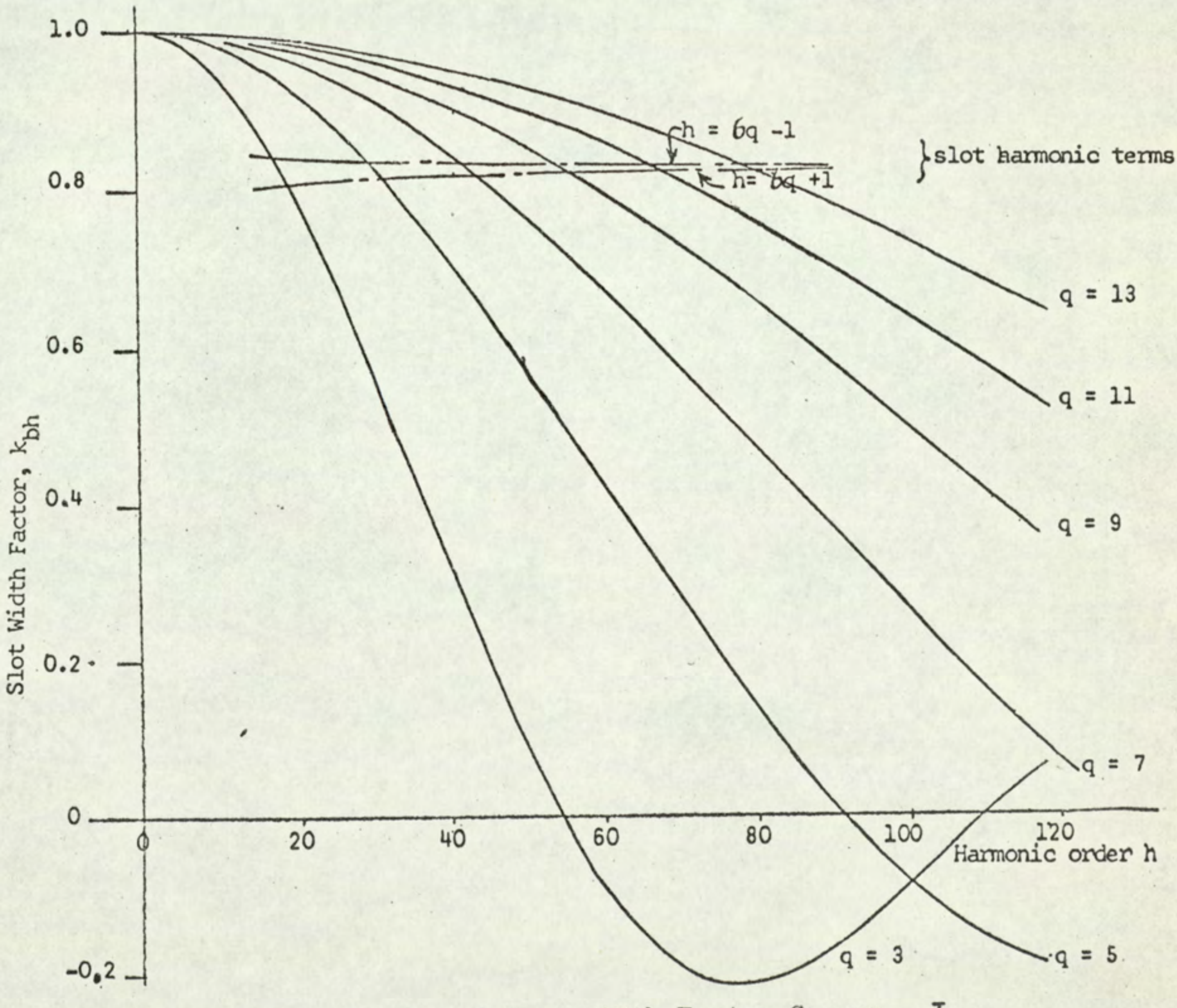

Fig. 12.1.2 Family of Slot Width Factor Curves - I

k_{bh} against harmonic order for discrete values of slots/pole/phase, q.
Slot width/slot pitch ratio, $b/\lambda_s = \frac{1}{3}$.

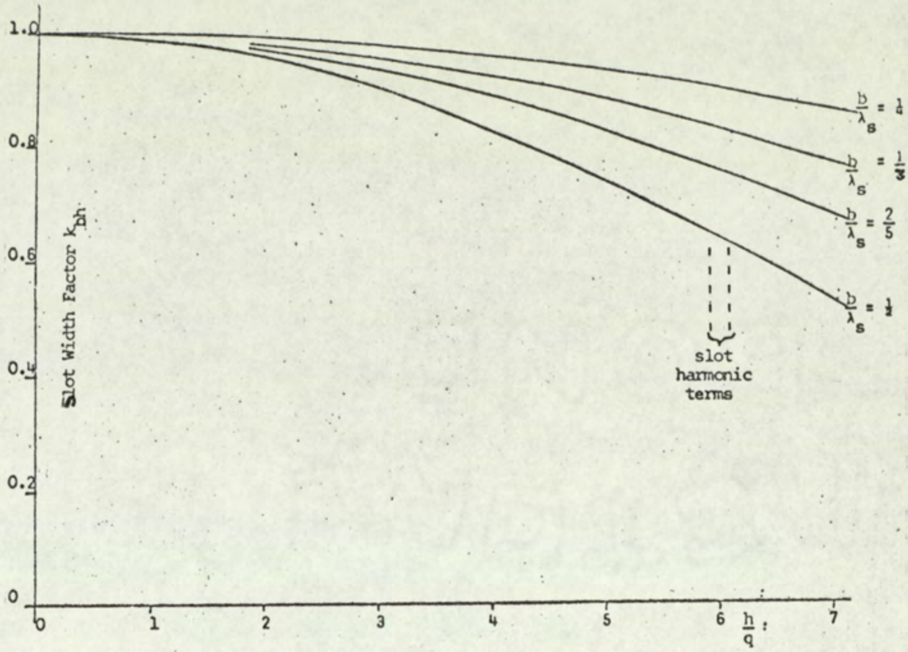

Fig. 12.1.3. Family of slot width factor curves - II

k_{bh} against harmonic order per s/p/p, $\frac{h}{q}$, for discrete values of slot width/slot pitch ratio, b/λ of an integral slot winding.
For the slot harmonic terms $h = 6q \mp 1$, i.e. $\frac{h}{q} = 6 \mp \frac{1}{q}$.

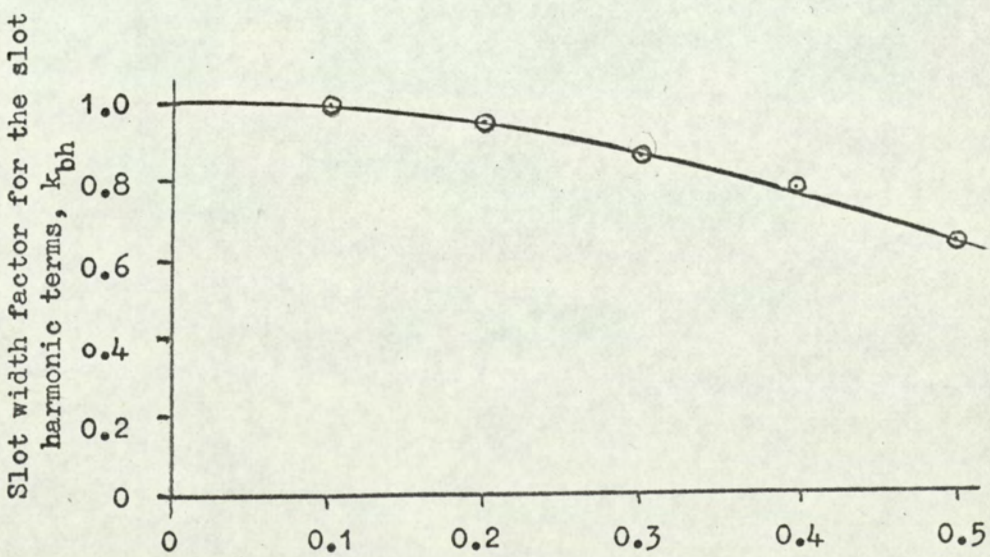

Fig. 12.1.4. The slot harmonic slot width factor.

k_{bh} against slot width/slot pitch ratio, b/λ_s, for the slot harmonic terms of an integral slot winding, $h = 6q \mp 1$.

APPENDIX 12.2 POLE FACE LOSS THEORY

12.2.1 Pole Profile

An example of a machine with a non-uniform gap is given in Fig. 12.2.1 for which the pole profile is concentric with the bore (parallel gap) from B to C and chamfered from A to B and C to D.

Further to the list of symbols given in section 1,

let w' = the computed loss figure per unit length of pole periphery

= $W_{TOT}/p\lambda_1$ watts per metre

g_1 = air gap length over potion BC

g_2 = air gap length at A and D

x = o at B, and x = a at A

and w' = w_1' over BC

Note that λ_1 = a double pole pitch

Then the loss over the chamfered section is represented by the shaded area of Fig. 12.2.1.:

$$\int_{x=b}^{x=a} w'\,dx$$

This can be determined either graphically, by computing w' for varying g, or by an approximate formula such as the one derived below. Because the loss due to m.m.f. harmonics is expected to be a comparatively small proportion of the total load loss, it is considered expedient to save computing time by using the formula thereby reducing the number of

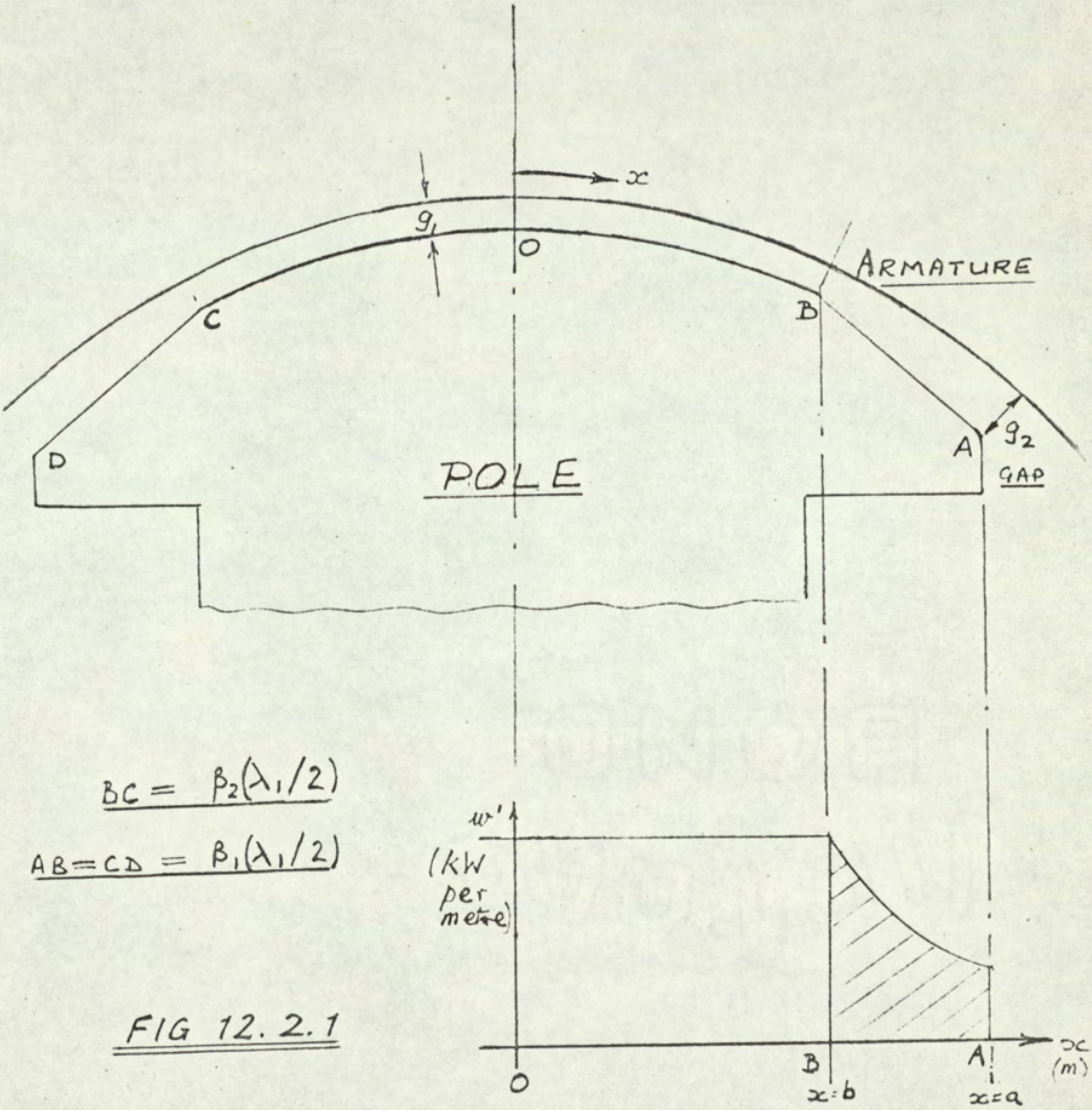

$BC = \beta_2(\lambda_1/2)$

$AB = CD = \beta_1(\lambda_1/2)$

FIG 12.2.1

computations involved to one - that for the 'parallel air gap' section. Section 3.9 states that the loss due to m.m.f harmonics is inversely proportional to $g^{(1.5 \text{ to } 3)}$, the lower index usually predominating. As a first approximation, take the loss to be inversely proportional to g

$$\text{i.e.} \quad w' = \frac{c}{g^2} \tag{12.2.1}$$

where c is a constant which may be evaluated at x = 0 from known values of w' and g,

$$\text{i.e.} \quad c = w'_1 g_1^{\ 2}$$

Ignoring the curvature of the stator iron over surface AB,

$$g = g_1 + \frac{g_2 - g_1}{a - b}(x - b) \tag{12.2.2}$$

where $a - b = AB = \frac{1}{2} \beta_1 \lambda_1$

$$\therefore \frac{dg}{dx} = (g_2 - g_1)/(a - b)$$

$$\therefore w' = \frac{w'_1 g^2{}_1}{\left(g_1 + \frac{g_2 - g_1}{a - b}(x - b)\right)^2}$$

whence the loss over the chamfered section AB $= \int_{x=b}^{x=a} w' \, dx$

$$= w' \frac{g_1}{g_2}(a - b)$$

$$= w'_1 \frac{g_1}{g_2} \cdot \frac{\beta_1 \lambda_1}{2} \qquad \left[\text{using eqn. } (12.2.2)\right]$$

$\therefore$ The loss over both chamfered sections of 2p poles

$$= 2 \times 2p \frac{g_1}{g_2} \cdot w_1' \frac{\beta_1 \lambda_1}{2} \qquad (12.2.3)$$

The loss over the parallel sections of 2p poles

$$= 2p \times BC \times w'$$

$$= 2p \times w' \beta_2 \lambda_1 / 2 \qquad (12.2.4)$$

$\therefore$ Total loss per machine

$$= p \lambda_1 w_1' \times \{ 2 \beta_1 \frac{g_1}{g_2} + \beta_2 \}$$

$$= W_{TOT} \times \{ 2 \beta_1 \frac{g_1}{g_2} + \beta_2 \} \qquad (12.2.5)$$

where W_{TOT} is the computed loss figure for a cylindrical rotor with a gap $= g_1$, and is assumed inversely proportional to g^2.

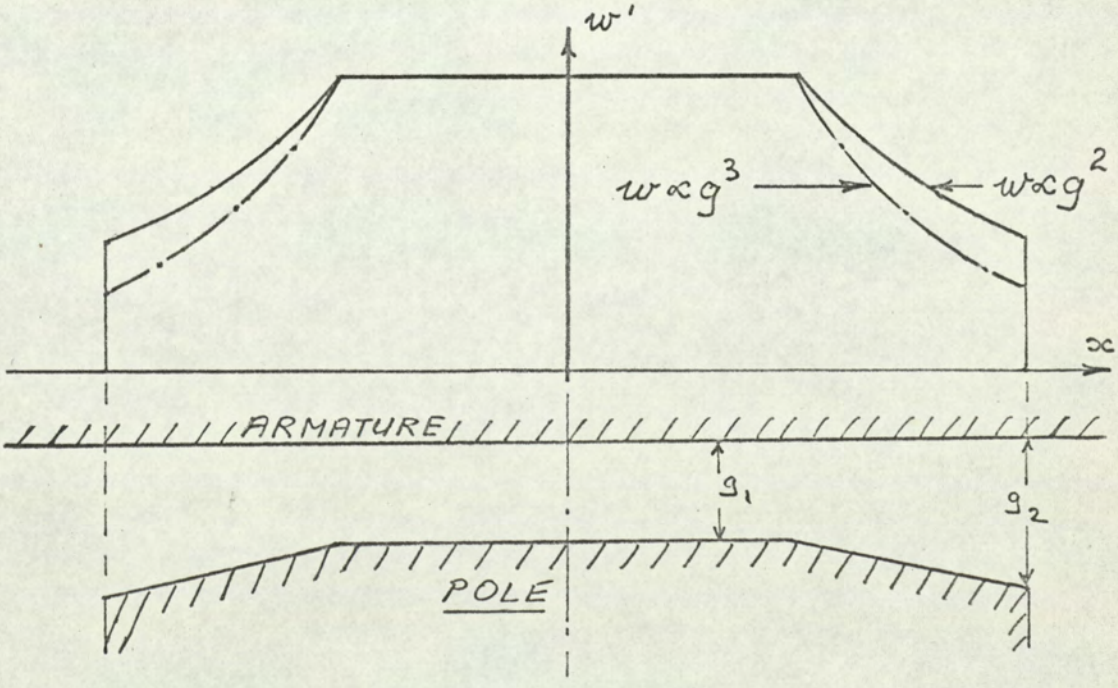

If the loss is taken to vary inversely as g^3 and the integration repeated, the loss over the chamfered periphery is given by equation 12.2.3. reduced by the ratio

$$\frac{\text{average gap over AB}}{\text{gap at pole tip}} \quad \text{or} \quad \frac{g_1 + g_2}{2g_2}$$

taking g_2/g_1 as 1.5 the reduction would be about 20% over AB, which would not affect the loss over the whole surface by more than a few percent. In view of the other assumptions made in this work, in particular the arithmetic summation of harmonic losses, equation 12.2.5. is considered suitable for practical purposes.

12.2.2. Peripheral Flux Leakage

The modified eddy current coupling theory predicts the loss when all the harmonic fluxes leaving the armature (primary member) enter the pole face (secondary member). A correction factor, K_L, accounting for flux leakage around the air gap, is now derived. The corrected loss figure is then obtained by evaluating K_L for each harmonic order, say K_{Lh}, in a given machine, and summating the products of harmonic loss power and K_L in the manner described in paragraph 3.7.

The theory is based on the equations expressed in polar co-ordinates for the flux distribution in an annular air gap space from the book by P. L. Alger.[36] The assumptions are listed below. The first, in particular, produces a pessimistic estimate of K_L, the last two being common to section 3.3.

(1) The primary and secondary members are both assumed to have infinite permeability and infinite resistivity throughout.

(2) Any core-end leakage is neglected.

(3) Excitation is by a sinusoidally distributed m.m.f. of peak value A ampere turns and p pole pairs at the primary gap surface.

Nomenclature

The following symbols are used in lieu of or in addition to those in the main text:-

suffix o refers to the primary surface, i.e. that on the diameter of the air gap

suffix i refers to the secondary surface, i.e. the inner diameter of the airgap.

ϕ = total flux at a gap/iron surface per unit length of core

R = radius of a gap/iron surface (see Fig.12.2.2)

C = a constant

a, b, r = functions of g, λ, R etc. defined below

Fig. 12.2.2

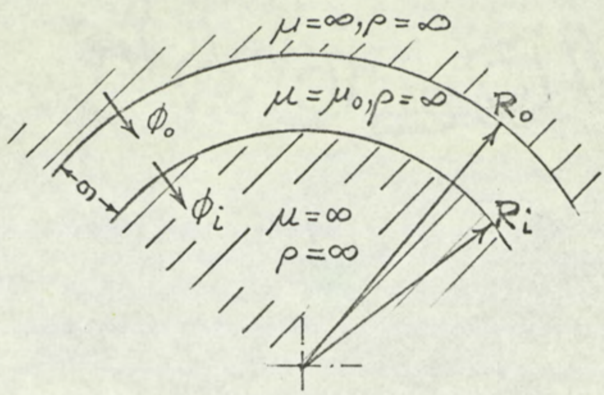

Taking B as solenoidal in the airgap and using the circuital law for H, Alger shows that the total flux leaving the primary member per unit length of core is given by his equation 7.21.B.:

$$\phi_o = \frac{CA(R_o^{2p} + R_i^{2p})}{R_o^{2p} - R_i^{2p}} \tag{12.2.6.}$$

The flux entering the secondary member is given by Alger's equation 7.29.B.

$$\phi_i = \frac{2CAR_o^{p} R_i^{p}}{R_o^{2p} - R_i^{2p}} \tag{12.2.7.}$$

The quotient of 12.2.6. and 12.2.7. gives the proportion of the total flux, which enters the rotor.

$$\frac{\phi_i}{\phi_o} = \frac{2R_o^{p} R_i^{p}}{R_o^{2p} + R_i^{2p}}$$

It is usually more convenient to express ϕ_i/ϕ_o in terms of g and D_o by substituting

$$R_i = R_o - g$$

$$\text{and} \qquad \lambda = \pi D_o/p = 2\pi R_o/p$$

to give

$$\frac{\phi_i}{\phi_o} = \frac{2R_o^{2p}(1 - g/R_o)^p}{R_o^{2p} + R_o^{2p}(1 - g/R_o)^{2p}}$$

$$= \frac{2(1 - g/R_o)^p}{1 + (1 - g/R_o)^{2p}}$$

For the hth harmonic term p becomes p_h (= h x p)

hence

$$\frac{\phi_i}{\phi_o} = \frac{2(1 - g/R_o)^{hp}}{1 + (1 - g/R_o)^{2hp}} \qquad (12.2.8)$$

This can also be expressed in terms of the gap to harmonic wavelength ratio by putting $r = g/\lambda_h$

$$= \frac{ghp}{2\pi R_o}$$

$$\text{i.e.} \qquad \frac{g}{R_o} = \frac{2\pi r}{hp}$$

As a preliminary investigation, ϕ_i/ϕ_o was calculated for a few synchronous machines having different gap/diameter ratios and plotted on Fig. 12.2.3.

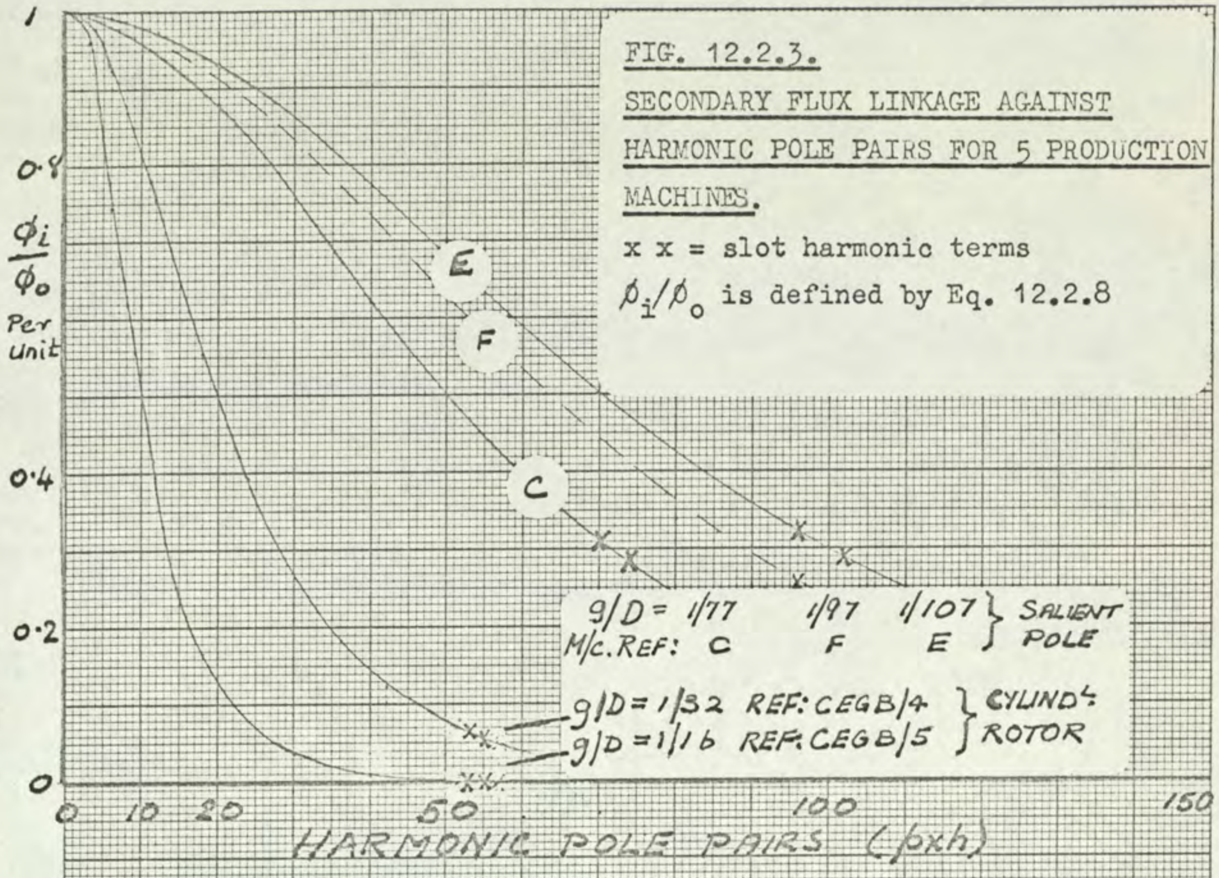

FIG. 12.2.3.

SECONDARY FLUX LINKAGE AGAINST HARMONIC POLE PAIRS FOR 5 PRODUCTION MACHINES.

x x = slot harmonic terms

ϕ_i/ϕ_o is defined by Eq. 12.2.8

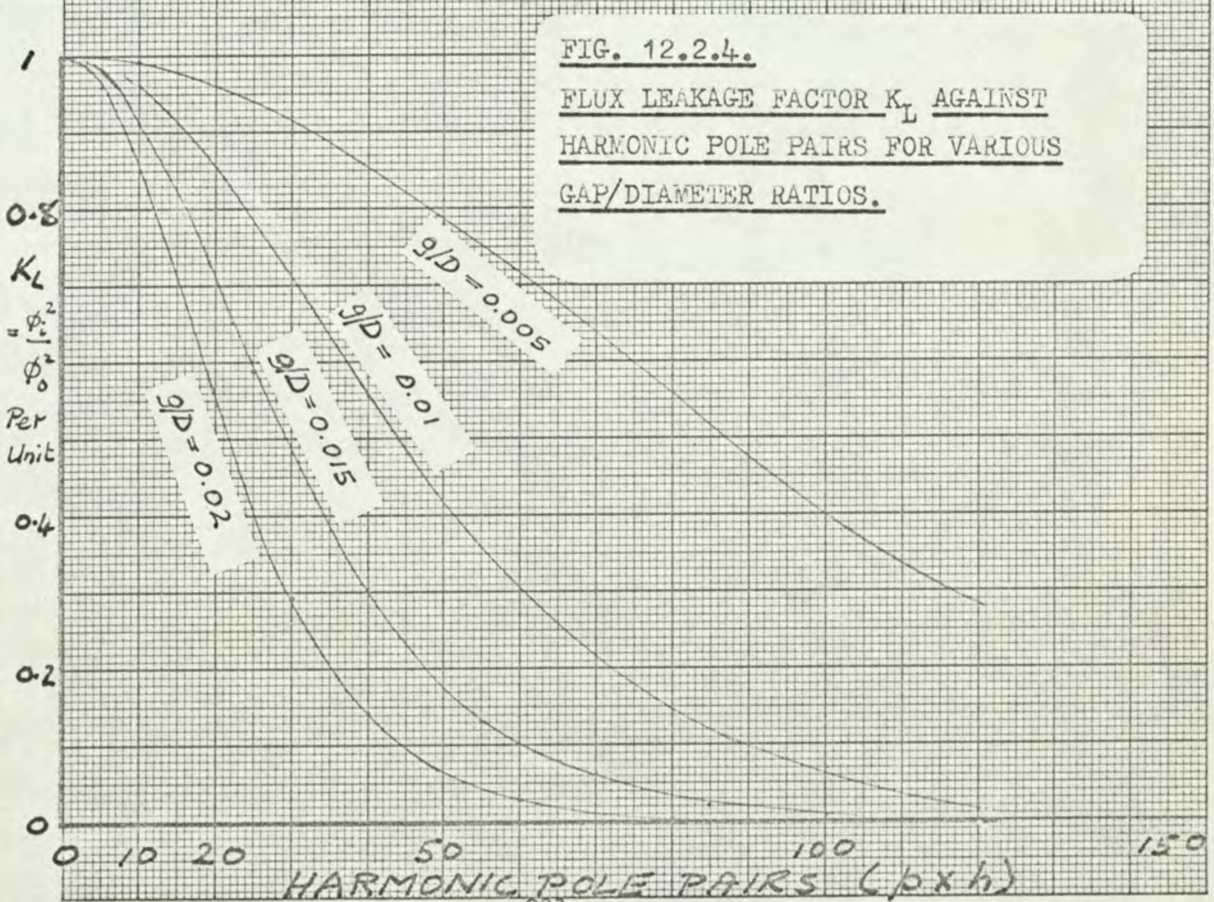

FIG. 12.2.4.

FLUX LEAKAGE FACTOR K_L AGAINST HARMONIC POLE PAIRS FOR VARIOUS GAP/DIAMETER RATIOS.

The eddy current loss W_h is usually taken to be proportional to the square of the flux density. This is discussed in section 6.3.1 with reference to the eddy current coupling theory.

Putting $W_h \propto \phi^s$, the loss reduction factor is defined as:

$$K_L = \frac{\text{actual loss for harmonic order h}}{\text{calculated loss assuming no leakage flux, order h}}$$

$$= \frac{K_L W_h}{W_h}$$

Taking $K_L W_h \propto \phi_i^s$ and $W_h \propto \phi_o^s$, we get:

$$K_L = (\phi_i/\phi_o)^s \quad \text{where s is to be specified}$$

For reasons given in section 6.3.1 (iii), the value of s for the family of K_L curves in Fig. 12.2.4 is 2.

Appendix 12.3 The Computer Programmes

The first programme to calculate the m.m.f. harmonic loss in a smooth cylindrical rotor was written in Elliott Autocode using the magnetisation parameters k_1 and m evaluated for ingot iron. The print-out format and method of calculation were improved in stages (see Tables 6.3 to 6.9, section 6.3.1), programme 8 being the final version.

A change of magnetisation parameters to those of the experimental machine alters the arithmetical values of various multipliers in the first section. This requirement has been met (a) in the autocode programmes by re-writing the programme and reading in points on a hand-calculated normalised curve, (b) in the Algol programme by reading k_1 and m as preliminary data and computing the normalised curve applicable to the particular pole steel. Two of the programmes are included by way of illustration, namely MS-1L, and FS-4M. Block flow diagrams for these and for AL-1 are shown in Figs. 12.3.1., 12.3.2., and 12.3.3. The requisite normalised torque is obtained by linear interpolation between points on the stored normalised curve.

Programme Reference Numbers:

MS-1L indicates the "long" version of the mild steel programme in inch units corresponding to programme 8 for ingot iron, in Elliott Autocode. Most intermediate steps are printed using Punches 1 and 2 if parameter A13 < 0.

If A13 > 0, Punch 2 is not called.

MS-1 indicates the "short" version of MS-1L where all terms are computed but only the significant terms are printed, i.e. those for which W_h > 1% of ΣW_h — see next programme Fig. 12.3.2.

FS-4M indicates the "short" fractional slot programme in m.m. units, where the fraction is always $\frac{1}{2}$, corresponding to programme MS-1 for integral slot windings. In addition, FS-4M prints the fundamental winding factors.

AL-1 indicates the first version of the Algol programme in inch units for integral slot windings.

The data sheets for the autocode programmes are given in sections 3.7.1 and 6.3.2; that for the Algol programme precedes Fig. 12.3.3. In some programmes, the constants, G_o, G_1, & G_2 are titled CF, CT and CN since they occur in the equations for m.m.f. normalised torque and normalised speed respectively.

$ signifies "less than"

and % signifies "greater than".

Other principal symbols are included on the data sheets alongside each programme.

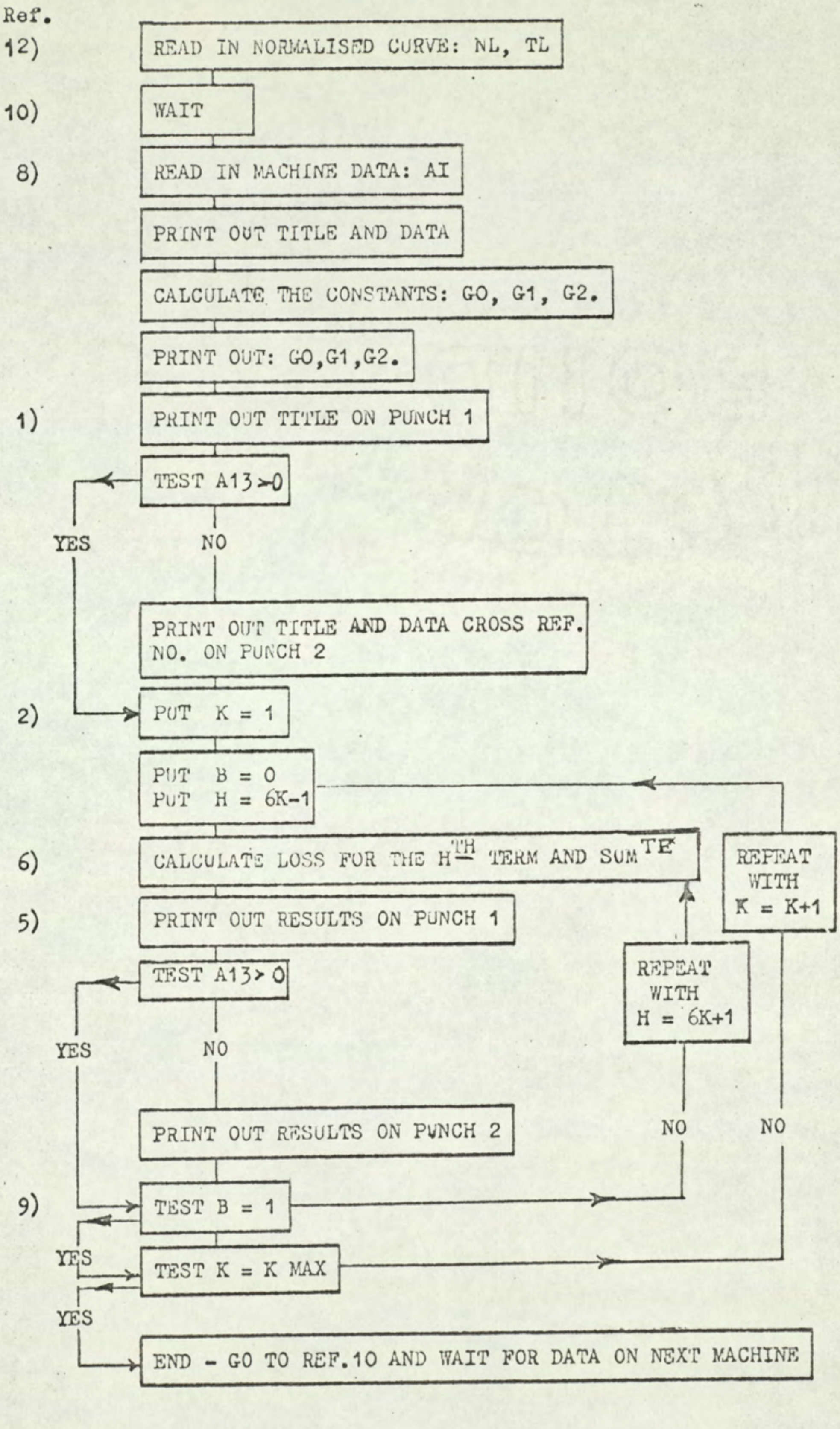

Fig. 12.3.1. Block Flow Diagram for Programme No. MS-1L

<u>PROGRAMME NO. MS-1L.</u>

```
::        PROGRAMME NO MS-1L 20/10/65
::      LOSS DUE TO HARMONICS IN MMF WAVEFORM
SETV A(16)C(4)DH(1)KP(12)ZN(30)T(30)E
SETS BIJLM
SETF TRIG PUNCH LOG EXP INT
SETR:12
12)SUBR:3
10)WAIT
PUNCH 1
LINES 10
8)VARY I=0:1:17
READ AI
REPEAT I
TITLE
                    LOSS DUE TO HARMONICS IN MMF WAVEFORM  PROG MS-1L

PROGRAMME ACCOUNTS FOR SLOT WIDTH AND PRINTS ALL TERMS

  PPRS      NS       Z       Y       C       I     A13  KMAX    REF
LINE
VARY I=0:1:6
PRINT AI,4
REPEAT I
PRINT A13,2
PRINT A14,2
PRINT A16,6
LINE
TITLE
 S/P/P   PITCH    SPREAD     D        G        L       RHO    SLOT
LINE
VARY I=6:1:7
PRINT AI,5
REPEAT I
PRINT A15
LINE
A14=A14+.1
J=INT A14
P11=0
A15=0.0254*A15
```

Continued. . .

```
A9=0.0254*A9
A10=0.0254*A10
A11=0.0254*A11
Z=A2*A5
Z=Z/A3
Z=Z/A4
C0=1.35*Z
C0=A6*C0
C1=A0*A9
C1=C1*A11
C1=C1*4.08
C1=C1/A10
C1=C1/10000000
C3=LOG A9
C3=C3*3.176
C3=EXP C3
C4=LOG A0
C4=2.176*C4
C4=EXP C4
C2=C4/C3
C2=A10*C2
C2=A10*C2
C2=A12*C2
C2=318000*C2
TITLE
   CF            CT            CN
LINE
VARY I=0:1:3
PRINT CI,5/
REPEAT I
LINE
1)TITLE
 K      H     KPH        KDH        KBH     T/TM    N/NM      KW   KW TOT
JUMP IF A13%0@2
PUNCH 2
LINES 5
PRINT A16,6
TITLE
 H      FH         FH9         TM          N       NM        T
2)VARY K=1:1:J
```

Continued. . .

```
B=0
H=6*K
H=H-1
6)P=H*A7
P=P/2
P=SIN P
D=A8/A6
D=D/360
D=H*D
P1=SIN D
P1=P1*A6
D=D*A6
D=SIN D
P1=D/P1
P12=2*A10
P12=A9+P12
D=A*H
D=D*A15
D=D/P12
P12=D/3.14159
P12=SIN P12
P12=P12/D
P12=MOD P12
P=MOD P
P1=MOD P1
P2=C0*P0
P2=P2*P1
P2=P2*P12
P2=P2/H
P2=MOD P2
P3=LOG P2
P3=P3*0.824
P3=EXP P3
P4=C1*H
P4=P4*P2
P4=P4*P2
P5=6*K
P5=P5*A1
P5=P5/H
```

```
D=LOG H
D=D*2.176
D=EXP D
D=D*C2
P6=D/P3
P7=P5/P6
SUBR:4
5)PUNCH 1
LINE
PRINT K,2
PRINT H,3
PRINT P,5
PRINT P1,5
PRINT P12,5
PRINT P8,3
PRINT P7,3
PRINT P10,4
PRINT P11,4
JUMP IF A13%0@9
PUNCH 2
LINE
PRINT H,3
VARY I=2:1:3
PRINT PI,3/
REPEAT I
PRINT P5,4
PRINT P6,3/
PRINT P9,3/
9)JUMP IF B=1@7
B=1
H=H+2
JUMP @6
7)
CHECK K
REPEAT K
LINE
JUMP @10
STOP
3)VARY L=0:1:24
READ NL
READ TL
CHECK N
CHECK T
REPEAT L
EXIT
```

```
4)VARY M=1:1:31
JUMP IF P7$N(M)@11
REPEAT M
11)E=N(M)-N(M-1)
P8=T(M)-T(M-1)
P8=P8/E
E=P7-N(M-1)
P8=P8*E
P8=P8+T(M-1)
P9=P8*P4
P10=P9*P5
P10=P10*0.0001047
P11=P11+P10
E=P10/P11
EXIT
START 12

0 0
0.0026 0.0337
0.0185 0.159
0.0425 0.297
0.067 0.418
0.102 0.515
0.174 0.678
0.257 0.790
0.352 0.875
0.459 0.927
0.577 0.965
0.707 0.985
0.849 0.995
1.000 1.000
1.34 0.991
3.52 0.855
4.70 0.790
6.59 0.719
11.2 0.605
16.5 0.520
23.9 0.451
41.6 0.358
104 0.296
15200 0.0034
```

Normalised Curve

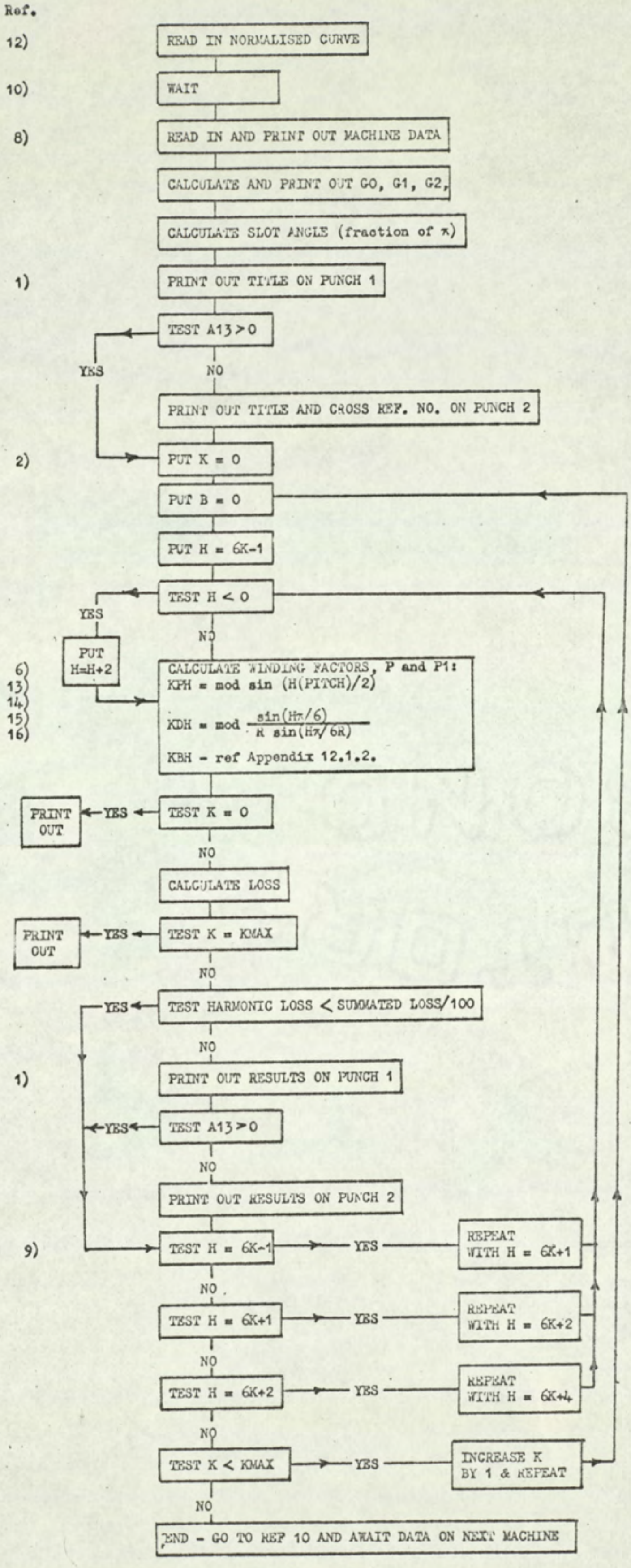

Fig. 12.3.2 Block-flow Diagram for Programme No. FS-4M

```
::            PROGRAMME NO. FS-4M 29/6/66
::      LOSS DUE TO HARMONICS IN MMF WAVEFORM OF 3PH FRACT SLOT WDGS
::      SUB-HARMONICS NOT COMPUTED                R/2 S/P/P
::      KBH AND KW PRINTED FOR EACH HARMONIC IFKW EXCEEDS 0.01KWTOT
SETV A(16)C(4)DH(1)KP(12)ZN(30)T(30)EF
SETS BIJLMQ
SETF TRIG PUNCH LOG EXP INT
SETR 16
12)SUBR 3
10)WAIT
PUNCH 1
LINES 10
VARY I=0:1:17
READ AI
REPEAT I
TITLE
            LOSS DUE TO HARMONICS IN MMF WAVEFORM
                                                      PROGRAMME FS-4M
PRINTS IF KW EXCEEDS 0.01KWTOT                        R/2 S/P/P

    PPRS      NS       Z       Y       C       I       A13  KMAX  REF
LINE
VARY I=0:1:6
PRINT AI,4
REPEAT I
PRINT A13,2
PRINT A14,2
PRINT A16,6
LINE
TITLE
 S/P/P       S/P/P   PITCH
  NUM        DENOM   P.U.     D        G        L        RHO      SLOT
LINE
VARY I=6:1:7
PRINT AI,5
REPEAT I
PRINT A15
LINE
A14=A14+1.1
J=INT A14
P11=0
A9=0.001*A9
A10=0.001*A10
A11=0.001*A11
A15=0.001*A15
Z=A2*A5
Z=Z/A3
Z=Z/A4


C0=1.35*Z
C0=A6*C0
C0=C0/A7
C1=A0*A9
C1=C1*A11
C1=C1*4.08
C1=C1/A10
C1=C1/10000000
C3=LOG A9
C3=C3*3.18
C3=EXP C3
C4=LOG A0
C4=C4*2.18
C4=EXP C4
C2=C4/C3
C2=A10*C2
C2=A10*C2
C2=A12*C2
C2=C2*318000
C3=3*A6
C3=C3+1
C4=C3/6
C3=C4/A6
```


Continued. . .

```
TITLE
   CF              CT              CN
LINE
VARY I=0:1:3
PRINT CI,5/
REPEAT I
LINE
TITLE
 K      H           KPH          KDH          KBH     T/TM   N/NM      KW      KW TOT
JUMP IF A13%0@2
PUNCH 2
PRINT A16,6
TITLE
 H        FH                FH9            TM             N              NM            T

2)VARY K=0:1:J
B=0
P5=6*K
H=P5-1
JUMP IF H$0@9
6)P=H*A8
P=P/2
P=SIN P
P=MOD P
P1=H*C4
13)JUMP IF P1$2@14
P1=P1-2
JUMP @13
14)P1=COS P1
D=H*C3
15)JUMP IF D$2@16
D=D-2
JUMP @15
16)D=COS D
D=D*A6
P1=P1/D
P1=MOD P1
P12=2*A10
P12=A9+P12
D=A*H
D=D*A15
D=D/P12
P12=D/3.14159
P12=SIN P12
P12=P12/D
P12=MOD P12
P2=C0*P0
P2=P2*P1
P2=P2*P12
P2=P2/H
P2=MOD P2
P3=LOG P2
P3=P3*0.824
P3=EXP P3
P4=C1*H
P4=P4*P2
P4=P4*P2
JUMP IF P5$0.5@1
P5=P5*A1
P5=P5/H
D=LOG H
D=D*2.18
D=EXP D
D=D*C2
P6=D/P3
P7=P5/P6
SUBR 4
F=K+0.1
Q=INT F
JUMP IF Q=J@1
JUMP IF E$0.01@9
```

```
1)PUNCH 1
LINE
PRINT K,2
PRINT H,3
PRINT P,5
PRINT P1,5
PRINT P12,5
PRINT P8,3
PRINT P7,3
PRINT P10,4
PRINT P11,4
JUMP IF A13%0@9
PUNCH 2
LINE
PRINT H,3
VARY I=2:1:3
PRINT PI,3/
REPEAT I
PRINT P5,4
PRINT P6,3/
PRINT P9,3/
9)JUMP IF B%0@5
B=1
H=H+2
P5=H-1
JUMP @6
5)JUMP IF B%1@8
B=2
H=H+1
P5=H+1
JUMP @6
8)JUMP IF B%2@7
B=3
H=H+2
P5=H-1
JUMP @6
7)REPEAT K
LINE
JUMP @10
STOP
3)VARY L=0:1:30
READ NL
READ TL
REPEAT L
EXIT
4)VARY M=1:1:24
JUMP IF P7$N(M)@11
REPEAT M
11)E=N(M)-N(M-1)
P8=T(M)-T(M-1)
P8=P8/E
E=P7-N(M-1)
P8=P8*E
P8=P8+T(M-1)
P9=P8*P4
P10=P9*P5
P10=P10*0.0001047
P11=P11+P10
E=P10/P11
EXIT
START 12
```

0	0
0.0026	0.0337
0.0185	0.159
0.0425	0.297
0.067	0.418
0.102	0.515
0.174	0.678
0.257	0.790
0.352	0.875
0.459	0.927
0.577	0.965
0.707	0.985
0.849	0.995
1.000	1.000
1.34	0.991
3.52	0.855
4.70	0.790
6.59	0.719
11.2	0.605
16.5	0.520
23.9	0.451
41.6	0.358
104	0.296
15200	-0.0034

Normalised Curve

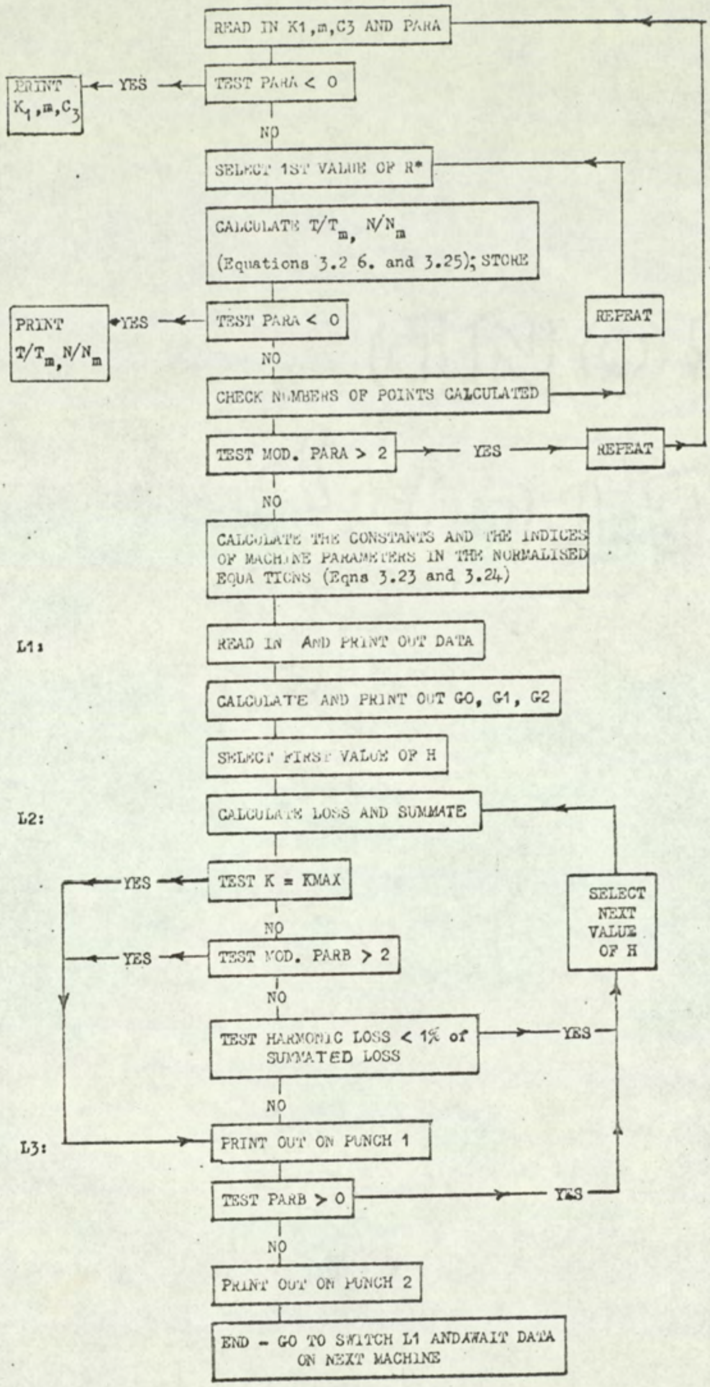

Footnotes

* The symbol "R" is used for "Q" in equations 3.25 and 3.26 to avoid confusion with the slots/pole/phase. "q".

@ By means of parameter A, several normalised curves can be calculated and printed out in succession, but the last (by putting $-2 < \text{PARA} < 2$) will be stored and used in the loss calculation.

Fig. 12.3.3. Block Flow Diagram for Programme No. AL-1

LAYOUT OF DATA SHEET FOR ALGOL PROGRAMME AL-1

Pole Face Loss due to m.m.f. Harmonics

Machine Reference No.

	K1	magnetisation curve
	M	parameters
	C	theoretical constant C_3
	PARA	parameter A
A0	P	pole pairs
A1	NS	synchronous speed (r.p.m.)
A2	U	conductors/slot
A3	Y	parallel paths/coil side
A4	C	parallel paths/phase
A5	I	total phase current (amp)
A6	Q	slots/pole/phase
	S	coil span (slots)
A15	B	slot width (ins.)
A9	D	rotor diameter (ins.)
A10	GAP	effective air gap (ins.)
A11	L	rotor length (ins.)
A12	RHO	pole shoe resistivity ($\mu\Omega$- cm)
A73	PARB	parameter B
A14	KMAX	highest K-term required
A16	REF	cross reference no.

The symbols used in the autocode programme are given in the first column.

The symbols used in the Algol programme are given in the second column.

If parameter $A < 0$, K1, m and C3 T/T_m, N/T_m are printed.

If modulus of parameter $A > 2$, then only normalised curves can be computed.

If modulus of parameter $B < 2$, the programme prints only those terms for which the harmonic loss exceeds 1% of the summated loss.

If parameter $B > 0$, punch 1 only is called.

If parameter $B < 0$, punches 1 and 2 are called.

Appendix 12.4. The Calculation of Primary Iron Loss in the Experimental Synchronous Load Loss Dynamometer

The primary iron loss is calculated for rated line voltage from the manufacturer's loss curves for the year of purchase. Design details are given in Fig. 12.4.1.

Assuming a 2% volt drop across the primary impedance the flux per pole is given by

$$0.98V = \sqrt{3} \times 4.44 \times (\text{cond/slot} \times s/p/p \times p)\ f\phi k_p k_d$$

$$\therefore \phi = \frac{210 \times 0.98}{\sqrt{3} \times 4.44 \times 8 \times 2 \times 50 \times 1 \times 1} = 33.4 \text{ mWb}$$

Assuming a stacking factor of 0.94,

the core length = 0.25 x 0.94 = 0.235 m

Since the machine has 3 kidney ducts and 4 poles, the inner core diameter is taken as the outer duct diameter = 129 mm

Root tooth diameter = 290 - 0.6 - (2 x 26) = 237.4 mm

Mean core diameter = 237.4 - 108.4/2 = 183 mm

$\therefore$ Core area $= 10^{-3}(237.4 - 129)\frac{1}{2} \times 0.235$

$= 127 \times 10^{-4}\ m^2$

Assuming core flux $= 100\%$ of $\phi \div 2 = 16.7$ mWb

$B_c = 33.4 \times 10^{-3} \times 10^4/254 = 1.315$ Wb/m

Assuming iron density = 7.78 gm/c.c.

$$\text{Core weight} = \frac{183\pi \times 54.2 \times 235 \times 7.78}{10^3 \times 10^3}$$

= 56.7 Kg.

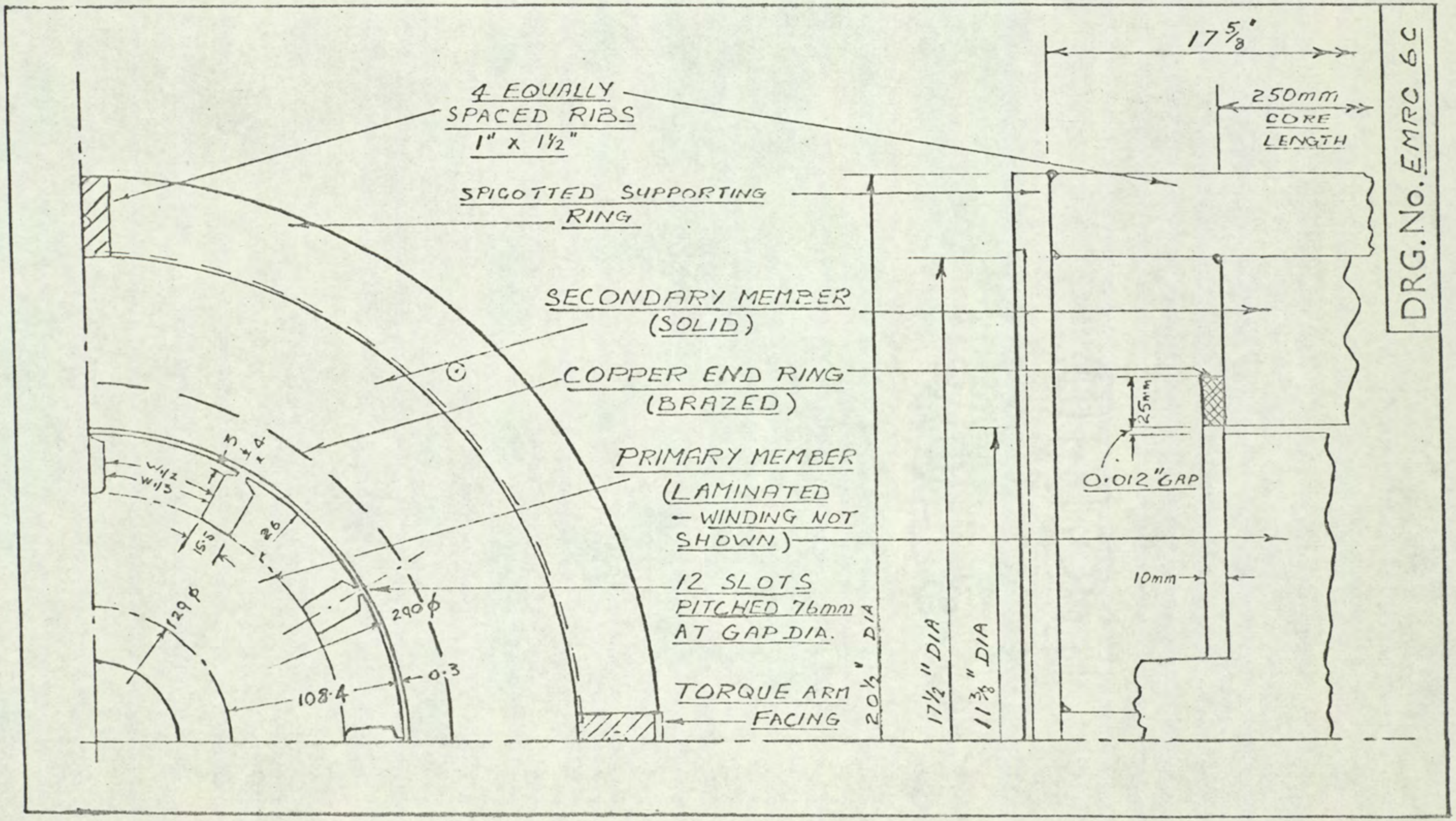
DRG. No. EMRC 6C
17 5/8"
250mm CORE LENGTH
4 EQUALLY SPACED RIBS 1" x 1½"
SPIGOTTED SUPPORTING RING
SECONDARY MEMBER (SOLID)
COPPER END RING (BRAZED)
PRIMARY MEMBER (LAMINATED — WINDING NOT SHOWN)
12 SLOTS PITCHED 76mm AT GAP DIA.
TORQUE ARM FACING
0·012" GAP
25mm
10mm
20½" DIA
17½" DIA
11 3/8" DIA
290 ϕ
129 ϕ
108·4
0·3
26
15·5
W.12
W.13

FIG. 12.4.1.

Diameter at $w_{1/3}$ $= 290 - 0.6 - 0.026 \times \frac{4}{3} = 255$ mm

$\therefore \quad w_{1/3} = \frac{\pi \times 255}{12} - 15.5 = 51.2$ mm

$\therefore$ Tooth area $= 51.2 \times 3 \times 235 \times 10^{-6} = 361 \times 10^{-4} m^2$

Assuming tooth flux $= 98.5\%$ of ϕ,

$$B_{t.mean} = \frac{0.985 \times 33.4 \times 10^{-3}}{361 \times 10^{-4}} = 0.912 \text{ Wb/m}$$

$$\therefore \quad B_{t.max} = \frac{\pi}{2} \times B_{t.mean} = 1.433 \text{ Wb/m}$$

$$W_{\frac{1}{2}} = \frac{\pi \times 263.4}{12} - 15.5 = 53.4 \text{ mm}$$

$$\therefore \text{ Wt. of teeth} = \frac{12 \times 26 \times 235 \times 53.4 \times 7.78}{10^3 \times 10^3}$$

$$= 30.5 \text{ Kg.}$$

The core loss is taken as

2.1 x value from manufacturer's curves at

$B = \phi/\text{core area}$

and the tooth loss as

1.25 x value from manufacturer's curves at

$$B = \frac{\pi}{2} \times \frac{\phi}{\text{tooth area at 1/3 point}}$$

From the manufacturer's curves, the loss at 50 c/s is:

4.9 W/Kg when $B = 1.315$ Wb/m^2

5.8 W/Kg when $B = 1.433$ Wb/m^2

$\therefore$ Core loss $= 2.1 \times 56.7 \times 4.9 = 580$

and tooth loss $= 1.25 \times 30.5 \times 5.8 = \underline{220}$

$\therefore$ Calculated primary iron loss = $\underline{800 \text{ Watts}}$

Compare this with the measured value:

Taking the gap flux as 98.5% of

$$B_{mean} = \frac{0.985 \times 33.4 \times 10^{-3}}{0.25 \times 0.228}$$

$$= 0.58 \text{ Wb/m}^2$$

From Fig. 5.25, the measured primary iron loss = 750 watts

Appendix 12.5. The E.M.F. Distribution Across the Pole Face

It is shown in sections 2.3., 7.3., and 12.6. that the alternating e.m.f's. induced in the secondary surface vary circumferentially. In this appendix, an expression for any harmonic component of the e.m.f. induced in a secondary surface search coil is derived from Faraday's law. The e.m.f., which has components caused by the m.m.f. harmonics and the primary slot openings, is expressed in terms of the harmonic flux densities. Whilst these are not predicted theoretically, the derived expressions are used in the analysis of the test results obtained in chapter 7.

12.5.1. The General Case

Consider any search coil on the secondary surface such as DE in Fig. 7.3., section 7.

Let e_h = the e.m.f. induced in DE by the hth harmonic of the primary m.m.f. wave, F_h

where F_h is defined by equation 3.1

Let h = $6K - 1$, the lower order of each pair of terms

B_h = maximum surface value of flux density for the hth m.m.f. harmonic (= B_{y0} at $y = 0$)

Let $\not{y}\pi$ = π/h_1 = the pitch of DE in electrical radians

and θ_2 = the displacement of search coil axis from the m.m.f. direct axis.

Then DE is full-pitched for the harmonic term order h_1 and the $6K + 1$ harmonic orders are designated $h + 2$.

The induced e.m.f. depends on the time rate of change of the surface flux density and this in turn is related to F_h by Fig. 12.5.1.

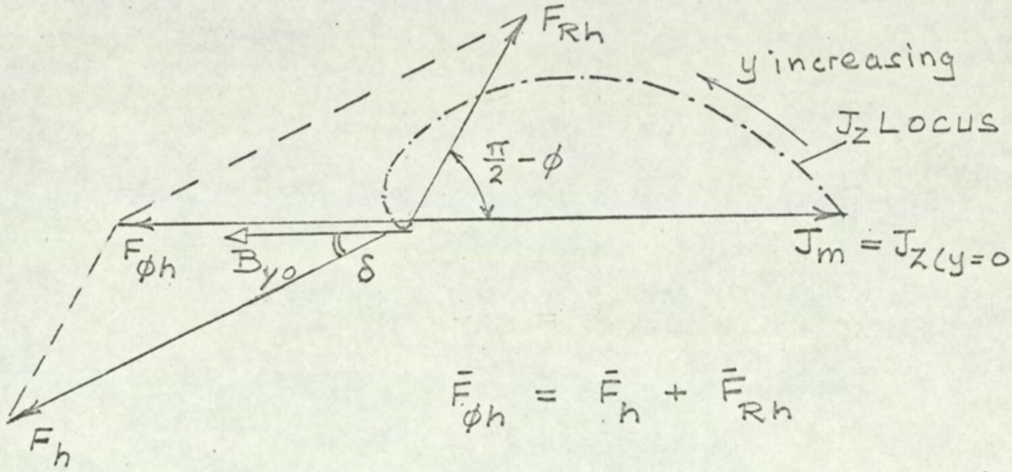

Fig. 12.5.1. Values of Electromagnetic Quantities in the Secondary

The surface current density J_m, given by equation 3.3. is taken as reference vector and the locus of J_z with depth is shown dotted. J_z leads J_m by αy radians and decreases exponentially with y.

The eddy current reaction m.m.f., expressed in section 3.6.3., leads J_m by the angle $\pi/2 - \phi$. In the linear theory[3] $\phi \rightarrow \pi/4$, but in the non-linear[38] ϕ is about half this value. In this work ϕ is not evaluated but assumed to have the same value for those harmonic terms which induce identical frequencies in the secondary.

The flux density distribution at the secondary surface which has to be provided to cause the assumed J_z distribution is derived from equation (6) of reference 3 viz:

$$H_y = -(\pi/\lambda\alpha^2)\, J_m e^{-\alpha y} \cos\,(\omega t - 2\pi x/\lambda - \alpha y)$$

$$= -\pi J_z/\lambda\alpha^2$$

$$B_y = \mu_r \mu_o H_y$$

$$= \frac{-2\pi}{\lambda} \cdot \frac{\rho J_z}{\omega} \quad .. \quad .. \quad .. \quad .. \qquad (12.5.1.)$$

i.e. at all points in the secondary, B_y is independent of μ and α and is in antiphase with J_z. B_{yo} is now drawn leading J_m by π and F_ϕ drawn in phase with B_{yo}.

The inducing m.m.f.,

$$F_h = F_\phi - F_R$$

leads B_{yo} by some angle δ, which is assumed constant for a particular induced frequency. Using the nomenclature of equation 7.1., we can write the instantaneous value of general term in the Fourier series of the B-wave at the secondary surface:

$$B_{h(inst)} = B_h \cos\,(h\theta_2 + 6K\omega_1 t + \delta) \qquad (12.5.2)$$

Integrating $B_{h(inst)}$ over the search coil area we get the flux linkage wave:

$$\Phi_h = \int_{\theta_2 - \psi\pi/2}^{\theta_2 + \psi\pi/2} B_{h(inst)} \frac{LD}{2p} \, d\theta_2$$

the search coil area being $L \times \frac{D}{2} \cdot \frac{\psi\pi}{p}$ for a machine with p pole pairs,

putting $\gamma = 6K\omega_1 t + \delta$

$$\Phi_h = \frac{LDB_h}{2hp} \Big[\sin (h\theta_2 + \gamma) \Big]_{\theta_2 - \pi/2h_1}^{\theta_2 + \pi/2h_1}$$

$$= \frac{LD}{2hp} B_h \left(\sin(h\theta_2 + \frac{h\pi}{2h} + \gamma) - \sin(h\theta_2 - \frac{h\pi}{2h_1} + \gamma) \right)$$

which reduces to

$$\Phi_h = \frac{LD}{hp} B_h \sin \frac{h\pi}{2h} \sin (h\theta_2 + 6K\omega_1 t + \delta)$$

$$\therefore e_h = d\Phi_h / dt$$

$$\therefore e_h = \frac{-6k\omega_1 LD}{hp} B_h \sin\frac{h\pi}{2h} \sin(h\theta_2 + 6K\omega_1 t + \delta) \text{ volts}$$

leaving aside the slot ripple e.m.f. for the moment, let us sum each pair of e.m.f's. having a common 'K' assuming:

$$\delta_{6K+1} = \delta_{6K-1}$$

and $B_h \propto F_h$ for a given pair of terms

i.e. $$\frac{F_{6K+1}}{F_{6K-1}} = \frac{B_{6K+1}}{B_{6K-1}} = \frac{6K-1}{6K+1} \times \frac{k_{w(6K+1)}}{k_{w(6K-1)}} = C_4$$

i.e. $$B_{6K+1} = C_4 \, B_{6K-1} \qquad \text{.. .. (12.5.4.)}$$

Note that the sign of C_4 may be positive or negative.

In this appendix, the subscript 'h' refers to the lowest order of any pair of terms. We can therefore write:

$$B_{h+2} = C_4 \, B_h$$

Hence

$$e_h = -\frac{6K\omega_1 LD}{hp} B_h \sin\frac{h\pi}{2h_1} \sin(h\theta_2 + \gamma) \qquad (12.5.5.)$$

$$e_{h+2} = \frac{-6K\omega_1 LD}{h+2} C_4 B_h \sin\frac{h+2}{2h_1} \sin(2\theta_2 + h\theta_2 + \gamma)$$

where $\gamma = 6K\omega_1 t + \delta$

These equations indicate that for the Kth pair of terms e_{h+2} leads e_h in time phase by $2\theta_2$ providing their winding factors have the same sign.

They may now be added together to give the total e.m.f. in a given search coil fully pitched for the harmonic order h_1. The summation is performed in the next section.

12.5.2. The 300c/s Induced E.M.F's. in the Experimental Load Loss Dynamometer

In this section, the e.m.f's. induced in two secondary search coils are evaluated. The subscript nomenclature is:

The first figure refers to the harmonic order for which the coil is full-pitched

and the second figure refers to the harmonic order of the inducing field.

e.g. For search coil No. 53 which is pitched $\pi/5$ radians (Elec), the flux linkages due to the 7th harmonic of the inducing field is designated Φ_{57}.

Putting $h_1 = 5$, $h = 5$, $p = 2$ and $\theta_2 = 0$ in equation 12.5.5., the resultant e.m.f. induced in coil 53 when that coil is situated at the direct axis is obtained by algebraic addition, noting the signs of the winding factors. The corresponding e.m.f. induced at the quadrature axis is then obtained. The ratio of these e.m.f's. is calculated here for use in chapter 7. The calculation is then repeated for the coil pitched $\pi/7$ (i.e $h_1 = 7$).

The constant C_4, defined by equation 12.5.4, is 5/7 numerically, making $B_7 = 5B_5/7$

Hence

$$e_{55} = -\frac{6\omega_1 LD}{2 \times 5} B_5 \sin\frac{\pi}{2} \sin(6\omega_1 t + \delta) \qquad (12.5.6)$$

and

$$e_{57} = -\frac{6\omega_1 LD}{2 \times 7} \cdot \frac{5B_5}{7} \sin\frac{7\pi}{10} \sin(6\omega_1 t + \delta) \qquad (12.5.7)$$

Since the winding factors for the 7th harmonic are negative (Table 7.1.), the total e.m.f. in coil 53 induced by the 5th harmonic of primary m.m.f. is

$$e_5 = e_{55} - e_{57}$$

$$= -6\omega_1 LDB_5 \left(\frac{1}{10} - \frac{5}{98} \times 0.809\right) \sin(6\omega_1 t + \delta)$$

$$= -6\omega_1 LDB_5 (0.1 - 0.041) \sin(6\omega_1 t + \delta)$$

$$\therefore \underline{E_{5max} = 6 \times 0.059\ \omega_1 LDB_5 \text{ at the direct axis}}$$

At the quadrative axis $\theta_2 = \pi/2$

$$\therefore \; e_{55} = -\frac{6\omega_1 LD}{10} B_5 \sin\frac{\pi}{2} \sin\left(\frac{5\pi}{2} + 6\omega_1 t + \delta\right)$$

$$\text{or} \quad e_{55} = -0.6\omega_1 LD\, B_5 \cos(6\omega_1 t + \delta) \qquad (12.5.8)$$

$$\text{and} \quad e_{57} = -\frac{6\omega_1 LD}{19.6} B_5 \sin\frac{7\pi}{10} \sin\left(\frac{7\pi}{2} + 6\omega_1 t + \delta\right)$$

$$\text{or} \quad e_{57} = +6 \times 0.041\omega_1 LDB_5 \cos(6\omega_1 t + \delta) \qquad (12.5.9)$$

Algebraic addition of e_{55} and e_{57} now gives:

$$e_5 = 6\omega_1 LD\, B_5(-0.1 + (-1)(0.041)) \cos(6\omega_1 t + \delta)$$

the peak value of which is:

$$E_{5_{max}} = 6 \times 0.141\ \omega_1\ LDB_5$$

$$\therefore \text{ The ratio } \frac{\text{direct axis value of } e_5}{\text{quad. axis value of } e_5} = \frac{0.059}{0.141} = 0.42$$

For coil 74 pitched $\pi/7$ radians (Elec), the corresponding calculation is:-

when $\theta_2 = 0$

$$\left.\begin{aligned} e_{75} &= -\frac{6\omega_1 LDB_5}{10} \sin\frac{5\pi}{14}\ \sin(6\omega_1 t + \delta) \\ &\text{and} \\ e_{77} &= -\frac{6}{19.6}\omega_1 LDB_5 \sin\frac{\pi}{2}\ \sin(6\omega_1 t + \delta) \end{aligned}\right\} \quad (12.5.10)$$

$$\therefore\ E_{7_{max}} = 6\omega_1 LDB_5\ (0.0902 - 0.051) = 6 \times 0.392\omega_1 LDB_5$$

when $\theta_2 = \pi/2$

$$e_{75} = -\frac{6}{10}\ \omega_1 LDB_5 \sin\frac{5\pi}{14}\ \sin\left(\frac{5\pi}{2} + 6\omega_1 t + \delta\right)$$

and

$$\left.\begin{aligned} e_{77} &= -\frac{6}{19.6}\omega_1 LDB_5 \sin\frac{\pi}{2}\quad \sin\left(\frac{7\pi}{2} + 6\omega_1 t + \delta\right) \\ \therefore\ e_7 &= 6\omega_1 LDB_5(-0.0902 - 0.051) \cos(6\omega_1 t + \delta) \end{aligned}\right\} \quad (12.5.11)$$

since k_{p7} is negative

$$\therefore\ E_{7_{max}} = 6 \times 0.1412\ \omega_1 LDB_5$$

$$\therefore \text{ The ratio } \frac{\text{d.a. value of } e_7}{\text{q.a. value of } e_7} = \frac{0.392}{0.141} = 0.28$$

12.5.3. The Summation of m.m.f. and slot ripple harmonics

The frequency of the induced e.m.f's. in the pole face of a synchronous machine having an integral slot winding due to armature slot openings ($6qf_1$) equals that due to the slot harmonic pairs of m.m.f. harmonics. ($6Kf_1$ when K = a simple multiple of q.

In the experimental load loss dynamometer having 1 s/p/p, this equality occurs for the first (and subsequent) m.m.f. harmonic terms, i.e. $K = q = 1$. The measured search coil e.m.f., filtered to exclude non-300 c/s terms, will contain the slot ripple components given by equation 12.6.22, in section 12.6.6. and m.m.f. harmonic components given by equations 12.5.5, section 12.5.1.

Putting $K = q$, the general expression for the total search coil e.m.f. is:

$$e_T = e_{h_1 5} + e_{h_1 7} + e_R$$

$$\therefore \quad e_T = - 6q\omega_1 LD\ (A + B + C + D)/p \quad .. \quad .. \quad (12.5.12.$$

where

π/h_1 = search coil pitch, ^{o}E

h = $6q - 1$

$$A = \frac{B_h}{h} \sin \frac{h\pi}{2h_1} \sin (h\theta_2 + 6q\omega_1 t + \delta)$$

$$C = \frac{C_5 a_n}{2h} \sin \frac{h\pi}{2h_1} \sin (h\theta_2 + 6q\omega_1 t + \delta_R)$$

$$B = \frac{C_4 B_h}{h + 2} \sin \frac{(h + 2)\pi}{2h_1} \sin (2\theta_2 + h\theta_2 + 6q\omega_1 t + \delta)$$

$$D = \frac{C_5 a_n}{2h + 4} \sin \frac{(h + 2)\pi}{2h_1} \sin (2\theta_2 + h\theta_2 + 6q\omega_1 t + \delta_R)$$

C_5 and δ_R account for changes in magnitude and phase caused by eddy current reaction.

Note:

(1) The m.m.f. components A and B are phase displaced from the slot ripple components C and D respectively by angle $(\delta - \delta_R)$.

(2) The sum (A + C) lags (B + D) by $2\theta_2$.

(3) When $\theta_2 = 0$, the sum of C and D is a maximum and of opposite polarity to (A + B) within the limitations of (4) below.

(4) A negative sign appearing in Table 7.1. against a_n, the winding factor, and in Table 12.6.2 against a_n indicates a phase shift of π harmonic electrical radians and modifies statements (1) to (3) accordingly.

(5) The reaction of slot ripple eddy currents on the inducing field was neglected in section 12.6.6. Eddy current reaction should reduce both the magnitude of the flux ripple and the phase displacement between A + C and B + D referred to

in (1) above. The factor C_4 and the angle δ_R have been introduced accordingly.

Whilst this limited theoretical analysis precludes the prediction of B_h, C_5 , δ and δ_R, it does deepen the understanding of the problem and affords a means of interpreting the test results of chapter 7. A realistic analysis of such a complex problem would presumably rely on test results to a considerable extent. It must not be forgotten that the total e.m.f. such as that shown in the oscillograms of chapter 7 contains a complete series of terms summated for $K = 1$ to ∞ , and $n = 1$ to ∞ .

12.6. The Influence of Armature Slot Openings

12.6.1. Introduction

In this appendix, the pole face loss due to slot openings is calculated for the experimental synchronous load loss dynamometer. The slot ripple loss, caused by the considerable diminution of the surface flux density opposite the primary slot openings is treated in sections 12.6.1. - 12.6.5. Whilst the calculation is based on several simplified assumptions, it is simple and conforms to current practice.

The surface e.m.f's. induced in the secondary by the "slot ripple flux" are important in this work since they affect the measured e.m.f's. induced in the secondary search coils. They are expressed in terms of the peak polarising gap flux density in section 12.6.6.

For reasons given in the introduction (section 2.4.5) the calculations in this appendix are based on publications by Gibbs[9] and Freeman[40]. The calculations is prolonged because certain constants, necessary to the calculation expressed in terms of the slot opening to gap ratio of 13.33 lie outside the ranges published by both Gibbs and Freeman. These are first determined by Schwartz-

Christoffel transformation in section 12.6.4. It is known that Gibbs' equations can be applied with confidence to conventional synchronous machines, but the application to a device having such a large s/g ratio is yet to be verified. Experimental work is being performed elsewhere on a model machine with an s/g ratio approaching that of the load loss dynamometer. It is hoped that future calculations will be based on the results of this work but, for the present time, the loss is calculated using Gibbs' formula (12.6.5).

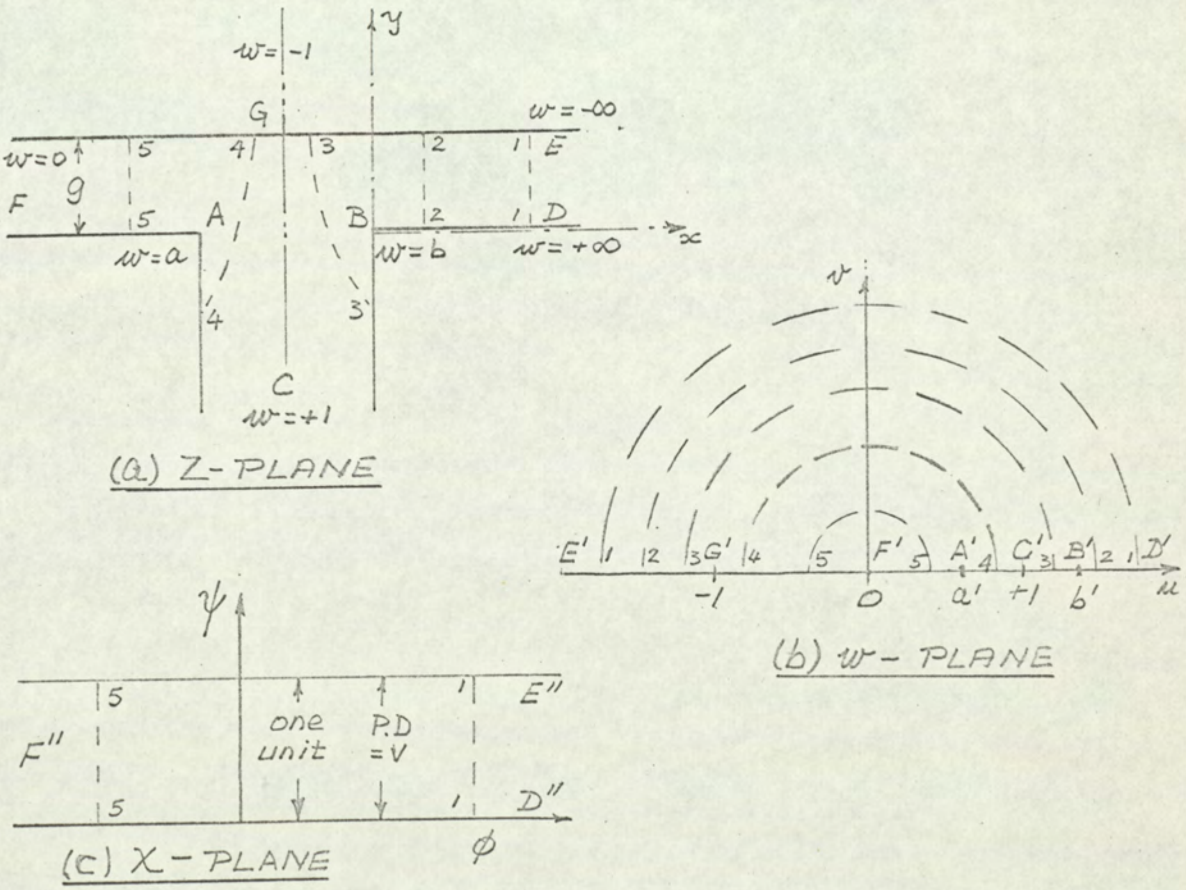

Fig. 12.6.1 Conformal Transformations

The calculations are based on Gibbs' and not Lawrenson's[7] work since the latter states that his results are not presented as the basis of a quantatative test of theory.

The values of β_1 and β_2 in Gibbs' formula are determined in section 12.6.4. ~~from the variation in~~ gap flux density opposite a slot opening. This variation is calculated in section 12.6.3. using the theory given in section 12.6.2.

Some of the terms used in this appendix are now introduced or re-stated to avoid ambiguity:-

z-plane = a plane through the machine perpendicular to its axis; $z = x + jy$, the positive directions of both x and y are those assigned in section 2.4.2 but y is now measured from the primary gap surface

w-plane = S-C transformation of the z-plane

a,b,p = parameters used in the w-plane

B_{max} = gap flux density at the secondary surface ($y = g$) opposite a tooth centre

B_{min} = gap flux density at the secondary surface ($y = g$) opposite a slot centre

B = gap flux density at the secondary surface ($y = g$) at any point

B_1 = the maximum value of polarising flux density at the secondary surface

B'_{mean} = mean gap flux density over a slot pitch in gauss

B_{Rn} = the nth harmonic of the ripple flux density

s = slot opening

t = tooth width

g = gap length

D = numerator of equation 12.6.6.

P = loss/unit area (Gibbs)

P_6 = loss per machine; ref. Fig. 5.15.

D' = pole face diameter in c.m.

λ'_s = slot pitch in c.m.

H' = magnetic intensity in oersted

μ_r = relative permeability

ρ' = resistivity in Ω-c.m.

β_1, β_2, R_1 = factors in Gibbs' equations defined in section 12.6.4.

Φ, Φ', Φ_s, Φ_t = gap fluxes defined in section 12.6.4. (and in Reference 5)

Φ_R = search coil flux linkages, section 12.6.6.

a_n = the amplitude of the nth harmonic in the gap flux density waveform

c_n = a_n/B_{max}

n = the harmonic order based on the slot pitch as the wavelength for which n = 1

ℓ_1 = any integer $>$ o

r = harmonic order defined in section 12.6.4.

12.6.2. Flux Density Distribution

The contribution the slot ripple makes to the total pole face loss will now be assessed in terms of the standing flux density. The equations are taken from the work of Gibbs[13] which uses the requisite Schwarz-Christoffel transformation to obtain the flux density distribution over one slot pitch when a constant m.m.f. exists across the air gap. The impressed m.m.f in the experimental machine, however, differs markedly from that of Gibbs by its being a Fourier series with time and space variables. Only the standing fundamental component of this series is considered as this makes a much bigger contribution to the slot ripple loss than the rotating harmonic components since the magnitude and angular velocity of the latter (with respect to the slot openings) are each 1/h of the fundamental.

The sinusoidal nature of the impressed m.m.f. is deferred for the moment whilst the flux density distribution is determined for the constant gap m.m.f. Gibbs' equations are now applied to one slot pitch.

The assumptions are:-

1) The curvature of the air gap can be neglected

2) The slot depth is infinite (see Gibbs p.104)

3) End-effects are negligible

4) The tooth width is large enough to allow the single-slot theory to be used (justifiable for experimental machine)

Transformation from z-plane to w-plane

The mathematical model in the z-plane is labelled in Fig. 12.6.1. Gibbs uses the transformation for which the resulting streamlines in the w-plane are semicircles, i.e. the point F, at which the real part of z is at minus infinity, transforms to the origin in the w-plane (F'). The other points A'B'C'D'E'G' in the w-plane correspond to ABCDEG in the z-plane.

$$\text{if } F'A' = a$$

$$F'B' = b$$

$$F'C' = 1$$

and
$$p^2 = \frac{w - b}{w - a} \quad .. \quad .. \quad .. \quad (12.6.1.)$$

Gibbs shows;

(i) the transformation, expressed in terms of the parameter p, is

$$z = \frac{g}{\pi}\left\{\log\left|\frac{1 + p}{1 - p}\right| - \log\left|\frac{b + p}{b - p}\right| - \frac{2s}{g}\tan^{-1}\frac{p}{\sqrt{b}}\right\} \quad (12.6.2.)$$

<u>Note</u>:- The origin in the z-plane occurs when p is zero, i.e. when $p = 0$, $z = 0$ and $w = b$ (points B, B')

The origin in the w-plane occurs when z is minus infinity (F & F')

(ii) a and b are interdependent:

$$a = \frac{1}{b} \quad .. \quad .. \quad .. \qquad (12.6.3.)$$

(iii) b is directly related to the slot/gap ratio:

$$\frac{b - 1}{\sqrt{b}} = \frac{s}{g} \quad .. \quad .. \quad .. \qquad (12.6.4.)$$

It is easy to show further that

$$\frac{a - 1}{\sqrt{a}} = -\frac{s}{g}$$

(iv)

$$B = \frac{w - 1}{(w - a)^{\frac{1}{2}} (w - b)^{\frac{1}{2}}} B_{max} \qquad (12.6.5.)$$

whence

$$\frac{B_{max}}{B_{min}} = \frac{(a + b + 2)^{\frac{1}{2}}}{2} \quad .. \qquad (12.6.6.)$$

From equations (iii) and (iv) above it can be shown that

$$\frac{B_{max}}{B_{min}} = \sqrt{\tfrac{1}{4}(\tfrac{s}{g})^2 + 1} \quad .. \qquad (12.6.6a)$$

2.6.3 Flux Density Calculations

For the experimental machine $s/g = 13.33$,

$$\therefore B_{min} = 15\% \text{ of } B_{max}$$

i.e. opposite the centre of each slot opening the flux density drops to 15% of the "smooth primary value" (neglecting tooth saturation).

The variation in flux density from B_{min} to B_{max} is obtained by varying the parameter w in equation 12.6.5. The same parameter is present in equation 12.6.1. which, in conjunction with equation 12.6.2., yields the distance along the pole face. B and x are calculated in Table 12.6.1., the steps in the process being indicated in the left-hand columns. The equations necessary for this calculation are now derived.

Re-writing equation 12.6.4:

$$b = 1 + \tfrac{1}{2}\left(\frac{s}{g}\right)^2 + \sqrt{\left(1 + \tfrac{1}{2}\left(\frac{s}{g}\right)^2\right)^2 - 1} \quad .. \quad .. \quad (12.6.7)$$

and putting

$\frac{s}{g} = 13.33$, gives

$b = 180$

$a = 1/180 = 0.00556$

Equation 12.6.1. then becomes:

$$p = \frac{w - 180}{w - 1/180} = \frac{180 - w}{0.00556 - w} \quad .. \quad .. \quad (12.6.8)$$

Substituting these values in equation 12.6.2. and taking values for which z is wholly real yields an expression for the abscissa x:

Table 12.6.1. The Calculation of the Flux Density Distribution over Half of One Slot Pitch.

A constant gap m.m.f is assumed.

Two typical calculations are given.

Equation used	w	-1.0	- 0.00005
	(1) = .00556 - w	+1.006	0.00561
	(2) = 180 - w	181	180
	(3) = $\sqrt{((2) \times (1))}$	13.45	1.005
(8)	p = $\sqrt{((2)/(1))}$ = (3)/(1)	13.40	179.0
	(4) = $\left\lvert\frac{p+1}{p-1}\right\rvert$	1.16	1.011
(9)	(5) = $\left\lvert\frac{180+p}{180-p}\right\rvert$	1.16	359
	(6) = Log (4)	0.148	0.0109
	(7) = Log (5)	0.148	5.883
	(8) = (6) - (7)	0	- 5.872
	$\tan^{-1}$(p/ 13.41) (rad)	0.785	1.534
(9)	(9) = 26.67 $\tan^{-1}$(p/13.41)	20.95	41.0
(9)	(10) = (8) - (9) = $\pi x/g$	-20.95	- 46.9
(9)	x = (10) x $\frac{0.3}{\pi}$ mm	- 2.00	-4.48
(10)	θ = x/1.267 ^{o}E	-1.58	-3.65
(11)	$\frac{B}{B_{max}}$ = (1 - w)/(3)	0.148	0.995
	θ' = $2\theta_{(w=-1)} - \theta_w$	-1.58	+0.49

θ' and θ are symmetrical about the slot centre line.

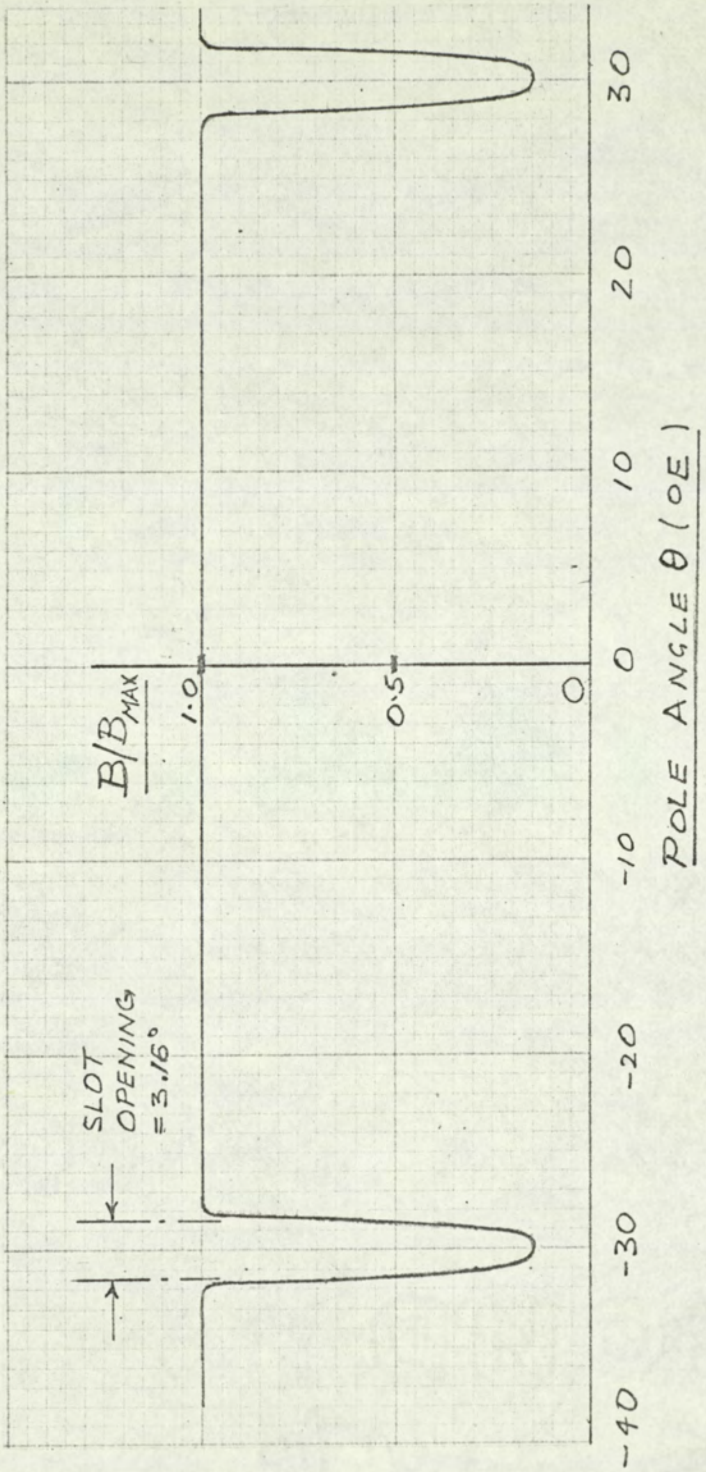

Fig. 12.6.2. The Flux Density Distribution in the Experimental Machine for a constant gap m.m.f.

$$x = \frac{\pi}{2}\left\{ \log \left|\frac{1 + p}{1 - p}\right| - \log \left|\frac{180 + p}{180 - p}\right| - 26.7 \tan^{-1} \left(\frac{p}{13.41}\right)\right\} \qquad (12.6.9)$$

With q (= 1) slots/pole/phase, x is changed to fundamental electrical radians by putting

$$\theta \doteq \frac{2\pi x}{(s + t)q} = \frac{2\pi x}{76 \times 6} \times \frac{180}{\pi} = \frac{60x}{76} = x/1.267 \ {}^{o}E \qquad (12.6.10)$$

where $s + t = 76$ m.m.

The flux density for each value of x, given by equation 12.6.5, becomes:

$$B = B_{max} \frac{w - 1}{\sqrt{\{(0.00556 - w)(180 - w)\}}} \qquad (12.6.11)$$

B is plotted against θ in Fig. 12.6.2.

12.6.4. The Determination of the Slot Ripple Loss Factors, β_1, β_2 and R_1.

The pole face loss per unit area due to the slot openings is given by Gibbs[9] in his equation (8):

$$P = 5.9\lambda_s' \beta_2 B'_{mean} (R.P.M.)(6q) H' \times 10^{-10} \text{ watts/c.m.}^2$$

The total loss per machine is therefore

$$P_6 = 1.85(2p) D'(R.P.M.)(\beta_2 \Phi') H' \times 10^{-9} \text{ watts} \qquad (12.6.12)$$

c.g.s. units are used for primed symbols
m.k.s. units for the remainder.

The value of H' is found from a graph of H' against $H'\sqrt{\rho'\mu_r}$, Fig. 12.6.5 ; $H'\sqrt{\rho'\mu_r}$ being calculated again from Gibbs, this time from his equation (7):

$$H'\sqrt{\rho'\mu_r} = 1.81\,\lambda'_s\ \beta_2 B'_{max} \sqrt{(R.P.M.)(6pq)} \times 10^{-6} \quad (12.6.13)$$

B'_{max} is defined in section 12.6.1.

The factor β_2 is the product of a flux oscillation factor, β_1, and a harmonic loss factor, R_1. Gibbs calls β_2 the modified flux oscillation factor.

Gibbs presents graphs of β_1 and β_2 plotted as families of curves for s/g $\leqslant$ 8. The s/g ratio of the experimental load loss dynamometer is too far outside Gibbs' range to permit extrapolation of the β_1 and β_2 curves. Therefore β_1 and β_2 are calculated from the flux distribution already established in section 12.6.3.

By definition $\beta_1 = \dfrac{\text{The Lost Flux}, \Phi'}{\text{The Total Flux}}$

$$= \frac{\Phi_t - \Phi_s}{\Phi_t + \Phi_s}$$

Where Φ_t = the maximum amount of flux embraced in half a slot pitch.

and Φ_s = the corresponding minimum amount in the remaining half.

It is straightforward therefore to determine β_1 either graphically from Fig. 12.6.2. or algebraically using the integral calculus.

For the second method equation 9.26. of ref. 13 is used:

$$\Phi' = \frac{2s}{\pi}\left\{\tan^{-1}\frac{s}{2g} - \frac{g}{s}\log\left(1 + \frac{s^2}{4g^2}\right)\right\}$$

for unit axial length and unit B_{mean}

For the experimental machine (g = 0.3 m.m., s = 4 m.m., and t = 72 m.m.) the lost flux is:

$$\Phi' = \frac{8}{1000\pi}\left\{81.5 \times \frac{\pi}{180} - \frac{3}{40}\log_e 45.4\right\} = 0.00294$$

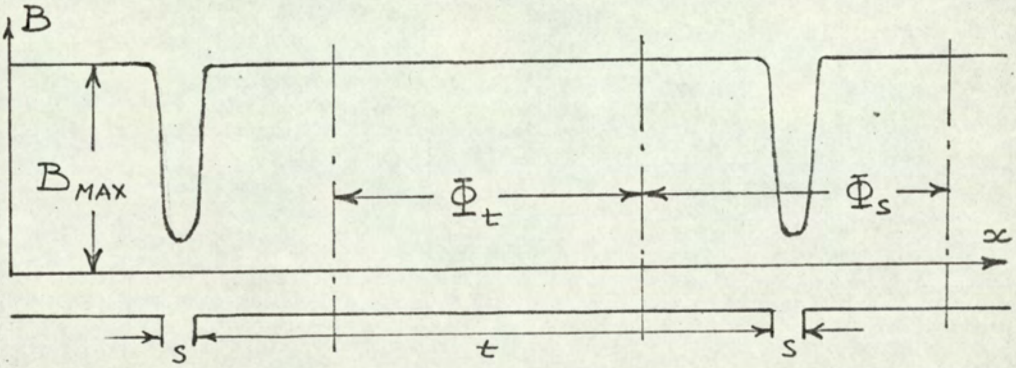

Fig. 12.6.3.

For an unslotted primary the undisturbed flux would be:

$$\Phi = B \times (s + t) \times L = 1 \times (76 \times 10^{-3}) \times 1 = 0.076$$

$$\therefore \beta_1 = \frac{\Phi_s - \Phi_t}{\Phi_s + \Phi_t} = \frac{\Phi'}{\Phi - \Phi'} = \frac{0.00294}{0.07306} = 0.0402$$

Table 12.6.2. Fourier Analysis of Flux Density Wave over One Slot Pitch, by Computer.

Gap m.m.f. constant (Fig. 12.6.2.)

120 ordinates

B_{max} = 1000

B_{mean} = 960.90

n	a_n	$\frac{a_n^2}{100}$	$\frac{a_n^2}{100\sqrt{n}}$	c_n	$b_n = \frac{a_n \times 100}{B_{mean}}$
1	77.89	60.6	60.6	0.00	8.11
2	-76.96	59.2	41.8	0.00	8.03
3	75.42	56.9	32.8	0.00	7.85
4	-73.31	53.8	26.9	0.00	7.64
5	70.65	50.0	21.4	0.00	7.36
6	-67.49	45.6	18.7	0.00	7.05
7	63.87	40.8	15.4	0.00	6.67
8	-59.86	35.9	12.7	0.00	6.24
9	55.51	30.7	10.2	0.00	5.80
10	-50.89	25.9	8.2	0.00	5.30
11	46.07	21.2	6.4	0.00	4.80
12	-41.12	16.9	4.9	0.00	4.28
13	36.10	13.1	3.6	0.00	3.76
14	-31.10	9.7	2.6	0.00	3.26
15	26.17	6.8	1.8	0.00	2.73
16	-21.38	4.6	1.2	0.00	2.24
17	16.79	2.8	0.7	0.00	1.74
18	-12.45	1.6	0.4	0.00	1.20
19	8.41	0.7	0.2	0.00	0.81
20	- 4.70	0.2	0.0	0.00	0.50
Total			272.5		

a_n and c_n are the coefficients of the general term in the F.S. :-

$$\sum_{n=0}^{\infty} (a_n \cos n\theta + c_n \sin n\theta)$$

This value is in close agreement with the figure of 0.0397 obtained using the graphical method. Reference to Gibbs' curves shows the average value 0.040 to be reasonable.

This value of β_1 must now be modified to account for harmonics in the flux ripple. The most convenient method is that discussed by Freeman[40] who defines the harmonic loss factor R_1 in his section 7 as:

$$R_1 = \frac{1}{{a_1}^2} \sum_{n=1}^{n=\infty} \frac{{a_n}^2}{\sqrt{n}} \quad .. \quad .. \qquad (12.6.14)$$

where a_n = the amplitude of the n-th harmonic in the gap density waveform.

The values of a_n were determined by Fourier analysis in two ways, one constituting a check on the other:

(i) The waveform in Fig. 12.6.2 was analysed by taking 120 ordinates per slot pitch, with the origin at the tooth centre (Table 12.6.2).

(ii) The sinusoidal standing flux density waveform was modified by taking the product of 360 ordinates of the sinusoidal waveform and 360 corresponding ordinates of the B/B_{max} waveform of Fig. 12.6.2. Two positions of the primary slot openings with respect to the standing flux were selected:-

(a) tooth centre on the primary m.m.f. direct axis

(b) slot centre on the primary m.m.f. direct axis.

The harmonics in the resulting flux density waveforms, sketched in Figs. 12.6.4. (a) and (b) respectively, are listed in Table 12.6.3.

In method (i), the wavelength of the first harmonic term always equals the slot pitch, $\lambda_1/6q$, and its frequency that of the m.m.f. slot harmonics, $6qf_1$ (= slots per pole pair x synchronous frequency). Both Gibbs[9] and Freeman[40] call this the fundamental frequency.

To avoid confusion with other parts of this thesis, the adjective "fundamental" is reserved for the frequency of the primary currents, f_1, and the order of the harmonic currents referred to f_1.

Let r = the harmonic order of the general term w.r.t. f_1

Then $r = \ell \times 6q$ where ℓ is an integer > 0

The amplitudes of the first 20 terms are listed in Table 12.6.2. in tenths of 1% of B_{max}.

In method (ii), the series of terms is different in both order and magnitude. The first 40 terms are listed

Table 12.6.3. The Calculation of the Harmonic Loss Factor for a Sinusoidally Distributed M.M.F. Wave, Fig. 12.6.4.

Harmonic Order $r = 6n \pm 1$	Amplitude of the r-th Harmonic b_r (a)	b_r (b)	n	a_n	a_n^2	$\frac{a_r^2}{\sqrt{n}}$
1	95.91	95.89				
5	+4.07	-4.04	1	8.15	67.3	67.3
7	-4.07	+4.11				
11	+4.03	+4.00	2	8.02	64.2	45.4
13	-4.02	-4.00				
⋮	⋮	⋮	⋮	⋮	⋮	⋮
113	+0.33	-0.29	19	0.64	0.04	0.01
115	-0.33	+0.32				
119	+0.09	+0.01	20	0.15	0.02	0
121	-0.07	-0.04				
				Total		303.9

$$a_n = \tfrac{1}{2}\left\{ b_r(a)_{6K-1} + b_r(a)_{6K+1} + b_r(b)_{6K-1} + b_r(b)_{6K+1} \right\}$$

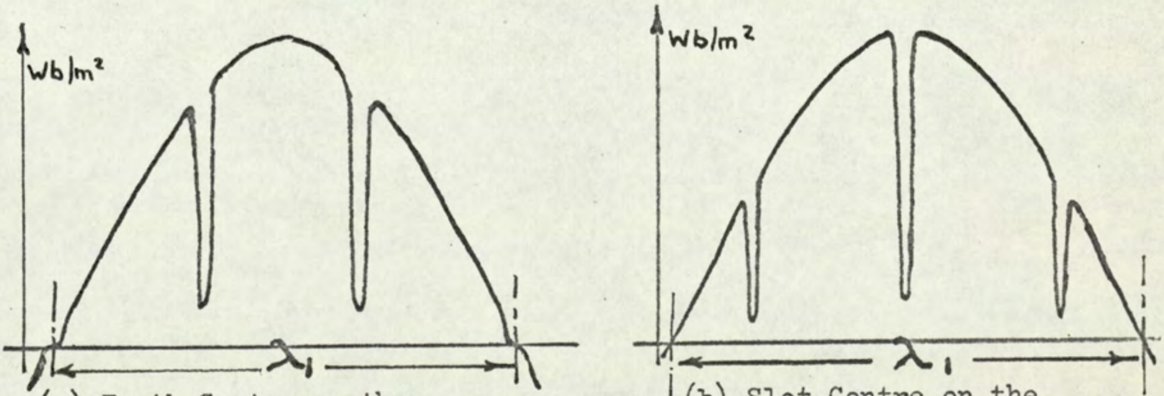

(a) Tooth Centre on the M.M.F. Direct Axis.

(b) Slot Centre on the M.M.F. Direct Axis.

Fig. 12.6.4. Flux Density Distribution in the Experimental Machine with a Sinusoidally Distributed Gap M.M.F.

in Table 12.6.3. An expression for "r", evident in Table 12.6.3 but derived mathematically in section 12.6.6, is:

$$r \;=\; 6\ell q \pm 1$$

i.e. when the standing flux density distribution is sinusoidal, each harmonic term order r splits into two terms of equal magnitude whose wavelength and frequency each correpspond to one of the slot harmonic terms in the primary m.m.f. wave.

The amplitude, b_r, of the rth term in Table 12.6.3 for slot position (a), Fig. 12.6.4, equals that for position (b), and that of the $(6\ell q - 1)$th term equals that of the $(6\ell q + 1)$th. These terms form distinct sub-groups which may be averaged either before or after summation, the sign changes merely bring the negative peaks of the harmonic cosine waves into alignment at the slot centre.

In Table 12.2.3, "n" is defined in section 12.6.1 and used in equation 12.6.14; a_n is the mean value of the sum of the harmonic amplitudes taken in pairs for slot positions (a) and (b) (i.e. ½ of the sum of 4 grouped values of b_r).

Using equation 12.6.14, we get:

From Table 12.6.2 $\quad R_1 = \dfrac{1}{60.6} \quad 272.5 \;=\; 4.49$

From Table 12.6.3 $\quad R_1 = \dfrac{1}{67.3} \quad 303.9 \;=\; 4.51$

$\therefore$ Mean Value of $R_1 \;=\; 4.50$

$\therefore \quad \beta_2 \;=\; R_1\beta_1 \;=\; 0.18$

R_1 is expectedly high due to the sharp dip in the gap flux density creating a wide harmonic spectrum. It is a reasonable extrapolation of Freeman's R_1 curves.

12.6.5. Slot Ripple Loss Calculations

The method of calculation was outlined at the beginning of section 12.6.4., where the necessary equations derived by Gibbs[9] were quoted. The method requires a graph of H' against $H'\sqrt{\rho'\mu_r}$. These co-ordinates, calculated from preliminary tests on the secondary steel used in the experimental machine, are plotted in Fig. 12.6.5. for three values of steel temperature. With the exception of the modified flux oscillation factor β_2 and $H'\sqrt{\rho'\mu_r}$, which have been determined above, Gibbs' equations (12.6.13. and 12.6.12.) can now be evaluated from the design data in terms of B_{mean}.

Substituting in equation 12.6.13:

$\lambda_s = 7.6$ c.m. and $\beta_2 = 0.180$, we get

$$H'\sqrt{\rho'\mu_r} = 1.81\lambda_s\,\beta_2\,B'_{mean}\sqrt{(R.P.M.)(6pq)} \times 10^{-6} \text{ c.g.s.u.}$$

$$= 1.81 \times 7.6 \times 0.180 \times (B_{mean} \times 10^4)\sqrt{N}\sqrt{6\times2\times1}\times10^{-6}$$

$$= 8.56\,B_{mean}\sqrt{N} \times 10^{-2} \text{ c.g.s.u.} \qquad (12.6.15)$$

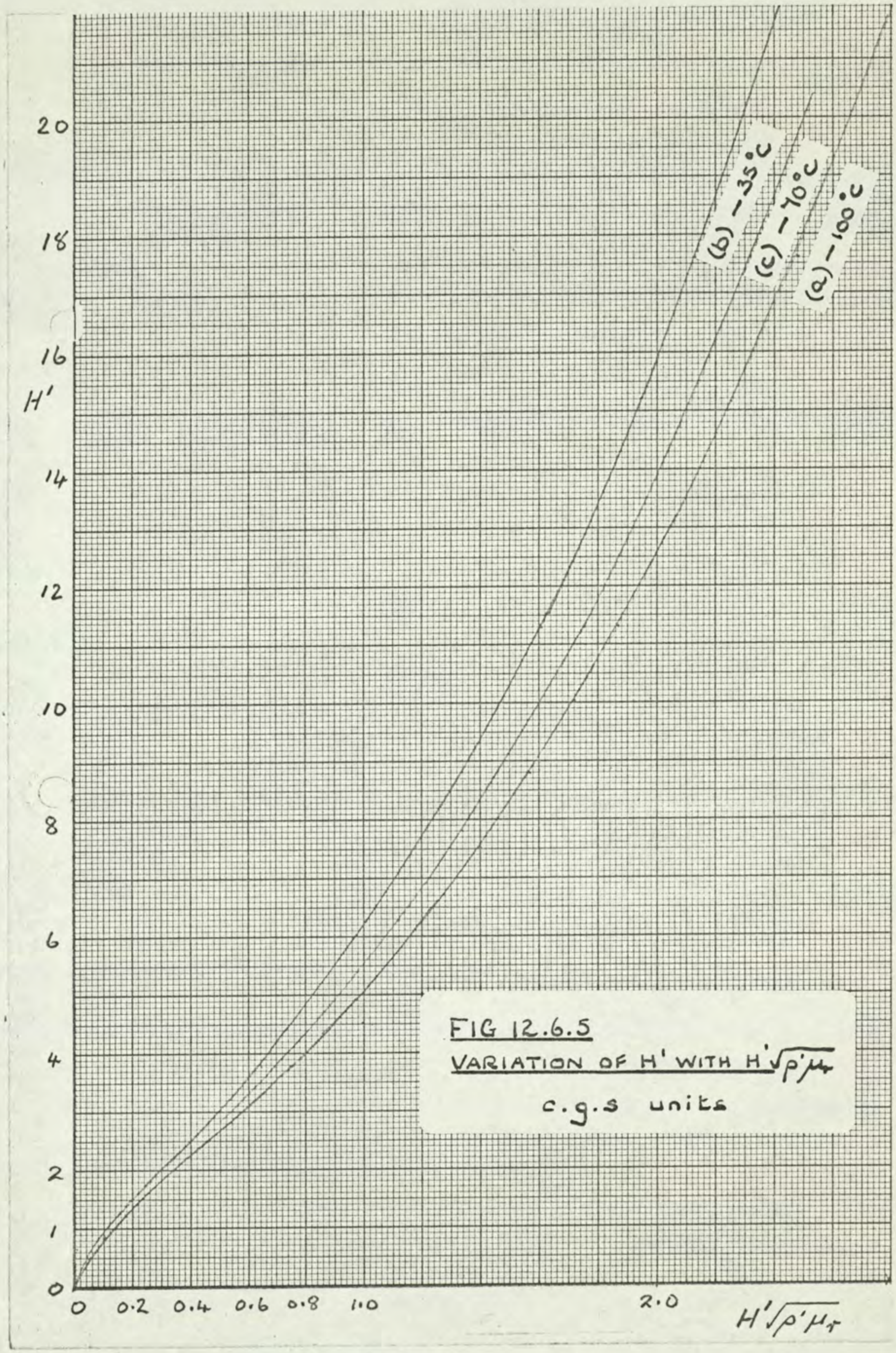

FIG 12.6.5
VARIATION OF H' WITH $H'\sqrt{\rho'\mu_r}$
c.g.s units

Table 12.6.4. The Calculation of the Slot Ripple Loss at 1500 r.p.m.

Ref. equation 12.6.16, equation 12.6.18, and Fig.12.6.5.

B_{mean} Wb/m^2	$H'\sqrt{p'\mu_r}$ c.g.s.u.	H' c.g.s.u.	P_6 kW	H' c.g.s.u.	P_6 kW	H' c.g.s.u.	P_6 kW
	(a) 100°C			(b) 35°C		(c) 70°C	
0.1	0.331	2.00	0.066	2.15	0.071		
0.2	0.662	3.40	0.225	3.95	0.261		
0.3	0.993	5.00	0.496	6.15	0.611	5.48	0.544
0.4	1.324	7.05	0.932	8.72	1.154	7.75	1.026
0.5	1.655	9.53	1.578	11.75	1.945	10.45	1.73
0.6	1.986	12.45	2.49	15.75	3.13	13.7	2.72
0.7	2.317	15.9	3.68	20.4	4.72		
0.8	2.648	19.75					

If N = 1500,

$$H'\sqrt{\rho'\mu_r} = 0.331\ B_{mean} \quad \text{c.g.s.u.} \quad .. \quad (12.6.16)$$

Equation (12.6.12.) becomes

$$P_6 = 5.9 \times 7.6 \times 0.180 \times (B_{mean} \times 10^4)\ N \times 12H' \times 10^{-10} \times \pi \times 29 \times 25 \quad \text{watts (total per secondary)}$$

$$= 0.2205\ N\ H'\ B_{mean} \quad \text{watts} \quad .. \quad .. \quad (12.6.17)$$

If N = 1500,

$$P_6 = 331\ H'B_{mean} \quad \text{watts} \quad .. \quad .. \quad (12.6.18)$$

P_6 is now calculated at 1500 r.p.m. for three different surface temperatures in Table 12.6.4. and plotted in Fig. 5.28 for use in the mains frequency tests in chapter 5. For the variable frequency tests, P_6 is calculated from equation 12.6.17. as required.

12.6.6. The Slot Ripple E.M.F's.

In sections 12.6.1. to 12.6.5., equations derived from conformal-transformation theory have been used to calculate the shape and hence the harmonic content of the tooth ripple flux density waveform at the secondary surface of the experimental machine. When the impressed m.m.f. is uniform over a slot pitch, the equation of the waveform may be written[40] as:

$$B = B_{mean} + \sum_{n=1}^{\infty} a_n \cos n\theta_2 \quad .. \quad .. \quad (12.6.19.)$$

The selection of the tooth centre as the origin eliminates all sine terms.

The per-unit harmonic amplitude $= b_n = a_n/B_{mean}$

The value of B_{mean} and the first 4 values of b_n, listed in Table 12.6.2, agree closely with the corresponding values plotted by Freeman in Figs. 5-9 of Reference 40 in both magnitude and sign. However, in the experimental machine, the impressed m.m.f. is not constant but varies over 2 pole pitches in the manner described in sections 2.3. and 12.5., namely a precisely defined set of rotating m.m.f. waves. The influence of the slot openings will be much greater on the fundamental wave than on the harmonic waves since the magnitude and angular speed of the harmonics are both reduced in proportion to the harmonic order. In the derivation of an expression for the slot ripple e.m.f's., the m.m.f. harmonics will be neglected and the impressed waveform assumed sinusoidal, thereby producing a sinusoidal flux density waveform of peak value B_1 upon which is superimposed the slot ripple (e.g. Fig. 12.6.4.). Under these circumstances, the nth component of the ripple flux density wave, B_{Rn}:

(i) has a wavelength $= \lambda_1/6qn$

(ii) is moving relative to the secondary surface at an angular velocity $= 6q\omega_1$

(iii) will be modified in magnitude and phase by eddy current reaction (section 12.5.3.)

and (iv) in the absence of (iii), has a peak value (which varies with θ_2) equal to

$$a_n \cos\theta = b_n B_1 \cos\theta_2$$

which is a maximum when $\theta_2 = 0 = t$ (Fig. 7.3.)

i.e. $$B_{Rn} = (b_n B \cos\theta_2) \times (\cos 6qn\theta_2 + 6q\omega_1 t) \qquad (12.6.20)$$

Concentrating attention on the first term which induces 300 c/s e.m.f's. in the secondary, we can write:

$$n = 1$$

$$a_1 = b_1 B_1 \cos\theta_2$$

$$\therefore \quad B_R = B_{R_1} = a_1 \cos\theta_2 \cos(6q\theta_2 + 6q\omega_1 t)$$

The e.m.f. induced in a search coil having a pitch $\psi\pi$ is determined by calculating the time rate of change of flux linkages in the manner described in section 12.5.1.

i.e. $$\Phi_R = \int_{\theta_2 - \psi\pi/2}^{\theta_2 + \psi\pi/2} B_R L \frac{D}{2} \frac{d\theta}{p}$$

$$= \frac{LDa_1}{2p} \int \tfrac{1}{2} \left[\cos\{(6q + 1)\theta_2 + 6q\omega_1 t\} + \cos\{(6q - 1)\theta_2 + 6q\omega_1 t\} \right] d\theta$$

$$= + \frac{LDa_1}{4p}\left[\frac{\sin\{(6q+1)\theta_2+6q\omega_1 t\}}{6q+1} + \frac{\sin\{(6q-1)\theta_2+6q\omega_1 t\}}{6q-1}\right]_{\theta_2 - \psi\pi/2}^{\theta_2 + \psi\pi/2}$$

The e.m.f. induced in the search coil therefore possesses two components which can be considered to be caused by two B-waves rotating in the same direction and at the same angular velocity but having different wavelengths. Their wavelengths are identical to those of the m.m.f. harmonics for which $k = q$, i.e. the slot harmonic terms. Their frequencies ($= 6qf_1 = 6kf_1$) are also identical.

Putting $6q - 1 = h$

$$6q + 1 = h + 2$$

and $\psi\pi = \pi/h_1$ as in section 12.5

we get:

$$\Phi_R = \frac{LDa_1}{4ph}\left[\sin\left(h\theta_2 + \frac{h\pi}{2h_1} + 6q\omega_1 t\right) - \sin\left(h\theta_2 - \frac{h\pi}{2h_1} + 6q\omega_1 t\right)\right]$$

$$- \frac{LDa_1}{4p(h+2)}\left[\sin\left\{(h+2)\theta_2 + \frac{(h+2)\pi}{2h_1} + 6q\omega_1 t\right\}\right.$$

$$\left. - \sin\left\{(h+2)\theta_2 - \frac{(h+2)\pi}{2h_1} + 6q\omega_1 t\right\}\right] \qquad (12.6.21)$$

The e.m.f. induced by the term in the first square bracket has been determined in section 12.5.1 and can be simply restated. That by the second square bracket can be obtained by substituting $(h + 2)$ for h:

$$\therefore \quad e_R = -\frac{3q\omega_1 LDa_1}{ph} \sin\frac{h\pi}{2h_1} \sin(h\theta_2 + 6q\omega_1 t)$$

$$- \frac{3q\omega_1 LDa}{p(h+2)} \sin\frac{(h+2)\pi}{2h} \sin(h\theta_2 + 2\theta_2 + 6q\omega_1 t) \qquad (12.6.22)$$

The phase angle between these two terms is $2\theta_2$ (as for the m.m.f. harmonics), bringing the two components in phase at the m.m.f. axis where the flux density ripple is a maximum and in antiphase at the quadrature axis where the ripple flux density is zero.

Putting $q = 1$, $h = 5$ and $h_1 = 5$ or 7 for the coils pitched $\pi/5$ and $\pi/7$ respectively, we can obtain expressions for the 300 c/s slot ripple e.m.f's. e_{5R} and e_{7R} in search coils 53 and 74 respectively.

(a) $h_1 = 5$

(i) when $\theta_2 = 0$

$$e_{5R} = -3\omega_1 LDb_1 B_1 \left(\frac{1}{10} + \frac{0.809}{14}\right) \sin 6\omega_1 t \quad .. \qquad (12.6.23)$$

$$= -6 \times 0.0789 \ LDb_1 B_1 \sin 6\omega_1 t$$

c.f. equations 12.5.6 and .7.

(ii) when $\theta_2 = \pi/2$

$$e_{5R} = -3\omega_1 LDb_1 B_1 \left(\frac{1}{10} - \frac{0.809}{14}\right) \cos 6\omega_1 t \quad .. \qquad (12.6.24)$$

$$= -6 \times 0.0212 \ \omega_1 LDb_1 B_1 \cos 6\omega_1 t$$

c.f. equations 12.5.8 and .9.

(b) $h_1 = 7$

(i) when $\theta_2 = 0$

$$e_{7R} = -3\omega_1 LDb_1 B_1 \left(\frac{0.902}{10} + \frac{1}{14}\right) \sin 6\omega_1 t \quad .. \qquad (12.6.25)$$

$$= -6 \times 0.0808\ \omega_1 LDb_1\ B_1 \sin 6\omega_1 t$$

c.f. equations 12.5.10.

(ii) when $\theta_2 = \pi/2$

$$e_{7_R} = -3\omega_1 LDb_1 B_1 (0.0902 - 0.0714) \cos 6\omega_1 t$$

$$= -6 \times 0.0094\ \omega_1 LDb_1\ B_1 \cos 6\omega_1 t \quad .. \qquad (12.6.26.)$$

c.f. equations 12.5.11.

Equations 12.6.23. to 12.6.26 are used in appendix 12.5.3. They represent e.m.f's. induced in the secondary having the same frequency and wavelength as those induced by the slot harmonic order m.m.f. wave but need modifying in magnitude and phase to account for eddy current reaction. Assuming that both e_{7_R} and e_{5_R} are influenced to the same extent by eddy current reaction, the above summations will give for coils pitched $\pi/5$ the ratio

$$\frac{\text{d.a. value of slot ripple e.m.f.}}{\text{q.a. value of slot ripple e.m.f.}}$$

$$= \frac{0.0789}{0.0212} = 3.7.$$

For coils pitched $\pi/7$, the ratio is

$$\frac{0.0808}{0.0094} = 8.6.$$

Appendix 12.7. The Supply of Power to the Pole Face

12.7.1. Introduction

In an eddy current coupling, and an unloaded unparallelled separately excited d.c. or a.c. generator, the exciter power source provides only the power consumed in the copper conductors of the field winding. All other electrical power losses (tooth-ripple, end-region, armature, iron loss, etc.) are provided by the mechanical shaft power, i.e. by mechanical/electrical energy conversion.

The pole face loss problem differs from the above in that the excitation is provided by an a.c. winding and therefore both mechanical/electrical and electrical/electrical means of energy conversion are possible.

Basically, the machine consists of a set of primary conductors producing a precise series of rotating magnetic fields. Each causes an induced current pattern in a secondary member, producing losses therein and also a reaction m.m.f. This modifies the primary m.m.f. and induces mains frequency e.m.f's. in the primary conductors. It was pointed out in section 2.4.5.(iii) that the pole face loss due to armature reaction m.m.f. harmonics is analogous to the loss in the secondary member of solid rotor induction motors and eddy current couplings. This analogy has been used by Wagner and Evans (Ref. 41 p. 92) to determine the power source of negative phase sequence currents in synchronous generators under unbalanced load or fault conditions. Whilst in this appendix the method is extended to pole face loss problems in general, it has a direct bearing on the experimental work of section 5 regarding the method of loss separation.

12.7.2. Theory

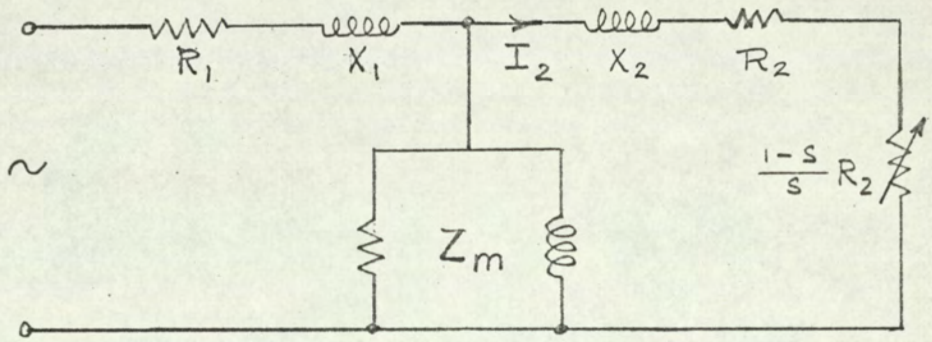

Fig. 12.7.1.

Consider an induction motor having the equivalent circuit of Fig. 12.7.1.

I_2, X_2 and R_2 are equivalent phase values of secondary currents, reactance and resistance referred to the primary.

Let ω_h = the angular velocity of the hth harmonic space wave relative to the secondary.

and ω_1 = the angular velocity of the secondary relative to the primary.

The 3-phase stator produces harmonic field patterns each rotating at an angular velocity of $\pm \frac{\omega_1}{h}$ with respect to the stator (or primary) when the mains frequency is $\omega_1/2\pi$.

Since the secondary is rotating at a speed of $+\omega_1$ the slip per unit for each harmonic term will be

$$s = \frac{\pm\omega_1/h - \omega_1}{\pm\omega_1/h} = \frac{\pm\omega_1 - \omega_1(6K \pm 1)}{\pm\omega_1} \doteq \pm 6K$$

The power absorbed by R_2 represents the secondary loss and that by $R_2(1 - s)/s$ represents the useful shaft output power per phase. Let us assume that the analogous induction motor is coupled to a reversible machine.

For the 5th and $(6K - 1)$ terms, the secondary is being driven in the opposite direction to the rotating harmonic magnetic field and the system corresponds to the braking mode of the induction motor. Slip is positive and equal to 6K.

$\therefore$ The mechanical power output

$$= 3 \times I_2{}^2 R_2 \frac{1 - s}{s} = -3I_2{}^2 R_2 \frac{6K - 1}{6K}$$

The negative sign signifies the flow of mechanical power to the secondary member.

$\therefore$ The mechanical power supplied by the shaft

$$= 3I_2{}^2 R \frac{h}{h + 1} \quad (\text{since } h = 6K - 1)$$

Now the total power consumed in the secondary = $3I_2^2 R_2$

Therefore the power supplied by the primary equals the total power consumed less the shaft power supplied

$$\text{i.e. } P_E = \frac{3I_2{}^2R_2}{6K} = \frac{3I_2{}^2R_2}{h+1}$$

hence the ratio,

$$\frac{\text{power supplied electrically}}{\text{power supplied mechanically}} = \frac{1}{h}$$

For the 7th and (6K + 1) terms, the pole face is being driven in the same direction as, but faster than the rotating harmonic magnetic field. The situation therefore corresponds to the generating mode of the induction motor. The slip is negative and equal to -6K. Therefore the mechanical power expressed as an "output" power will again be negative.

$$= 3I_2{}^2R_2 \frac{1-s}{s} = -3I_2{}^2R_2 \frac{6K+1}{6K}$$

i.e. the mechanical power supplied

$$= 3I_2{}^2R_2 \frac{h}{h-1} \quad (\text{since } h = 6K + 1)$$

This is greater than the pole face (rotor) loss, the surplus P_E being generated viz:

$$P_E = 3I_2{}^2R_2 \frac{1}{h-1} = \frac{3I_2{}^2R_2}{6K}$$

In practice, the harmonic m.m.f. losses produced by the 6K - 1 and 6K + 1 terms are usually unequal and not simply expressed. It is convenient therefore to terminate the algebraic analysis here and demonstrate that most of the loss power is supplied from the shaft in Table 12.7.1.

Table 12.7.1. lists the pole face loss for each of the predominant harmonics in the experimental load loss dynamometer (computed by the modified eddy current coupling theory in chapter 3) divided into their component parts. The error in assuming that the loss is provided entirely by mechanical means is very small (2% for the rated primary current of 29.8 amps.)

Table 12.7.1. Analysis of Secondary M.M.F. Loss in the Experimental Machine

K	Harmonic order, h $6K \pm 1$	Computed harmonic loss "KW" $\frac{h}{6K}$	Power supplied: Mechanical Component $=$ "KW" $\times \frac{h}{6K}$	Power supplied: Electrical Component $= \{$"KW"$_{(6K+1)}$ $-$"KW"$_{(6K-1)}\}/6$
1	5	0.443	0.370	$\frac{0.108}{6} = 0.018$
	7	0.335	0.391	
2	11	0.304	0.278	$\frac{0.100}{12} = 0.008$
	13	0.204	0.221	
3	17	0.147	0.139	$\frac{0.05}{18} = 0.003$
	19	0.097	0.102	
4	23	0.065	0.062	$\frac{0.020}{24} = 0.001$
	25	0.045	0.047	
Total of 1st 8 terms:			$P_M = 1.612$	$P_E = 0.030$

∴ The error in neglecting electrical component of m.m.f. loss power when assessing the primary iron loss

$$= \frac{P_E}{P_E + P_M} \times 100 = 2\%$$

12.7.3 Conclusion

By assuming that the experimental load loss dynamometer can be represented by the equivalent circuit of Fig. 12.7.1, it is shown that for any harmonic of order h:

$$\frac{\text{the electrical power supplied}}{\text{the mechanical power supplied}} = \frac{1}{h}$$

The electrical power is positive for the 6K - 1 harmonics but negative for the 6K + 1 harmonics (indication generation). The pole face loss caused by the harmonic m.m.f's. of armature reaction is supplied almost entirely in the form of mechanical shaft power, the electrical powers tending to cancel.

The expressions derived are valid for any practicable value of h and also for negative phase sequence m.m.f's. For these, h = 1 and s = +2 giving $P_E = P_M = \frac{1}{2}$(eddy current loss in the pole face).

Appendix 12.8 Production Machines

The predicted <u>component</u> of stray load loss caused by the armature reaction m.m.f. harmonics using the proposed theory is compared in Table 12.8.1 with the <u>total</u> measured stray load loss on several salient pole and solid rotor alternators.

Table 12.8.1. Predicted M.M.F. Losses for a Small Selection of Large Synchronous Machines.

Machine Reference		S	T	U	V	W	X (1)	Y (1)
Cross Reference		1.2803	1.3006	1.201746	1.201679	CEGB/5	CEGB/6	CEGB/11
Programme No.		MS-1	MS-1	MS-1	MS-1	7	7	7
Data								
Electric loading	AC/in	1210	2576	1230	820	1800	3070	4250
Rating	MW	1	4.9	1.5	1.0	-	-	-
Pole pairs	p	3	2	3	2(25c/s)	1	1	1
Synchronous speed	N_s r.p.m.	1000	1500	1000	750	3000	3000	3000
Effective conductors per slot	Z/Y	22	8	3	2	2	2	2
Parallel paths/phase	C	1	1	6	4	2	2	2
Total phase current	I	55	322	2460	1640	4650	6276	11000
Slots/pole/phase	q	4	5	7	9	9	12	10
Pitch	p.u	1.0	0.800	0.809	0.740	0.815	0.833	0.833
Spread	deg.	60	60	60	60	60	60	60
Rotor diameter	D mm	764	876	764	890	1020	1020	1090
Effective airgap	g mm	19.8	13.1	5.8	14	61	89	85
Slot width	b mm	18.5	13.0	9.7	12.2	-	-	-
Slot pitch	λ_s mm	35	47	19.5	26	65	50	65
Active rotor length	L	650	1200	635	825	4800	3750	5200
Rotor iron resistivity	ρ μΩ-cm	21	21	17.2	17.2	27.5	27.5	27.5
Gap/diameter ratio	$g/(D+2g)$	0.022	0.013	0.007	0.014	0.05	0.07	0.06
Slot pitch/gap ratio	λ_s/g	1.9	3.9	3.5	2.1	1.4	0.7	1
Slot harm. pole pairs	6qp	72	60	126	108	54	72	60
Calculated m.m.f. harmonic loss:								
Belt terms	kW	0.52	3.54	0.38	1.2	26 (2)	52 (2)	230 (2)
Slot terms: Loss	P_L kW	0.05	15.3	0.37	0.1	42	21	250
Slot terms: Leakage factor	K_L	0.02	0.19	0.18	0.02	0	0	0
Slot terms	$P_L K_L$ kW	0	2.92	0.07	0	0	0	0
Total (3)	kW	0.5	6.5	0.5	1.2	26	52	230
Test stray load loss	kW	1.9	22.3	13.75	4.73	170	390	1090
Ratios:								
Calc^d Total m.m.f./test stray	%	26	29	3.6	25	15	13	21
Calc^d Belt m.m.f./test stray	%	26	16	2.8	25	15	13	21

Footnotes:

(1) The test stray load loss is the average of two machines.

(2) Programme 7 does not include the slot width factor.

(3) The total calculated loss includes the peripheral flux leakage factor for the slot terms only (Fig. 12.2.4.).

13. REFERENCES

13. REFERENCES

1. KUYPER W.W. — "Pole-face Loss in Solid-rotor Turbine Generators", Trans. Amer. Inst. Elect. Engrs., 1943, 62, p.827.

2. BARELLO G. — "Eddy Currents Produced in the Solid Pole Pieces of Alternators by the Stray Rotating Fields of Armature Reaction". Revue Générale de L'Électricité, 1955, 64, p.557.

3. DAVIES E.J. — "An Experimental and Theoretical Study of Eddy-current Couplings and Brakes". Trans AIEE Power App. & Systems, 1963, 67, p.401.

4. DAVIES E.J. — "General Theory of Eddy Current Couplings and Brakes", Proc. IEE. 1966, 113, p.825.

5. GIBBS W.J. — "The Theory and Design of Eddy Current Slip Couplings" BEAMA Journal, 1946, p.123, p.172, p.219.

6. CHALMERS B.J. — "Electromagnetic problems of A.C. Machines (book) 1965, Chapman & Hall Ltd.

7. LAURENSON P.J. and Others — "Tooth Ripple Losses in Solid Poles". Proc. IEE, 1966, 113, p.657.

8. RICHARDSON P. — "Stray Losses in Synchronous Electrical Machinery" Proc. IEE 1945, 92, II, p.291.

9. GIBBS W.J. "Tooth Ripple Losses in Unwound Pole Shoes", Journal I.E.E., 1947, 94, II. p.2.

10. GIBBS W.J. "Induction and Synchronous Motors with Unlaminated Rotors", ibid., 1948, 95 pt.II. p.411.

11. HUGHES E. "Errors in Magnetic Testing of Ring Specimens", ibid., 1927, 65, p.932.

12. RAWCLIFFE G.H. & MENON A.M. "A Simple New Test for Harmonic Frequency Losses in A.C. Machines", Proc. I.E.E., 1952, 99 pt.II.p.145.

13. GIBBS W.J. Conformal Transformations in Electrical Engineering (book), Chapman and Hall, 1958.

14. POSTNIKOV "Eddy Currents in Synchronous and Asynchronous Machines with Unlaminated Rotors", Electrichestvo 1958, No. 10 7 - 14.

15. ASTON K. and RAO M.V.K. "Pole Face Losses Due to open slots on Grooved and Ungrooved Faces", Proc. I.E.E., 1953, 100, IV, p.104.

16. POHL R. "Electromagnetic and Mechanical Effects in Solid Iron due to an Alternating or Rotating Magnetic Field", Journal I.E.E., 1944, 91 pt.II, p.239.

17. ANEMPODISTOV et al. Problems in the Design and Development of 750 MW Turbo-generators (book, English Translation) Pergamon Press, 1963.

18. BRATOLJIC, T. "Recent Studies of Stray Losses in Solid Pole-Pieces of Synchronous Machines", Brown Boveri Review, 1966, 53, p.521.

19. HEAVISIDE, O. The Induction of Currents in Cores, The Electrician, 1884. Vol. 13.

20. THOMPSON J.J. "On the Heat produced by Eddy Currents in an Iron

plate Exposed to an Alternating Magnetic Field", The Electrician, April 1892, p.599.

21. CARTER G.W. — The Electromagnetic Field in its Engineering Aspects (book) Longmans, 1962.

22. OLSEN E. — Applied Magnetism, A Study in Quantities (book), Phillips, 1966.

23. RUDENBERG, R. — "Energie der Wirbelströme in Electrischen Bremsen und Dynamomaschinen", Publ. by Enke, Stuttgart, 1906.

24. RUDENBERG, R. — "Zusätzliche Verluste in Synchronmaschinen und ihre Messung", Elecktrotechnische Zeitschrift 1924, 45, p.37

25. ROSENBERG, E. — "Eddy Currents in Iron Masses", The Electrician, August 1923, p.188.

26. GILLOTT, D.H. & CALVERT J.F. — "Eddy Current Loss in Saturated Solid Magnetic Plates, Rods, and Conductors, I.E.E.E. Trans. on Magnets June 1965 p.126.

27. ABRAMS M.D. & GILLOTT D.H. — "Numerical Analysis of Hysteresis and Eddy Current Losses in Solid Cylindrical Rods of No. 1010 Steel", I.E.E.E. Trans., 1967, PAS-86, p.1077

28. AHAMED S.V. & ERDELYI E.A. — "Non Linear Theory of Salient Pole Machines", I.E.E.E. Trans. 1966, PAS-85, p.61.

29. ANGST G. — "Polyphase Induction Motor with Solid Rotor; Effects of Saturation and Finite Length", Trans. A.I.E.E. 1961, 80, III, p.902.

30. MUKHERJI K.C. — "Pole Face Losses in Rotating Electrical Machinery", E.R.A. Report Z/T98, 1955.

31. BOON C.R. & THOMPSON J.E. "Rotational Hysteresis Loss in Single-Crystal Silicon Iron". Proc. I.E.E. 1964, III, p.605.

32. BOON C.R. & THOMPSON J.E. "Alternating and Rotational Power Loss at 50 c/s in 3% Silicon Iron Sheets" ibid., 1965, 112, p.2147.

33. POLLARD "Load Losses in Salient Pole Synchronous Machines", Trans. A.I.E.E., 1935, 54, p.1332.

34. BALL J.D. "The Unsymmetrical Hysteresis Loop" Trans. A.I.E.E. 1915, 34, p.2275.

35. RICHARDSON P. "Large Solid Rotor Asynchronous Generators" Proc. I.E.E. 1958, 105A, p.332.

36. ALGER P.L. The Nature of Induction Machines (book) Gordon and Breach, 1965.

37. BUCKINGHAM H. & PRICE E.M. Principles of Electrical Measurements (book) EUP. 196

38. JAMES B. Electromagnetic Fields in the End Region of Eddy Current Couplings. M.Sc. Thesis, University of Aston, to be submitted in August 1968.

39. CLAYTON R. & WHITTAKER C. "Losses in Ferromagnetic Materials near current carrying conductors", Undergraduate Project Report, 1 University of Aston.

40. FREEMAN E. "The Calculation of Harmonics, due to slotting, in th Flux Density Waveform of a Dynamo - Electric Machine" Proc. I.E.E., 1962, 109C, p.581.

41. WAGNER C.F. & EVANS R. Symmetrical Components (book) McGraw Hill 1933.

42. DAVIES E.J. "A Slotless Turbogenerator", Electronics and Power, May 1968, p.209.